MDC E0648

FINAL REPORT
FOR
DIGITAL RECEIVER STUDY AND IMPLEMENTATION

1 JUNE 1971 – 1 JUNE 1972

CONTRACT NO.: NAS5-11424

PREPARED BY

MCDONNELL DOUGLAS ASTRONAUTICS COMPANY - EAST

St. Louis, Missouri 63166

MCDONNELL DOUGLAS ...ATION

FOR

GODDARD SPACE FLIGHT CENTER

GREENBELT, MARYLAND

MDC E0648

COPY NO. 36

FINAL REPORT
FOR
DIGITAL RECEIVER STUDY AND IMPLEMENTATION

1 JUNE 1971 – 1 JUNE 1972

CONTRACT NO.: NAS5-11424

GODDARD SPACE FLIGHT CENTER

CONTRACTING OFFICER : K.G. WILLIAMS CODE 245

TECHNICAL MONITOR: W. ALFORD CODE 563

PREPARED BY

MCDONNELL DOUGLAS ASTRONAUTICS COMPANY - EAST

St. Louis, Missouri 63166

MCDONNELL DOUGLAS CORPORATION

D.A. FOGLE, DR. G.M. LEE, J.C. MASSEY

FOR

GODDARD SPACE FLIGHT CENTER

GREENBELT, MARYLAND

ABSTRACT

Computer software is developed which makes it possible to use any general purpose computer with A/D conversion capability as a PSK receiver for low data rate telemetry processing. Carrier tracking, bit synchronization, and matched filter detection are all performed digitally. To aid in the implementation of optimum computer processors, a study of general digital processing techniques was performed which emphasized various techniques for digitizing general analog systems. In particular, the phase-locked loop was extensively analyzed as a typical non-linear communication element. Bayesian estimation techniques for PSK demodulation were studied. A hardware implementation of the digital Costas loop was developed.

TABLE OF CONTENTS

PAGE

TABLE OF CONTENTS ii

LIST OF FIGURES v

1. INTRODUCTION 1

2. DEVELOPMENT OF DIGITIZED PHASE-LOCKED LOOP 3

2.1 Synthesis of Equations 3

2.1.1 Choice of Phase-Locked Loop Filter 3

2.1.2 Analysis of Linear Loop 4

2.1.3 Differential Equation Approach 6

2.1.4 Difference Equation Formulation 9

2.2 Development of Computer Programs 12

2.3 Comparison of Techniques 21

2.3.1 Non-Linear Phase-Locked Loop 21

2.3.2 Linear Filters 25

2.4 Determination of System Constraints 30

2.4.1 Sampling Rate 30

2.4.2 Quantization 33

2.4.3 Scale Factor 35

2.5 Automatic Gain Control (AGC) 40

2.5.1 Bandpass Limiter 40

2.5.2 Closed Loop AGC 43

2.5.3 Comparison of Techniques 48

2.6 Acquisition 50

2.6.1 Swept Frequency Method 50

2.6.2 Fast Fourier Transform Acquisition 52

TABLE OF CONTENTS (Continued)

PAGE

2.6.3 Free Running Acquisition 57
2.6.4 Comparison of Techniques 57
2.7 Hybrid Simulation 61
2.7.1 Input Filter 61
2.7.2 Results 66
2.8 Evaluation of Performance 70
2.8.1 Phase Error Variance 71
2.8.2 Phase-Locked Loop Threshold 73
2.8.3 Acquisition 75
3. DEVELOPMENT OF DIGITIZED PSK RECEIVER 79
3.1 Synthesis of PSK Receiver Software 79
3.1.1 Sampling and A/D Conversion of Data 79
3.1.2 Rejection of DC Bias 84
3.1.3 Input Filter Design 86
3.1.4 Generation of PSK Modulated Noisy Carrier 88
3.1.5 Study of Carrier Synchronization 89
3.1.6 Automatic Gain Control 100
3.1.7 Study of Bit Synchronization 103
3.1.8 Development of Integrated Program 137
3.1.9 Study of Acquisition Techniques 147
3.2 Digital PSK System Analysis 156
3.2.1 Sampling Losses 157
3.2.2 Losses Due to Imperfect Phase Synchronization 164
3.2.3 Losses Due to Imperfect Bit Synchronization 167
3.2.4 Performance Evaluation 171

TABLE OF CONTENTS (Continued)

PAGE

4. STUDY OF NON-ANALOG SYNTHESIS TECHNIQUES 179

4.1 Bayesian Estimation 179

4.2 Performance Evaluation 186

5. DEVELOPMENT OF HARDWARE COSTAS LOOP 193

5.1 Machine Organizations 195

5.2 Parallel, 3 Arithmetic Logic Unit Design 195

5.2.1 General Description 197

5.2.2 Function Block 198

5.2.3 Logic Diagrams 202

5.2.4 Cost Estimate 219

5.3 Future Effort 219

REFERENCES 220

APPENDIX I - ANDERSON, BALL, VOSS METHOD I-1

APPENDIX II - DERIVATION OF DIFFERENCE EQUATIONS FOR LINEAR FILTERS . . II-1

APPENDIX III - BIT SYNCHRONIZATION ERROR III-1

APPENDIX IV - LISTING OF DIGITAL RECEIVER WITHOUT SAMPLE STORAGE BIT SYNCHRONIGATION IV-1

APPENDIX V - LISTING OF DIGITAL RECEIVER WITH SAMPLE STORAGE BIT SYNCHRONIGATION V-1

APPENDIX VI - LISTING OF DIGITAL RECEIVER WITH SAMPLE STORAGE BIT SYNCHRONIGATION (SPLIT-PHASE DATA) VI-1

APPENDIX VII - LISTING OF BASEBAND DIGITAL RECEIVER VII-1

APPENDIX VIII - LISTING OF DIGITAL RECEIVER WITH SWEPT FREQUENCY ACQUISITION VIII-1

LIST OF PAGES

Title Page
ii thru xii
1 thru 222
I-1 thru I-3
II-1 thru II-9
III-1 thru III-6
IV-1 thru IV-6
V-1 thru V-11
VI-1 thru VI-11
VII-1 thru VII-5
VIII-1 thru VIII-10

LIST OF FIGURES

FIGURE NO.	TITLE	PAGE
1	Linearized Phase-Locked Loop	4
2	Phase-Locked Loop Block Diagram	6
3	Differential Equation Implementation	8
4	Finite Difference Model of Phase-Locked Loop	9
5	Computer Program for Runge-Kutta Method	13
6	Computer Programs for Euler's and the Z-Transform Method	14
7	Computer Program for Tustin's and ABV Method	15
8	Mechanization of the Z-Transform Method	16
9	Mechanization of Euler's Method	17
10	Routine for Calculating Sine	18
11	Accuracy of Sine Wave Generator	20
12	Comparison of Numerical Methods for a Ramp Input	22
13	Comparison of Numerical Methods for a Step Input	22
14	Methanization of the ABV Method and Tustin's Method	24
15	Comparing Numerical Methods for Ramp Input as a Function of Computation Time	26
16	Comparing Numerical Methods for Step Input as a Function of Computation Time	27
17	Comparison of Numerical Techniques for Linear Filter with Ramp Input	28
18	Comparison of Numerical Techniques for Linear Filter with Step Sine Wave Input	29
19	Phase Variance Versus Sample Interval	31
20	Phase Error Curve (Digital Simulation)	32

LIST OF FIGURES (continued)

FIGURE NO.	TITLE	PAGE
21	Mean Squared Error Versus Offset Frequency for Different Sample Intervals	34
22	Standard Deviation of Phase Output Versus the Number of Quantization Levels	36
23	Phase Error Variance Versus the Number of Quantization Levels	37
24	Scale Factor Determination	39
25	Phase-Locked Loop with Input Limiter	40
26	Sawtooth Comparator	42
27	Phase Error Variance for Limiter	44
28	Phase Error Variance for Sawtooth Comparator	45
29	Closed Loop Analog AGC	46
30	Implementation Diagram for AGC Loop	47
31	Phase Error Variance Versus Input SNR	49
32	Swept Frequency Acquisition	51
33	Determining Relationship Between LPF Bandwidth and Sweep Rate	53
34	Computer Program for Acquisition	54
35	Digital Computer Program for FFT Generation	55
36	Mean Pull-in Time Versus Offset Frequency	58
37	Variance in Pull-in Time Versus Frequency Offset	59
38	Probability of Acquisition Versus Sweep Data	60
39	Optimizing Second Order Input Filter	64
40	Comparing Input Filters (L Versus R)	65
41	Comparing Input Filters (K Versus R)	66
42	Hybrid Configuration	67

LIST OF FIGURES (continued)

FIGURE NO.	TITLE	PAGE
43	Tracking Noisy Sine Wave	68
44	Phase Error Variance without Limiter (Hybrid Simulation)	69
45	Phase Error Variance with Limiter (Hybrid Simulation)	70
46	Comparing Digital Simulation Results with Quasi-Linear Approximation	72
47	Comparing Digital Simulation Results with Fokker-Plank Solution	74
48	Comparing Measured and Calculated Pull-in Time	76
49	Comparing Digital Simulation and Theoretical Results for Probability of Acquisition	77
50	Generation of Noisy PSK Modulated Carrier	80
51	Direct IF Sampling and A/D Conversion	81
52	Sample Timing for 1 kHz Operation	83
53	Sample Timing for 244 Hz Operation	84
54	DC Bias Remover	85
55	Digital Signal Generation	90
56	The Squaring Loop for Phase-Tracking a Binary-Modulated Suppressed-Carrier Input	91
57	The Costas Loop for Phase-Tracking a Binary PSK Carrier	91
58	Decision-Oriented Carrier Tracking	92
59	Bit Error Probability for Costas Loop and Decision Feedback	94
60	Linearized Costas Loop	96
61	Phase Error Variance	102
62	Square Law Bit Synchronizer	105

LIST OF FIGURES (continued)

FIGURE NO.	TITLE	PAGE
63	Delay and Multiply Bit Synchronizer	107
64	Autocorrelation Function for Output of Delay and Multiply Bit Synchronizer	107
65	Gate Location	109
66	Gated Bit Synchronizer	109
67	Comparison of Bit Synchronizers	111
68	Bit Synchronizer Acquisition Time	112
69	Bit Synchronization Loop	114
70	Loop Error Signal	116
71	Time Points Defining Early, Late, and Data Integrals	117
72	Reduced Bit Synchronization Loop	118
73	Bit Synchronization Feedback Loop	120
74	Bit Error Rate for Digital Receiver with and without Sample Storage Bit Synchronizer	125
75	Standard Deviation of Bit Jitter	126
76	Standard Deviation of Bit Jitter - 5% Timing Error	127
77	Bit Error Rate - NRZ and Split-Phase	130
78	Standard Deviation of Bit Jitter - NRZ and Split-Phase	131
79	Bit Error Rate - NRZ and Split-Phase	132
80	Standard Deviation of Bit Jitter - NRZ and Split-Phase	133
81	Standard Deviation of Bit Jitter; AGC and No AGC	135
82	Digital Receiver with Sample Storage Bit Synchronizer and AGC	136

LIST OF FIGURES (continued)

FIGURE NO.	TITLE	PAGE
83	Costas Loop with Hard Line Sync	138
84	Flow Chart of Digital PSK Receiver with Data Derived Sync	140
85	Acquisition Indicator - Simulation	150
86	Acquisition Indicator - Experimental	151
87	Loss Caused by Noise Aliasing	159
88	Loss Caused by Intersymbol Interference	160
89	Total Sampling Loss	161
90	Costas Loop Phase Error Variance	166
91	Probability of Error with a Noisy Phase Reference	168
92	Standard Deviation of Bit Jitter Versus Signal-to-Noise Ratio	169
93	Bit Synch Error Versus Signal-to-Noise Ratio (Theoretical)	170
94	Effect of Sample Rate on Bit Sync Error	172
95	Bit Error Rate - Sample Storage Bit Sync	173
96	Bit Error Rate - AGC	175
97	Bandpass Filter	176
98	Bit Error Rate - Optimized IF Filter	177
99	Bit Error Rate Split-Phase Data	178
100	Reduction of Dimensionality	183
101	Probability of Bit Error with Bayesian Estimation	191
102	Typical Learning Curve for Bit Synchronization	192
103	Phase Estimation Processor	194
104	Candidate Systems Versus Speed	196

LIST OF FIGURES (continued)

FIGURE NO.	TITLE	PAGE
105	Time Slot Operations	196
106	Functional Block Diagram	199
107	Operation Sequencer and Clock	203
108	Timing Diagram	205
109	Arithmetic Logic Units A and C	206
110	Arithmetic Logic Unit B	209
111	Method A Sine-Cosine ROM	214
112	Method B Sine-Cosine ROM	216
113	Input-Output Registers	217
III1	Bit Synchronization Model	III-1
III2	Bit Synchronization Integrals	III-4
III3	Standard Deviation of Bit Jitter Versus Signal-to-Noise Ratio	III-6

1. INTRODUCTION

Potential applications of digital computers in communications systems continue to expand. Many ground stations have ready access to general purpose computers that could be used as data processors. In this study, we have developed the digital signal processing techniques necessary for performing all the functions of an analog communication receiver.

The computer software developed for the MDAC Digital PSK receiver makes it possible to use any general purpose computer (with A/D conversion capability) as a receiver for low data rate telemetry processing. The first step in the receiver processing is sampling and A/D conversion. The sampling can either be performed directly on the IF signal, or on the quadrature components of the IF signal derived from mixing the IF with a frequency oscillator. We have operated our receiver with both sampling techniques without any noticeable difference in performance.

The sampled quadrature components are A/D converted for further processing by a set of digital algorithms which are roughly equivalent to a digital Costas loop. The output of the Costas loop is mixed with the input signal to develop the NRZ video signal. Bit synchronization is performed by a set of digital algorithms which constitute an early-late gate type synchronizer. The bit synchronizer uses four offset integrators to perform phase detection along with a digital phase locked loop for tracking. A digital integrator and threshold is then used for bit detection.

The logic speed of general purpose computers makes this software useful for data rates of 0-100 bits/second. Very low bit rates are difficult to demodulate with analog processors due to the need for very long time constant filters, precise component values, and very stable timing references. Thus,

the digital software discussed in this report provide a low cost, efficient, and versatile solution to the low data rate receiver problem. This software can also easily be modified to incorporate any data format desired. Measurements of receiver performance (i.e., probability of error/bit) indicate that the Digital PSK Receiver will operate as close to the theoretical optimum as the logic speed and tracking bandwidths will permit.

The Digital Receiver Study and Implementation conducted under contract NAS5-11424 for NASA GSFC, included the optimization of the MDAC digital PSK receiver software (developed under contract NAS5-21021), an expanded study of digital bit synchronization algorithms, and a preliminary study of digital processing techniques which have no real analog equivalent. This report also contains the principal results from the previous contract NAS5-21021, the study of Digital Phase Lock Techniques. The results of both contracts were combined since they are highly interrelated and are both incomplete without the other. All system simulations for both contracts were performed on the MDAC CDC 6400 and CDC 6600 computers, and all receiver software was optimized for the GSFC CDC 3200 computer.

2. DEVELOPMENT OF DIGITIZED PHASE-LOCKED LOOP

This effort consisted of designing, implementing, and evaluating a digitized phase-locked loop capable of tracking a carrier imbedded in wide band noise. As part of the design effort, we compared the various numerical techniques available for implementing a digital filter, synthesized and analyzed the loop equations, and evaluated the performance by determining curves of phase error variance as a function of the signal-to-noise ratio, sampling rate, and quantization interval size. We also investigated digital techniques for implementing AGC and acquisition circuits.

2.1 Synthesis of Equations

We selected a phase-locked loop filter by considering its effect on transient response (damping), bandwidth, and steady state tracking-offset for a ramp input. Utilizing this filter, we analyzed the linear loop in order to determine the filter and gain constants as a function of the damping factor (ζ), and the undamped natural frequency (ω_o). Finally, we analyzed the non-linear loop and developed numerical equivalents for it using both the differential and difference equation approach.

2.1.1 Choice of Phase-Locked Loop Filter

The filter in a second order phase-locked loop can have any of the forms given in Equations (1-3).

$$F_1(s) = \frac{b}{s+b} \tag{1}$$

$$F_2(s) = \left(\frac{b}{a}\right) \frac{(s+a)}{(s+b)} \tag{2}$$

$$F_3(s) = \frac{s+a}{s} \tag{3}$$

We determined the effect of the three phase-locked loop filters on the transient response (damping), bandwidth, and steady state tracking offset for a ramp input to the associated phase-locked loop. The filter represented by Equation (1) was not chosen because the bandwidth and phase offset both depend on the loop gain and thus cannot be chosen independently. If the filter given in Equation (2) is utilized, the filter constant (a) and the loop gain are chosen to give the proper bandwidth and damping, and the filter constant (b) is chosen to give an acceptable phase offset. Since the phase offset will normally be made small, the constant (b) for $F_2(s)$ will be near zero, and $F_3(s)$ and $F_2(s)$ are essentially the same. Therefore, the choice must be made in terms of implementation complexity. Since the digital implementation of $F_3(s)$ requires one less multiplication, it was selected as the phase-locked loop filter. $F_2(s)$ would be our choice for an analog implementation because of the difficulty associated with implementing the open loop integrator associated with $F_3(s)$. This decision is also supported by the fact that for an input consisting of a ramp of phase the third filter form minimizes the mean squared error at the loop output.

2.1.2 Analysis of Linear Loop

A block diagram of the linearized phase-locked loop is given in Figure 1 where the input signal is assumed to be of the form $A \sin(\omega_o t + \Theta_{in})$.

LINEARIZED PHASE – LOCKED LOOP

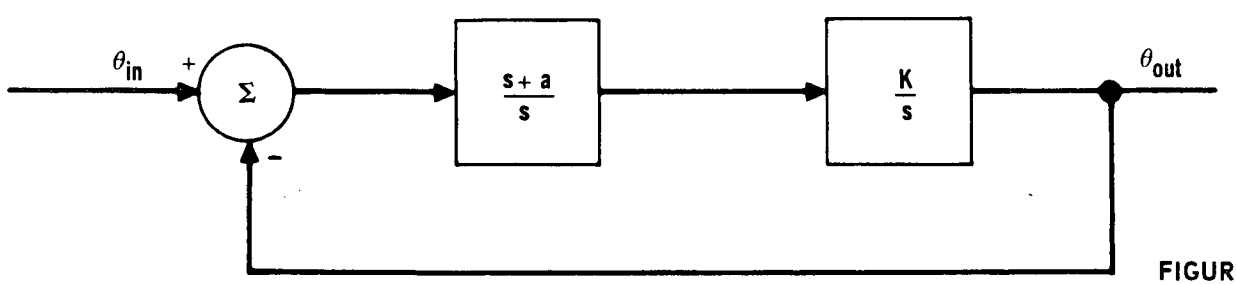

FIGURE 1

The loop transfer function can then be determined as shown in Equations (4) and (5).

$$\frac{\theta_{out}}{\theta_{in}} = \frac{\frac{AK(s+a)}{s^2}}{1+\frac{AK(s+a)}{s^2}} \tag{4}$$

$$\frac{\theta_{out}}{\theta_{in}} = \frac{AK(s+a)}{s^2 + AKs + aAK} \tag{5}$$

This transfer function can then be put in the standard form given in Equation (6).

$$\frac{\theta_{out}}{\theta_{in}} = \frac{2\zeta\omega_0 s + \omega_0^2}{s^2 + 2\zeta\omega_0 s + \omega_0^2} \tag{6}$$

$$AK = 2\zeta\omega_0 \tag{7}$$

$$aAK = \omega_0^2 \tag{8}$$

If the input amplitude, the damping factor (ζ), and the undamped natural frequency (ω_0) are known, the phase-locked loop gain and filter constant can be determined from Equations (7) and (8) and are given in Equations (9) and (10).

$$K = \frac{2\zeta\omega_0}{A} \tag{9}$$

$$a = \omega_0/2\zeta \tag{10}$$

The response of the above loop to a ramp input of slope ω is given in Equation (11).

$$\theta_{out}(t) = \omega t - \frac{2\omega\delta^2}{\omega_0\sqrt{1-\zeta^2}} e^{-\delta\omega_0 t} \sin \omega_0\sqrt{1-\zeta^2}\, t \tag{11}$$

The above result shows that the effective time constant of the loop is $\frac{1}{\delta\omega_0}$ seconds. The noise and 3 db bandwidth of the above loop are given in Equations (12) and (13).

$$\text{Noise Bandwidth} = B_N = \omega_0 \left(\frac{2\zeta + \frac{1}{2\zeta}}{4} \right) \quad \text{Hz} \tag{12}$$

$$\text{3 db Bandwidth} = \frac{\omega_0}{2\pi} \sqrt{(2\zeta^2 + 1) \pm \sqrt{(2\zeta^2 + 1)^2 + 1}} \quad \text{Hz} \tag{13}$$

2.1.3 Differential Equation Approach

With the loop parameters established in terms of standardized functions, we proceeded to develop the numerical equivalents for the differential equations which describe the loop operation. From the block diagram of the phase-locked loop presented in Figure 2, the loop equations can be derived as shown in Equations (14-17).

PHASE – LOCKED LOOP BLOCK DIAGRAM

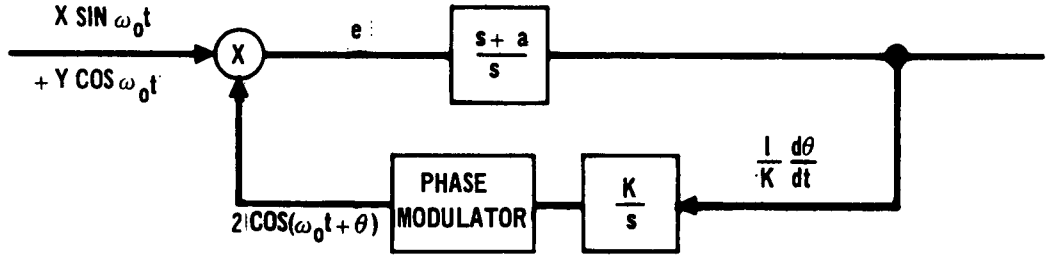

FIGURE 2

$$e = 2(X \sin \omega o t + Y \cos \omega o t) \cos (\omega o t + \theta) \tag{14}$$

$$e = -X \sin \theta + Y \cos \theta + \text{(second harmonic terms)} \tag{15}$$

$$\frac{d^2\theta}{dt^2} = K\left(\frac{d}{dt} + a\right)e \tag{16}$$

$$\frac{d^2\theta}{dt^2} = aK \left[Y \cos \theta - x \sin \theta\right] + K \frac{d}{dt} \left[Y \cos \theta - X \sin \theta\right] \quad (17)$$

To avoid taking the derivative of the quadrature components, the above equation can then be converted to the form shown in Equations (18) and (19).

$$\frac{dc}{dt} = aK \ (Y \cos \theta - X \sin \theta) \quad (18)$$

$$\frac{d\theta}{dt} = c + K \ (Y \cos \theta - X \sin \theta) \quad (19)$$

One discrete time technique that was used to solve the above equations is the Runge-Kutta Method. Using results obtained from Scarborough[1], the equations for this technique are shown in Figure 3. A second technique investigated was Euler's Method. The equations for this method are also given in Figure 3. A comparison of these and other techniques is presented in Section 2.3.

DIFFERENTIAL EQUATION IMPLEMENTATION

A	= INPUT SINE WAVE AMPLITUDE
h	= TIME INCREMENT
θ_n	= OUTPUT PHASE AT TIME t_n
C_n	= DUMMY VARIABLE C AT TIME t_n
X_n, Y_n	= QUADRATURE COMPONENTS OF INPUT SIGNAL AT TIME t_n
K	$= 2\zeta\omega_0/A$
a	$= \omega_0/2\zeta$

RUNGE – KUTTA METHOD

$F(\theta, X, Y)$	$= Kh\,(Y \cos\theta - X \sin\theta)$
G_1	$= F(\theta_{n-2}, X_{n-2}, Y_{n-2})$
A_1	$= hC_{n-2} + G_1$
B_1	$= aG_1$
G_2	$= F(\theta_{n-2} + A_1/2, X_{n-1}, Y_{n-1})$
A_2	$= h[C_{n-2} + B_1/2] + G_2$
B_2	$= aG_2$
G_3	$= F(\theta_{n-2} + A2/2, X_{n-1}, Y_{n-1})$
A_3	$= h[C_{n-2} + B2/2] + G_3$
B_3	$= aG_3$
G_4	$= F(\theta_{n-2} + A_3, X_n, Y_n)$
A_4	$= h[C_{n-2} + B_3] + G_4$
B_4	$= aG_4$
C_n	$= C_{n-2} + (B_1 + 2B_2 + 2B_3 + B_4)/6$
θ_n	$= \theta_{n-2} + (A_1 + 2A_2 + 2A_3 + A_4)/6$

EULER'S METHOD

G	$= Y_{n-1} \cos\theta_{n-1} - X_{n-1} \sin\theta_{n-1}$
θ_n	$= \theta_{n-1} + h\,C_{n-1} + KhG$
C_n	$= C_{n-1} + aKhG$

FIGURE 3

2.1.4 Difference Equation Formulation

The difference equation approach is basically a method of determining the present value of the phase-locked loop output in terms of past output values and past and present input values. In order to formulate the difference equations for the phase-locked loop, the block diagram of Figure 4 is utilized.

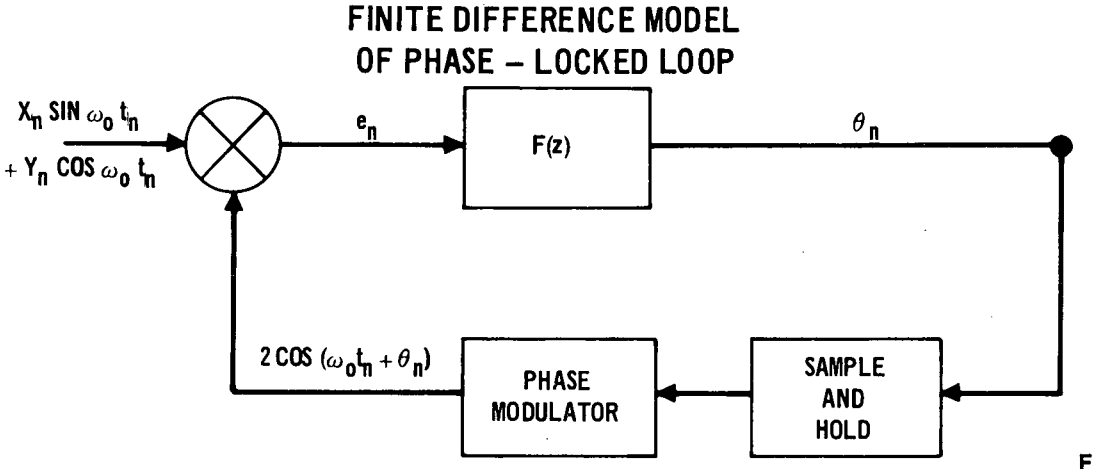

FIGURE 4

The difference equations for the above model can be written as shown in Equations (20-23).

$$e_n = 2(X_n \sin \omega_o t_n + Y_n \cos \omega_o t_n) \cos (\omega_o t_n + \theta_n) \quad (20)$$

$$e_n = -X_n \sin \theta_n + Y_n \cos \theta_n + \text{(second harmonic terms)} \quad (21)$$

$$\frac{\theta(z)}{e(z)} = \frac{A_2 z^2 + A_1 z + A_0}{B_2 z^2 + B_1 z + B_0} \quad (22)$$

$$\theta_n = \frac{1}{B_2} (A_2 e_n + A_1 e_{n-1} + A_o e_{n-2} - B_1 \theta_{n-1} - B_o \theta_{n-2}) \quad (23)$$

z = Z-Transform operator

The first technique we investigated for implementing difference equations was the Z-Transform method. In order to use this technique a hold circuit must be placed in front of the phase-locked loop filter. F(z) can then be determined as shown

$$F(z) = (1-z^{-1}) \quad Z \quad \left[\frac{Ks + aK}{s^3}\right] \quad (24)$$

$$F(z) = \frac{(2Kh + aKh^2)z + (aKh^2 - 2Kh)}{2\,(z^2 - 2z + 1)} \tag{25}$$

The difference equation for the loop can be written as shown in Equations (26-28).

$$e_{n-1} = Y_{n-1} \cos \Theta_{n-1} - X_{n-1} \sin \Theta_{n-1} \tag{26}$$

$$e_{n-2} = Y_{n-2} \cos \Theta_{n-2} - X_{n-2} \sin \Theta_{n-2} \tag{27}$$

$$\Theta_n = 2\Theta_{n-1} - \Theta_{n-2} + \frac{1}{2}(2Kh + aKh^2)\, e_{n-1} + \frac{1}{2}(aKh^2 - 2Kh)\, e_{n-2} \tag{28}$$

The second technique investigated was Tustin's Method. This technique corresponds to trapezoidal rule integration. In order to obtain the difference equation from the transfer function, the integration operators are replaced by

$$\frac{1}{s} \longrightarrow \frac{h(1 + z^{-1})}{2(1 - z^{-1})} \tag{29}$$

$$\frac{1}{s^2} \longrightarrow \frac{h^2(1 + z^{-1})^2}{4(1 - z^{-1})^2} \tag{30}$$

F(z) can then be obtained

$$F(s) = \frac{\theta(s)}{e(s)} = \frac{Ks + aK}{s^2} = K\left(\frac{1}{s}\right) + aK\left(\frac{1}{s^2}\right) \tag{31}$$

$$F(z) = F(s) \Bigg|_{\frac{1}{s^2} = \frac{h^2(1+z^{-1})^2}{4(1-z^{-1})^2}\,,\quad \frac{1}{s} = \frac{h(1+z^{-1})}{2(1-z^{-1})}} \tag{32}$$

$$F(z) = \frac{\theta(z)}{e(z)} = \frac{2Kh(z^2-1) + aKh^2(z^2 + 2z + 1)}{4(z^2 - 2z + 1)} \tag{33}$$

Since the phase output θ_n depends on e_n, a unit delay must be added in the feedback path. The results are given in Equations (34-37).

$$e_n = Y_n \cos\theta_{n-1} - X_n \sin\theta_{n-1} \tag{34}$$

$$e_{n-1} = Y_{n-1} \cos\theta_{n-2} - X_{n-1} \sin\theta_{n-2} \tag{35}$$

$$e_{n-2} = Y_{n-2} \cos\theta_{n-3} - X_{n-2} \sin\theta_{n-2} \tag{36}$$

$$\theta_n = 2\theta_{n-1} - \theta_{n-1} + \frac{1}{4}(2Kh + aKh^2)e_n + \frac{1}{2} aKh^2 e_{n-1} + \frac{1}{4}(aKh^2 - 2Kh) e_{n-2} \tag{37}$$

The final technique considered was the Anderson, Ball, Voss Method. This technique consists of approximating the input signal by a polynomial in t and then computing the response at the output of the filter. The input signal was approximated by a second order polynomial, and the resulting difference equation is given in Equations (38-41). The unit delay is again added in the feedback path because of the problem mentioned with respect to Tustin's Method. Because of the complexity associated with this technique, the derivation of this result appears in Appendix I.

$$e_n = Y_n \cos\theta_{n-1} - X_n \sin\theta_{n-1} \tag{38}$$

$$e_{n-1} = Y_{n-1} \cos\theta_{n-2} - X_{n-1} \sin\theta_{n-2} \tag{39}$$

$$e_{n-2} = Y_{n-2} \cos\theta_{n-3} - X_{n-2} \sin\theta_{n-3} \tag{40}$$

$$\theta_n = 2\theta_{n-1} - \theta_{n-2} + (\frac{1}{2} Kh + \frac{1}{12} aKh^2) e_n + \frac{5}{6} aKh^2 e_{n-1} + (\frac{1}{12} aKh^2 - \frac{1}{2} Kh) e_{n-2} \tag{41}$$

Equations (38-41) show that the Anderson, Ball, Voss technique gives results that are almost identical with those obtained using Tustin's Method. Therefore, for this particular filter, the higher order approximation used with the Anderson, Ball, Voss technique does not increase the accuracy of the result. We also investigated the Madwed-Truxal and the Boxer-Thaler Techniques. These

methods are similar to Tustin's method except that different approximations are used for the higher order integration operators. Our results showed that these techniques give only an insignificant increase in accuracy and are more unstable than Tustin's method. Therefore, it was concluded that these techniques did not merit further consideration.

2.2 Development of Computer Programs

We developed digital computer programs for the five techniques considered in Section 2.1. These programs were written in the Fortran IV language which is compatible with the CDC 3200 computer. The Runge-Kutta Method is shown in Figure 5; Euler's Method and the Z-Transform technique is shown in Figure 6; and Tustin's Method and the Anderson, Ball, Voll (ABV) Method is illustrated in Figure 7. In these figures ADC (01) and ADC (02) represent the digitized values of the sampled quadrature components which have been sent through the analog to digital converters.

Mechanization block diagrams for the Z-Transform technique and for Euler's method are shown in Figures 8 and 9 respectively. As is shown in the following section, these two approaches give near optimum results for the non-linear phase-locked loop. The blocks containing Z^{-1} represent a storage register which delays the signal by one sample period.

The most complex and time consuming portion of these implementations is the sine and cosine calculation. One possible method of simplifying this calculation is to compute new values of the sine and cosine from the previous values by using the small angle approximation as shown in Equations (42) and (43).

COMPUTER PROGRAM FOR RUNGE – KUTTA METHOD

ADC(01) = DIGITIZED VALUE OF X QUADRATURE COMPONENT FROM ANALOG CIRCUITRY
ADC(01) = DIGITIZED VALUE OF Y QUADRATURE COMPONENT FROM ANALOG CIRCUITRY
H = TIME BETWEEN SAMPLES
AK = KH
AA = a
C6 = H/2
T = θ_n
TM1 = θ_{n-1}
TM2 = θ_{n-2}
C = C_n
CM1 = C_{n-1}
CM2 = C_{n-2}
XM = x_n
YM = y_n
SMI = x_{n-1}
YMI = y_{n-1}
XM2 = x_{n-2}
YM2 = y_{n-2}

```
XM   = ADC(01)
YM   = ADC(02)
C3   = CM2 * H
C2   = AK * (XM2 * SIN(TM2) -YM2 * COS(TM2))
A1   = C3 + C2
B1   = AA * C2
C4   = TM2 + .5 * A1
C2   = AK * (XM1 * SIN(C4) -YM1 * COS(C4))
A2   = C3 + C6 * B1 + C2
B2   = AA * C2
X4   = TM2 + .5 * A2
C2   = AK * (XM1 * SIN(C4) -YM1 * COS(C4))
A3   = C3 + C6 * B2 + C2
B3   = AA * C2
C4   = TM2 + A3
C2   = AK * (XM * SIN(C4) -YM * COS(C4))
A4   = C3 + H * B3 + C2
B4   = AA * C2
T    = TM2 + (A1 + 2 * (A2 + A3) + A4)/6.
C    = CM2 + (B1 + 2 * (B2 + B3) + B4)/6.
YM2  = YM1
XM2  = XM1
YM1  = YM
XM1  = XM
TM2  = TM1
TM1  = T
CM2  = CM1
CM1  = C
```

FIGURE 5

COMPUTER PROGRAMS FOR EULER'S AND THE Z-TRANSFORM METHOD

EULER'S METHOD

H	= TIME BETWEEN SAMPLES
AK	= KH
AA	= a
T	$= \theta_n$

X	= ADC(01)
Y	= ADC (02)
TEMP	= AK * (Y * COS(T) −X * SIN(T))
T	= T + C * H + TEMP
C	= C + AA * TEMP

Z − TRANSFORM METHOD

H	= TIME BETWEEN SAMPLES
A1	$= KH + \frac{1}{2}aKH^2$
A2	$= \frac{1}{2}aKH^2 - KH$
T	$= \theta_n$
TM1	$= \theta_{n-1}$
TM2	$= \theta_{n-2}$
EM1	$= e_{n-1}$
EM2	$= e_{n-2}$
XM1	$= x_{n-1}$
YM1	$= y_{n-1}$

XM1	= ADC(01)
YM1	= ADC(02)
EM1	= YM1 * COS(TM1) −XM1 * SIN(TM1)
T	= 2 * TM1 −TM2 + A1 * EM1 + A2 * EM2
TM2	= TM1
TM1	= T
EM2	= EM1

FIGURE 6

COMPUTER PROGRAM FOR TUSTIN'S AND ABV METHOD

```
T   = θ_n
TM1 = θ_n-1
TM2 = θ_n-2
EM1 = e_n-1
EM2 = e_n-2
XM  = x_n-1
YM  = y_n-1
```

```
TUSTIN'S METHOD
  H  = TIME BETWEEN SAMPLES
  C1 = KH/2 + aKH^2/2
  C2 = aKH^2/2
  C3 = aKH^2/4 - KH/2
```

```
XM  = ADC(01)
YM  = ADC(02)
EM  = YM * COS(TM1) - XM * SIN(TM1)
T   = 2 * TM1 - TM2 + C1 * EM + C2 * EM1 + C3 * EM2
EM2 = EM1
EM1 = EM
TM2 = TM1
TM1 = T
```

```
ANDERSON, BALL, VOSS METHOD (ABV)
  H  = TIME BETWEEN SAMPLES
  C1 = KH/2 + aKH^2
  C2 = 5aKH^2/6
  C3 = aKH^2/12 - KH/2
```

```
XM  = ADC(01)
YM  = ADC(01)
EM  = YM * COS(TM1) - XM * SIN(TM1)
T   = 2 * TM1 - TM2 + C1 * EM + C2 * EM1 + C3 * EM2
EM2 = EM1
EM1 = EM
TM2 = TM1
TM1 = T
```

FIGURE 7

MECHANIZATION OF THE Z-TRANSFORM METHOD

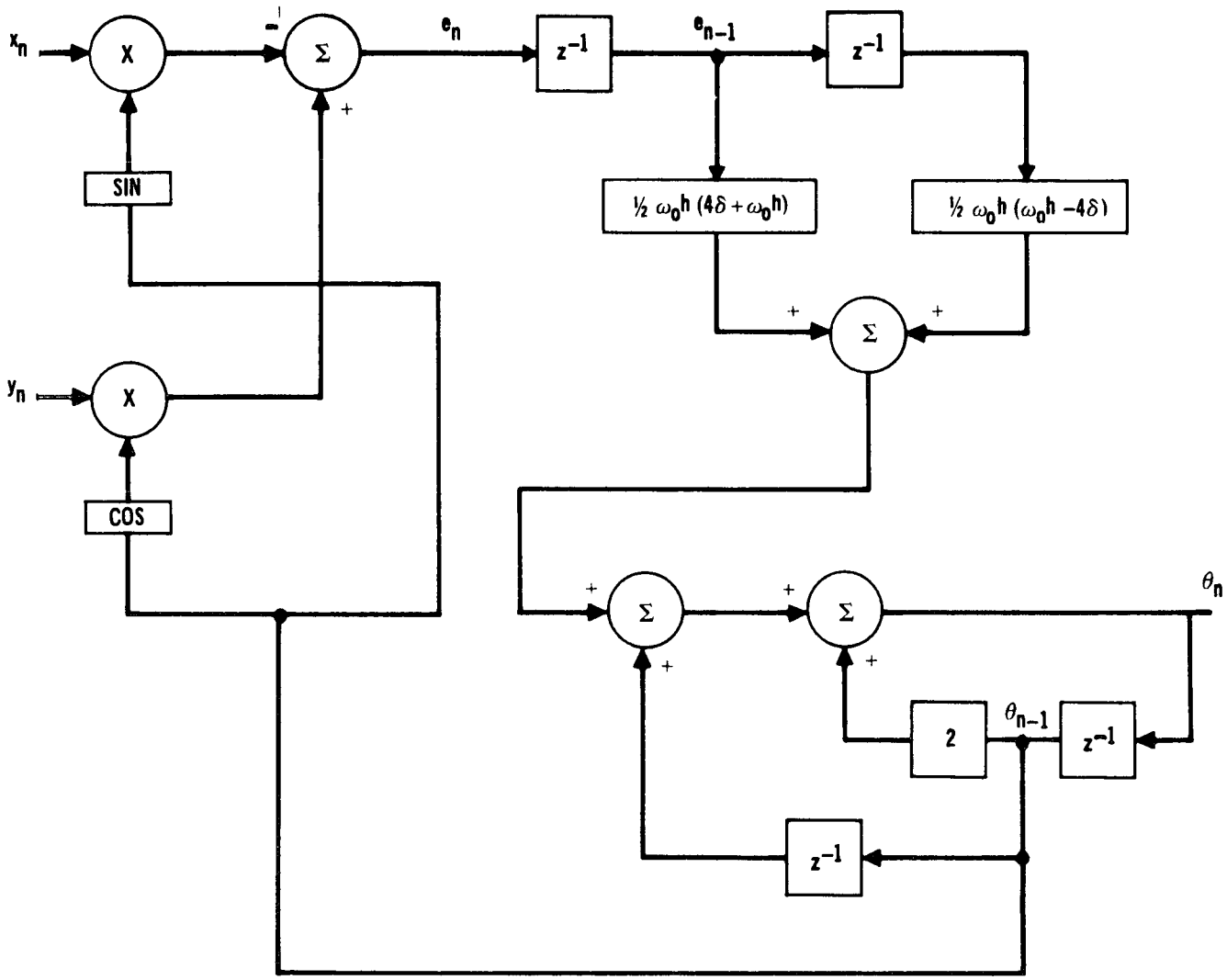

FIGURE 8

MECHANIZATION OF EULER'S METHOD

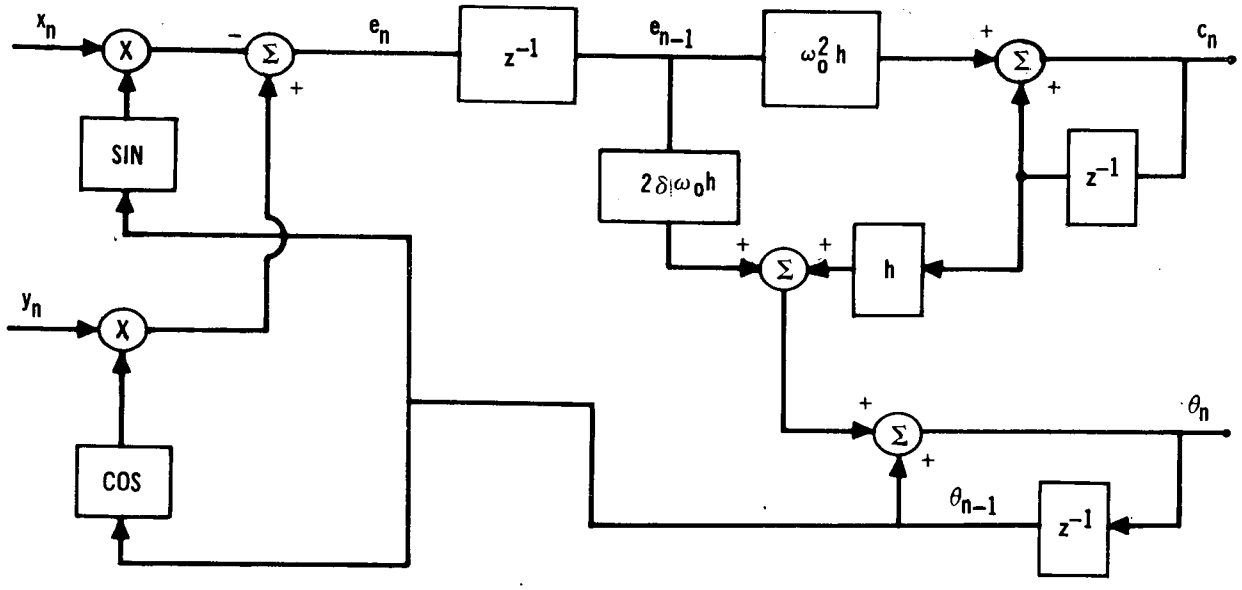

FIGURE 9

$$\cos(\Theta + \Delta\Theta) = \cos\Delta\Theta\cos\Theta - \sin\Delta\Theta\sin\Theta \qquad (42)$$

$$\sin(\Theta + \Delta\Theta) = \sin\Delta\Theta\cos\Theta + \cos\Delta\Theta\sin\Theta \qquad (43)$$

If $\Delta\Theta$ is small, this result can be simplified as shown in Equations (44) and (45).

$$\cos(\Theta + \Delta\Theta) = \cos\Theta - \Delta\Theta\sin\Theta \qquad (44)$$

$$\sin(\Theta + \Delta\Theta) = \sin\Theta + \Delta\Theta\cos\Theta \qquad (45)$$

Starting with an initial value for sin Θ and cos Θ, the above formulas can be used to recursively evaluate the sine and cosine if $\Delta\Theta$ is small. However, Larimore[2] shows that this technique will become unstable unless a correction

factor is applied to the above calculation. He suggests that this correction factor make the sum of the squares of the sine and cosine equal to one as shown in Equations (46-51).

K = correction factor

$$K^2 \left[\cos^2 (\theta + \Delta\theta) + \sin^2 (\theta + \Delta\theta)\right] = 1 \qquad (46)$$

$$K = 1/\left[\cos^2 (\theta + \Delta\theta) + \sin^2 (\theta + \Delta\theta)\right]^{\frac{1}{2}} \qquad (47)$$

$$\text{let } E = \cos^2 (\theta + \Delta\theta) + \sin^2 (\theta + \Delta\theta) - 1 \qquad (48)$$

$$\therefore K = 1/\sqrt{1 + E} = (1 + E)^{-\frac{1}{2}} \qquad (49)$$

$$\text{if } E \approx 0 \qquad (50)$$

$$K \approx 1 - \frac{1}{2} E \qquad (51)$$

A Fortran program for continuously making the above calculation is given in Figure 10.

ROUTINE FOR CALCULATING SINE

```
CMI = PREVIOUS VALUE OF SINE
SMI = PREVIOUS VALUE OF COSINE
DTHE = Δθ
SM = PRESENT VALUE OF SINE
CM = PRESENT VALUE OF COSINE
-----------------------------
CMP = CMI - DTHE * SMI
SMP = SMI + DTHE * CMI
DN = 1.5 - 0.5 * (SMP **2 + CMP **2)
CM = DN * CMP
SM = DN * SMP
CMI = CM
SMI = SM
```

FIGURE 10

Utilizing the CDC 6400 computer, a timing calculation was made for both the above routine and the standard subroutine used in the 6400 for computing the sine and cosine. The results showed that the simple technique required 49 μsec of central processor time per iteration, while the more complex method required 251 μsec per iteration. Although the simple technique is 5 times faster, its accuracy degrades as a function of both the number of calculations and the increment size, as shown in Figure 11. If we sample at a rate ten times the maximum offset frequency, the average output phase change would be 36°. Therefore, from the results given in Figure 11, it would be necessary to update the sine and cosine generator after only a small number of iterations, thus making the usefulness of this technique questionable. One possible method of updating the calculation would be to store several values of the sine and cosine uniformly spaced between zero and ninety degrees, and then selecting the nearest angle after a fixed number of calculations. In order to implement this approach logic statements must be added to the program, which would result in an increased computation time. A transient will also occur in the phase-locked loop each time an update is made. A better solution to this problem might be to write a more efficient routine for generating the sine and cosine or to use a table look-up technique. A trade-off between accuracy and speed could then be made to determine the optimum approach. Designing an optimum sine and cosine generator for use in this phase-locked loop program represents a prime area for further study.

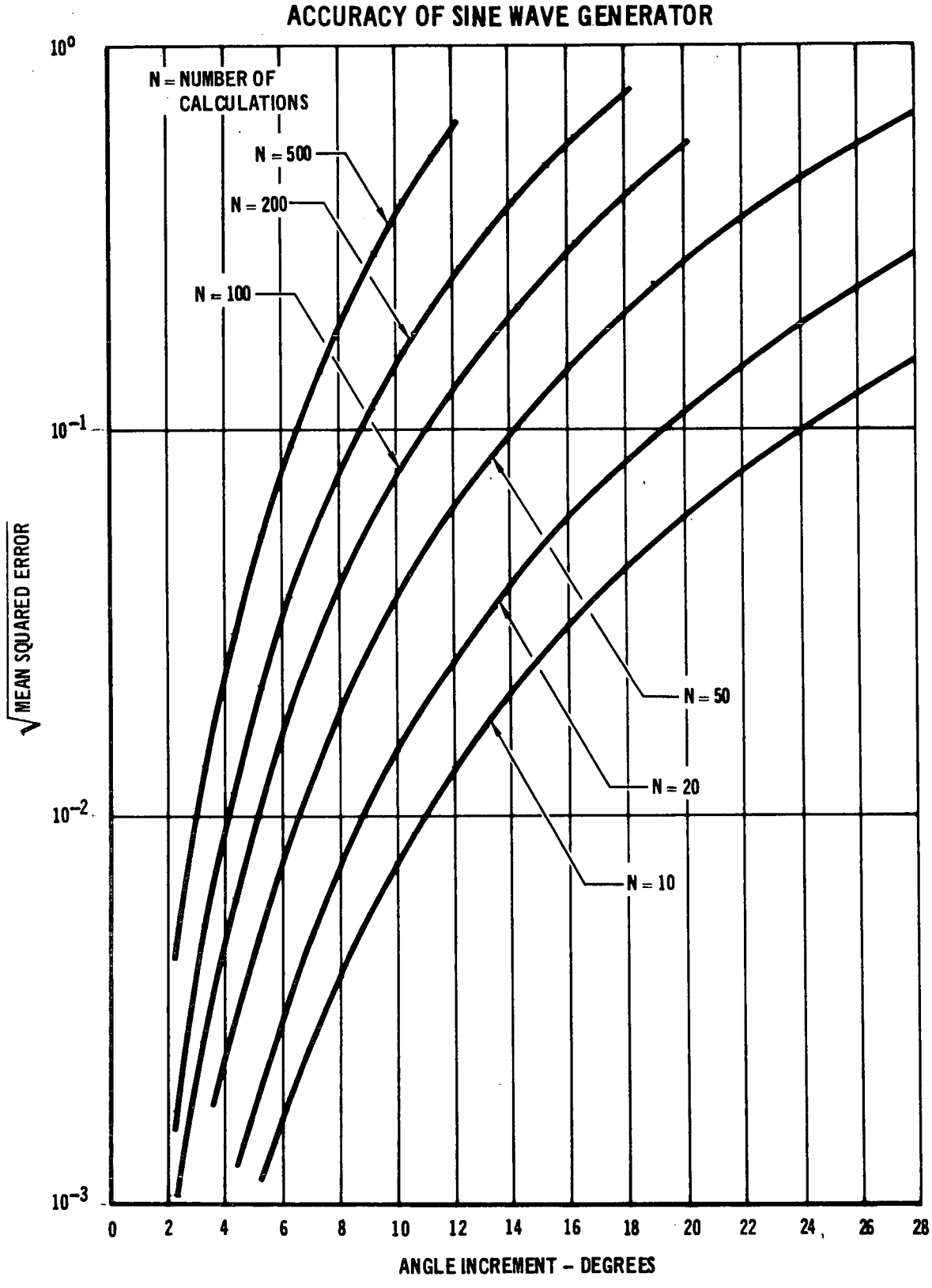
ACCURACY OF SINE WAVE GENERATOR
N = NUMBER OF CALCULATIONS
N = 500
N = 200
N = 100
N = 50
N = 20
N = 10
10^0
10^{-1}
10^{-2}
10^{-3}
$\sqrt{\text{MEAN SQUARED ERROR}}$
0 2 4 6 8 10 12 14 16 18 20 22 24 26 28
ANGLE INCREMENT – DEGREES

FIGURE 11

2.3 Comparison of Techniques

In this section the five selected numerical techniques are compared on the basis of accuracy and speed for two linear second order filters and a phase-locked loop with various inputs. The second order filter and phase-locked loop were chosen because they represent a typical linear and non-linear subsystem component. The analog linear filter output can easily be calculated and thus the error of the discrete filter measured.

2.3.1 Non-Linear Phase-Locked Loop

As a first step in comparing the five numerical methods described in Sections 2.1 and 2.2, we determined the central processor time required for one iteration of each of the candidate techniques using the standard machine subroutine for sin and cos. These times, which apply to our CDC 6400 computer, are given below.

Euler	240.3 μsec
Tustin	273.7 μsec
Anderson, Ball, Voss	273.7 μsec
Z-Transform	311.9 μsec
Runge-Kutta	1334.0 μsec

We also determined the mean-squared error between the output of a continuous loop and the digitized implementation for both ramp and step inputs. The ramp input signal was started at a sample point, while the step input was begun at a point halfway between the sample points. The results of this comparison are given in Figures 12 and 13. These curves indicate that Tustin's Method and the Anderson, Ball, Voss Method, two techniques which normally give high accuracy, show results considerably below the other candidate approaches. The reason is that a unit delay must be added in the feedback path because of the non-linearity associated with the phase-locked loop. In Section 2.3.2, the above techniques are compared for two linear filters, and the increased accuracy of Tustin's Method and the ABV Method is evident.

COMPARISON OF NUMERICAL METHODS FOR A RAMP INPUT

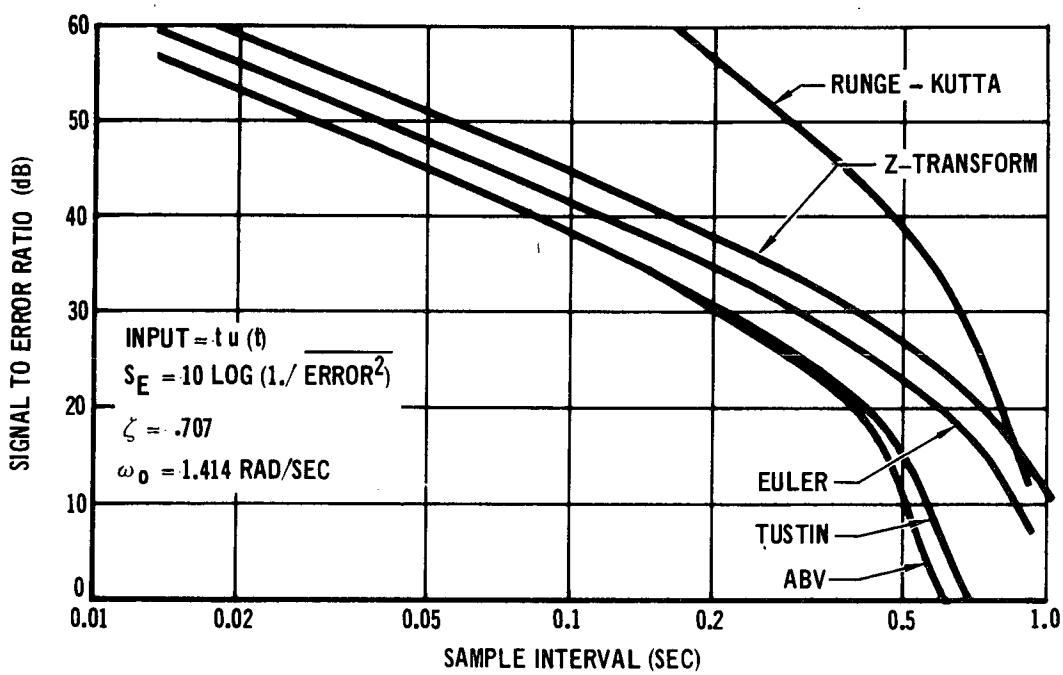

FIGURE 12

COMPARISON OF NUMERICAL METHODS FOR A STEP INPUT

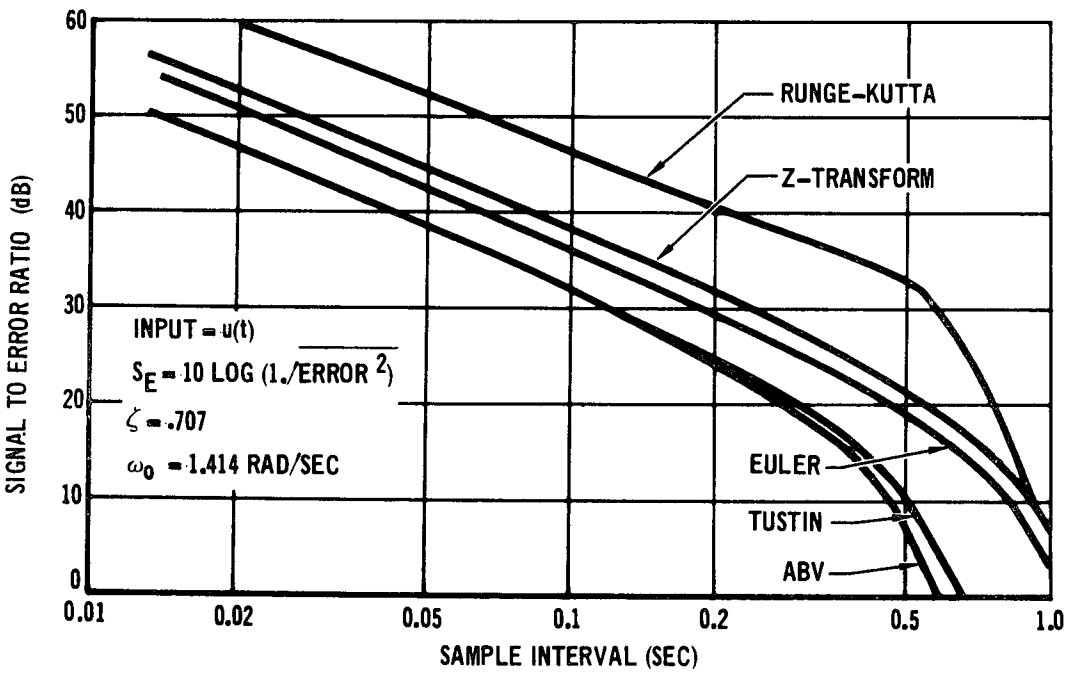

FIGURE 13

The complexity of the candidate techniques was assessed by drawing block diagrams, using the unit delay element, showing how the different methods can be implemented. Diagrams for Euler's Method and the Z-Transform Method were given previously in Figures 8 and 9. A block diagram showing the implementation of Tustin's Method and the ABV Method is given in Figure 14. One diagram suffices for these two techniques since they differ only by the value of the constants.

The numerical techniques described above were then compared using the preceding information on accuracy, complexity, and speed as the criteria of goodness. The Runge-Kutta Method was immediately discarded because of its complexity and slowness. Tustin's Method and the ABV Method were discarded because of low accuracy. This leaves the Z-Transform Method and Euler's Method, two techniques which give very similar performance as is evidenced by the preceding results. A more quantitative indication of this fact can be obtained by determining the central processor times (per .2 second interval) for a constant value of error. The Z-Transform technique with a sample time of 1/5 the loop time constant was chosen as a reference. This choice was made because 1/5 the loop time constant is a near optimum sample time for the phase-locked loop as will be shown in the next section, and also because this point is on the linear portion of Figure 12 and 13. The results are given below for both the step and ramp input. Note that for a fixed error the Z-Transform requires a slightly greater central processor usage than Euler's Method for a step input and slightly less usage for a ramp input.

Ramp Input

Z-Transform = 311.9 μsec

Euler = 331.5 μsec

Step Input

Z-Transform = 311.9 μsec

Euler = 292.3 μsec

MECHANIZATION OF THE ABV METHOD AND TUSTIN'S METHOD

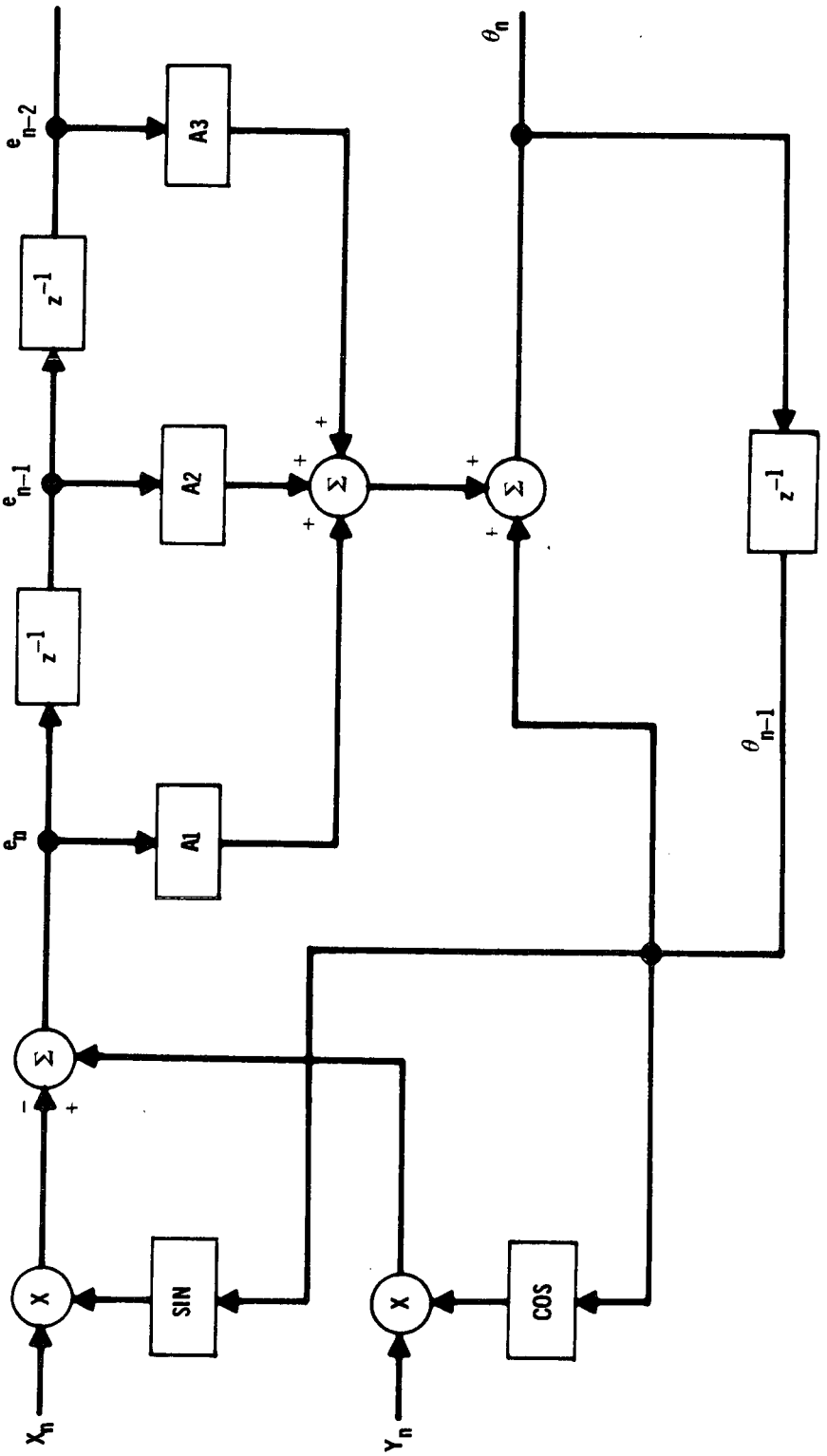

$$\theta_n = 2\theta_n - \theta_{n-2} + A_1 e_n + A_2 e_{n-1} + A_3 e_{n-2}$$

FIGURE 14

A more complete comparison of the numerical techniques is given in Figures 15 and 16 where the signal to error ratio is plotted versus the ratio of sample time to computation time. The above results indicate the near equality between the techniques in terms of speed and accuracy. Since Euler's Method is slightly easier to implement than the Z-Transform Method (the former technique requires three unit delay elements whereas the latter necessitates four), Euler's technique was selected and is used to determine the simulation results given in subsequent sections.

2.3.2 Linear Filters

We also applied the five numerical techniques described above to the two second order filters given in Equations (52) and (53).

$$H_2(s) = \frac{2\zeta\omega_0 s + \omega_0^2}{s^2 + 2\zeta\omega_0 s + \omega_0^2} \qquad (52)$$

$$H_1(s) = \frac{\omega_0^2}{s^2 + 2\zeta\omega_0 s + \omega_0^2} \qquad (53)$$

The difference equations for each of the numerical techniques is derived in Appendix II for $H_1(S)$ and $H_2(S)$. Utilizing these formulas, the central processor time for the CDC 6400 computer was determined for each of the methods and is given below.

Euler	35.0 μsec	
Z-Transform	50.9 μsec	
Tustin	62.9 μsec	
ABV	62.9 μsec	
Runge Kutta	214.5 μsec	$[H_2(s)]$
	274.1 μsec	$[H_1(s)]$

COMPARING NUMERICAL METHODS FOR RAMP INPUT AS A FUNCTION OF COMPUTATION TIME

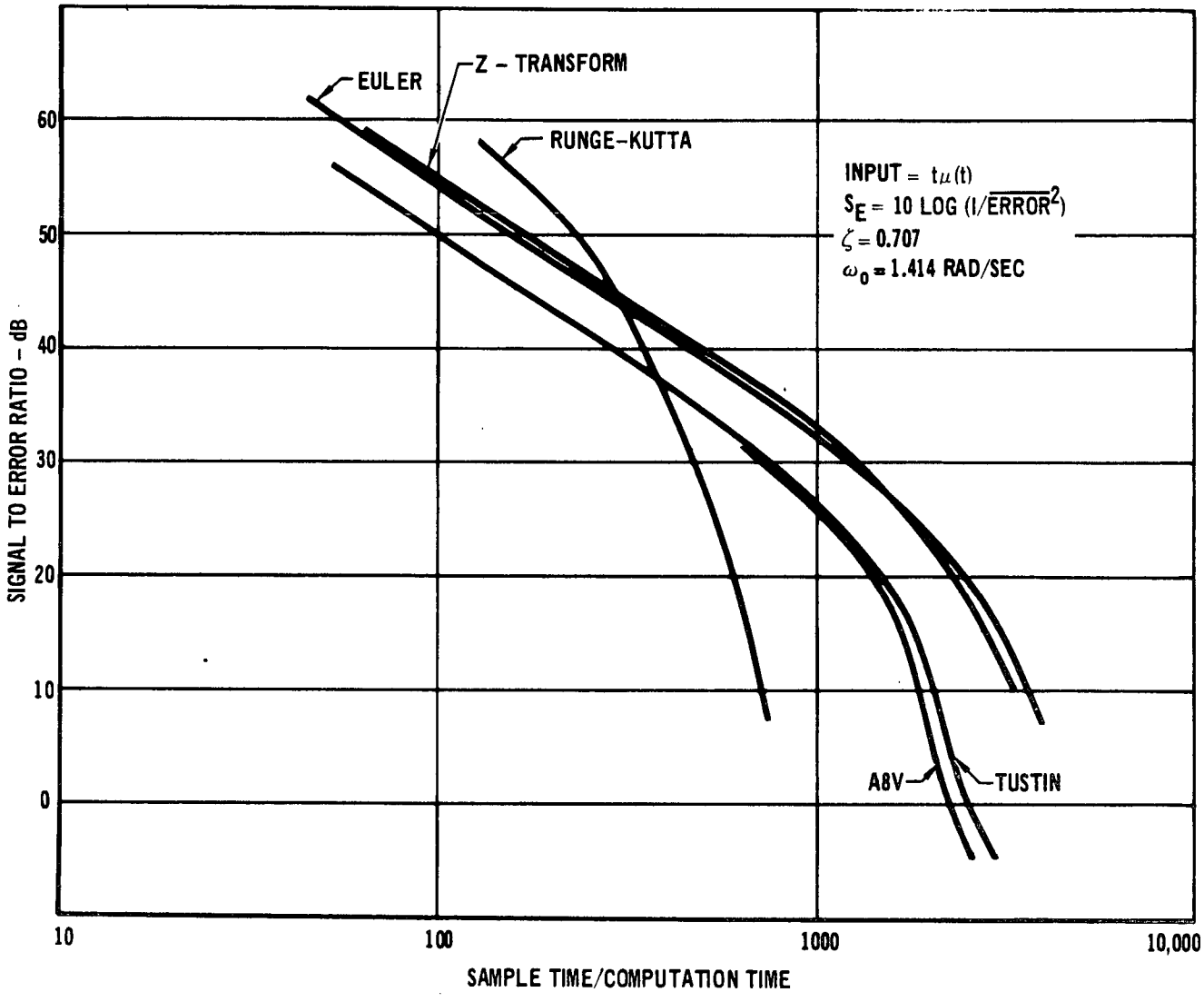

FIGURE 15

COMPARING NUMERICAL METHODS FOR STEP INPUT AS A FUNCTION OF COMPUTATION TIME

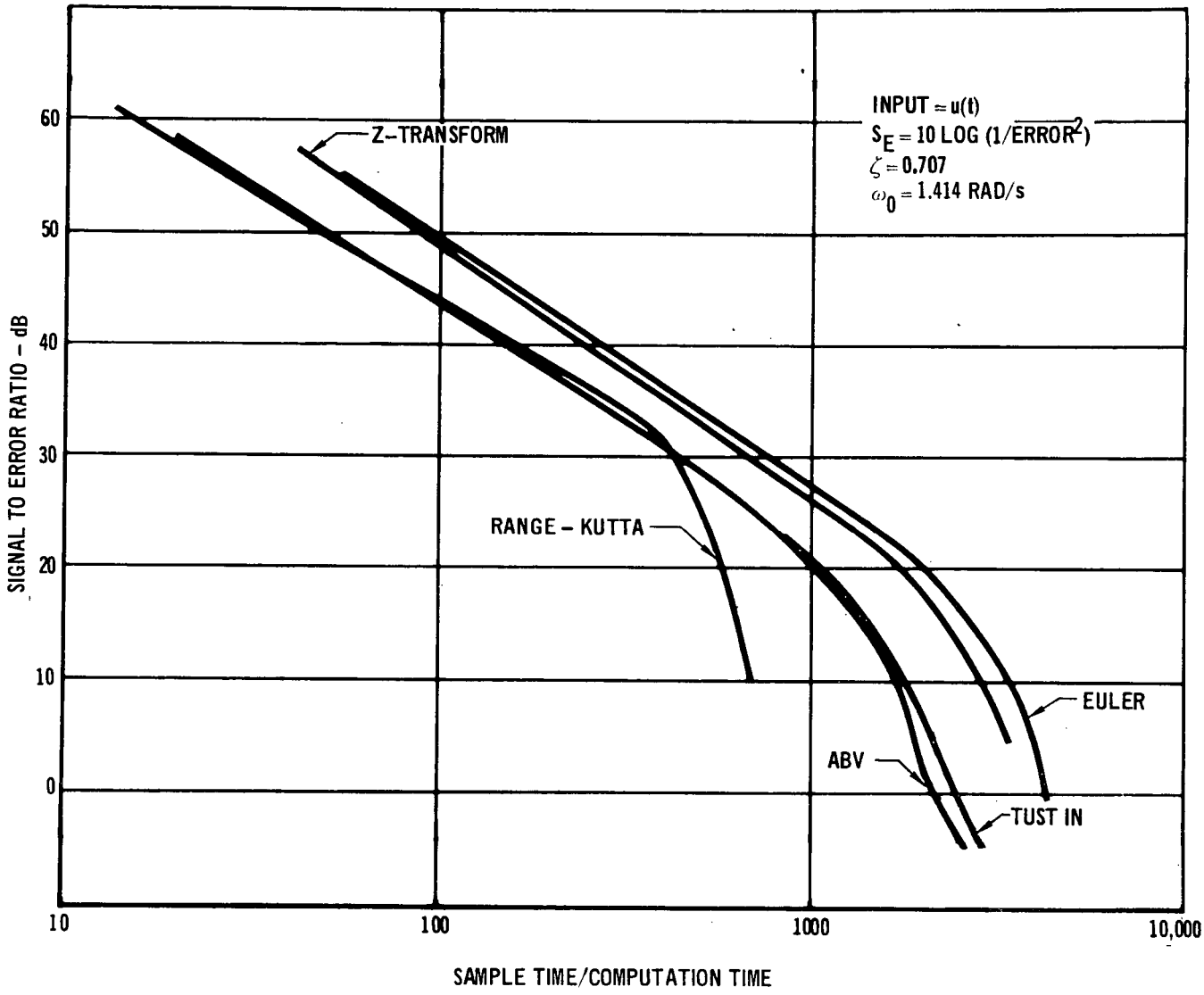

FIGURE 16

We also determined the mean-squared error between the output of the continuous filter and its digitized equivalent for ramp and step sine wave inputs, where the step occurred at a sample point. Since the filter is linear, the output of the continuous filter with the above inputs was calculated. Graphs showing the signal to error ratio versus sampling rate for the two filters are shown in Figures 17 and 18. Thus for a linear system Anderson, Ball, Voss Method is significantly better than Euler's Method due to greater accuracy. However, the non-linearity in the phase lock loop makes Anderson, Ball, Voss unappropriate for our application.

COMPARISON OF NUMERICAL TECHNIQUES FOR LINEAR FILTER WITH RAMP INPUT

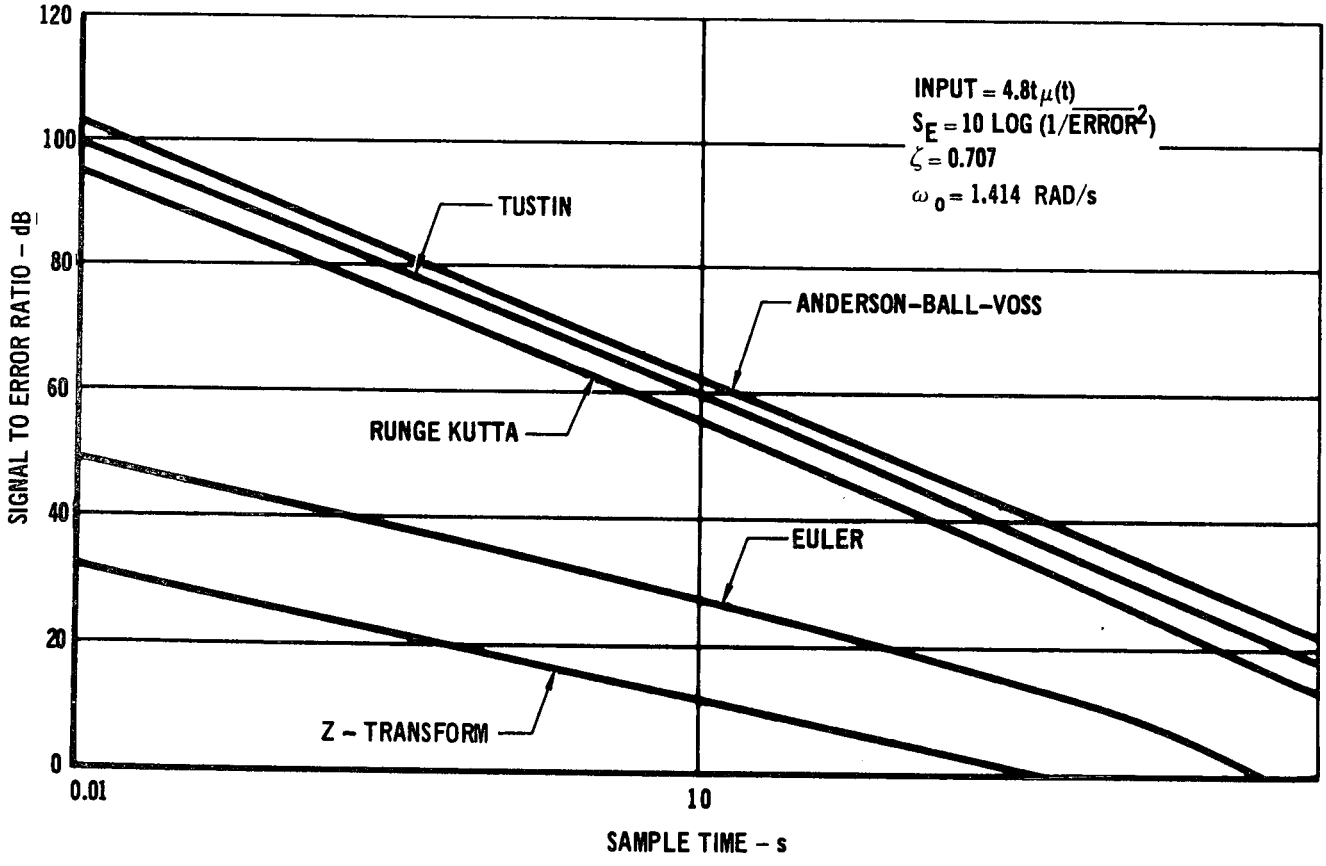

FIGURE 17

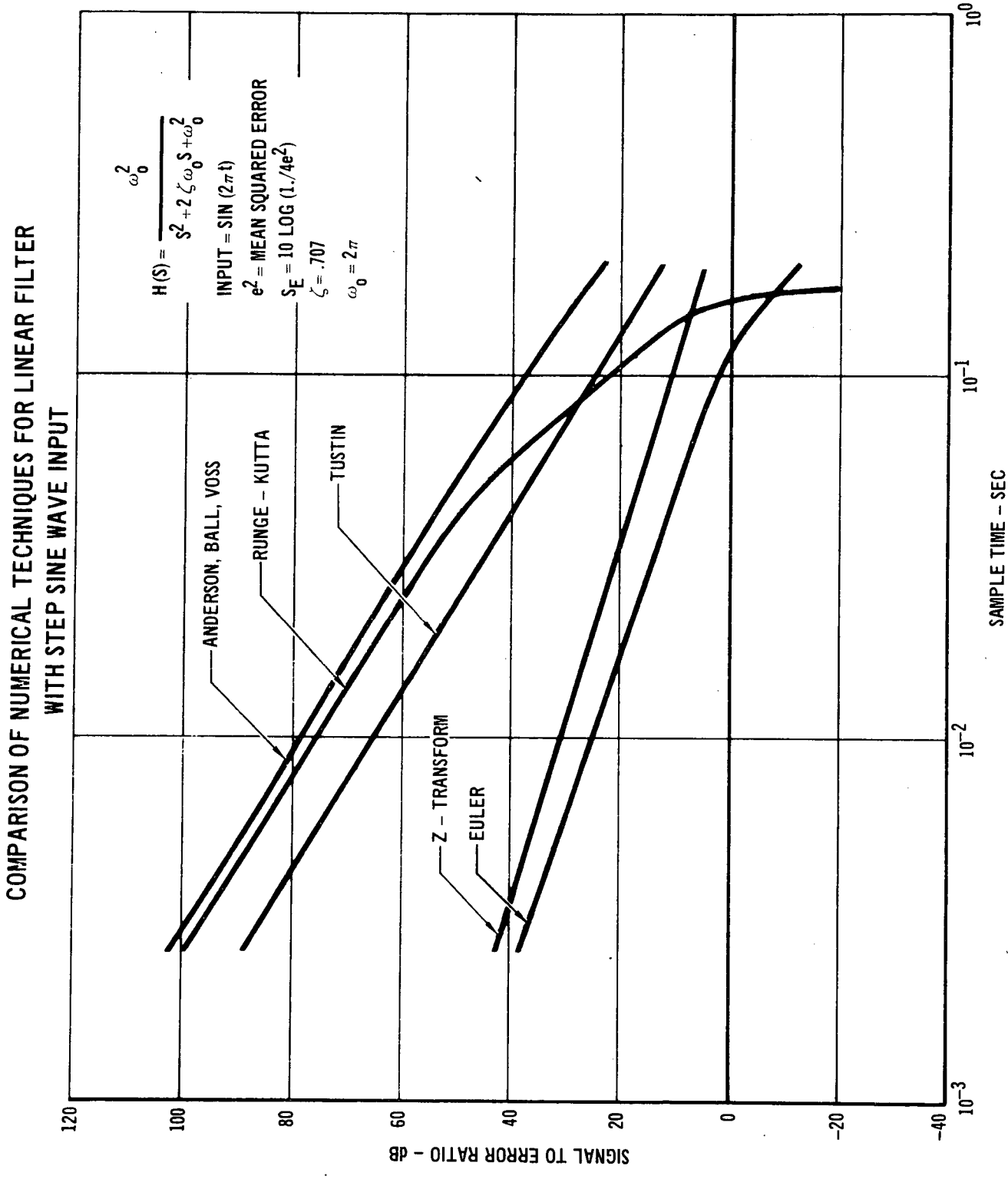
COMPARISON OF NUMERICAL TECHNIQUES FOR LINEAR FILTER
WITH STEP SINE WAVE INPUT
$H(S) = \frac{\omega_0^2}{S^2 + 2\zeta\omega_0 S + \omega_0^2}$
INPUT = SIN (2πt)
e^2 = MEAN SQUARED ERROR
S_E = 10 LOG (1./4e^2)
ζ = .707
$\omega_0 = 2\pi$
ANDERSON, BALL, VOSS
RUNGE – KUTTA
TUSTIN
Z – TRANSFORM
EULER
SIGNAL TO ERROR RATIO – dB
120
100
80
60
40
20
0
-20
-40
10^0
10^{-1}
10^{-2}
10^{-3}
SAMPLE TIME – SEC

FIGURE 18

2.4 Determination of System Constraints

The effect of sampling rate, quantization noise, and dynamic range on digital phase-locked loop performance is determined in this section.

2.4.1 Sampling Rate

The necessary sampling rate depends on the numerical technique being used, the bandwidth of the phase-locked loop, and the offset frequency at the input to the loop. Since Euler's Method has already been selected as the numerical method, only the latter two effects will be considered here. The effect of sampling rate was determined by measuring phase variance versus sample interval for a fixed input noise spectral density using an all digital simulation. The input noise was generated using a Gaussian random number generator. It was assumed for all digital simulations in Section 2 of this study that the quadrature components were prefiltered with an integrate and dump filters. The resulting curve, Figure 19, shows that for the phase-locked loop being considered ($\zeta = 0.707$ and $\omega_o = 1.414$ rad/sec) the sample interval must be less than 70% of the loop time constant to keep the loop from going unstable. We also determined a graph of phase variance versus $\frac{(N_o B_n)}{A^2}$, the loop signal-to-noise ratio, as a function of the sampling rate using an all digital simulation. This graph, which is shown in Figure 20, indicates that a serious degradation occurs for sample intervals between 20% and 40% of the loop time constant. Therefore, a sampling interval of 20% of the loop time constant represents a nearly optimum selection for the case of no offset frequency since this value is well below the point of instability and also allows the digital phase-locked loop to operate at a point where its transient performance approaches that of the continuous analog loop. We next determined the effect of an offset frequency on the sampling rate requirements. This was accomplished by computing the mean squared value of the difference between the continuous loop output and the

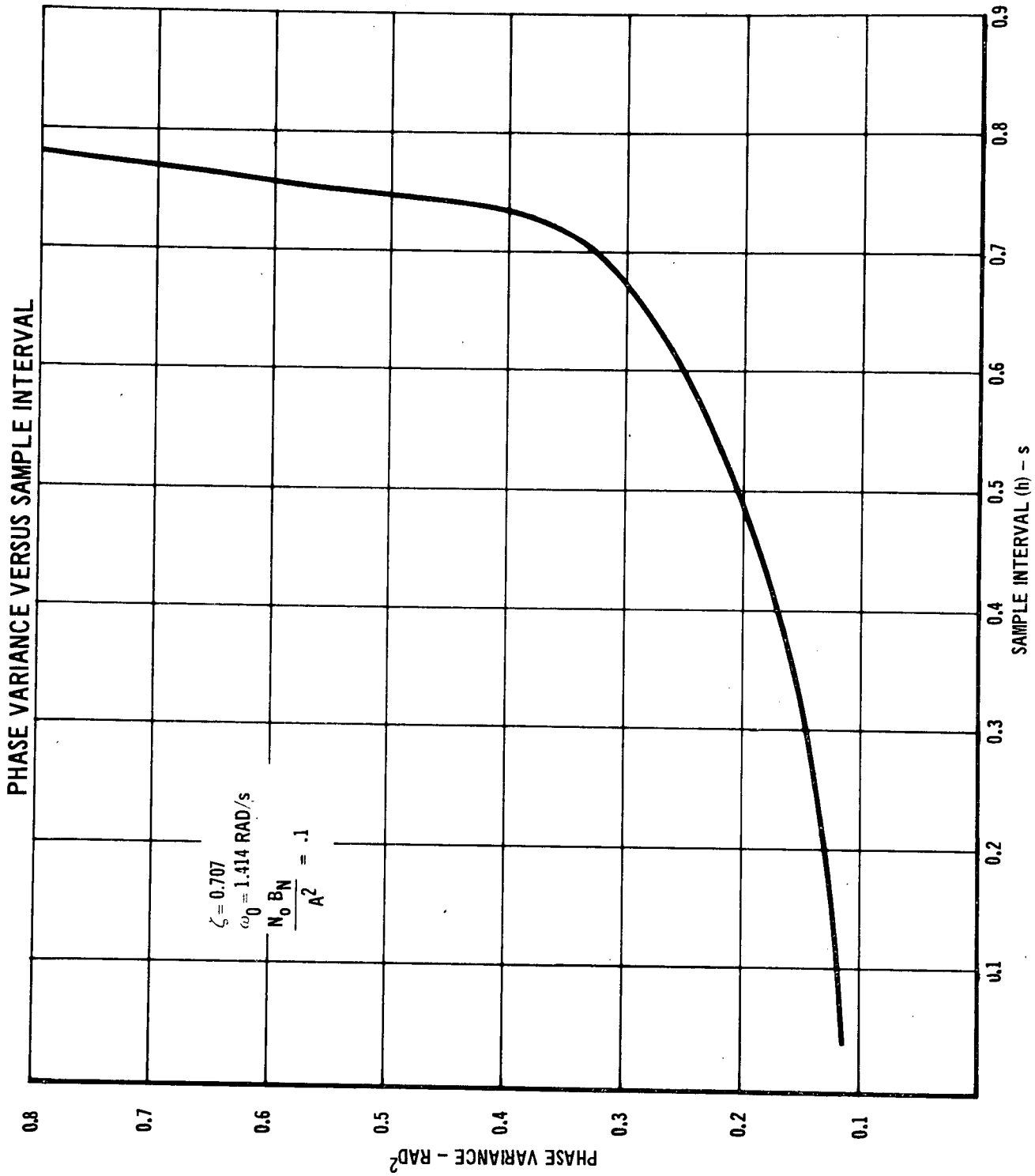
PHASE VARIANCE VERSUS SAMPLE INTERVAL
$\zeta = 0.707$
$\omega_0 = 1.414$ RAD/s
$\frac{N_0 B_N}{A^2} = .1$
PHASE VARIANCE – RAD²
0.8
0.7
0.6
0.5
0.4
0.3
0.2
0.1
SAMPLE INTERVAL (h) – s
0.9
0.8
0.7
0.6
0.5
0.4
0.3
0.2
0.1

FIGURE 19

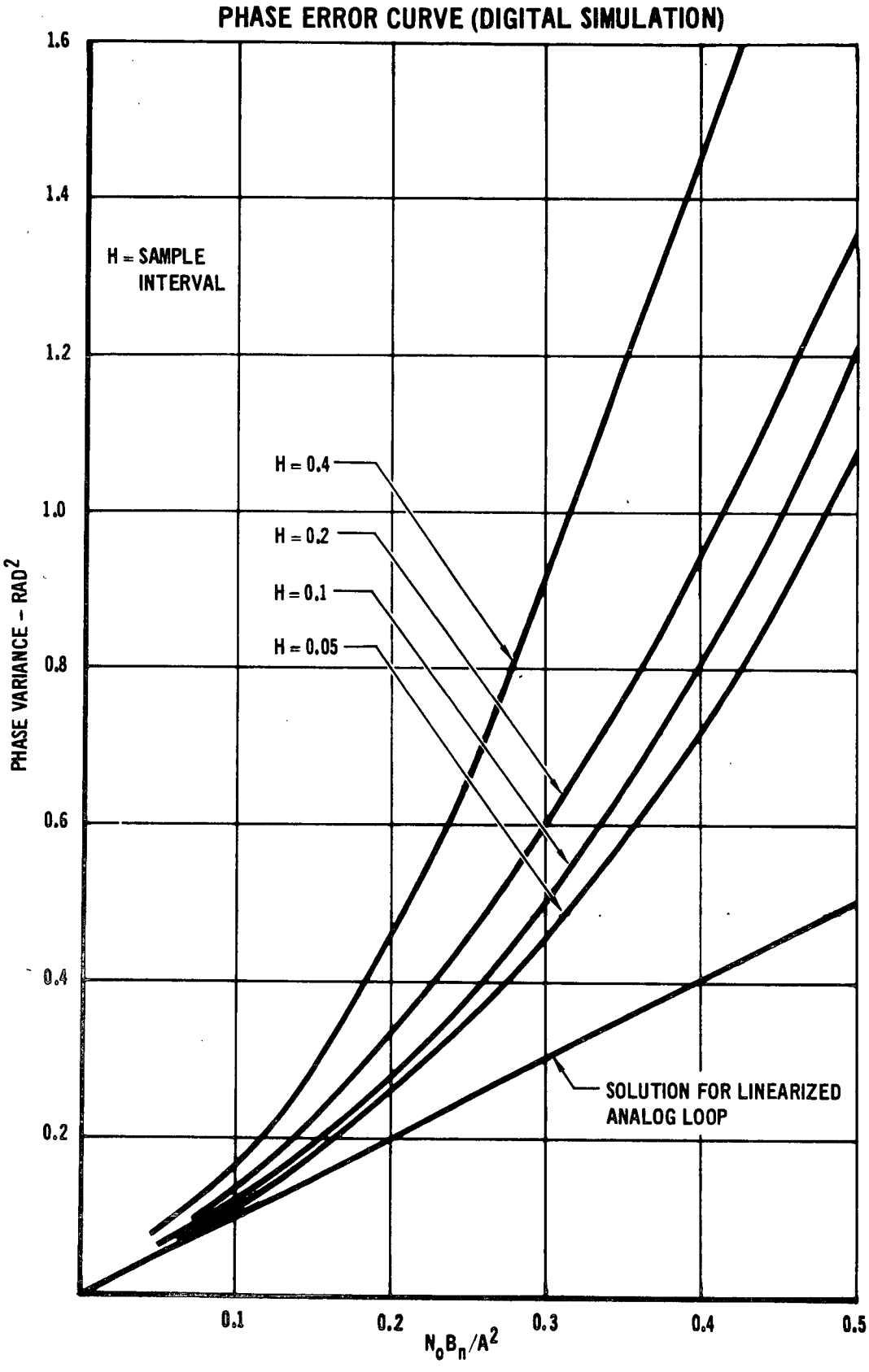
PHASE ERROR CURVE (DIGITAL SIMULATION)
1.6
1.4
1.2
1.0
0.8
0.6
0.4
0.2
PHASE VARIANCE - RAD^2
H = SAMPLE INTERVAL
H = 0.4
H = 0.2
H = 0.1
H = 0.05
SOLUTION FOR LINEARIZED ANALOG LOOP
0.1
0.2
0.3
0.4
0.5
N_0B_n/A^2

FIGURE 20

digitized loop for different frequency offsets. A graph showing the error versus the offset frequency for two different sampling rates is given in Figure 21. This curve shows that decreasing the sampling interval from 20% to 10% of the loop time constant does not increase the accuracy significantly and also does not allow operation at a much higher offset frequency. Therefore, if the offset frequency is within the bandwidth of the loop, a sampling interval of 20% of the loop time constant gives adequate results. For frequency offsets much greater than the loop bandwidth, the sampling rate is dependent on both the input filter and the frequency of the offset. This dependency will be given more attention in the section on input filters.

2.4.2 Quantization

In order to determine the effect of quantization on the operation of the phase-locked loop, we analytically determined the phase error variance as a function of the number of quantization levels. If the quantization error is assumed to be uniform, the noise variance caused by this error is given by the following formula.

$$\sigma_Q^2 = \frac{a^2}{12} \tag{54}$$

$$a = \frac{V_p}{L} \tag{55}$$

V_p = peak voltage

L = number of positive quantization levels

If it is assumed that adjacent samples of the quantization noise are independent, the phase variance at the output of the linearized phase-locked loop can be determined as shown below. It is also assumed that the noise samples are held for one sample interval.

$$\sigma_\phi^2 = \frac{N_o B_n}{A^2} \tag{56}$$

N_o = Spectral density of quantization noise

$$N_o = 2\,\sigma_Q^2\, h$$

MEAN SQUARED ERROR VERSUS OFFSET FREQUENCY FOR DIFFERENT SAMPLE INTERVALS

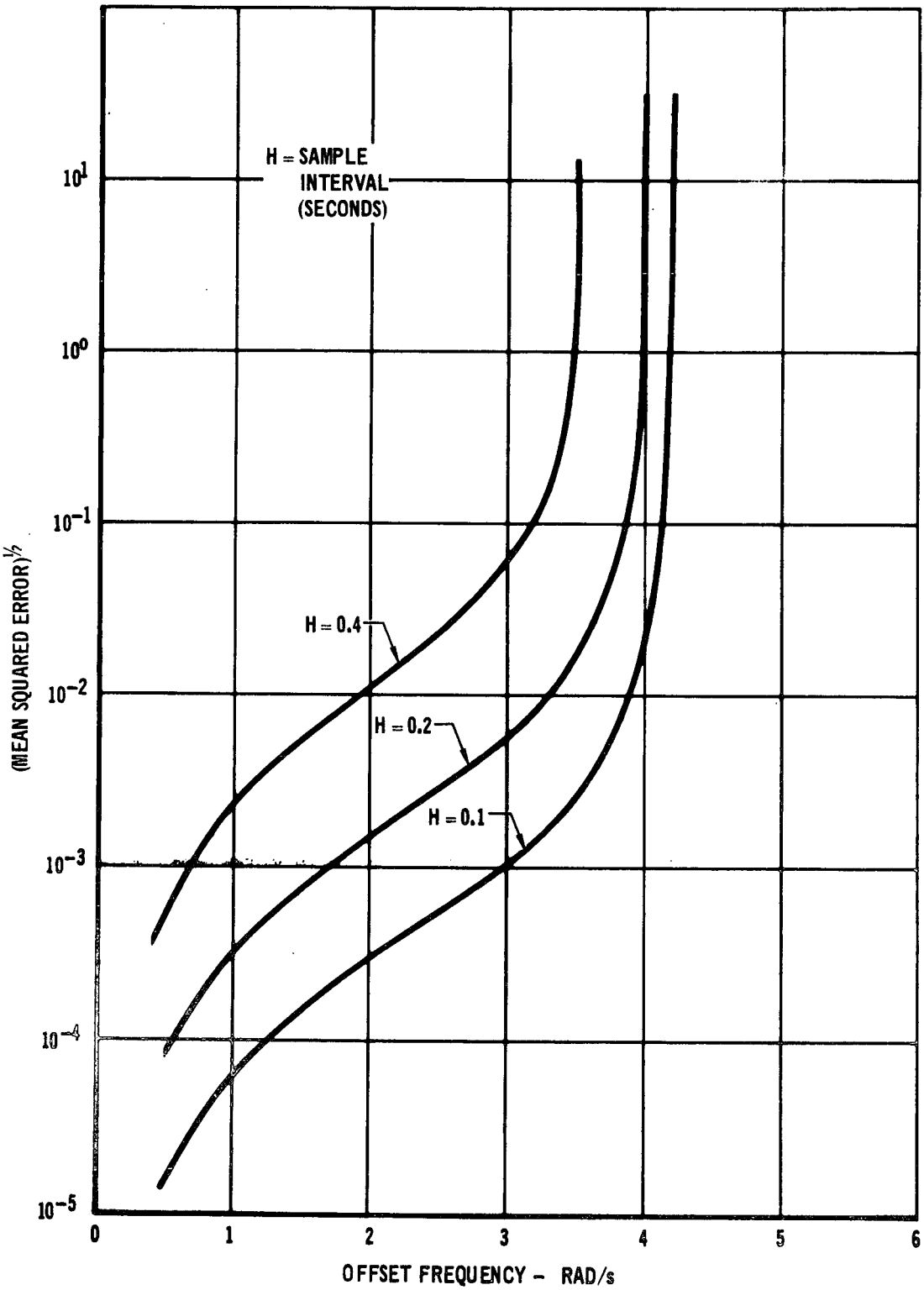

FIGURE 21

h = sample interval

A = amplitude of input sine wave

B_n = noise bandwidth of PLL

$$\sigma^2 = \frac{V_p^2 \, h \, B_n}{6 \, A^2 L^2} \qquad (57)$$

The phase variance was also determined using a digital simulation to check the analytical results. In order to get worst case results the offset frequency of the input sine wave was made small (.1 rad/sec). For low offset frequencies adjacent samples of quantization noise are no longer independent causing the loop to be less effective in filtering out quantization noise. A graph of phase variance versus the number of quantization levels for both the theoretical and the digital simulation results is shown in Figure 22. As the number of levels is increased, adjacent samples of quantization noise become more decorrelated and the two curves approach each other. The interaction between thermal noise and quantization noise was investigated using a digital simulation to determine the output phase variance as a function of the number of quantization levels for different values of the output signal-to-noise ratio ($\frac{A^2}{2N_o B_n}$). This graph, which is given in Figure 23, shows that the output phase variance is approximately independent of the number of quantization levels if the number of levels is greater than 16. Figure 23 shows that for 16 or more levels the standard deviation of the phase output is less than 1 degree for a wide range of signal-to-noise ratios. A phase error of this value in a PSK system would cause less than a 2×10^{-3} dB reduction in the effective output signal-to-noise ratio.

2.4.3 Scale Factor

Another important system constraint is the dynamic range of the A/D converter which precedes the digital computer. If the signal amplitude is greater than the dynamic range of the converter, signal energy will be lost resulting in a lower effective

STANDARD DEVIATION OF PHASE OUTPUT VERSUS THE NUMBER OF QUANTIZATION LEVELS

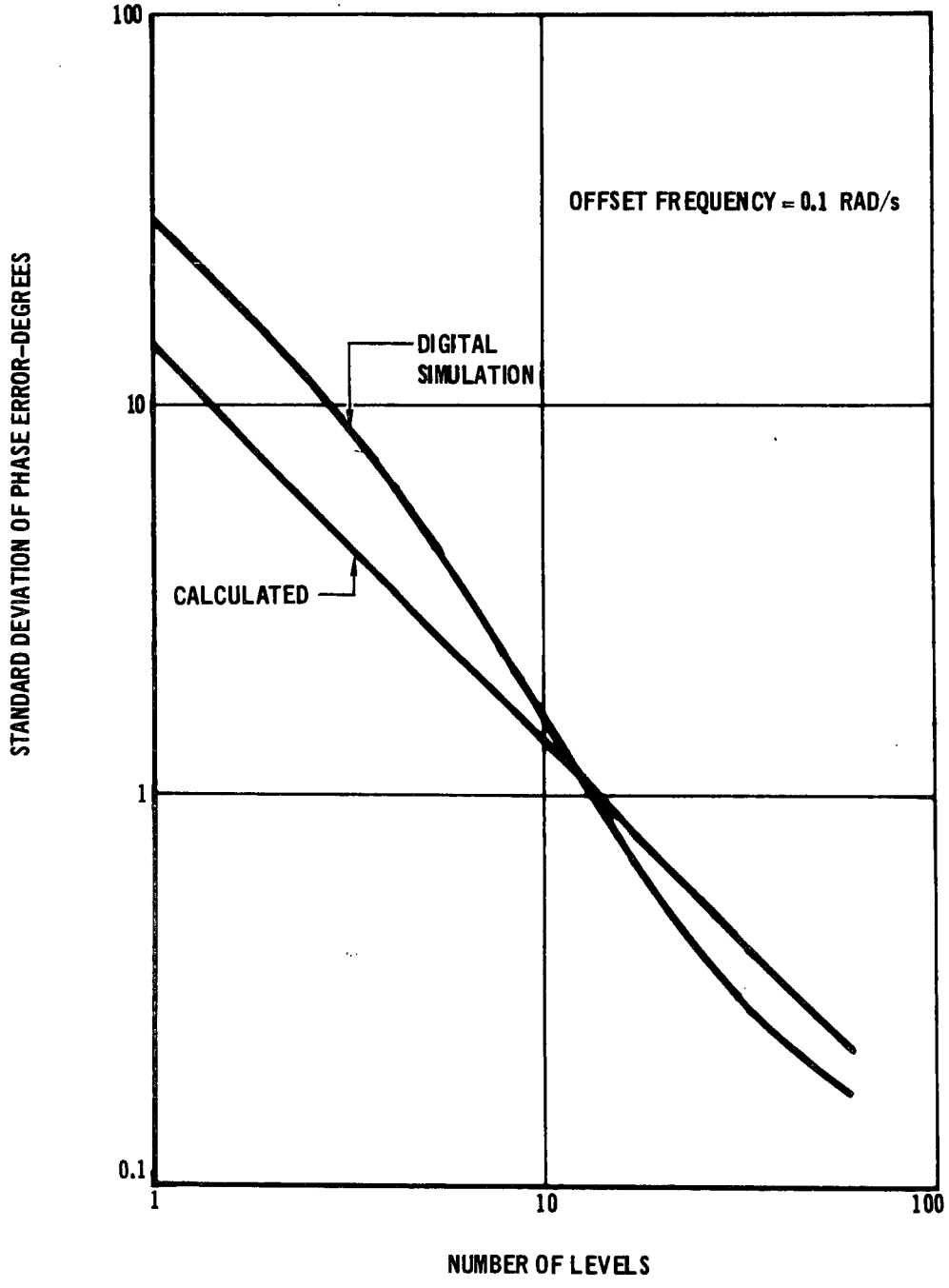

FIGURE 22

PHASE ERROR VARIANCE VERSUS THE NUMBER OF QUANTIZATION LEVELS

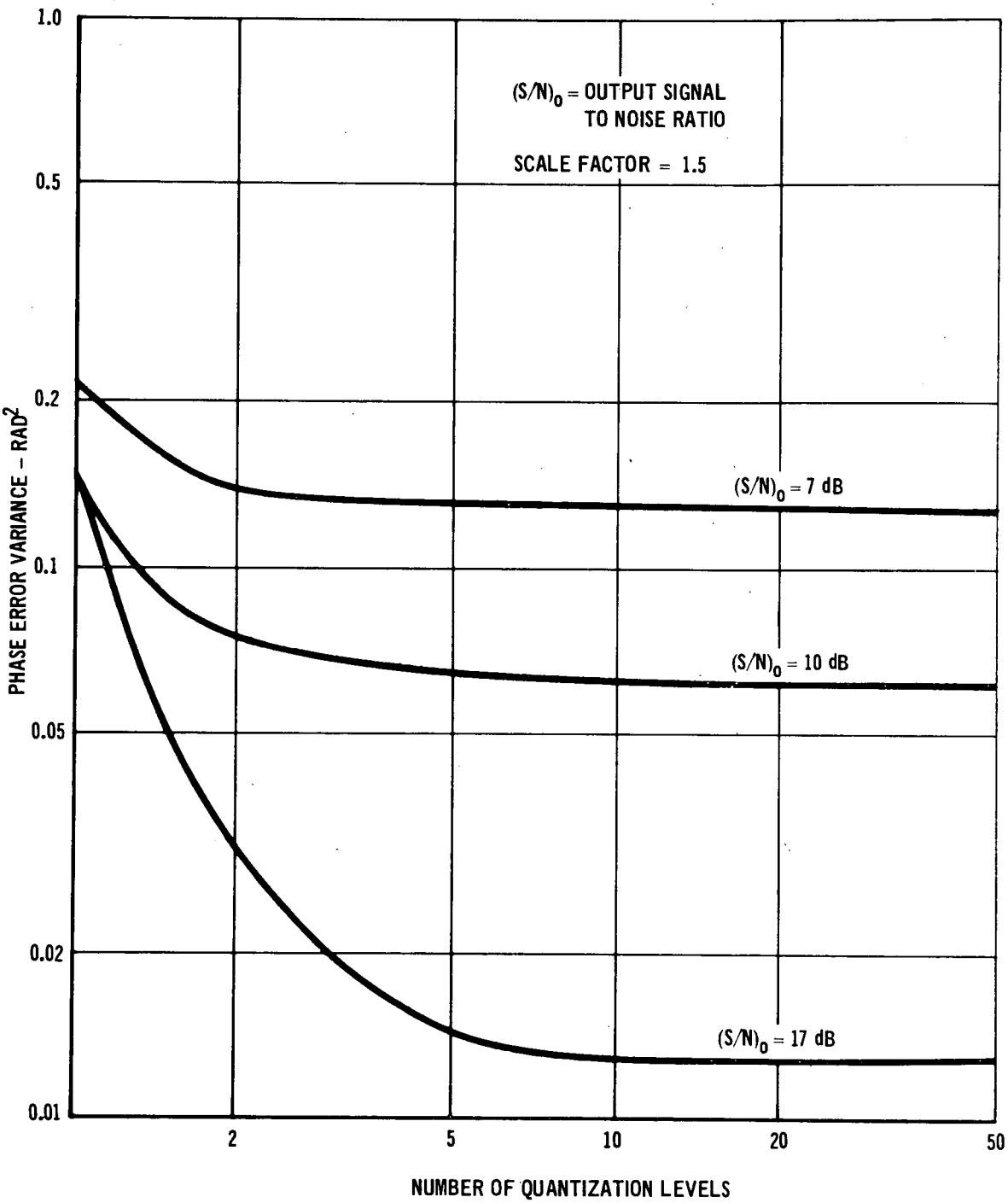

FIGURE 23

input signal-to-noise ratio. If the dynamic range is made much greater than the signal amplitude, the quantization noise will be increased because of the increased size of the quantization interval. Therefore, the dynamic range of the converter should be set somewhere between the above extremes. We determined the output phase variance as a function of the number of quantization intervals for several different dynamic range settings. These results showed that the output phase variance was independent of the dynamic range if it was greater than ($A = 3\sigma$), where A was the input sine wave amplitude, and σ is the input noise variance. A graph of the output phase variance versus the number of quantization levels as a function of the output signal-to-noise ratio and the dynamic range of the A/D converter is shown in Figure 24. This curve shows that the phase variance is reduced for a low number of quantization intervals as the dynamic range approaches the input singal amplitude. Our results indicate that a dynamic range of ($A + 2\sigma$) is a good compromise value.

SCALE FACTOR DETERMINATION

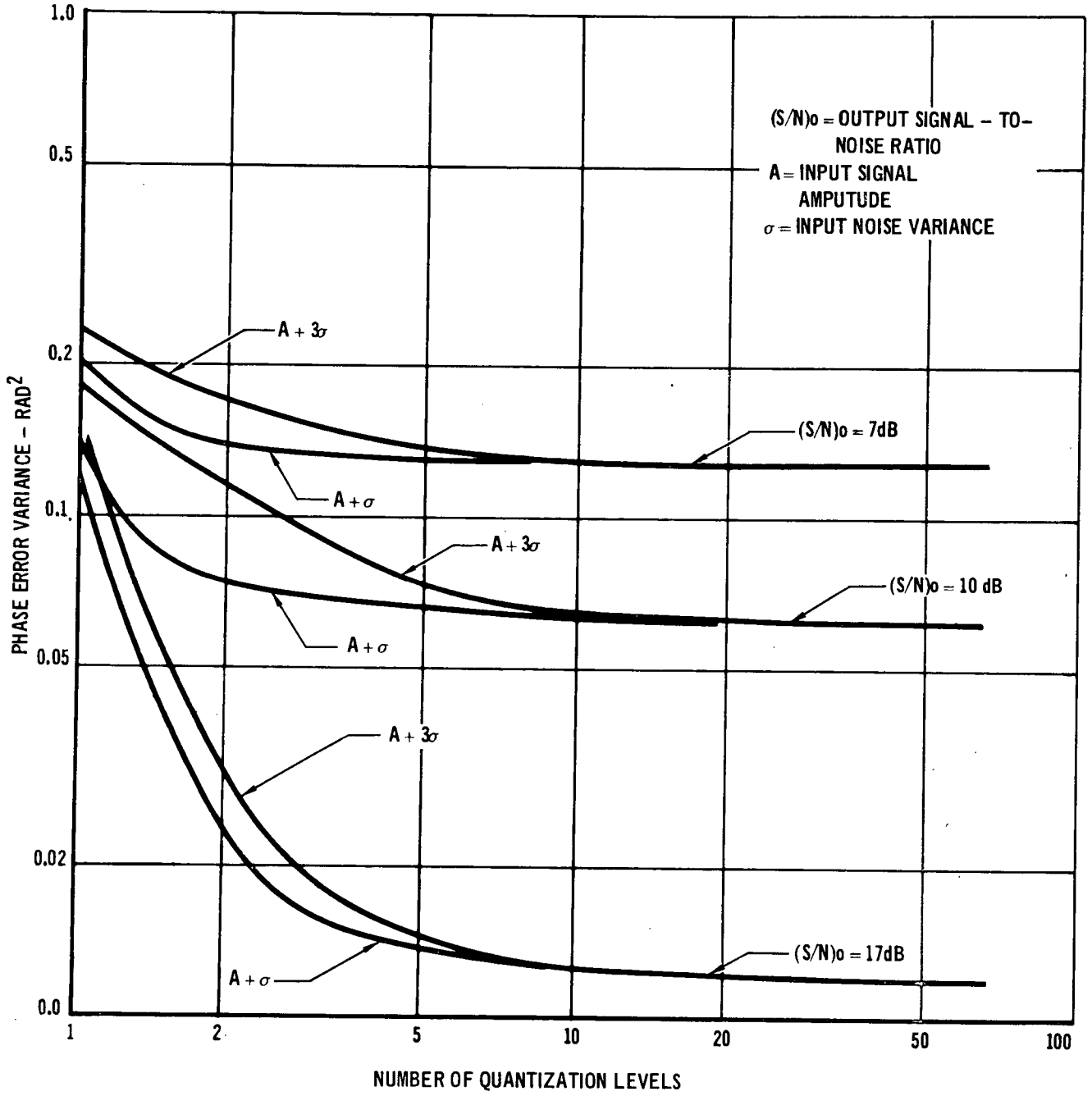

FIGURE 24

2.5 Automatic Gain Control (AGC)

Two AGC techniques were investigated. The first approach consisted of placing a bandpass limiter at the input to the phase-locked loop. We also investigated a slight variation of this method, using a sawtooth comparator in combination with the bandpass limiter. The second technique considered was to use a closed loop AGC preceding the phase-locked loop. Both of these techniques are analyzed in Sections 2.5.1 and 2.5.2, and computer implementations are determined.

2.5.1 Bandpass Limiter

A block diagram of the phase-locked loop preceded by a bandpass limiter is given in Figure 25.

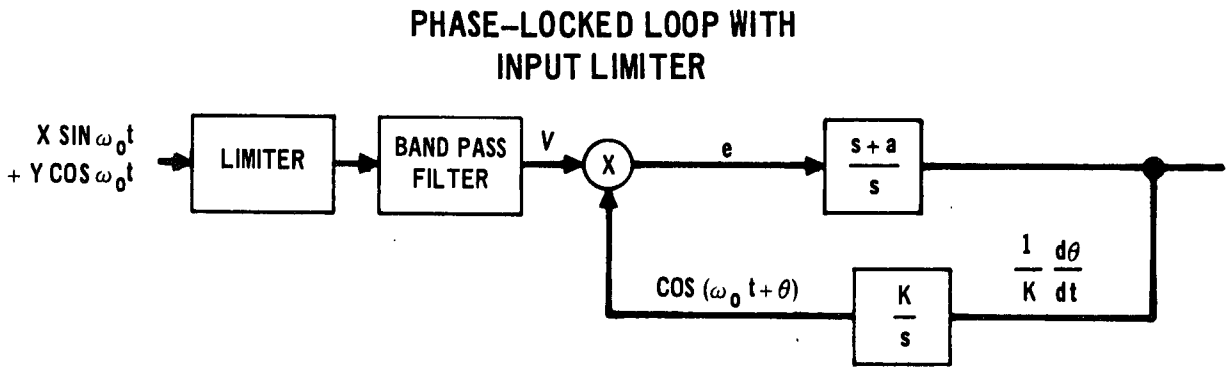

FIGURE 25

Assuming that the input signal is a narrow band process and that the higher harmonics will be removed by the bandpass filter following the limiter, the phase locked loop input will have the form given in Equation (58).

$$V = \sin\left(\omega_o t - \tan^{-1}\frac{Y}{X}\right) \tag{58}$$

The error signal at the input to the filter is given in Equations (59) and (60). It should be noted that the 1/2 factor resulting is omitted and considered part of the loop gain.

$$e = \sin\left(\tan^{-1}\frac{Y}{X} - \theta\right) \tag{59}$$

$$e = \frac{Y}{\sqrt{X^2 + Y^2}}\cos\theta - \frac{X}{\sqrt{X^2 + Y^2}}\sin\theta \tag{60}$$

The loop equation is then determined as shown in Equations (61) and (62).

$$\frac{d}{dt}\left(\frac{1}{K}\frac{d\theta}{dt}\right) = \left(\frac{d}{dt} + a\right)e \tag{61}$$

$$\frac{d^2\theta}{dt^2} = aKe + K\frac{de}{dt} \tag{62}$$

To avoid taking the derivative of the input signal, the above equation can be written as two first order equations by making the substitution $\frac{dc}{dt} = aKe$.

$$\frac{dc}{dt} = aK\left[\frac{Y}{\sqrt{X^2 + Y^2}}\cos\theta - \frac{X}{\sqrt{X^2 + Y^2}}\sin\theta\right] \tag{63}$$

$$\frac{d\theta}{dt} = c + K\frac{Y}{\sqrt{X^2 + Y^2}}\cos\theta - \frac{X}{\sqrt{X^2 + Y^2}}\sin\theta \tag{64}$$

Using Euler's Method, the difference equation for numerically solving the above equations will have the form given in Equations (65-67).

$$G = \frac{1}{\sqrt{X_{n-1}^2 + Y_{n-1}^2}}\left[Y_{n-1}\cos\theta_{n-1} - X_{n-1}\sin\theta_{n-1}\right] \tag{65}$$

$$\theta_n = \theta_{n-1} + hC_{n-1} + KhG \tag{66}$$

$$C_n = C_{n-1} + aKhG \tag{67}$$

Using the Equations (65-67), a Fortran computer program was written for Euler's method and is given below.

H = h = sample interval

AK = Kh

AA = a

T = phase output of loop

```
XXA = ADC(01)

YYA = ADC(02)

XNOR = SQRT(XXA**2 + YYA**2)

XA = XXA/XNOR

YA = YYA/XNOR

TEMP = AK*(YA*COS(T) - XA*SIN(T))

T = T + C*H + TEMP

C = C + AA* TEMP
```

A slight variation on the preceding technique consists of using a bandpass limiter preceding the phase-locked loop and a sawtooth comparator (inverse sine circuit) in front of the loop filter. The resulting block diagram is presented in Figure 26.

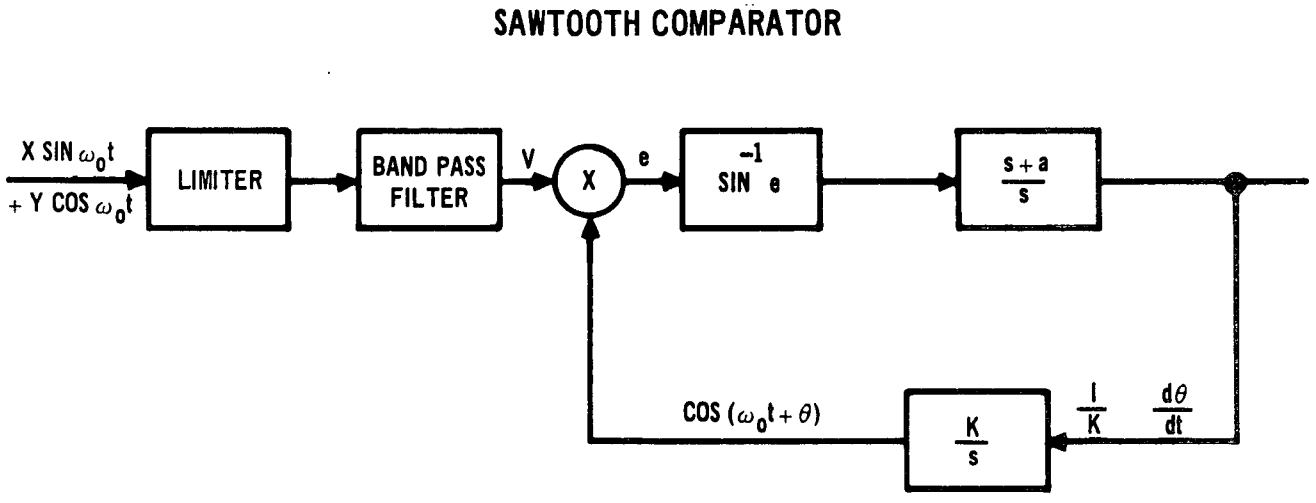

FIGURE 26

Using the same methods as were employed for the limiter, Equations (68) and (69) were derived.

$$\frac{dc}{dt} = aK\left(\tan^{-1}\frac{Y}{X} - \theta\right) \tag{68}$$

$$\frac{d\theta}{dt} = c + K\left(\tan^{-1}\frac{Y}{X} - \theta\right) \tag{69}$$

A Fortran computer implementation of this technique is given below.

```
H = h = sample interval

AK = Kh

AA = a

T = phase output of loop
XXA = ADC(01)

YYA = ADC(01)

ANG2 = ATAN2 (YYA, XXA)

ANG2 = ASIN (SIN(ANG2-T))

TEMP = AK*ANG2

T = T + C*H + TEMP

C = C + AA*TEMP
```

A curve showing the output phase variance as a function of the input noise spectral density for a phase-locked loop with, and without, a limiter is shown in Figure 27. This curve shows that as the input noise spectral density increases, the limiter reduces the gain of the loop, and as a result the output phase variance is reduced with respect to the loop with perfect AGC. A similar curve for the sawtooth comparator is shown in Figure 28. Since the sawtooth comparator exhibits more gain for large phase offsets than a loop with a sinusoidal comparator and a input limiter, the phase variance is greater for the sawtooth comparator configuration as low input signal-to-noise ratios. It should also be noted that the sawtooth comparator will track the input variations more effectively than the techniques described previously.

2.5.2 Closed Loop AGC

A block diagram for an analog configuration of a closed loop AGC is given in Figure 29.

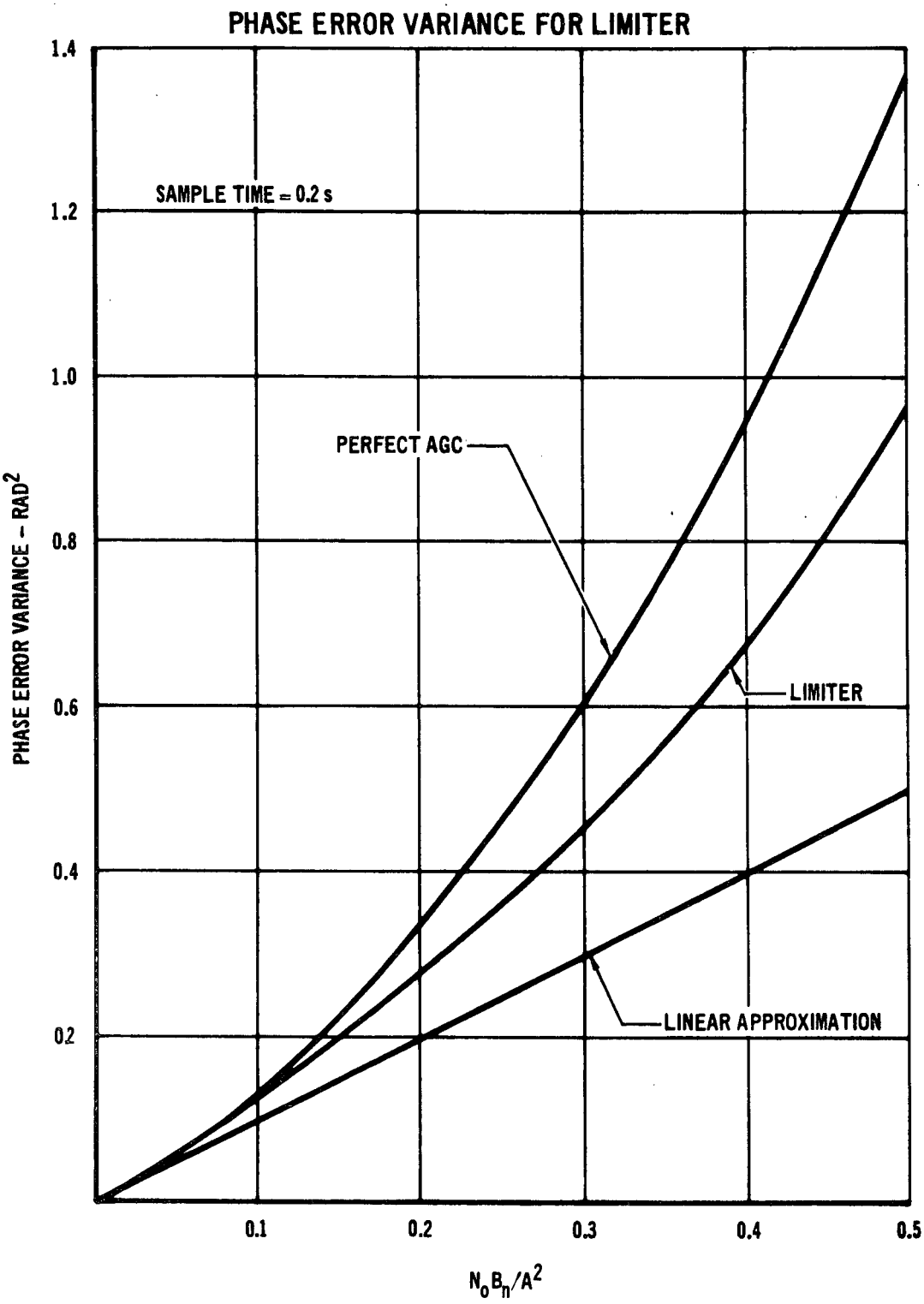
PHASE ERROR VARIANCE FOR LIMITER
SAMPLE TIME = 0.2 s
PERFECT AGC
LIMITER
LINEAR APPROXIMATION
PHASE ERROR VARIANCE - RAD^2
1.4
1.2
1.0
0.8
0.6
0.4
0.2
0.1
0.2
0.3
0.4
0.5
N_0B_n/A^2

FIGURE 27

PHASE ERROR VARIANCE FOR SAWTOOTH COMPARATOR

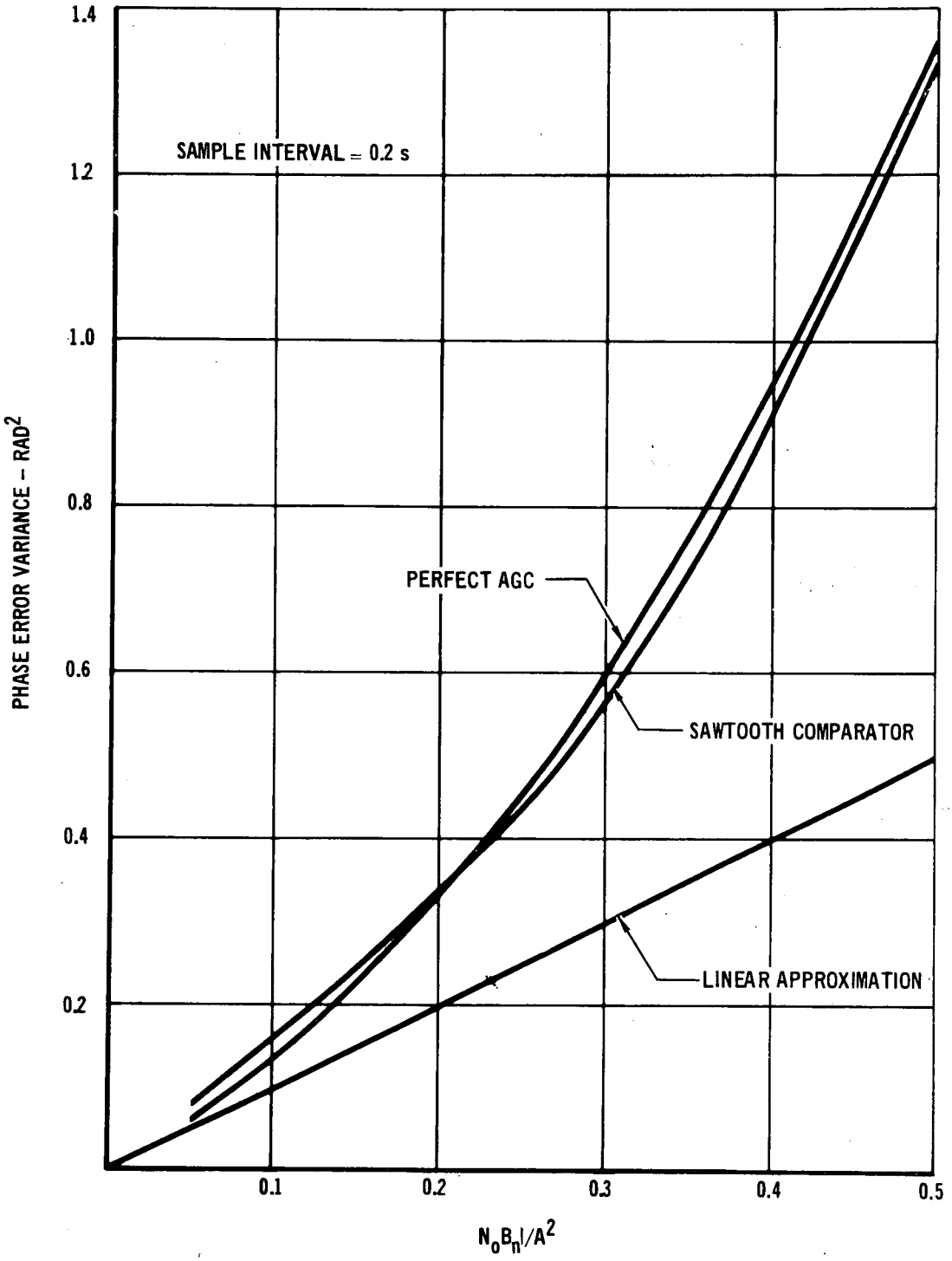

FIGURE 28

CLOSED LOOP ANALOG AGC

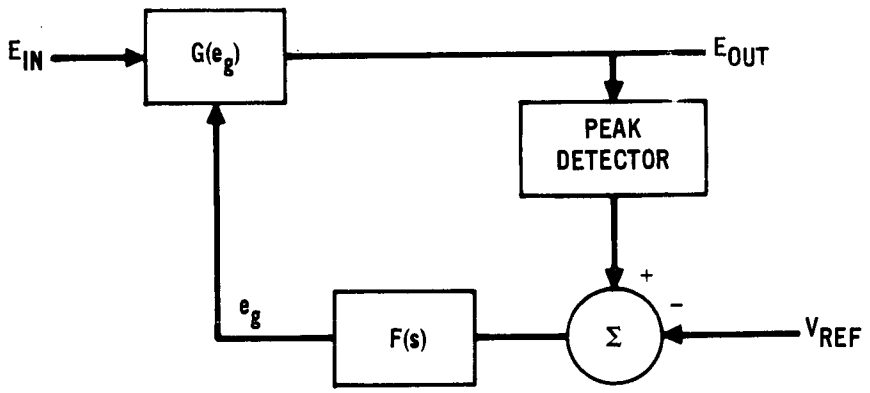

FIGURE 29

The incremental transfer function for this loop will have the form given in Equations (70) and (71) according to Povejsil, Raven, and Waterman.[3]

$$\frac{\Delta E_{out}}{\Delta E_{in}} = \frac{1}{1 + K_2 F(s)} \tag{70}$$

$$K_2 = \left.\frac{dE_{out}}{de_g}\right|_{E_{in} = \text{constant}} \tag{71}$$

In order to keep the loop gain independent of the input level, an exponential gain characteristic was used. An integrator was chosen for the loop filter to reduce the steady-state offset between E_{out} and V_{ref} to zero. The resulting loop transfer characteristic is given in Equations (72-75).

$$\frac{\Delta E_{out}}{\Delta E_{in}} = \frac{s}{s + K_2} \tag{72}$$

$$E_{out} = G(e_g)\, E_{in} \tag{73}$$

$$G(e_g) = e^{Be_g} \tag{74}$$

$$\left.\frac{\partial E_{out}}{\partial E_{e_g}}\right|_{E_{in} = \text{constant}} = K_2 = E_{in}\, Be^{Be_g} \tag{75}$$

A block diagram of the digital implementation of this circuit is shown below in Figure 30.

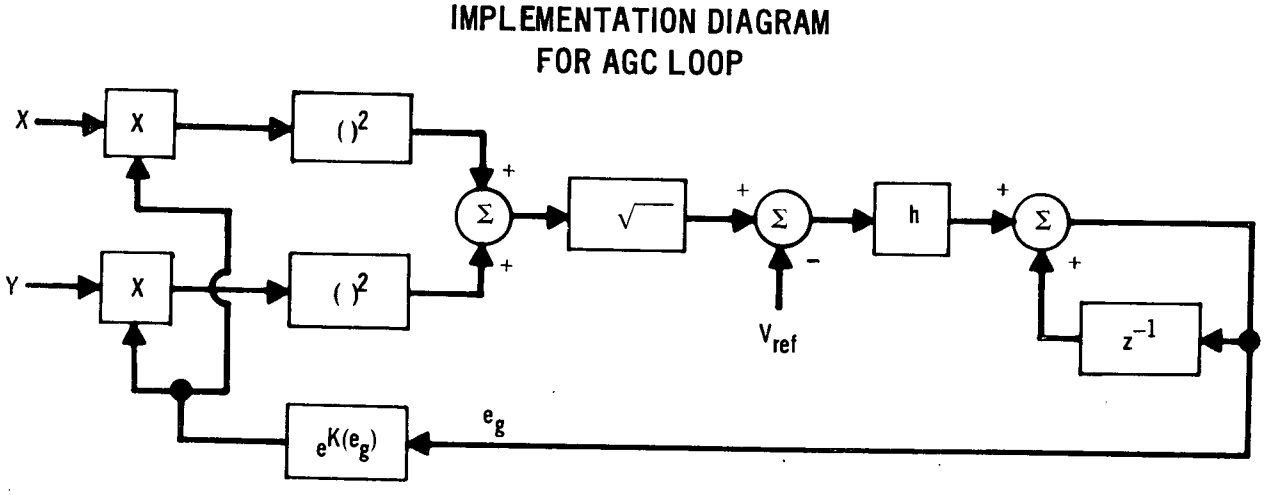

FIGURE 30

A Fortran computer program for implementing the above technique is given below.

H = h = sample interval

GAIN = K_2/V_{ref}

AK = Kh

AA = a

T = phase output of loop

REF = V_{ref}

X = G*ADC(01)

Y = G*ADC(02)

ENV = SQRT (X**2 + Y**2)

ERR = ENV - REF

EIT = EITM + ERR*H

EITM = EIT

```
G = EXP (-GAIN*EIT)

TEMP = AK*(X*COS(T)  - Y*SIN(T))

T = T + C*H + TEMP

C = C + AA*TEMP
```

2.5.3 Comparison of Techniques

In order to show that the two AGC implementations given above performed properly, we tested each technique by jittering the amplitude of the input signal and measuring the variance in the gain of the phase-locked loop. For a 5% input amplitude variance the gain of the loop varied by 3.4% for the closed loop configuration and 1.1% for the limiter. This result would be expected since the limiter has an effective time constant which is infinitely small, while the closed loop configuration that was investigated had a time constant of 5 seconds. The operation of the AGC circuit was also demonstrated by showing the effect of the input signal to noise ratio on the tracking ability of a phase-locked loop preceded by one of the above AGC circuits. Utilizing a digital simulation, a sine wave phase input was applied to the loop, and the phase error variance was determined as a function of the input signal-to-noise ratio. A graph of these results is shown in Figure 31 . For input signal-to-noise ratios above zero dB the output phase variance approaches the theoretical value for white noise passed through a linear loop. This indicates that the phase-locked loop is tracking the input sinusoidal phase variation with negligible error. As the input signal-to-noise ratio is reduced, the loop gain is reduced and the input phase variations can no longer be tracked. Figure 31 indicates that the threshold occurs at an input signal-to-noise ratio of -4 dB for the limiter and - 7 dB for the closed loop AGC with a 5 second time constant. Therefore, although the limiter

AGC reduces the gain variations by more than the closed loop configuration, it has a higher threshold than the latter method.

These results indicate that the limiter gives better regulation than the closed loop AGC, but it has a higher threshold. The previous Fortran computer programs showed that the limiter type AGC is faster and less complex than the closed loop approach. Since speed and complexity are important considerations in implementing a digitized receiver, the limiter AGC was chosen as the optimum method of obtaining automatic gain control.

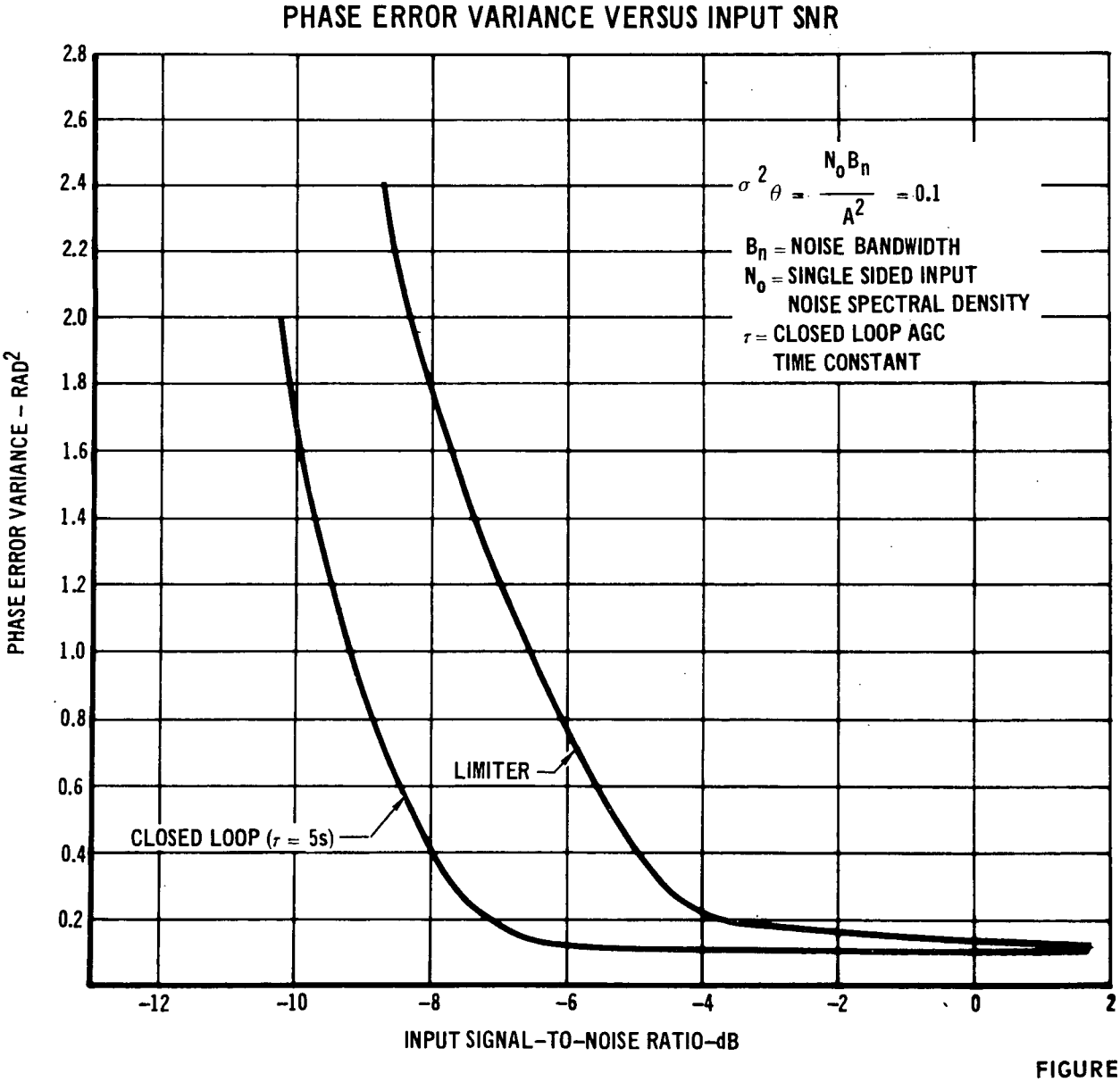

FIGURE 31

2.6 Acquisition

We analyzed and compared three approaches to phase-locked loop acquisition; the swept frequency method, the Fast Fourier Transform method, and the free-running mode. The first technique consists of beating the input signal with a swept frequency oscillator and passing the resultant signal through a low pass filter and a threshold detector. The second approach consists of computing the FFT of N input samples and then determining the Fourier coefficient of maximum amplitude. The final method allows the phase-locked loop to pull-in with no external controls.

2.6.1 Swept Frequency Method

The first technique, which was studied by Sterling[4], consists of beating the input signal with two oscillators that are 90° out of phase, filtering the resultant signal, and performing a threshold detection to determine when the swept frequency equals the input frequency. The two out-of-phase oscillators are necessary since the phase of the input signal is not known and thus a zero output could result if only one oscillator was used. A block diagram of this configuration is shown in Figure 32. The input multiplications shown in this figure are derived in Equations (76-81).

$$E_i = X \sin \omega_o t + Y \cos \omega_o t \tag{76}$$

$$E_{vco} = \cos (\omega_o t + \theta) \tag{77}$$

$$\theta = \omega_o t - kt^2 \tag{78}$$

$$k = \frac{w_h}{T} \tag{79}$$

T = sweep time

$$e_q = E_i E_{vco} = -X \sin \theta + Y \cos \theta \tag{80}$$

$$e_I = E_i E_{vco} = X \cos \theta + Y \sin \theta \tag{81}$$

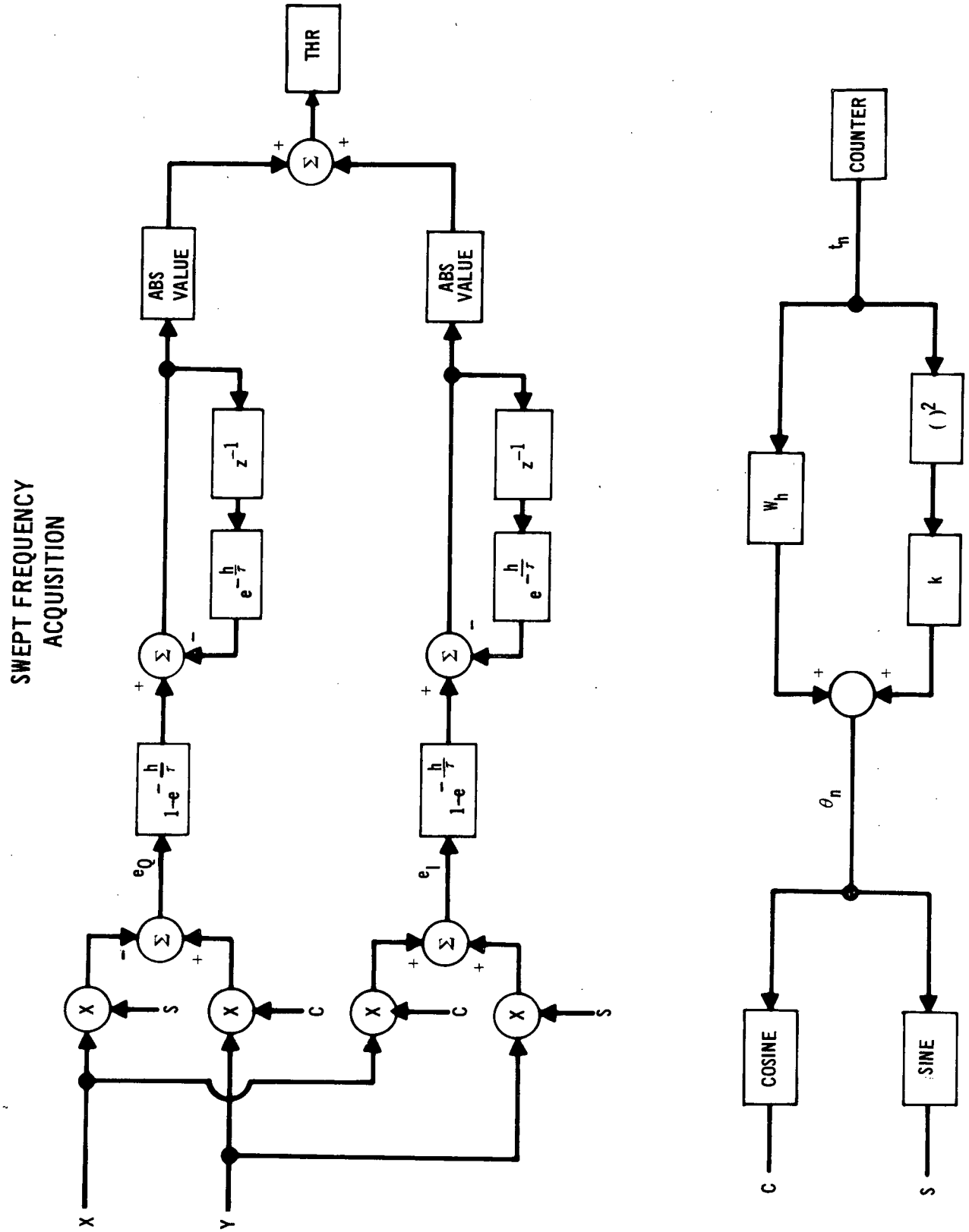
SWEPT FREQUENCY
ACQUISITION
THR
ABS VALUE
ABS VALUE
z^{-1}
z^{-1}
$e^{-\frac{h}{\tau}}$
$e^{-\frac{h}{\tau}}$
$1-e^{-\frac{h}{\tau}}$
$1-e^{-\frac{h}{\tau}}$
e_Q
e_I
S
C
C
S
X
Y
COUNTER
t_n
W_h
$(\ )^2$
k
θ_n
COSINE
SINE
C
S

FIGURE 32

Each of the quadrature components is passed through a low pass filter and an absolute value circuit. The resultant sum signal is applied to a threshold detector. The frequency of the sweep at the time the threshold is crossed is used as the initial condition on the frequency of the phase-locked loop. If this frequency is within the pull-in range of the phase-locked loop, the loop will almost instantaneously acquire the signal. The time constant of the low pass filter was chosen to maximize the ratio between the peak signal at the input to the threshold detector and the standard deviation of the noise at the output of the low pass filter. The measurement of peak signal to rms noise at the filter output is only an approximation of the actual signal-to-noise ratio since the noise should be taken at the input to the threshold detector. However, the absolute value circuit makes this difficult, and thus the approximate measurement was made. A graph of the signal-to-noise ratio versus the ratio of the low pass filter bandwidth squared to the sweep rate is shown in Figure 33. This graph shows that the signal-to-noise ratio is maximized for $(\omega_{LP}^2/2K)$ equal to 0.1715. However, this ratio can be varied between 0.1 and 0.275 with a resulting loss in signal-to-noise ratio of less than 0.1 dB. A computer program for the above acquisition circuitry with the phase-locked loop included is shown in Figure 34. When the variable E is greater than the threshold, the variable C is set equal to the swept frequency at that time, and the phase-locked loop calculations are begun at statement 2.

2.6.2 Fast Fourier Transform Acquisition

A second method for performing phase-locked loop acquisition is to utilize the Fast Fourier Transform (FFT). This technique consists of reading N samples into the computer and calculating the Discrete Fourier

Transform (DFT) which is given in Equation (82).

$$A_r = \sum_{k=o}^{N-1} X_k \exp(-2\pi jrk/N) \qquad (82)$$

$$r = 0, 1, ---, N-1$$

X_k = input samples

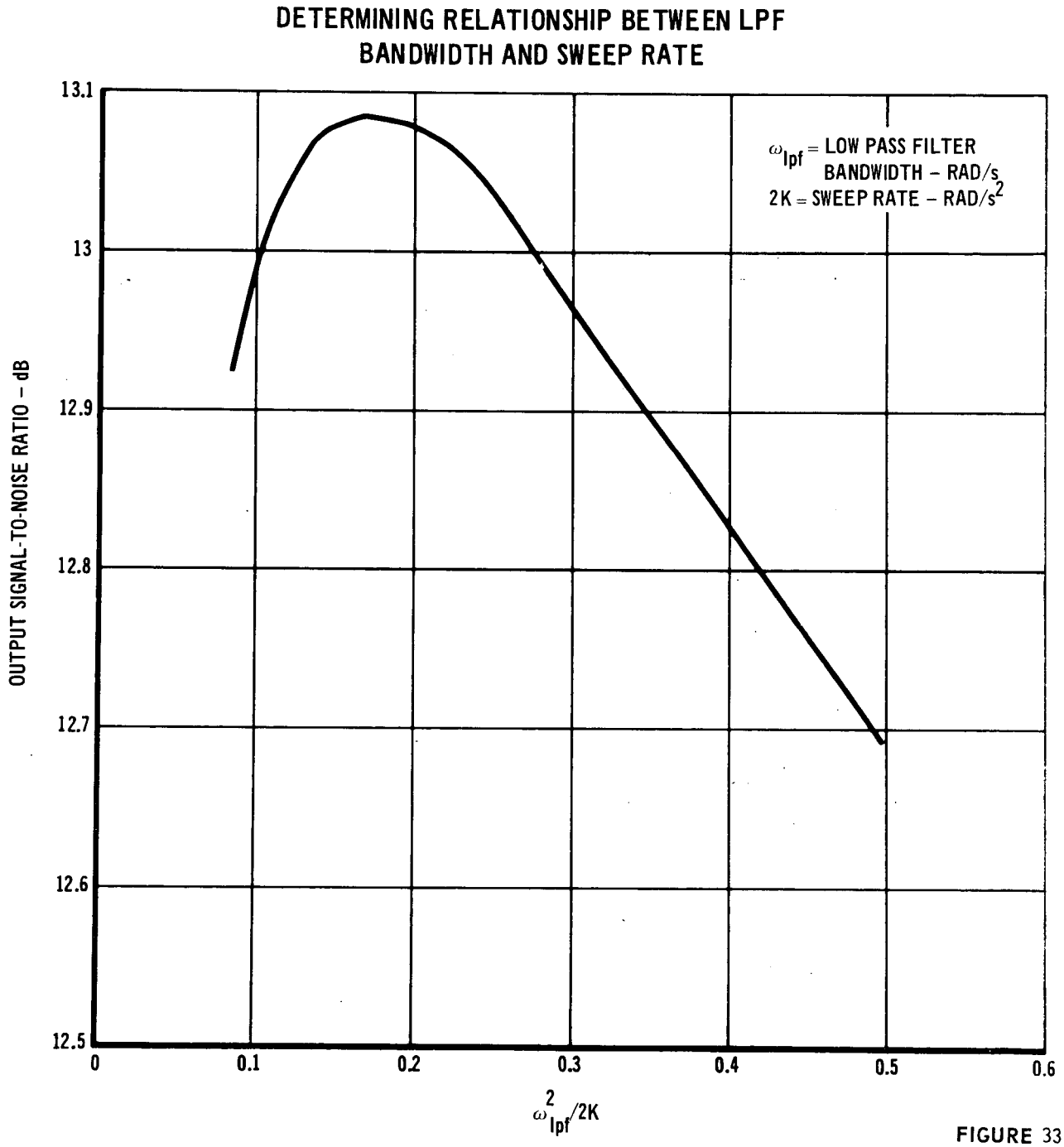

FIGURE 33

COMPUTER PROGRAM FOR ACQUISITION

```
      WH   = SWEEP START FREQUENCY AND ONE HALF OF SWEEP RANGE
      RK   = TWICE THE SWEEP RATE
      H    = TIME INTERVAL
      AK   = LOOP GAIN
      AA   = FILTER CONSTANT
      THR  = ACQUISITION THRESHOLD
      CON  = e ** (-ω_lpf * h)
      TTT  = SWEEP TIME
3     IF ( E. LT. THR) GO TO 1
      C    = WH - 2. * RK * TT
      GO TO 2
1     X    = ADC(01)
      Y    = ADC(02)
      THET = WH*TT - RK*(TT**2)
      CS   = COS (THET)
      SS   = SIN (THET)
      XX   = X*CS + Y*SS
      YY   = -X*SS+Y*CS
      EX   = XX + (EIX - XX) * CON
      EIX  = EX
      EY   = YY + (EIY - YY) * CON
      EIY  = EY
      E    = ABS (EX) + ABS (EY)
      TT   = TT + H
      IF (TT . GT . TTT) TT=0
      GO TO 3
2     X    = ADC(01)
      Y    = ADC(02)
      TEMP = AK * (Y*COS(T) -X*SIN(T))
      T    = T + C* H + TEMP
      C    = C + AA * TEMP
      GO TO 2
```

FIGURE 34

The FFT algorithm removes redundant operations from the calculations and reduces the number of operations from N^2 to $2N \log_2 N$. For large values of N this is an extremely significant reduction. The listing of a digital computer program for implementing the FFT algorithm is given in Figure 35.

DIGITAL COMPUTER PROGRAM FOR FFT GENERATION

```
C       COMPLEX W, X, Y
C       N = NUMBER OF SAMPLES
C       N = 2**L
C       X (J) = INPUT DATA
        PI = 3.141592653589793
        BBN = N
        AR = 2.* PI/BBN
        MM = 0
        K = 1
        NA = N/2
        KK = NA
        DO 2 J = 1, L
        IF (MM. EQ.1) GO TO 9
        MM = 1
        DO 1 I = 1, K
        IM = (I - 1) * KK
        AA = IM*AR
        W = CMPLX (COS (AA), - SIN (AA) )
        DO 1 II = 1, KK
        NZ = II + IM
        NQ = NZ + IM
        Y (NZ) = X (NQ) + W* X (NQ + KK)
        Y (NZ + NA) = X (NQ) - W* X (NQ + KK)
1       CONTINUE
        GO TO 12
9       MM = 0
        DO 10 I = 1, K
        IM = (I - 1) * KK
        AA = IM*AR
        W = CMPLX (COS (AA), - SIN (AA) )
        DO 10 II = 1,KK
        NZ = II + IM
        NQ = NZ + IM
        X (NZ) = Y (NQ) + W*Y ( NQ + KK)
        X (NZ + NA) = Y ( NQ) - W*Y (NQ + KK)
10      CONTINUE
12      KK = KK/2
        K = 2*K
2       CONTINUE
C       X(J) = OUTPUT DATA IF L IS EVEN
C       Y(J) = OUTPUT DATA IF L IS ODD
```

FIGURE 35

The program, which was written in Fortran IV, determines the FFT of a sequence of N complex input samples X(K). This program uses complex input samples which

is of great advantage since the Fourier Transform of the IF signal ($X \cos \omega_o t + Y \sin \omega_o t$) can be obtained by frequency shifting the transform of ($X + jY$) as is shown in Equations (83) and (84).

$$F\ (X + jY) = F(\omega) \tag{83}$$

$$F\ (X \cos \omega_o t + Y \sin \omega_o t) = \frac{1}{2}\ F^*(\omega - \omega_o) + \frac{1}{2} F\ (\omega + \omega_o) \tag{84}$$

The sampling rate must be greater than twice the maximum frequency of the sampled signal. The total number of samples determines the separation between the discrete spectral components. The program shown in Figure 35 has been written such that N must be an integral power of two ($N = 2^L$). This constraint is not usually restrictive in using this program for acquisition since the number of samples can usually be increased such that N becomes an integral power of two. The preceding program stores the DFT of the input signal in either the X or Y matrix depending on whether L is even or odd. The relationship between the coefficients A_r and the elements of the output matrix (assumed to be X for this example) is given below.

$$A_r = X(r + 1)$$

If the function ($X + jY$) is transformed, where X and Y are the quadrature components of the input signal, the complex value of the various spectral components are found in the storage locations given in Equation (85).

$$f_1 = \frac{1}{Nh} \tag{85}$$

h = sample interval

N = number of samples

$X(1) \longrightarrow f_o$ $\qquad$ $X(N) \longrightarrow f_o - f_1$

$X(2) \longrightarrow f_o + f_1$ $\qquad$ $X(N-1) \longrightarrow f_o - 2f_1$

$$X(3) \longrightarrow f_o + 2f_1 \qquad X(N-2) \longrightarrow f_o - 3f_1$$

$$\vdots$$

$$X(\tfrac{N}{2} - 1) \longrightarrow f_o + (\tfrac{N}{2} - 2)f_1 \qquad X(\tfrac{N}{2} + 1) \longrightarrow f_o - (\tfrac{N}{2} - 2)f_1$$

After computing and storing the complex Fourier coefficients, the magnitude of each coefficient is determined. The estimate of the input frequency is then made by determining the frequency associated with the complex Fourier coefficient of maximum magnitude. This value of frequency is then inserted as an initial condition in the the phase-locked loop as was done with the swept frequency method.

2.6.3 Free-Running Acquisition

This technique allows the phase-locked loop to pull-in without any external control. If the initial frequency offset is within the pull-in range of the loop, acquisition will occur. However, for large frequency offsets the loop will begin slipping cycles, and pull-in will occur in a much longer time. To show this effect we measured the mean and variance in pull-in time as a function of the frequency offset between the VCO and the input sine wave and the output signal-to-noise ratio. This investigation showed that the average pull-in time was independent of the output signal-to-noise ratio. A graph of pull-in time versus frequency offset is shown in Figure 36. The variance in pull-in time, which is affected by the output signal-to-noise ratio, is graphed in Figure 37 as a function of the frequency offset.

2.6.4 Comparison of Techniques

The free-running acquisition approach was discarded because of the excessive pull-in time required for large frequency offsets. The two remaining techniques were compared using digital simulation. The probability of acquisition was determined as a function of the sweep rate for two different output signal-to-noise ratios. In the simulation a correct acquisition was assumed to have

MEAN PULL-IN TIME VERSUS OFFSET FREQUENCY

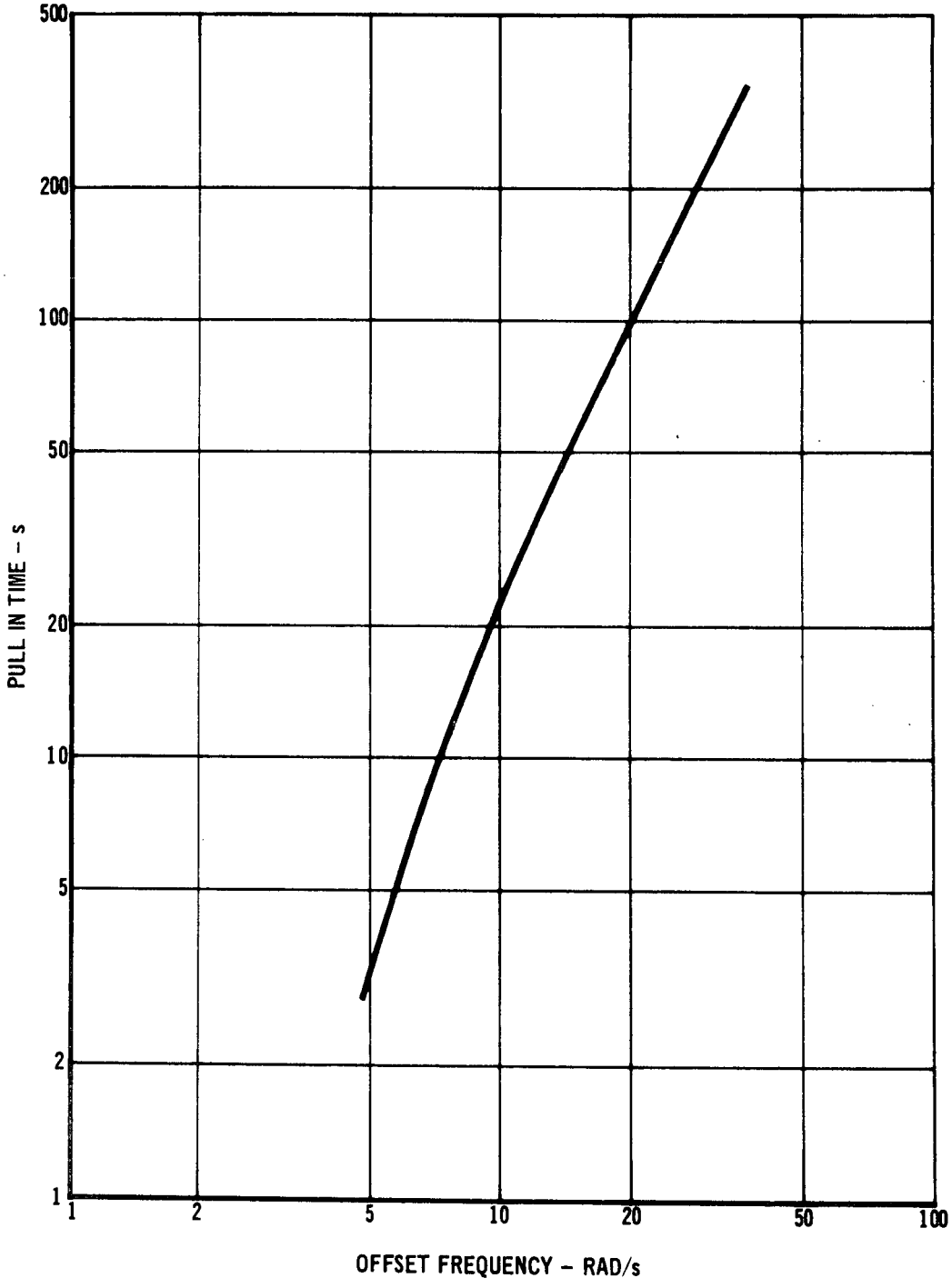

FIGURE 36

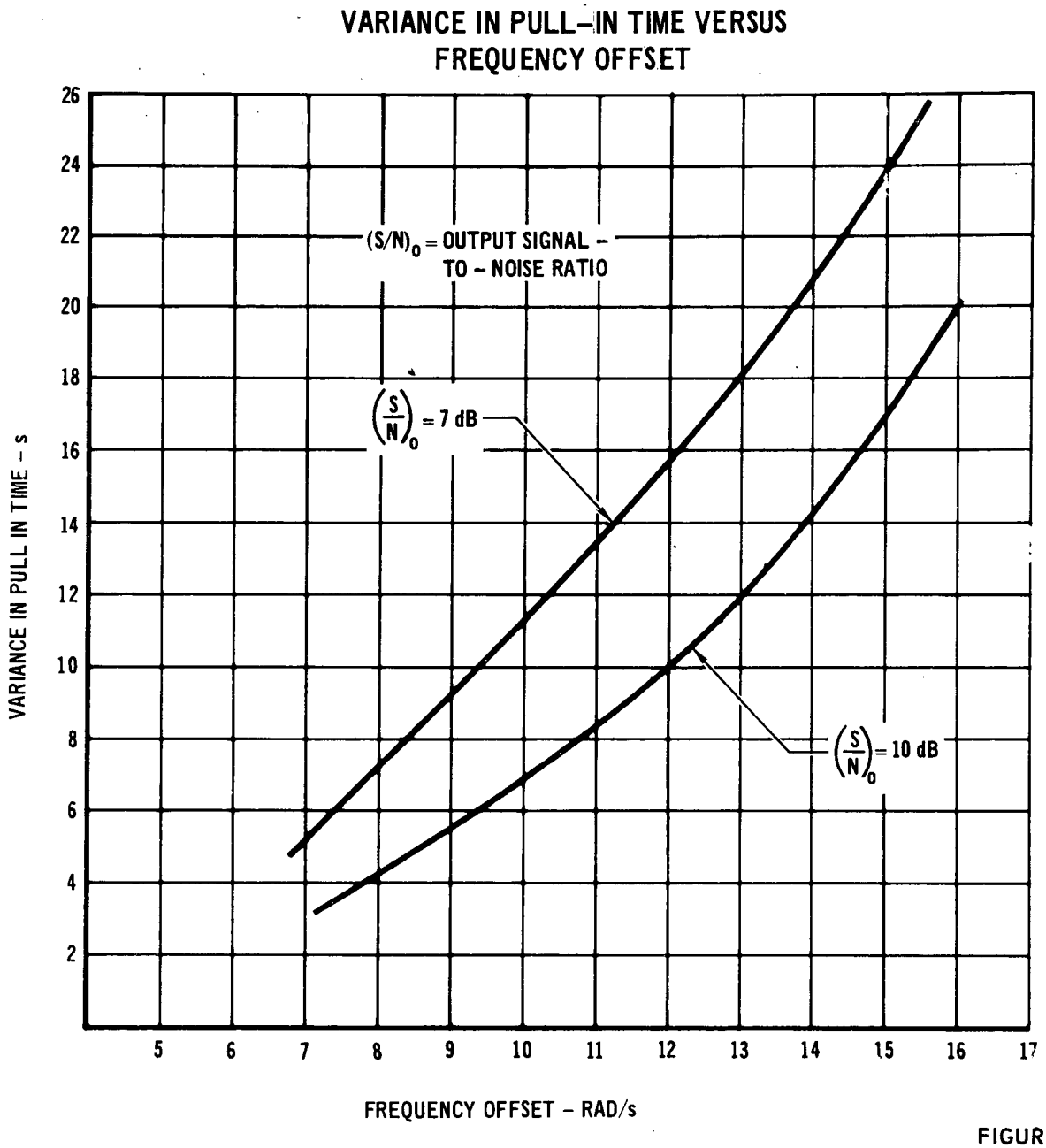

FIGURE 37

occurred if the difference between the estimate of the input frequency and the input frequency was within the pull-in range of the phase-locked loop. The loop pull-in range is considered to be the range over which the loop will acquire without slipping cycles. The results of this investigation are shown in Figure 38. The sweep rate for the FFT technique is determined by the frequency range, the sample interval, and the number of samples. Figure 38 indicates that the FFT

PROBABILITY OF ACQUISITION VERSUS SWEEPRATE

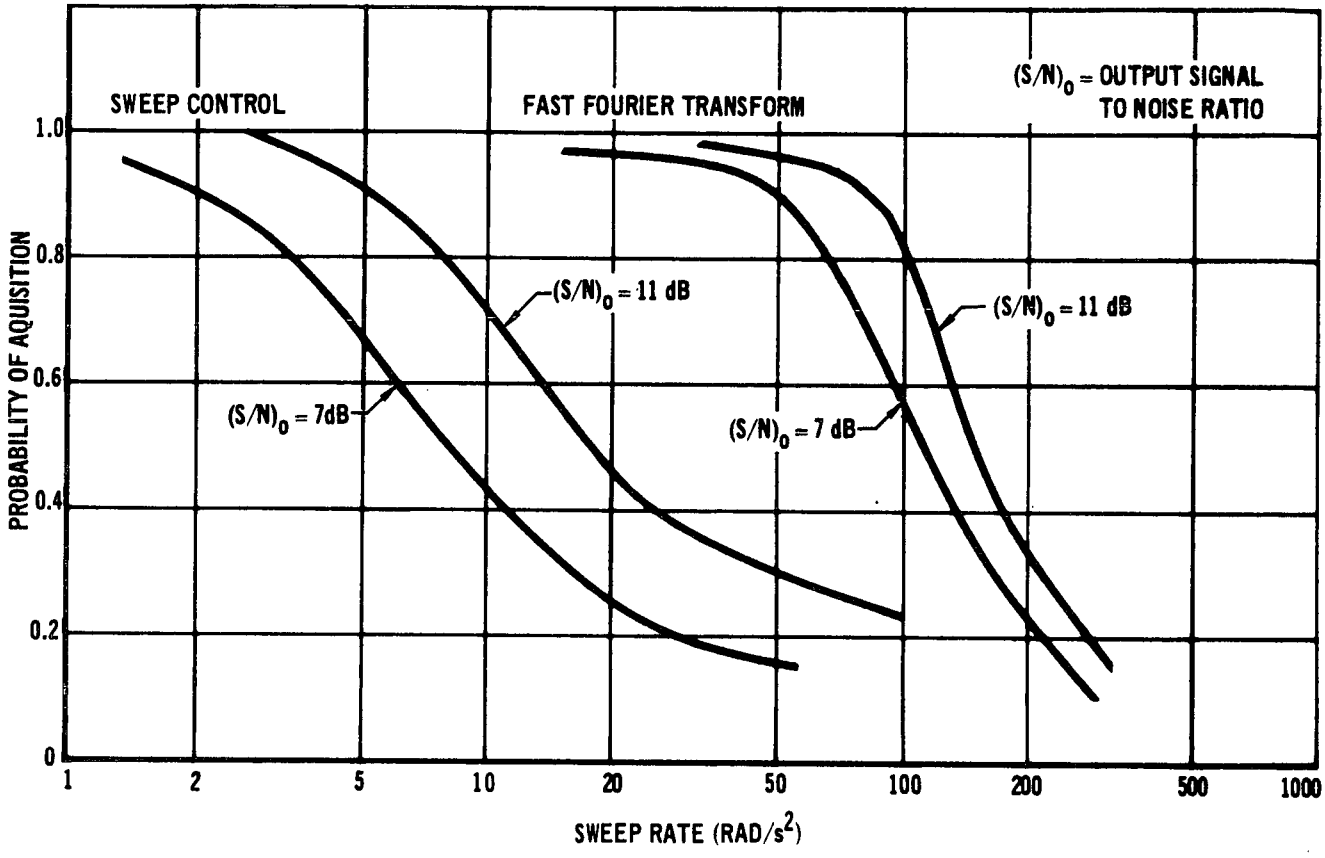

FIGURE 38

technique gives much better results than the sweep control method. This is due to the fact that the FFT method is similar to a parallel bank of matched filters centered on each of the spectral lines, while the latter method approximates a single matched filter which is switched from one spectral line to another. Therefore, the integration time is much longer for the FFT technique and the output noise power is reduced.

The main criteria used to choose between the acquisition techniques is speed and simplicity. One of the big disadvantages of the FFT technique is that it must be done sequentially. This means that no calculations can be made until all N samples are read into the digital computer, and that the digital

processor must be capable of storing these N samples. These constraints decrease the speed and increase the complexity associated with the processor. The calculations associated with the sweep control method can be made between samples and thus fewer modifications are necessary with this technique. Therefore, the sweep control method is the recommended approach for solving the acquisition problem.

2.7 Hybrid Simulation

One of the important decisions associated with implementing a digital processor is the determination of the filter which precedes the A/D converter. We first determined the effect of three candidate input filters, an integrate and dump filter, a single break low pass filter, and a double break low pass filter, on system performance. We then set up a hybrid simulation of the digitized phase-locked loop and determined the phase error variance as a function of noise-to-signal ratio.

2.7.1 Input Filter

Each of the quadrature components is filtered before being passed into the digital computer. This filter, which precedes the sample and hold circuit, eliminates the second harmonic of the input signal and reduces the loss caused by aliasing. If it is assumed that the input signal remains constant between samples, an integrate and dump filter, which integrates during the time between samples, is the optimum filter. The main problem associated with this technique is that a timing signal must be sent from the digital computer to dump the external integrator at the appropriate time. Because of the extra complexity associated with the above method, two alternative techniques, a single break low pass filter and a two break low pass filter, were considered. The transfer functions for these two filters are given in Equations (86) and (87).

$$F_1(s) = \frac{\alpha}{s + \alpha} \tag{86}$$

$$F_2(s) = \frac{\alpha^2}{(s + \alpha)^2} \tag{87}$$

In order to compare the three different filter implementations, we assumed that the input filter bandwidth was wide enough that the effective noise spectral density of the sampled and held input signal is constant over the noise bandwidth of the phase-locked loop. The loss in input signal to noise ratio is then defined as given in Equation (88),

$$L = 10 \log_{10} \frac{S_n(0)}{N_o \left| F(\omega_{max}) \right|^2} \tag{88}$$

L = loss in input signal-to-noise ratio (dB)

ω_{max} = maximum offset frequency

$F(\omega)$= filter transfer function

N_o = noise spectral density at filter input

$S_n(0)$ = effective noise spectral density at the output of the sample and hold circuit

For the integrate and dump filter $S_N(0)$ is equal to N_o. Therefore, the only loss results from the decrease in amplitude of the maximum offset sine wave at the output of the integrate and dump filter. This loss is then given in Equation (89).

$$L = 20 \log_{10} \left[\frac{\sin \pi/R}{\pi/R} \right] \tag{89}$$

$R = f_s/f_{max}$

f_s = sampling rate

f_{max} = maximum offset frequency

The increase in noise spectral density at zero frequency for the input filter F(s) was determined from Equation (90).

$$\frac{S_n(0)}{N_o} = \frac{1}{2} + \sum_{n=1}^{\infty} F(nw_s)^2 \tag{90}$$

This formula is determined from the fact that the spectral density at the input to a sampler is reproduced at multiples of the sampling frequency at the output of the sampler. Using the above relationships, the loss for filters $F_1(s)$ and $F_2(s)$ is given in Equations (91-94).

$$L_1 = 10 \log_{10} \frac{\frac{1}{2} + \sum_{n=1}^{\infty} \frac{1}{1 + (nK)^2}}{\left[\frac{R^2}{R^2 + K^2}\right]} \tag{91}$$

$$L_2 = 10 \log_{10} \frac{\frac{1}{2} + \sum_{n=1}^{\infty} \left[\frac{1}{1 + (nk)^2}\right]^2}{\left[\frac{R^2}{R^2 + K^2}\right]^2} \tag{92}$$

$$K = \frac{fs}{f_{LPF}} \tag{93}$$

$$R = f_s / f_{max} \tag{94}$$

In order to minimize the loss for each of the two filter configurations, we selected a value for R and plotted L as a function of K. One of these graphs for the second order filter for R=10 is shown in Figure 39. This curve shows that the minimum value of L_2 is .683 dB and that it occurs at K = 2.26. Utilizing the digital computer, we repeated the above procedure for different values of R. A graph of the minimum value of the loss versus R is shown in Figure 40 for all three filter configurations. Figure 41 shows a plot of the optimum value of K versus R. The integrate and dump circuit is not shown in this final figure since the ratio of sampling rate to filter bandwidth is a constant. The above results show that the integrate and dump filter is 1/2 dB better than a second order filter and 1 1/4 dB better than the first order filter for values of R equal to ten.

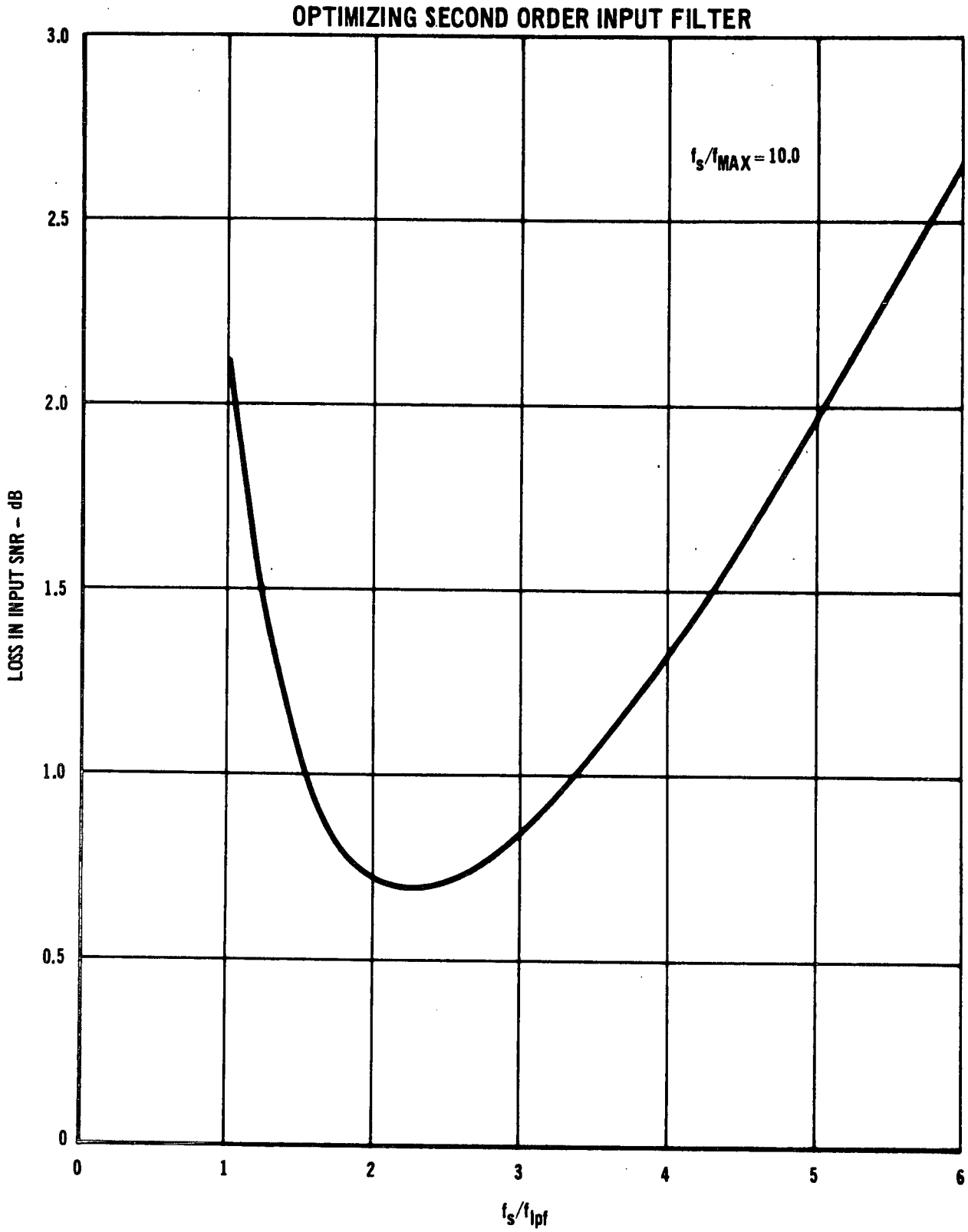
OPTIMIZING SECOND ORDER INPUT FILTER
$f_s/f_{MAX} = 10.0$
LOSS IN INPUT SNR - dB
3.0
2.5
2.0
1.5
1.0
0.5
0
0
1
2
3
4
5
6
f_s/f_{lpf}

FIGURE 39

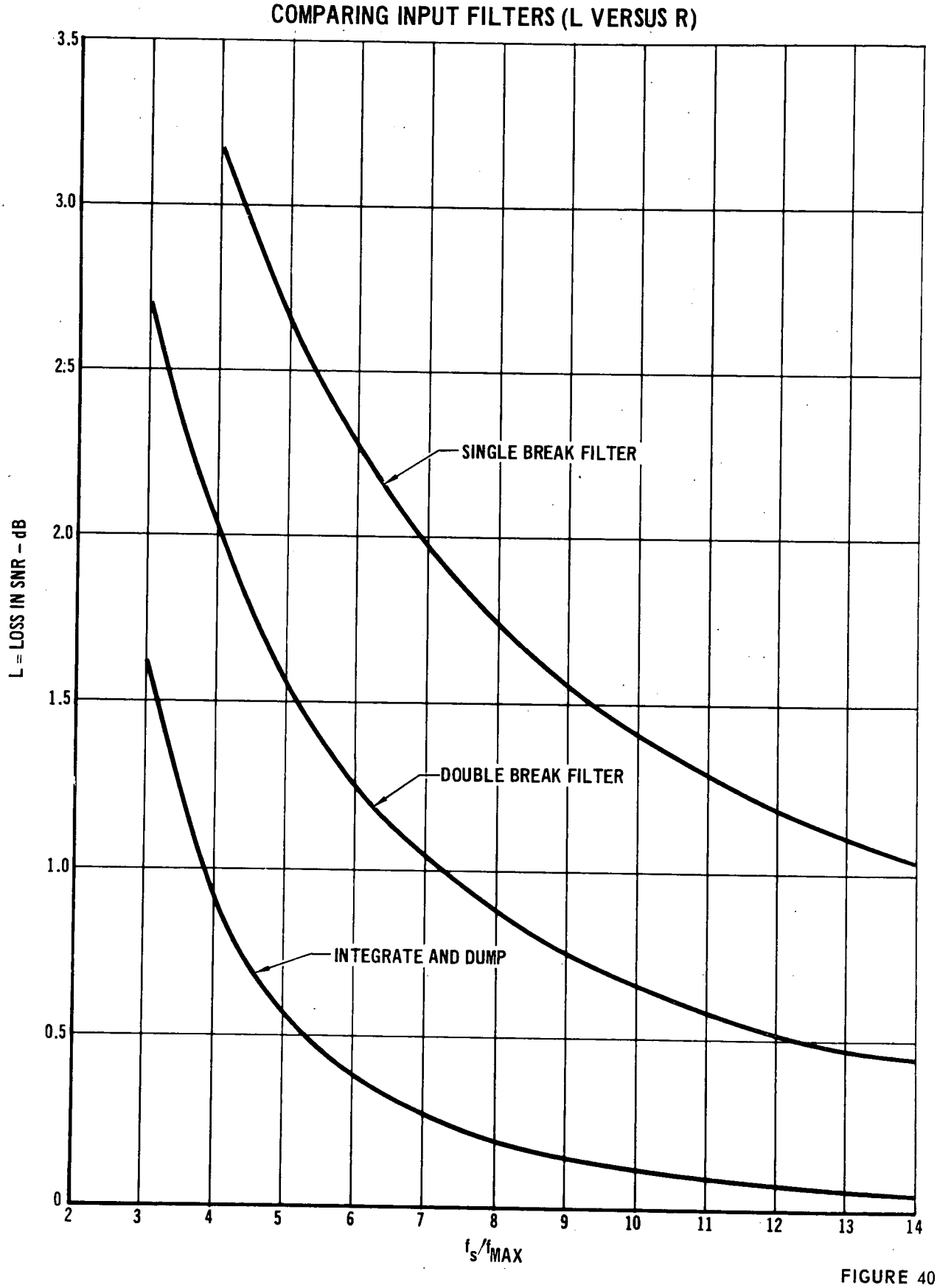
COMPARING INPUT FILTERS (L VERSUS R)
L = LOSS IN SNR - dB
3.5
3.0
2.5
2.0
1.5
1.0
0.5
0
2
3
4
5
6
7
8
9
10
11
12
13
14
f_S/f_{MAX}
SINGLE BREAK FILTER
DOUBLE BREAK FILTER
INTEGRATE AND DUMP

FIGURE 40

COMPARING INPUT FILTERS (K VERSUS R)

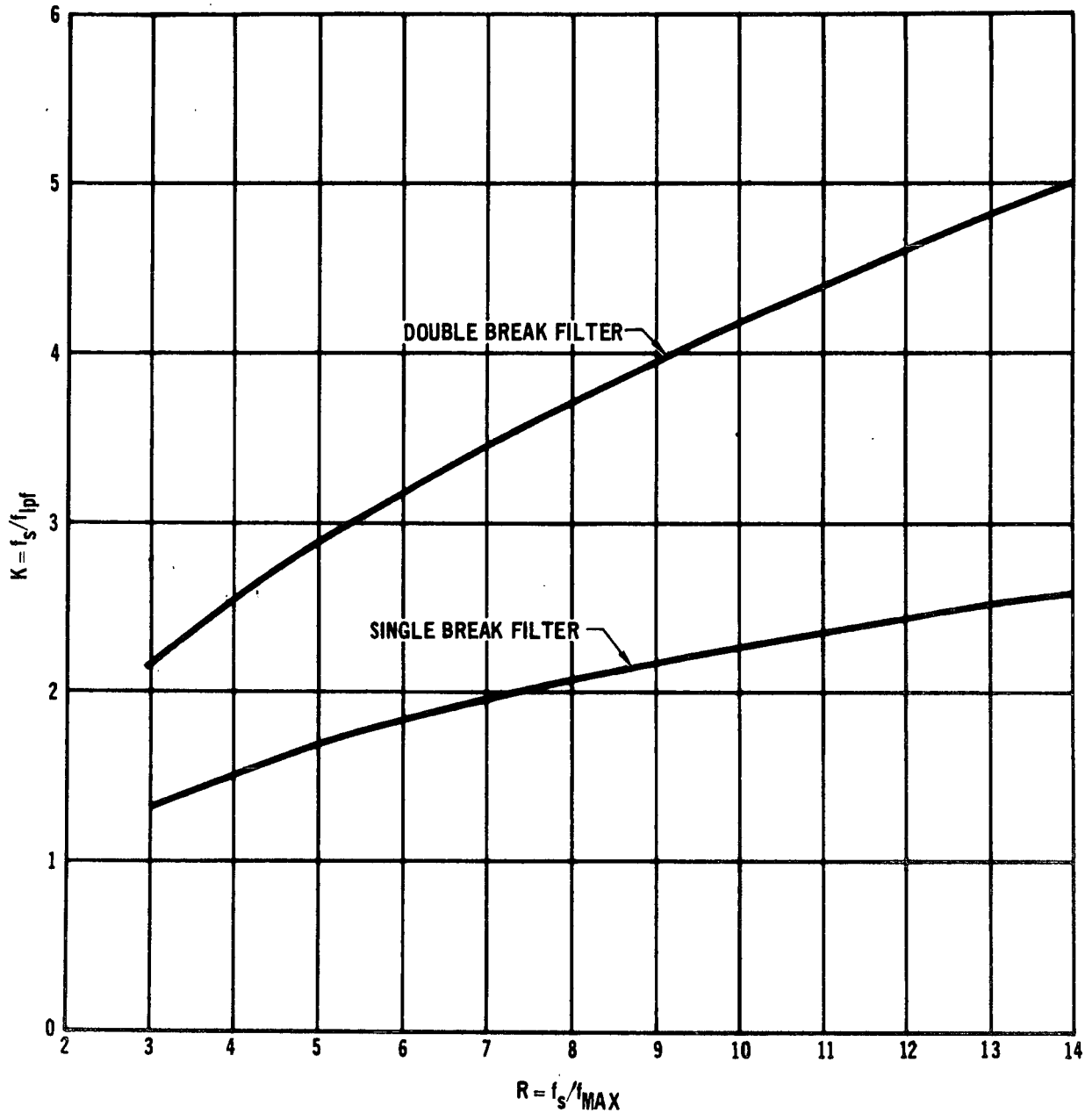

FIGURE 41

2.7.2 Results

Utilizing our 1 MHz "front end," the adage 770 A/D converter, and the CDC 6400 computer, a hybrid simulation of the digital phase-locked loop was conducted. A simplified block diagram of the configuration used is given in Figure 42.

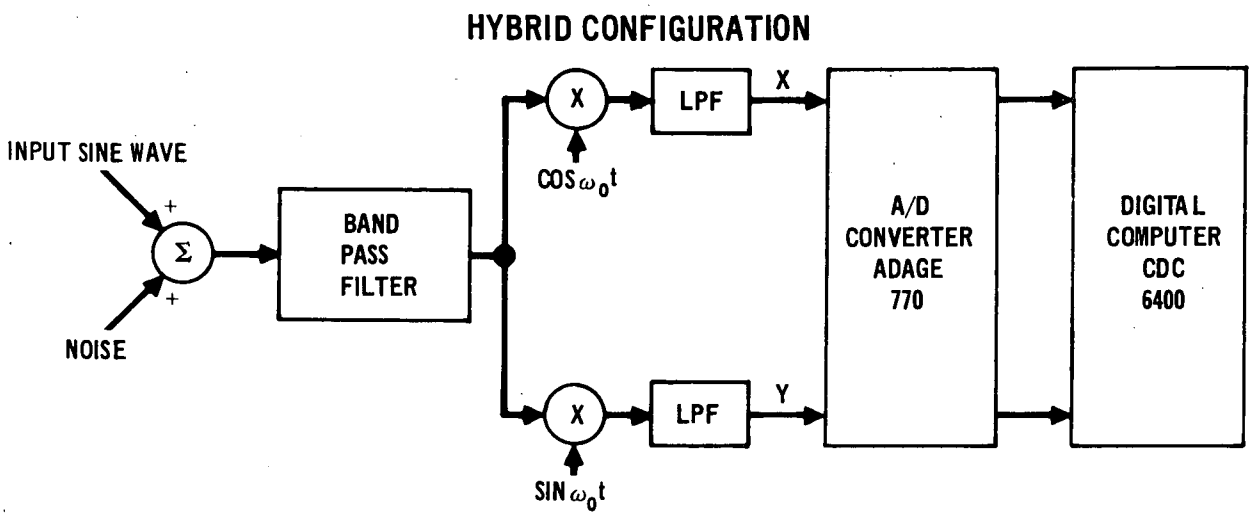

FIGURE 42

Figure 43 shows strip chart recordings of the input quadrature components and the phase output of the loop which was fed back from the digital computer. The phase error variance was then determined by generating an internal phase reference using a second phase-locked loop with a bandwidth 300 times smaller than the first. The only restriction on this technique is that the second loop must be allowed to run for a sufficient length of time before the phase error calculation begins so that any initial transient has decayed off. Another method of generating a phase reference would be to pass the non-noisy signal through an identical "front end" and compute the phase in the digital computer. This approach was discarded because of the problems associated with balancing the two channels and the added complexity associated with adding the two extra channels. Figures 44 and 45 show the phase error variance versus $(\frac{N_o B_n}{A^2})$ for the phase-locked loop without a limiter and with a limiter respectively. For both of these simulations the input filter consisted of a single break low pass filter with a 45 Hz bandwidth. We also set a .2Hz offset between the input frequency and the IF center frequency.

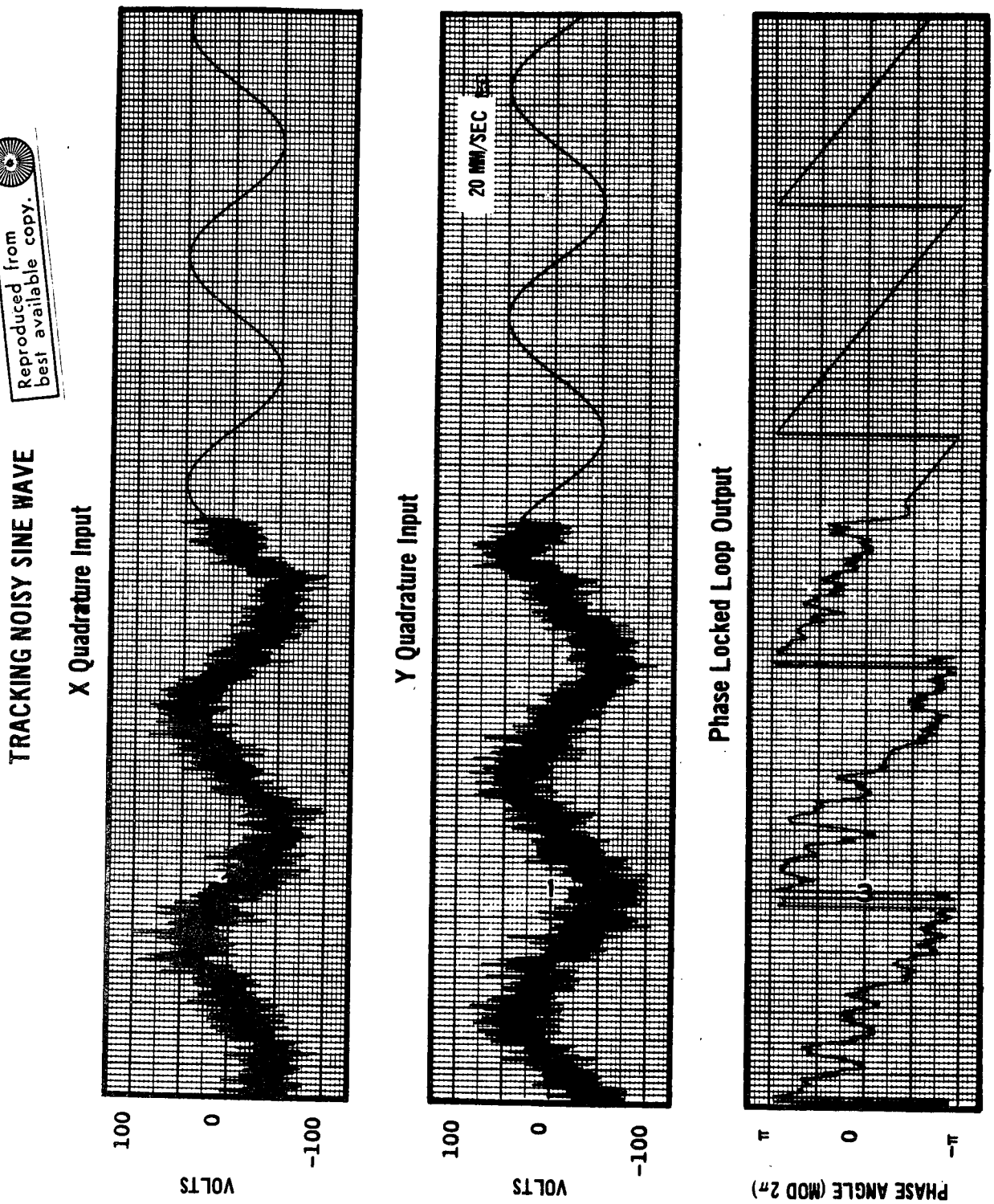

FIGURE 43

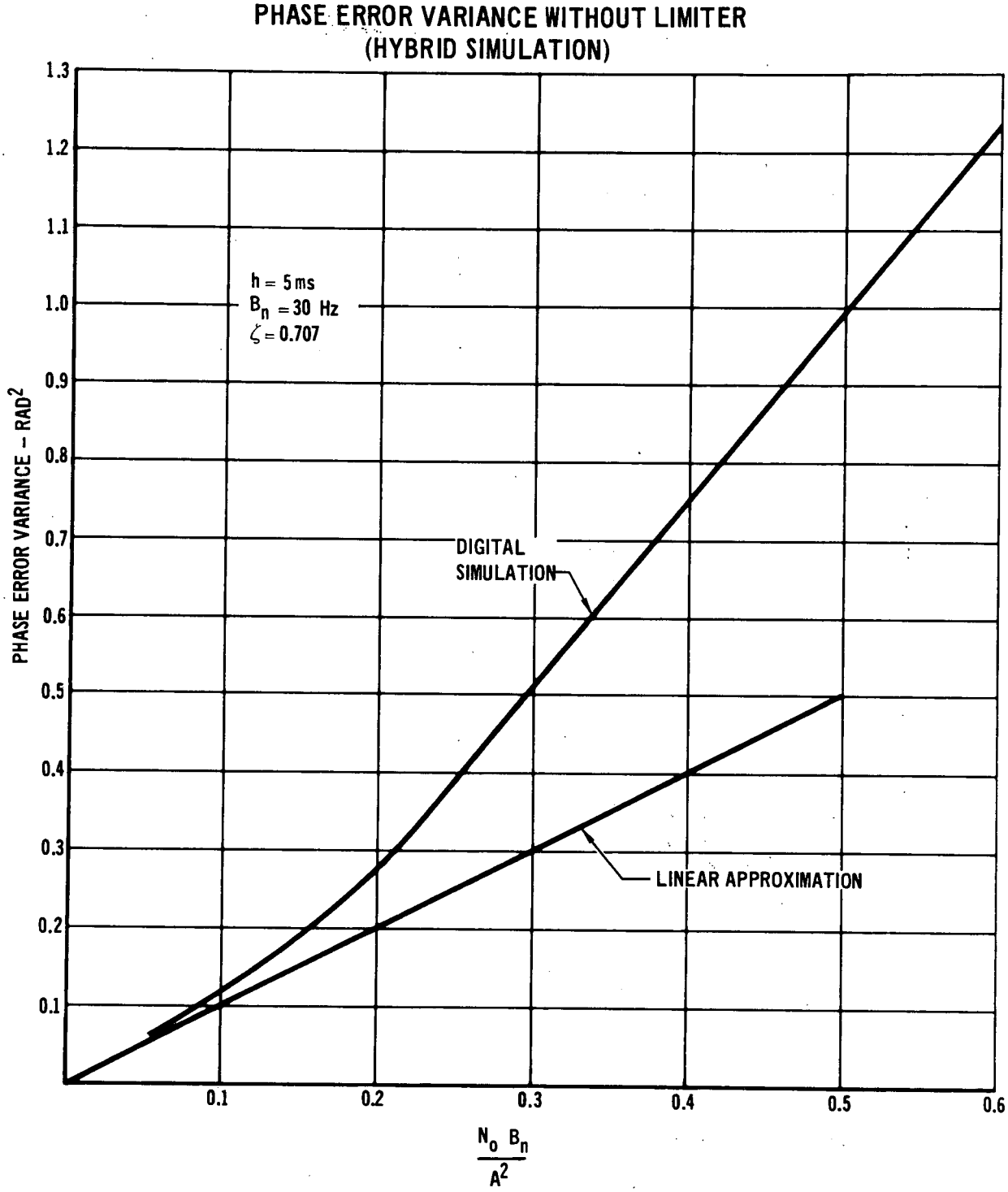
PHASE ERROR VARIANCE WITHOUT LIMITER
(HYBRID SIMULATION)
h = 5 ms
B_n = 30 Hz
ζ = 0.707
DIGITAL SIMULATION
LINEAR APPROXIMATION
PHASE ERROR VARIANCE - RAD^2
1.3
1.2
1.1
1.0
0.9
0.8
0.7
0.6
0.5
0.4
0.3
0.2
0.1
0.1
0.2
0.3
0.4
0.5
0.6
$\frac{N_o B_n}{A^2}$

FIGURE 44

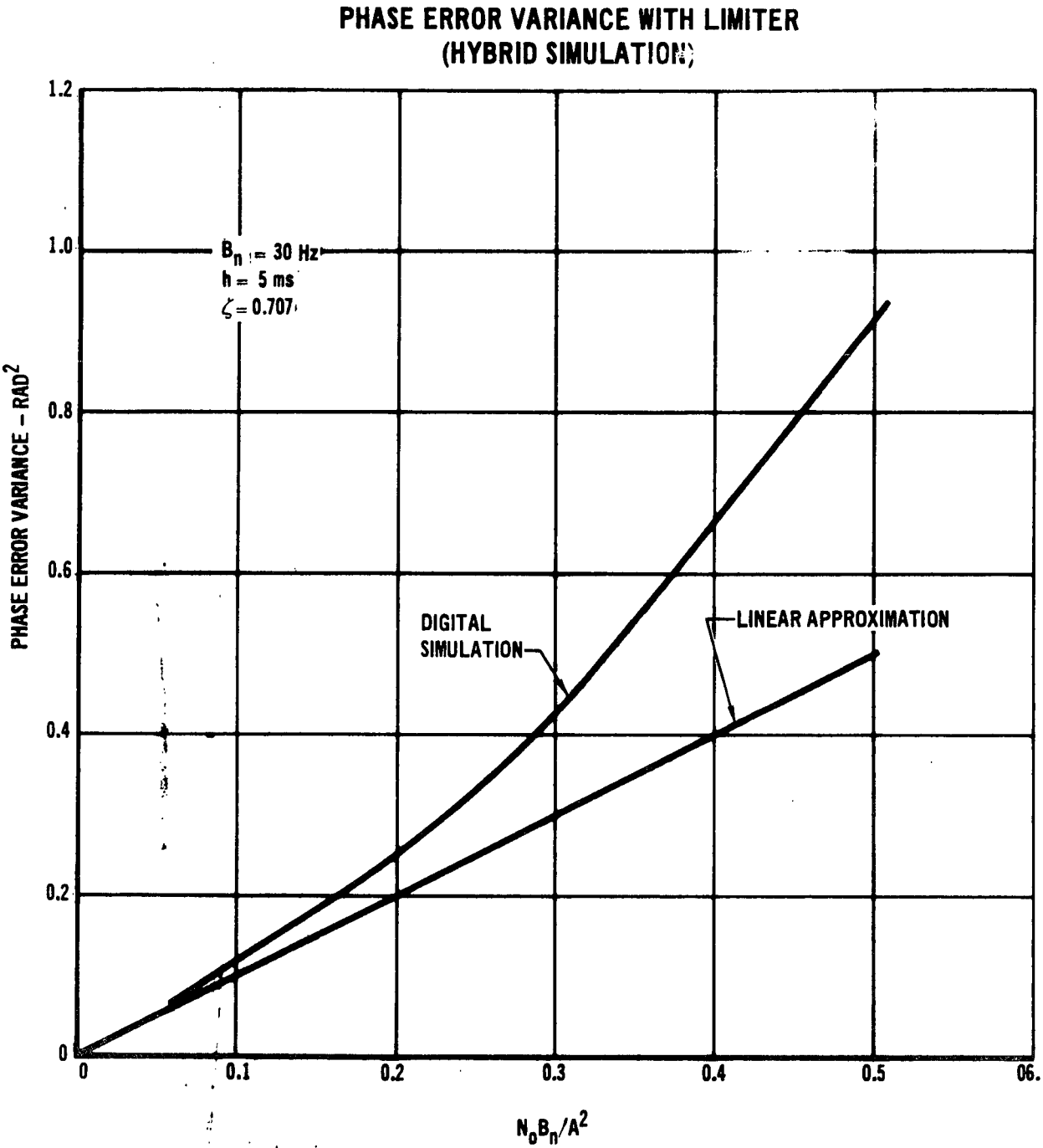

FIGURE 45

2.8 Evaluation of Performance

In this section we compare the results obtained during this study on phase error variance, phase-locked loop threshold, and acquisition with the results obtained by other investigators.

2.8.1 Phase Error Variance

In order to validate the results obtained during this portion of the study, we determined the relationship between the phase error variance and the noise-to-signal ratio using both an approximate technique, quasi-linearization, and an exact approach, the Fokker-Plank Method. Quasi-linearization consists of replacing the nonlinearity with an equivalent gain which is determined from a knowledge of the statistics at the input to the nonlinearity. If it is assumed that the input to the sine nonlinearity in the phase-locked loop is Gaussian with a variance σ^2_ϕ, Develet[5] shows that the equivalent gain can be determined as given in Equations (95) and (96).

$$G_{EQ} = \frac{AK}{\sqrt{2\pi}\ \sigma_\phi} \int_{-\infty}^{\infty} e^{-\theta^2/2\sigma_\phi^2} \cos\theta\ d\theta \qquad (95)$$

$$G_{EQ} = AK\ e^{-\sigma_\phi^2/2} \qquad (96)$$

A = input amplitude

K = VCO gain

This value of gain is substituted into the equation for phase variance at the output of the linear loop.

$$\frac{A^2}{N_o B_n} = \frac{e^{\sigma_\phi^2}}{\sigma_\phi^2} \left[\frac{1 + 4\delta^2 e^{-\sigma_\phi^2/2}}{1 + 4\zeta^2} \right] \qquad (97)$$

B_n = noise bandwidth of loop for $\sigma_\phi^2 = 0$

ζ = damping ratio of loop

A graph of this equation is given in Figure 46 along with the results obtained using our digital simulation. The maximum difference between the digital simulation results and the quasi-linear approximation is about 20%. As the phase error increases,

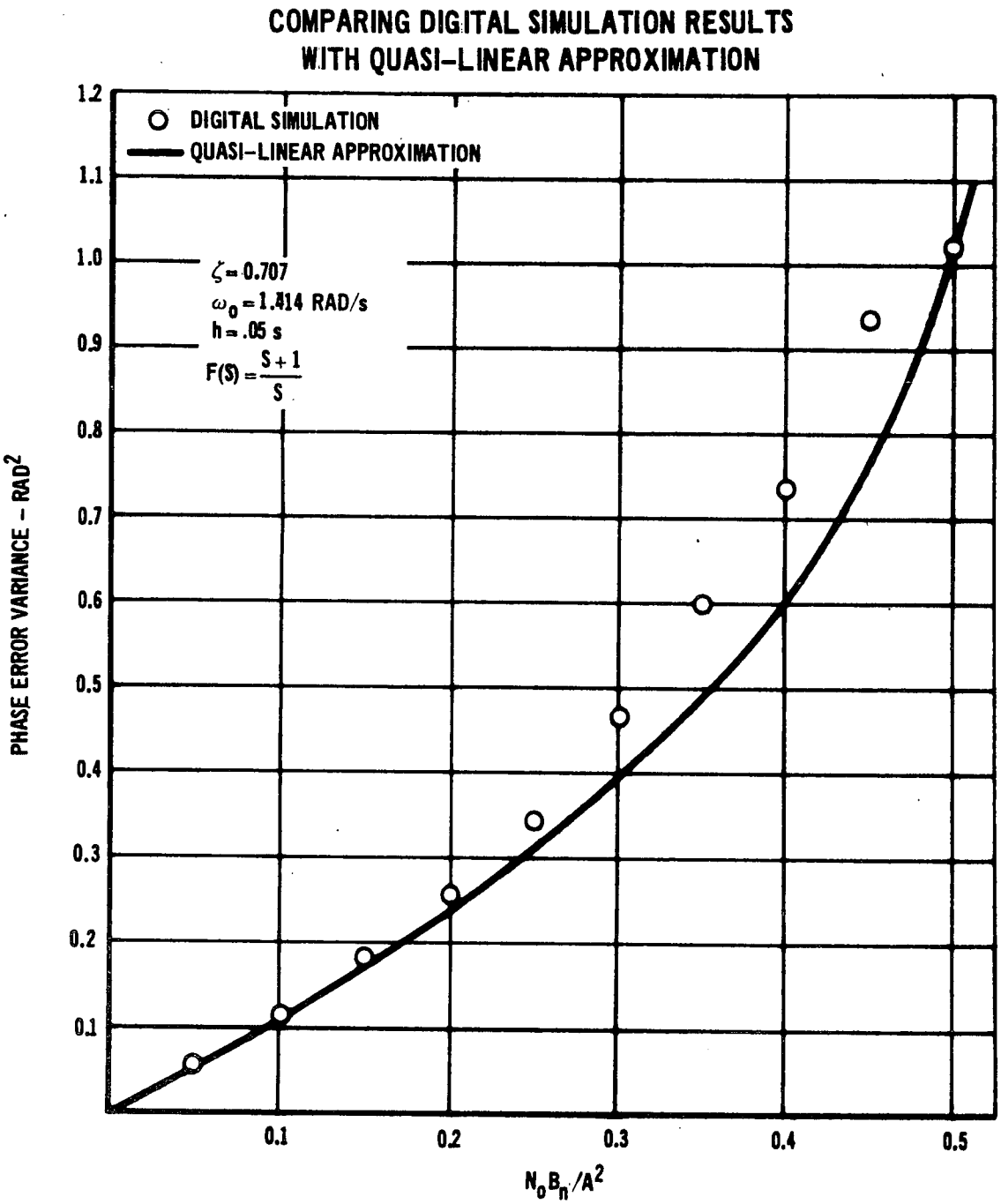

FIGURE 46

the Gaussian approximation no longer holds, and thus we would expect the curves to deviate as they do. A better method of validating the simulation results is to solve the Fokker-Plank equation of the phase-locked loop for the probability density of the phase error. The exact value of the phase error can then be determined as

a function of $(N_o B_n/A^2)$. However, no exact solution has been obtained for a second order loop with the filter $F(s) = \frac{s+a}{s}$. Therefore, we digitally simulated a phase-locked loop with the filter $F(s) = \frac{a}{s+a}$ for which a solution to the Fokker-Plank Equation can be obtained. Viterbi[6] and Lindsey and Tauseworthe[7] show that the probability density function of the phase error and the phase error variance will have the form given in Equations (98 - 100).

$$p(\phi) = \frac{e^{\alpha \cos \phi}}{2\pi I_o(\alpha)} \qquad -\pi < \phi < \pi \tag{98}$$

$$\alpha = \frac{A^2}{N_o B_n} \tag{99}$$

$$\sigma^2_\phi = \frac{\pi^2}{3} + 4 \sum_{n=1}^{\infty} \frac{(-1)^n I_n(\alpha)}{n \; I_o(\alpha)} \tag{100}$$

A graph of σ^2_ϕ versus $\frac{1}{\alpha}$ is shown in Figure 47. This plot shows that there is negligible error between the calculated and experimental results for a sample time of .05 seconds. For slower sampling rates, the curves will deviate slightly because of errors associated with the numerical technique. For $\alpha = 2$ the error between the two curves was 15% for a .1 second sampling interval and 30% for a .2 second interval.

2.8.2 Phase-Locked Loop Threshold

There are several different ways of defining the phase-locked loop threshold. The method employed by Viterbi[6] is to develop a model and then determine when the actual phase variance deviates by a specified amount from that predicted by the given model. In this section we will arbitrarily select the linear model as our standard and assume that the threshold occurs at the point where the error equals 50%. Using this criterion, the threshold noise-to-signal ratio, $N_o B_n/A^2$, is given for several different loop configurations and sampling intervals, h.

COMPARING DIGITAL SIMULATION RESULTS WITH FOKKER–PLANK SOLUTION

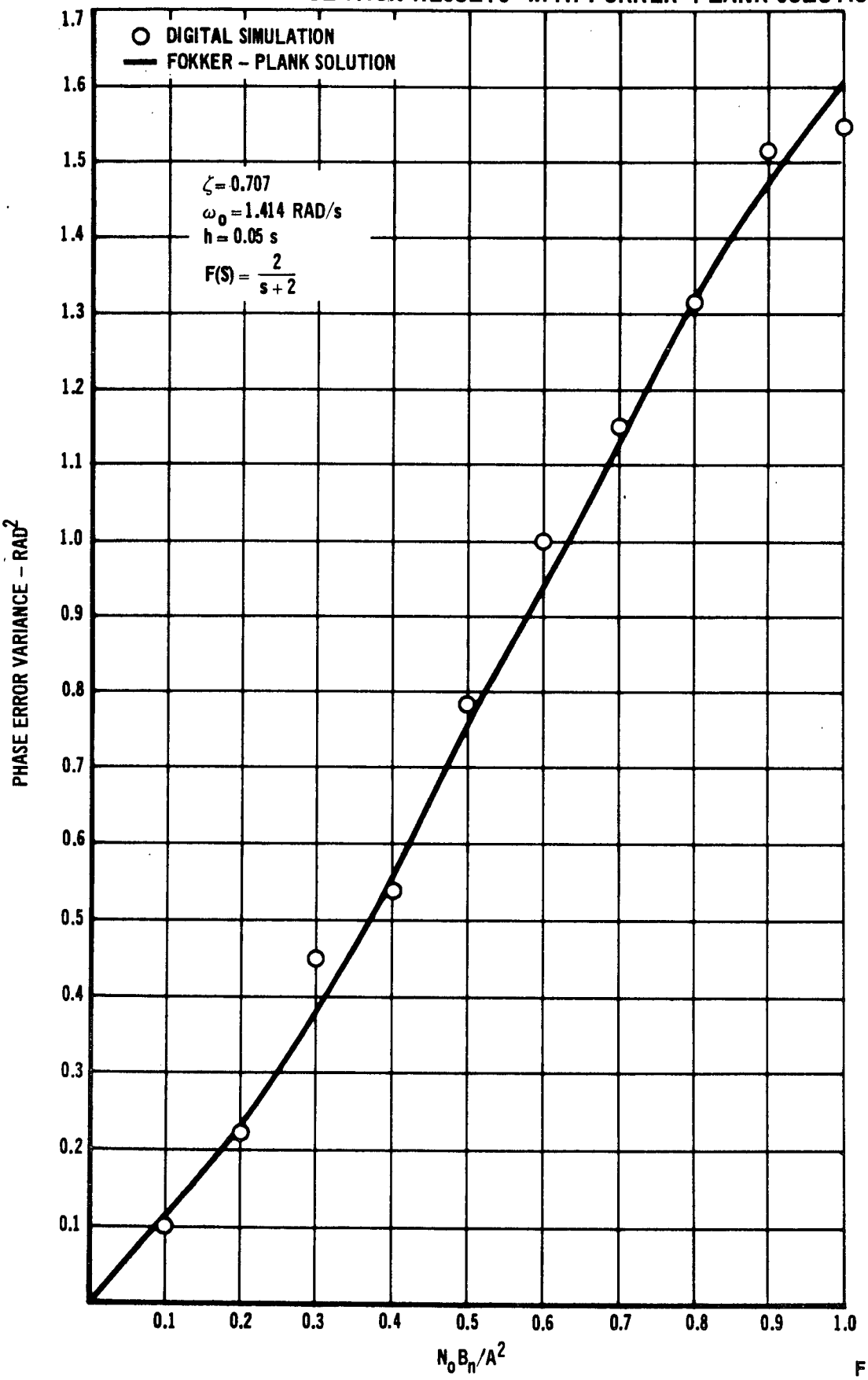

FIGURE 47

CONFIGURATION	h(sec)	$N_o B_n / A^2$
NO AGC	.05	.3
NO AGC	.1	.25
NO AGC	.2	.15
NO AGC	.4	.05
SAW TOOTH COMPARATOR	.2	.16
LIMITER	.2	.3

These results show that the threshold signal-to-noise ratio is increased as the sampling rate is increased. We have already shown that the results obtained with a sample interval of .05 seconds closely approximate the results obtained for an analog loop. For a .2 second sample interval, the threshold is increased by 3 db in going from the analog to the digitized loop.

2.8.3 Acquisition

We measured acquisition time as a function of the initial frequency offset and the results are presented in Section 2.6. Viterbi[8] determined an approximate formula for acquisition time for the second order phase-locked loop with filter $F(s) = \frac{s + a}{a}$, which is given in Equation (101).

$$t \approx \frac{1}{a} \left\{ \left[\frac{1}{AK} \frac{d\phi(o)}{dt} \right]^2 - \dot{\phi}_A^2 \right\} \qquad (101)$$

AK = loop gain

a = filter constant

$\dot{\phi}_A$ = limit of frequency lock = f $(\frac{a}{AK})$

The above approximation becomes increasingly crude as $\left[\frac{1}{AK} \frac{d\phi(o)}{dt} \right]$ approaches $\dot{\phi}_A$. A graph of this function is given in Figure 48 with the experimentally measured points superimposed. These results indicate that there is negligible difference between the digital simulation results and the theoretical values.

COMPARING MEASURED AND CALCULATED PULL-IN TIME

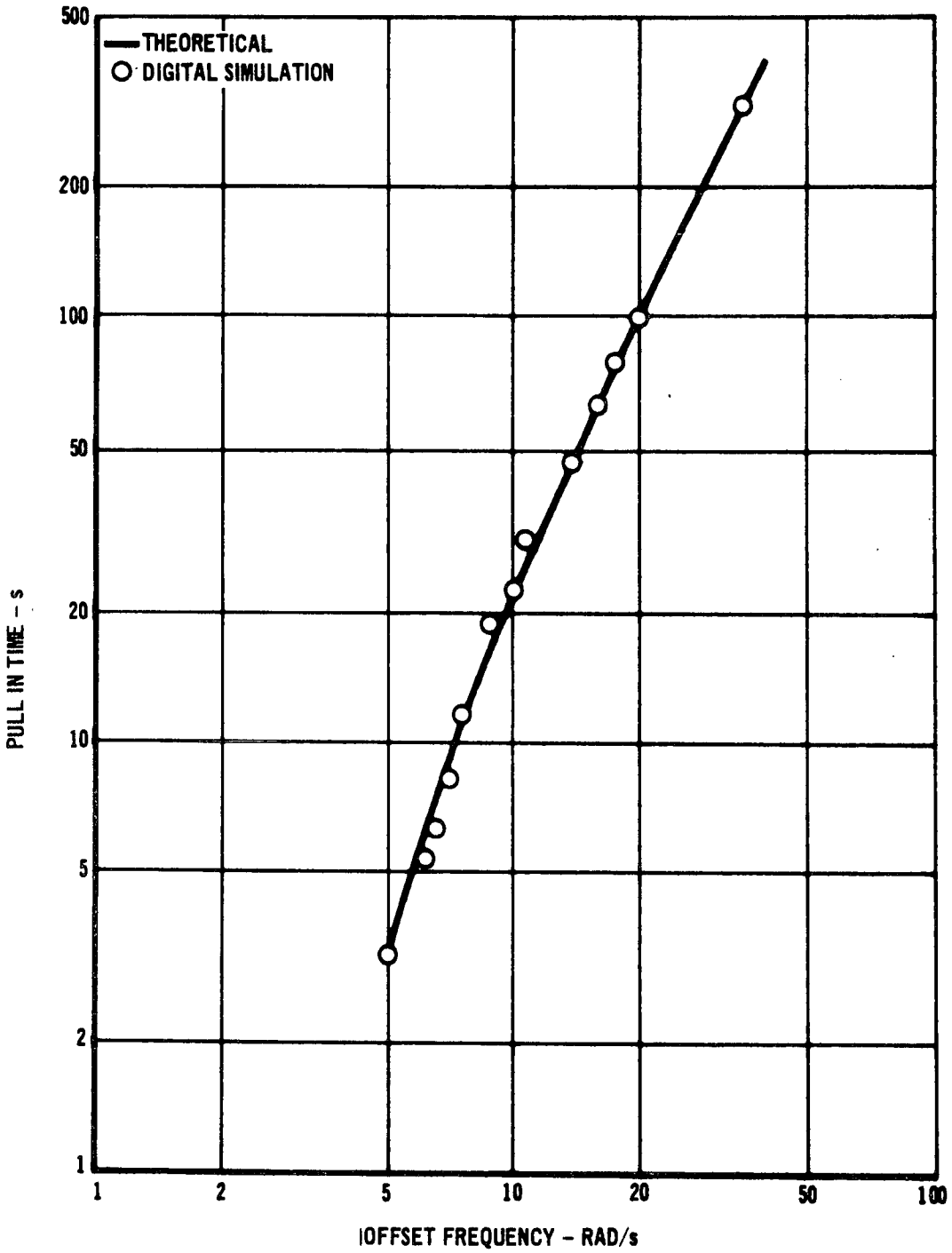

FIGURE 48

We also measured the probability of acquisition using a digital simulation of a system using a swept VCO. This technique is different from the one previously mentioned (Section 2.6.1) because the VCO sweep is not stopped when it is within the pull-in range of the loop. The loop must actually begin tracking the phase input which consists of a ramp of frequency. A graph of the results of this investigation is given in Figure 49 for an output signal-to-noise ratio of 10 dB. Also plotted on this graph are experimental results obtained by Frazier and Page [9] for an analog loop. They used a second order loop with a lead-lag filter of the form $F(s) = \frac{s+a}{s+b}$. However, since (a) is 1,000 times (b), this configuration

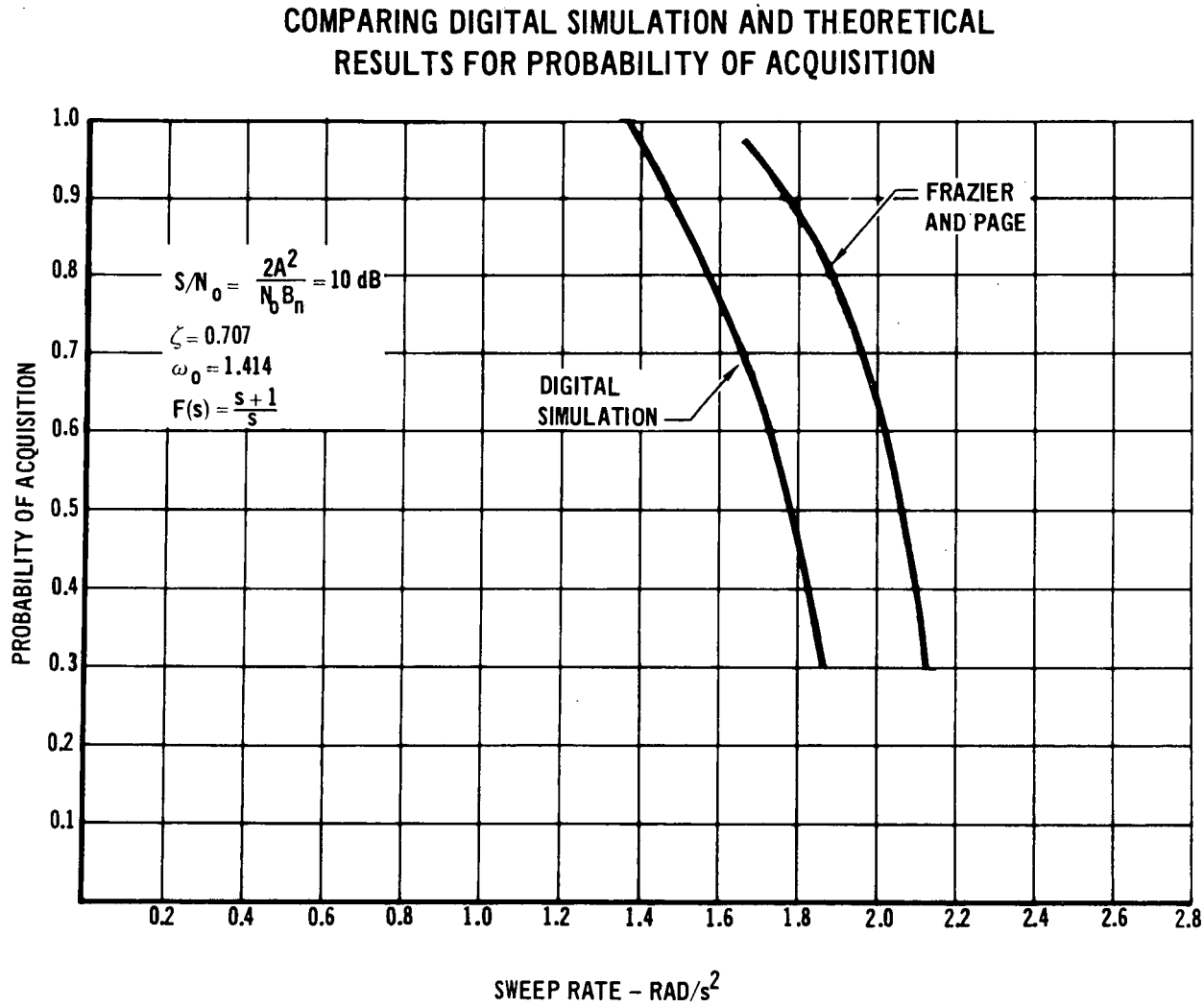

FIGURE 49

closely approximates that used in the digital simulation. The maximum error between the results for the digitized and the analog loops is 17%. This error is not significant when we consider the difficulty in determining whether acquisition has taken place and the fact that both results were experimentally obtained. The results for the digitized loop would also be closer to the analog results if the sampling rate was increased.

3. DEVELOPMENT OF DIGITIZED PSK RECEIVER

3.1 Synthesis of PSK Receiver Software

In Section 2. we studied techniques for synthesizing digital subsystems in general, and the phase-locked loop in particular. We applied these results in Section 3. to the development of a completely digital PSK receiver. Various solutions to the carrier and bit synchronization problem are compared on the basis of performance, speed, and complexity.

3.1.1 Sampling and A/D Conversion of Data

The first step in digital receiver design is the specification of a sampling technique. A brute force method would be to sample the noisy carrier at a rate which is fast enough to reproduce the carrier frequency. Digital logic and A/D converters, however, are not capable of operating at speeds compatible with typical carrier frequencies. For this reason the utility of the quadrature component signal sampling technique developed earlier in this report is of special importance in digital receiver design for narrowband binary PSK signals. With this technique the RF carrier is first heterodyned to a convenient IF frequency. There are two approaches to obtaining the quadrature components from the IF.

Quadrature Sampling

In one approach the quadrature components of the PSK carrier are generated by heterodyning the carrier with the best available estimate of the carrier and with a 90° phase shifted version of the carrier. Both of these products are then low pass filtered to eliminate the double-frequency terms (Figure 50a).

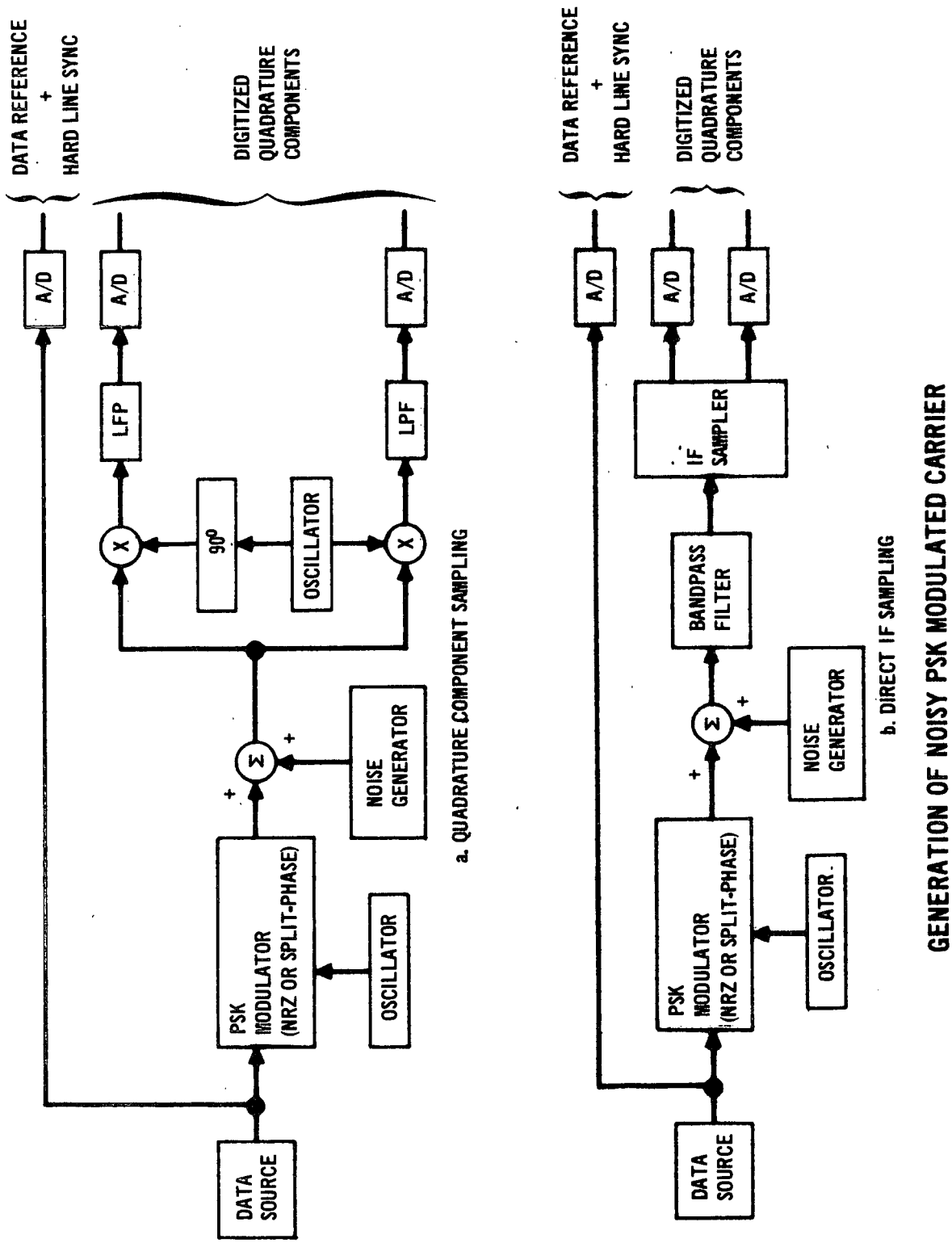

GENERATION OF NOISY PSK MODULATED CARRIER

Figure 50

The output of these filters are the quadrature components of the noisy PSK signal. Note that it is only necessary to sample the quadrature components at a rate consistent with the signal bandwidth. The technique is very efficient since it reduces the bandwidth and sampling rate to levels consistent with the information bandwidth and places the minimum possible demands on the A/D converter time resolution.

IF Sampling

This section describes the direct IF sampling approach (Figure 50b) and the usage of the ADCOM IF Sampler with the MDAC digital receiver.

The direct IF sampling technique generates a pair of quadrature samples by strobing a narrow aperture sampler at two instants of time separated by one-quarter of a period of the nominal IF (Figure 51). Denote the noisy PSK

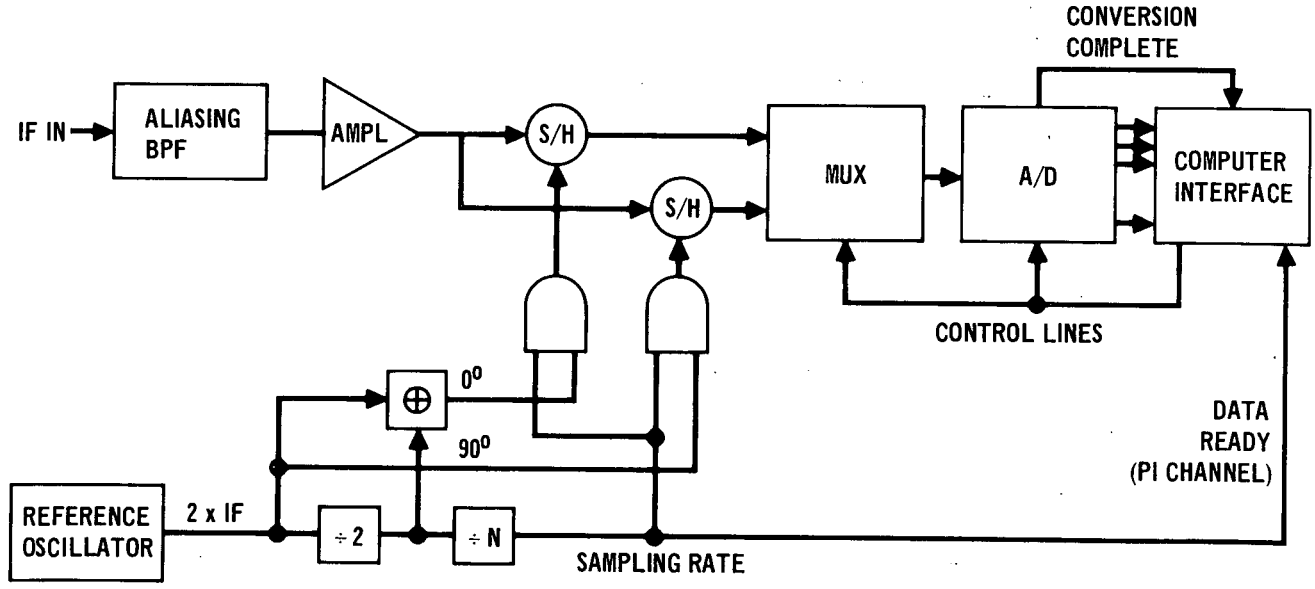

DIRECT IF SAMPLING AND A/D CONVERSION [10]

Figure 51

signal referred to the nominal IF frequency, ω_o, by Equation (102)

$$E(t) = A\, m(t) \sin\left[\omega_o t + \theta(t)\right] + n(t) \tag{102}$$

$$n(t) = n_1(t) \cos\left[\omega_o t + \theta(t)\right] + n_2(t) \sin\left[\omega_o t + \theta(t)\right] \tag{103}$$

$m(t)$ = modulation

In terms of its quadrature components, $x(t)$ and $y(t)$ defined in Equation (104) and Equation (105), the noisy signal can be represented as Equation (106).

$$x(t) = \left[A\, m(t) + n_2(t)\right] \cos\theta(t) - n_1(t) \sin\theta(t) \tag{104}$$

$$y(t) = \left[A\, m(t) + n_2(t)\right] \sin\theta(t) + n_1(t) \cos\theta(t) \tag{105}$$

$$E(t) = x(t) \sin\omega_o t + y(t) \cos\omega_o t \tag{106}$$

The first quadrature sample taken at $t_i = N\frac{2\pi}{\omega_o}$ is shown in Equation (107).

$$a_1 = E(t_i) = y(t_i) \tag{107}$$

The second quadrature sample taken at $t_i + \frac{\pi}{2\omega_o}$ is shown in Equation (108).

$$a_2 = E\left(t_i + \frac{\pi}{2\omega_o}\right) = x\left(t_i + \frac{\pi}{2\omega_o}\right) \tag{108}$$

$$a_2 \approx x(t_i) \tag{109}$$

Equation (109) follows because $m(t)$, $\theta(t)$, $n_1(t)$, and $n_2(t)$ are slowly varying compared to ω_o. Thus, a_1 and a_2 are the same quadrature samples that are obtained from the quadrature sampling technique.

The ADCOM IF Sampler is operable at three IF frequencies, 10 MHz, 1 MHz, and 1 KHz. For 1 KHz inputs the required 90° separation is achieved by operating each sample and hold with a repetition period of 256 μsec. The output of each sample and hold corresponds to samples spaced by 90° (i.e., 0°, 90°, 180°, 270°, ...) of an IF reference at $(4 \times 256)^{-1} \times 10^6 = 0.97$ KHz (Figure 52).

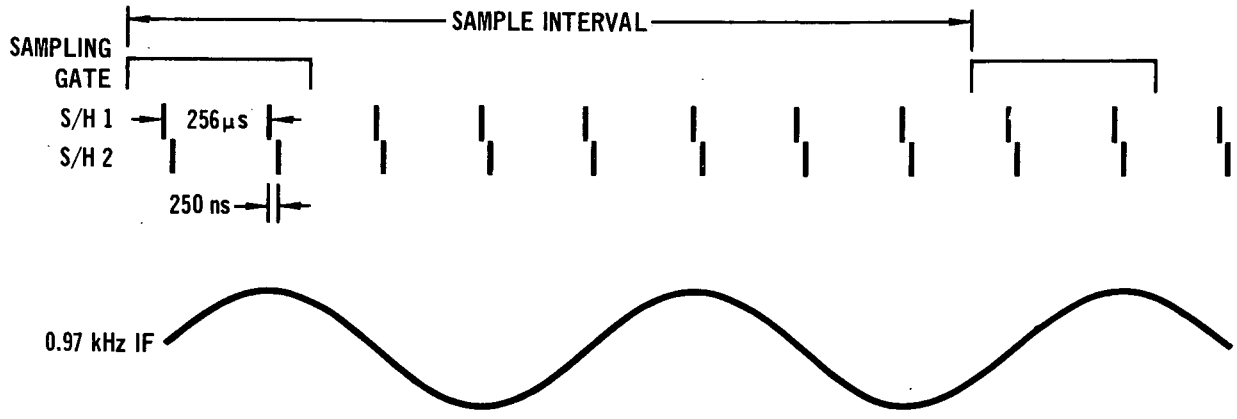

SAMPLE TIMING FOR 1 kHz OPERATION

Figure 52

The digital processor can change the effective sampling rate by discarding certain samples. For example, the first two samples from S/H 1 in Figure 52 are quadrature samples of 0.97 KHz IF. The digital processor fixes the interval between input samples of the quadrature components at 2.048 msec by discarding six samples from S/H 1 before accepting the ninth and tenth samples as the next pair of quadrature component samples.

The standard test parameters for the MDAC digital receiver were chosen to be a 244 Hz IF with a bit rate of 12.2 bits/second and a sample period of $\frac{1}{244}$ seconds (20 samples/bit). The ADCOM IF Sampler was adjusted so that the S/H's operate with a 1.024 msec period. The digital computer accepts four samples from the output of one sample and hold operating with a sample period of 1.024 msec. The first two samples are the quadrature components of the 244 Hz input signal (Figure 53). The remaining two samples are discarded.

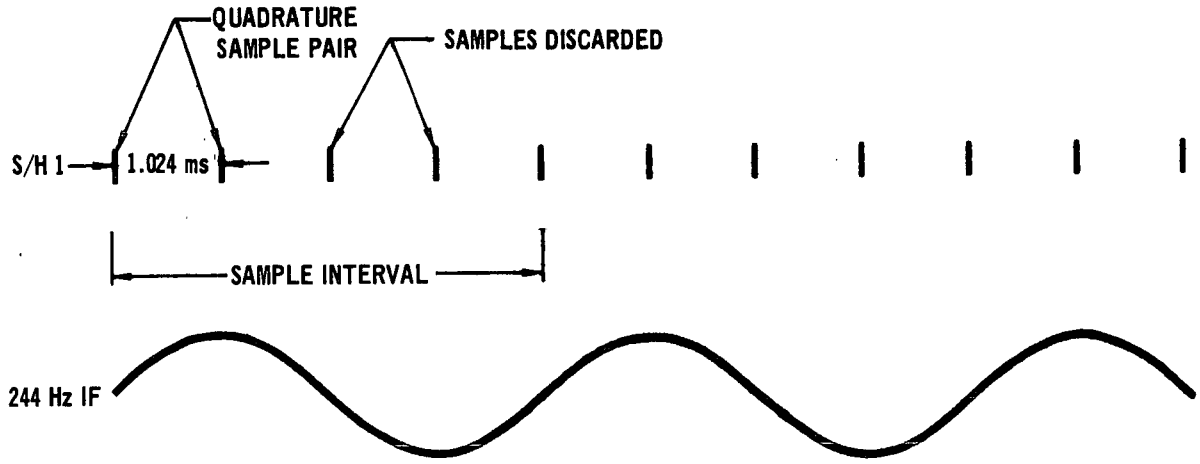

SAMPLE TIMING FOR 244 Hz OPERATION

Figure 53

For this sampling technique, there is one carrier cycle between successive quadrature sample pairs. Sampling with a noninteger number of carrier cycles between quadrature sample pairs introduces an apparent frequency offset at $\frac{d}{N+d}\,\omega_o$ rad/sec where N+d is the total number of carrier cycles between quadrature sample pairs. N is an integer and d is less than unity. The input signal to the digital receiver is then described by Equation (110) instead of Equation (102).

$$E(t) = A\,m(t)\,\sin\left[\omega_o t + \theta(t) + \frac{d}{N+d}\,\omega_o t\right] + n(t) \qquad (110)$$

When operating the MDAC digital receiver with a noninteger number of carrier cycles between sample pairs a frequency offset, $\frac{d}{N+d}\,\omega_o$ rad/sec is used as an initial condition in the Costas loop.

3.1.2 Rejection of DC Bias

In experimental evaluations of the digital receiver, we experienced difficulties with a DC bias at the output of the quadrature component generation circuitry. This bias appears to the Costas loop to be an interferring frequency component at the center frequency of the IF filter. If the bias is

large enough, the Costas loop will track the IF center frequency rather than the input signal frequency. We investigated both placing an analog high pass filter in the quadrature component circuitry and placing a digital high pass filter in the digital receiver. The most important trade-off between these techniques is the extra computation time associated with the digital implementation as opposed to the requirement of an added analog filter.

We first incorporated a digital high pass filter into the digital receiver as shown in Figure 54. Any DC bias in the quadrature components is eliminated

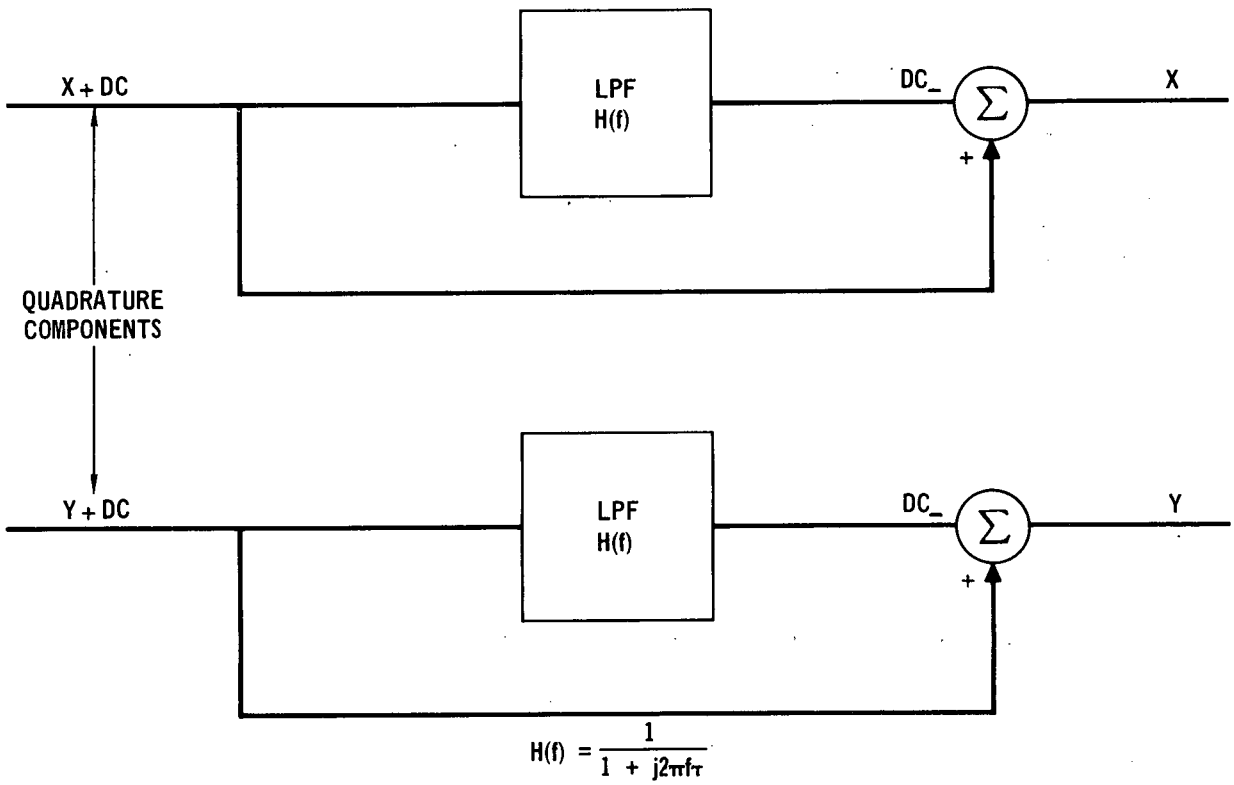

DC BIAS REMOVER

Figure 54

by first passing each quadrature component through a digital low pass filter and then subtracting the low pass filter output from the quadrature component. The Z transform implementation for a low pass filter whose transfer function is H(f) as defined in Figure 54 is given in Equation (111) where $E_i(n)$ is the n^{th} input sample, $E_o(n)$ is the n^{th} filter output, and h is the sample period.

$$E_o(n) = e^{-\frac{h}{\tau}} E_o(n-1) + (1 - e^{-\frac{h}{\tau}}) \; E_i(n-1) \tag{111}$$

for $\frac{h}{\tau} << 1$, $e^{-\frac{h}{\tau}} \approx 1 - \frac{h}{\tau}$

$$E_o(n) = E_o(n-1) - \frac{h}{\tau} \; E_o(n-1) + \frac{h}{\tau} \; E_i(n-1) \tag{112}$$

Equation (112) uses only two multiplications and two additions. One subtraction is then needed to remove the DC bias from the quadrature component. These operations do not add any significant computation time. We measured Costas loop tracking performance and phase error variance with the DC bias remover added and found no detrimental effect on receiver performance for τ = 200 bit periods. The digital high pass filter is easier to implement than an analog high pass filter and does not significantly increase computation time. For these reasons we chose the digital implementation.

3.1.3 Input Filter Design

Section 2.7.1 discussed the loss due to sampling or noise aliasing and showed that it was desirable to make the ratio of sampling rate to input bandwidth as large as possible. The input bandwidth is fixed by the bit rate and frequency instability. If all the input samples are passed through the entire digital receiver, the maximum sampling rate is determined by the maximum required computation time. However, one way to increase the effective sampling rate is to sample at a high rate, filter a group of these samples to

C2

produce one smoothed sample, and then process this one sample with the entire receiver. This is roughly equivalent to lowering the input filter bandwidth, but it is accomplished purely by digital means. The sampling loss is reduced due to the increase in the ratio of sampling rate to input bandwidth.

For instance, when operating at 244 Hz, the IF signal is sampled four times each carrier cycle (Figure 53). Normally, the first two samples are processed by the digital receiver and the remaining samples are discarded. In this section we use all of the input samples to obtain signal quadrature components.

Define the four samples in one sample interval as follows:

$$a_1 = y(t_1) \tag{113}$$

$$a_2 = x(t_1 + \frac{\pi}{2\omega o}) \approx x(t_1) \tag{114}$$

$$a_3 = y(t_1 + \frac{\pi}{\omega o}) \tag{115}$$

$$a_3 \approx -y(t_1) \tag{116}$$

$$a_4 = x(t_1 + \frac{3\pi}{2\omega o}) \tag{117}$$

$$a_4 \approx -x(t_1) \tag{118}$$

Equations (116) and (118) follow because $m(t)$, $\theta(t)$, $n_1(t)$, and $n_2(t)$ are slowly varying compared ω_o which has changed phase by 180°. One quadrature sample for the digital receiver is computed by low pass filtering a_1 and $-a_3$; the other by filtering a_2 and $-a_4$. We use the Z

transform implementation for a low pass filter discussed earlier in this report. The algorithm for filtering the input samples follows.

```
A(IDX)=input samples                    h   = step size = 2.048 sec.
Y     =quadrature component sample      τ   = low pass filter time constant
X     =quadrature component sample      CON = h/τ

QB= -1.0
Y =  0.0
X =  0.0
DO 930 IDX = 1, 3, 2
QB=QB
Y=Y-CON*Y+QB*CON*A(IDX)
930 X=X-CON*X+QB*CON*A(IDX+1)
```

3.1.4 Generation of PSK Modulated Noisy Carrier

A data stream, for simulation purposes, was generated by a pseudo-random generator with variable length sequences. The data (NRZ or split-phase) was phase modulated on a carrier, and wideband noise with a known noise density was added to the carrier. For quadrature component sampling, the noisy carrier was then multiplied by an estimate of the carrier frequency and by a 90° phase shifted version. Both products were then low-pass filtered to eliminate the double-frequency terms (Figure 50a). The outputs of the low pass filters are the quadrature components of the noisy PSK carrier. The quadrature components and a third channel, which contains the data stream and the hard-line bit-synchronization pulses, are then A/D converted. For direct IF sampling, the noisy carrier was bandpass filtered and processed by the ADCOM IF Sampler (Figure 50b). The outputs of the IF Sampler are the quadrature samples of the noisy PSK carrier. The quadrature samples and a third channel, which contains the data stream and the hard-line bit synchronization pulses, are then A/D converted. As in the unmodulated

carrier generation in Section 2.7, PSK carrier data was also generated by purely digital means to provide a check case for the bit error rates determined from the analog generated data.

By using digitally generated data, effects due to electronic instabilities in the A/D converter, noise generators, and the carrier oscillator are eliminated. The effects of different truncation levels were modeled in the CDC 6600 by internally reducing the number of bits/word to give a specified truncation error before entering the tracking loop. Figure 55 is a block diagram of the digital data generation subroutine which was used for generating the noisy PSK carrier.

3.1.5 Study of Carrier Synchronization

In order to demodulate PSK, it is necessary to estimate the phase and frequency of the subcarrier with as little error as possible. If the information process contains a residual component of sufficient strength at the subcarrier frequency, this component may be considered as a carrier and tracked as previously discussed. Several methods have been proposed for generating a reference subcarrier from the received signal when the residual subcarrier component is not available.

We will first consider the various analog carrier tracking techniques and then derive their digital equivalents. The squaring loop and the Costas loop which are common analog carrier tracking devices are shown in Figures 56 and 57. The analog Costas loop and squaring loop, although somewhat different in structure, are mathematically equivalent assuming that the effect of the presquaring bandpass filter is ignored. Neither method requires bit synchronization, but both are subject to 180 degree phase ambiguities. Since the two techniques are ideally mathematically equivalent, the digital Costas and squaring loop are identical. The digital Costas loop is developed later in this section.

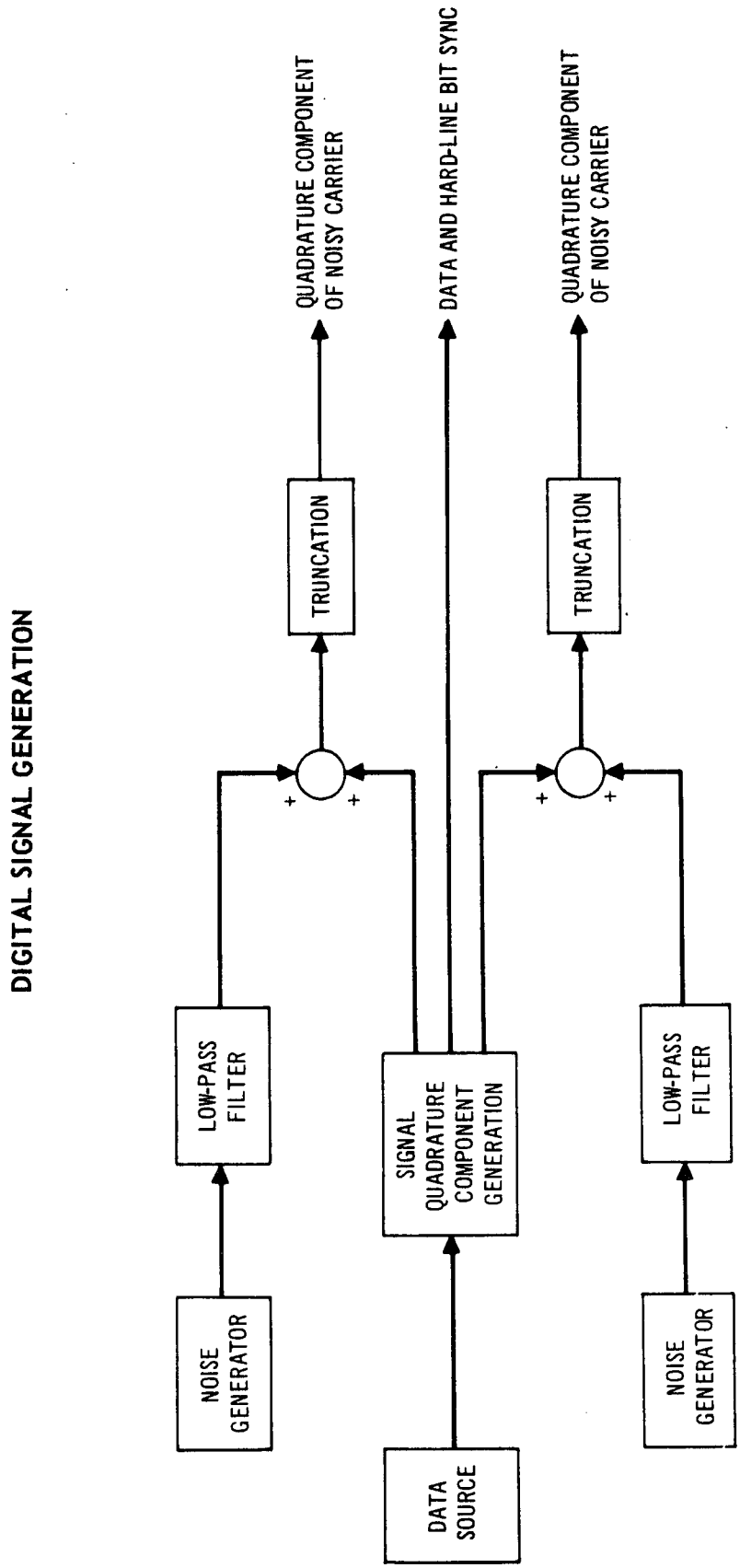
DIGITAL SIGNAL GENERATION
QUADRATURE COMPONENT OF NOISY CARRIER
DATA AND HARD-LINE BIT SYNC
QUADRATURE COMPONENT OF NOISY CARRIER
TRUNCATION
TRUNCATION
+
+
+
+
LOW-PASS FILTER
SIGNAL QUADRATURE COMPONENT GENERATION
LOW-PASS FILTER
NOISE GENERATOR
DATA SOURCE
NOISE GENERATOR

Figure 55

THE SQUARING LOOP FOR PHASE – TRACKING A BINARY – MODULATED SUPPRESSED – CARRIER INPUT

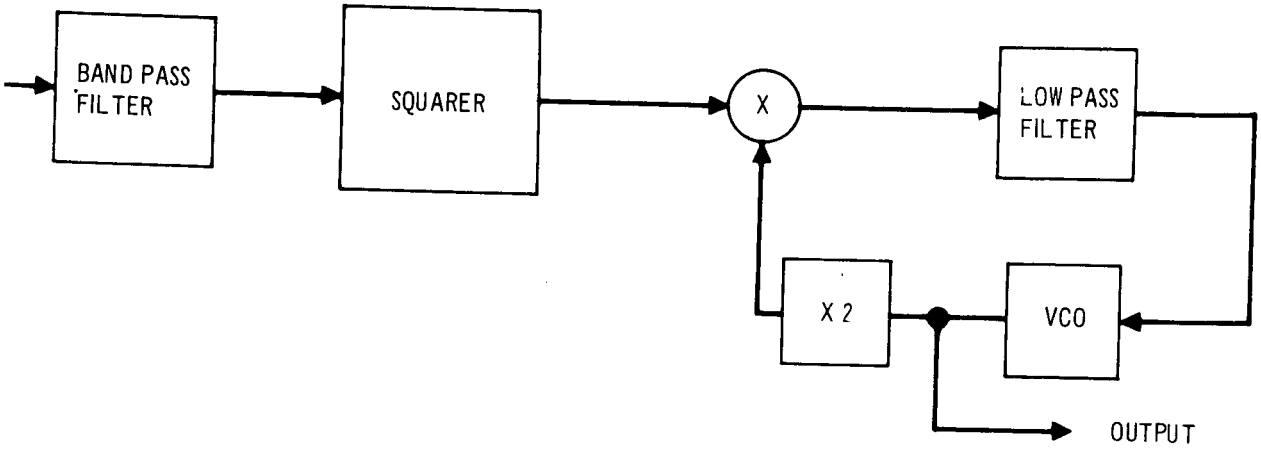

Figure 56

THE COSTAS LOOP FOR PHASE – TRACKING A BINARY PSK CARRIER

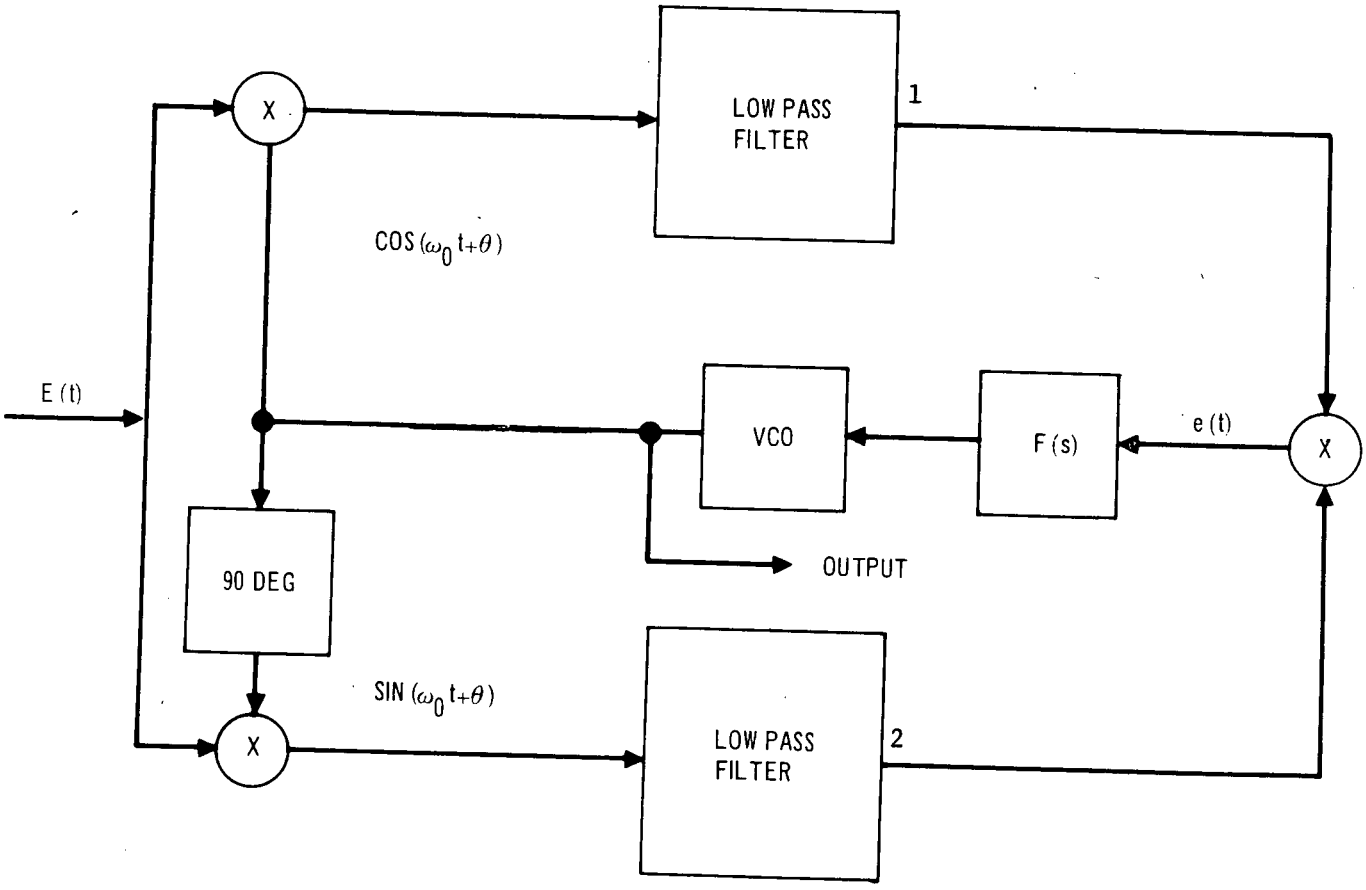

Figure 57

A third technique which has received considerable attention in the literature is the delayed decision feedback or the decision-directed carrier tracking. This method estimates the data bit and feeds this value back to be multiplied by a delayed version of the carrier (Figure 58). For

DECISION-ORIENTED CARRIER TRACKING

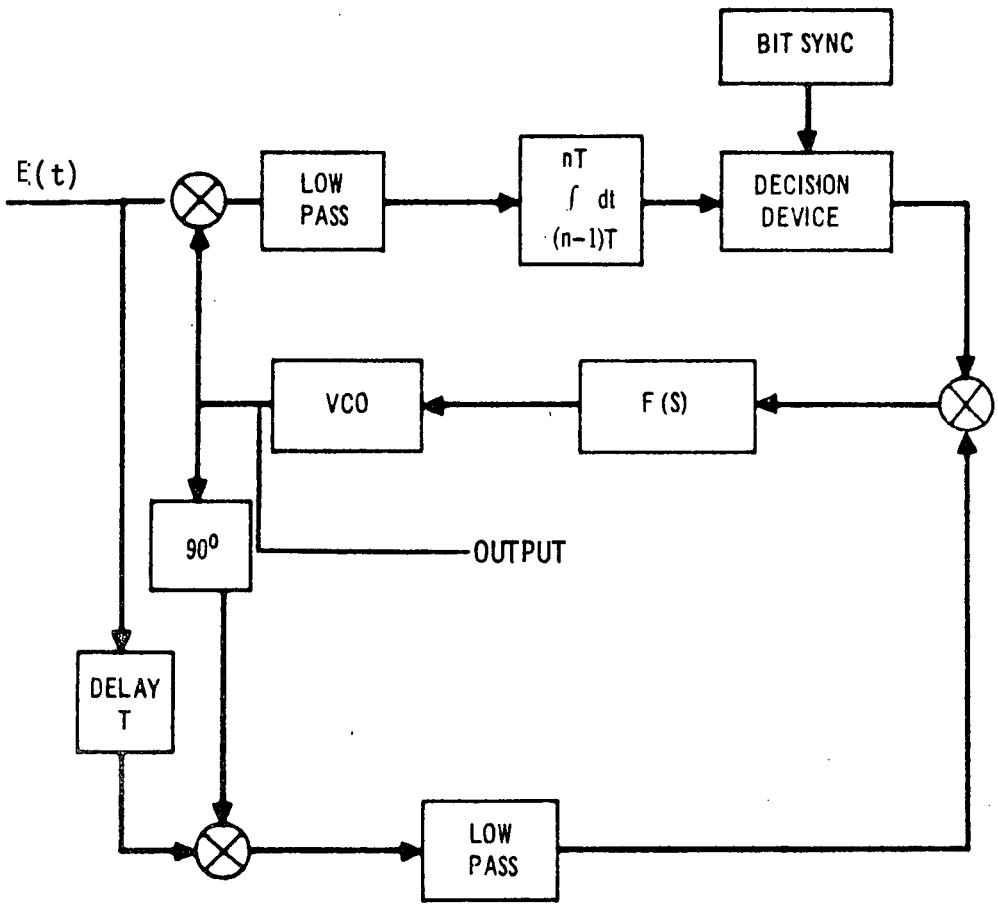

FIGURE 58

this technique good bit-synchronization is required for proper performance. Unfortunately, most bit synchronizers also require good carrier synchronization to work. Thus a circular problem results and careful attention must be given to the interrelationship between bit and carrier tracking.

The digital decision-directed carrier tracking loop is more complex than the Costas loop in that a shift register must be provided to obtain a one bit-period time delay. A decision-directed carrier tracking loop also tracks with phase offset equal to $\omega_o T$ radians where ω_o is the IF frequency and T is the bit period. This requires that the bit period and carrier frequency be accurately known or that the modulation be synchronized to the carrier phase. Probability of error with our digital Costas loop and Decision Feedback loop is shown in Figure 59. Note that the slight performance enhancement obtained by the digital decision-directed carrier tracking loop does not appear sufficient to outweigh the previously discussed disadvantages. Also the digital Costas loop gives tracking performance which is comparable to the other techniques, but yet is considerably simpler to instrument. Using the Costas loop also separates the bit and carrier synchronization algorithms which simplifies acquisition. Thus, the Costas loop appears to be the best analog technique for digital implementation.

Synthesis of Carrier Synchronization Algorithm

The differential equations describing the operation of the Costas loop in terms of the quadrature component samples are derived in this section. The set of digital algorithms for carrier synchronization consists of a numerical solution of these equations.

The input to the Costas loop, $E(t) = x(t)\sin \omega_o t + y(t)\cos \omega_o t$, was defined in Section 3.1.1 in terms of the quadrature components. The lowpass filters in the Costas loop are assumed to have the following effects at points (1) and (2) in Figure 57:

BIT ERROR PROBABILITY FOR COSTAS LOOP AND DECISION FEEDBACK

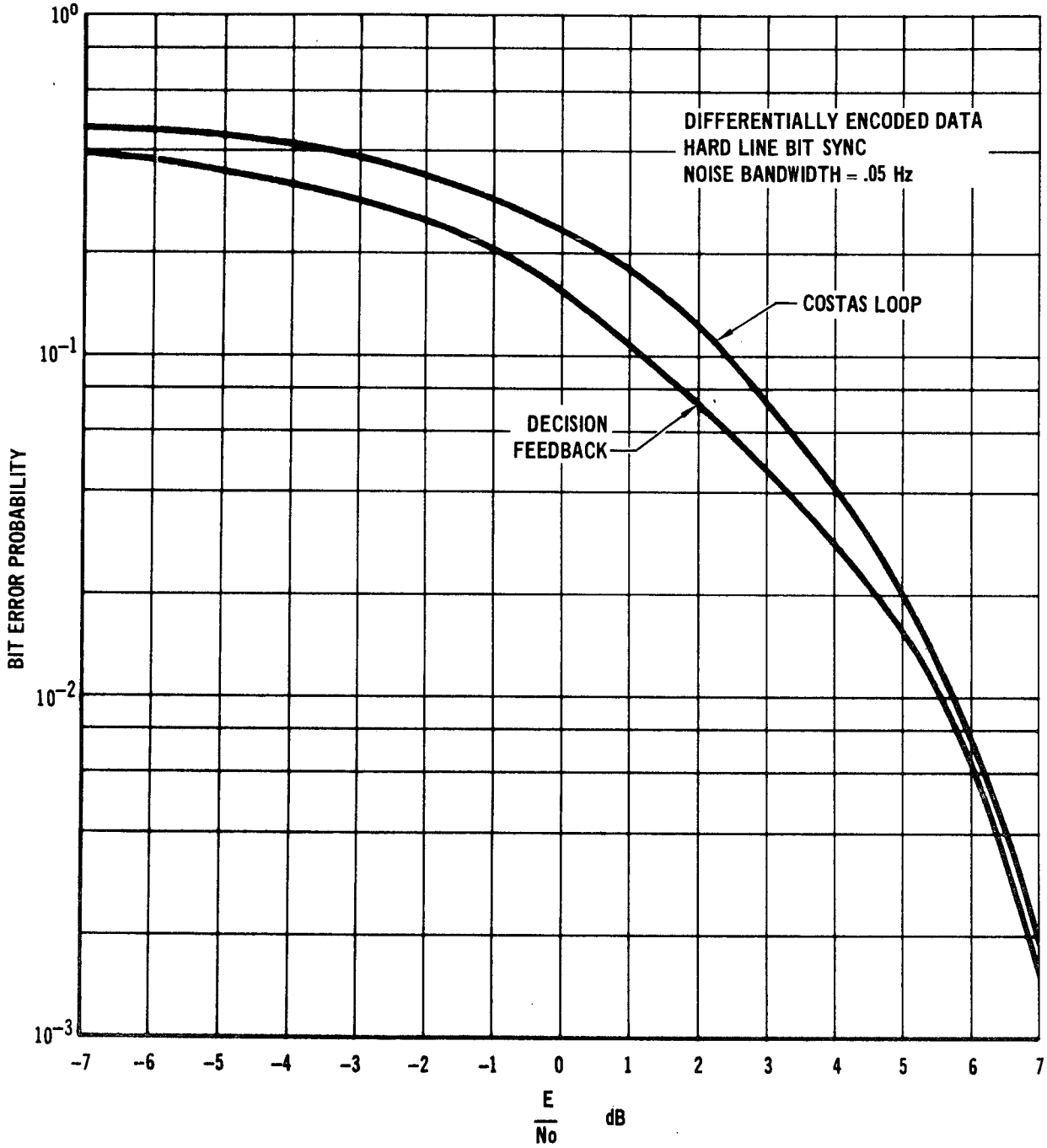

Figure 59

(1) The low frequency components of the signal and noise are passed without distortion;

(2) All double frequency components are completely rejected.

Let the output of the VCO be $\cos(\omega_o t + \hat{\theta}(t))$ where $\omega_o/2\pi$ is the free running frequency of the VCO in Hz, $\hat{\theta}(t)$ is the Costas loop estimate of the unknown phase $\theta(t)$. Using these assumptions the voltages at 1 and 2 can be expressed in terms of the quadrature components as

$$V_1(t) = -\frac{1}{2} x \sin \hat{\theta}(t) + \frac{1}{2} y \cos \hat{\theta}(t) \tag{119}$$

$$V_2(t) = \frac{1}{2} x \cos \hat{\theta}(t) + \frac{1}{2} y \sin \hat{\theta}(t) \tag{120}$$

and the voltage e(t) is

$$e(t) = \frac{1}{8} (y^2 - x^2) \sin 2\hat{\theta}(t) + xy \cos 2\hat{\theta}(t) \tag{121}$$

The differential equation describing the loop is

$$\frac{d\hat{\theta}(t)}{dt} = KF(p)e(t) \tag{122}$$

where

$p = \frac{d}{dt}$ is the differential operator,

K = multiplying constant for the VCO, and

F(p) = transfer function for the loop filter.

Because the Costas loop must extract a reference in the presence of frequency detuning, the loop filter F(s) is chosen for a second-order active loop.

$$F(s) = \frac{s+a}{s} \tag{123}$$

The Costas loop characteristics are defined in terms of the damping factor ζ, the undamped natural frequency ω_n, and the noise equivalent bandwidth B_N of the linearized loop. These parameters can be defined in terms of various loop and signal constants.

A block diagram of the linearized Costas loop is given in Figure 60, where the input to the Costas loop is assumed to be signal only.

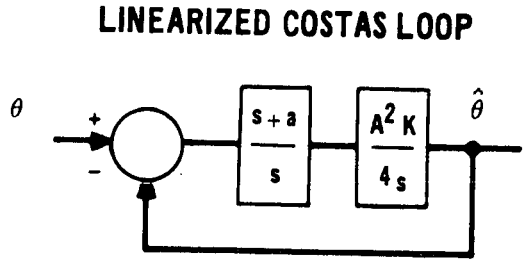

FIGURE 60

The loop transfer function can be determined as shown in Equation (124).

$$\frac{\hat{\theta}(s)}{\theta(s)} = \frac{\frac{A^2K}{4}s + \frac{A^2Ka}{4}}{s^2 + \frac{A^2K}{4}s + \frac{A^2Ka}{4}} \tag{124}$$

The transfer function can be written in the standard second order form.

$$\frac{\hat{\theta}(s)}{\theta(s)} = \frac{2\zeta\omega_n s + \omega_n^2}{s^2 + 2\zeta\omega_n s + \omega_n^2} \tag{125}$$

where $$K = \frac{85\omega_n}{A^2} \tag{126}$$

and $$a = \frac{\omega_n}{2\zeta} \tag{127}$$

The damping factor ζ is usually defined as $\frac{\sqrt{2}}{2}$ in Costas loops and that value will be used in the digital Costas loop. The undamped natural frequency ω_n is defined in terms of the damping factor and the loop noise bandwidth B_N.

$$\omega_n = \frac{8\zeta B_n}{4\zeta^2 + 1} \tag{128}$$

The loop noise bandwidth B_N is defined from linear phase-locked loop theory as

$$B_N = \frac{1}{2} \int_{-\infty}^{\infty} \frac{\hat{\theta}(f)}{\theta(f)} \, df \tag{129}$$

where $\frac{\hat{\theta}(f)}{\theta(f)}$ is defined by Equation (124) with $s = j2\pi f$.

If the constant amplitude factor A and the loop noise bandwidth B_N are known, the Costas loop gain K and loop filter constant a can be determined. It is convenient to describe the Costas loop in terms of its linear parameters even when it is operating in the nonlinear range. The Costas loop can be completely described in the time domain by substituting Equations (121) and (123) into (122)

$$\frac{d^2\hat{\theta}(t)}{dt^2} = Ka \left[\frac{1}{8}(y^2-x^2)\sin 2\hat{\theta}(t) + \frac{1}{4} xy \cos 2\hat{\theta}(t)\right] + K \frac{d}{dt}\left[\frac{1}{8}(y^2-x^2)\sin 2\hat{\theta}(t) + \frac{1}{4} xy \cos 2\hat{\theta}(t)\right] \tag{130}$$

The real time solution of Equation (130), where x and y are the signal quadrature components, is the real time estimate of the carrier phase which is mathematically equivalent to that of an ideal Costas loop.

To obtain the real time solution for $\hat{\theta}(t)$, Equation (130) can be represented by two first order simultaneous differential equations. Let $X1 = \hat{\theta}$ and X2 be a dummy variable, Equations (131) and (132) are equivalent to Equation (130).

$$\frac{d}{dt} X1 = X2 + K \left[\frac{1}{8}(y^2-x^2) \sin 2X1 + \frac{1}{4} xy \cos 2X1\right] \tag{131}$$

$$\frac{d}{dt} X2 = Ka \left[\frac{1}{8}(y^2-x^2) \sin 2X1 + \frac{1}{4} xy \cos 2X1\right] \tag{132}$$

The real time numerical solution of Equations (131) and (132) is the digital equivalent of the analog Costas loop.

A very simple numerical integration routine must be used to solve Equations (131) and (132) because all signal processing in the digital receiver is done in real time. Consequently, very complex integration routines that involve higher order derivatives like Taylor's algorithm [1] are not applicable. The Runge-Kutta method of order [1] is often used in the numerical integration of differential equations. This method requires four derivative evaluations per step. For real time calculations the computation time necessary for four derivative evaluations makes the Runge-Kutta method impractical. To satisfy the requirement for the least number of computations per step, Euler's method [1] was chosen. This method requires a small step size or high sampling rate, but uses only one derivative evaluation per step. In general, Euler's method for the solution of the differential equation

$$b' = f(a,b) \tag{133}$$

is $$b_n = b_{n-1} + hf(a_{n-1}, b_{n-1}) \tag{134}$$

where h is the step size.

The solution of the Costas loop equation by Euler's method where H is the sample interval is given in Equations (135) and (136).

$$X1_n = X1_{n-1} + H\left[X2_{n-1} + K\left[\frac{1}{8}(Y^2_{n-1} - X^2_{n-1})\sin 2X1_{n-1} + \frac{1}{4} X_{n-1}Y_{n-1}\cos 2X1_{n-1}\right]\right. \tag{135}$$

$$X2_n = X2_{n-1} + H\left\{Ka\left[\frac{1}{8} Y^2_{n-1} - X^2_{n-1}\right)\sin 2X1_{n-1} + \frac{1}{4} X_{n-1} Y_{n-1} \cos 2X1_{n-1}\right] \tag{136}$$

Equations (137) and (138) are difference equations for the Costas loop phase estimate and can be solved in real time on a digital computer. The computer algorithm for the Costas loop follows:

```
H = Sample Interval
DK = H*K
CK = H*K*a
X1 IS COSTAS PHASE ESTIMATE
X2 IS A DUMMY VARIABLE
ADC(1) AND ADC(2) ARE THE DIGITIZED QUADRATURE COMPONENTS

X = ADC(1)
Y = ADC(2)
TEMP = (Y**2 - X**2) *SIN(2*X1)/8.
       +X*Y*COS(2.*X1)/4.
X1 = X1 + H*X2 + TEMP*DK
X2 = X2 + TEMP*CK
```

The real time phase estimate from the digital Costas loop is used to establish a coherent reference for the cross-correlation or matched filtered detection process. The receiver cross-correlation operation is performed by a multiplier-integrator combination that multiplies the signal with the coherent reference and integrates over a bit period. The correlator output C is given by Equation (137).

$$C = \int_{nT}^{(n+1)T} E(t) \sin (\omega_o t + \hat{\theta}(t))\, dt \qquad (137)$$

where T is a bit period. Since the integration in the correlator averages out the double frequency terms, Equation (137) can be expressed in terms of the quadrature components as Equation (138).

$$C = \int_{nT}^{(n+1)T} \frac{1}{2} (x \cos\hat{\theta}(t) + y \sin\hat{\theta}(t))\, dt \qquad (138)$$

The digital correlator output is computed by performing the integration using the quadrature components and the phase estimate from the digital Costas loop. A bit decision is made by determining sgn[C]. The timing

command to make a decision on the correlator must be supplied from the bit synchronization algorithm. The digital algorithm for the correlator, performed using Euler's method is Equation (139).

$$C_n = C_{n-1} + H\left[\frac{1}{2}\left(X_{n-1}\cos\ Xl_{n-1} + Y_{n-1}\sin Xl_{n-1}\right)\right] \tag{139}$$

3.1.6 Automatic Gain Control

Earlier in this report we discussed two AGC techniques for use with a phase-locked loop. In the first approach we placed a bandpass limiter at the input of the phase-locked loop. In the second method we utilized a closed loop AGC preceeding the phase-locked loop. We chose the bandpass limiter as the preferred method for use with a phase-locked loop because of its simplicity and the small computation time required. In addition, this technique will correct amplitude variations instantaneously. In this section we will apply the limiter to our digital receiver to provide AGC for the Costas loop.

We incorporated the bandpass limiter into the Costas loop as we did in the phase-locked loop in Section 2.5.1. With a bandpass limiter the voltage e(t) (Figure 57) is Equation (140).

$$e(t) = \frac{1}{8}\frac{y^2 - x^2}{x^2 + y^2}\sin 2\hat{\theta}(t) + \frac{1}{4}\frac{xy}{x^2 + y^2}\cos 2\hat{\theta}(t) \tag{140}$$

The Costas loop equation with a bandpass limiter is Equation (141).

$$\frac{d^2\hat{\theta}(t)}{dt} = Ka\left[\frac{1}{8}\frac{y^2 - x^2}{x^2 + y^2}\sin 2\hat{\theta}(t) + \frac{1}{4}\frac{xy}{x^2 + y^2}\cos 2\hat{\theta}(t)\right] \tag{141}$$

$$+K\frac{d}{dt}\left[\frac{1}{8}\frac{y^2 - x^2}{x^2 + y^2}\sin 2\hat{\theta}(t) + \frac{1}{4}\frac{xy}{x^2 + y^2}\cos 2\hat{\theta}(t)\right]$$

To obtain the real time solution for $\hat{\theta}(t)$, Equation (141) can be represented by two first order differential equations. Let $X1 = \hat{\theta}$ and X2 be a dummy variable, Equations (142) and (143) are equivalent to Equation (141).

$$\frac{d}{dt} X1 = X2 + K\left[\frac{1}{8} \frac{y^2 - x^2}{x^2 + y^2} \sin 2X1 + \frac{1}{4} xy \cos 2X1\right] \quad (142)$$

$$\frac{d}{dt} X2 = Ka \left[\frac{1}{8} \frac{y^2 - x^2}{x^2 + y^2} \sin 2X1 + \frac{1}{4} xy \cos 2X1\right] \quad (143)$$

The real time numerical solution of Equations (142) and (143) is the digital equivalent of the analog Costas loop with a bandpass limiter. The numerical solution of Equations (142) and (143) using Euler's method where H is the step size, is given in Equations (144) and (145)

$$X2_n = X1_{n-1} + H\left[X2_{n-1} + K\left[\frac{1}{8} \frac{y^2_{n-1} - x^2_{n-1}}{x^2_{n-1} + y^2_{n-1}} \sin 2X1_{n-1} + \frac{1}{4} \frac{x_{n-1} y_{n-1}}{x^2_{n-1} + y^2_{n-1}} \cos 2X1_{n-1}\right]\right] \quad (144$$

$$X2_n = X2_{n-1} + H\left[\frac{1}{8} \frac{y^2_{n-1} - x^2_{n-1}}{x^2_{n-1} + y^2_{n-1}} \sin 2X1_{n-1} + \frac{1}{4} \frac{x_{n-1} y_{n-1}}{xn-1 + y^2_{n-1}} \cos 2X1_{n-1}\right] \quad (145$$

The computer algorithm for the Costas loop with a bandpass limiter follows.

```
H = Sample Interval
DK = H*K
CK = H*K*a
X1 IS COSTAS PHASE ESTIMATE
X2 IS A DUMMY VARIABLE
ADC(1) AND ADC(2) ARE THE DIGITIZED QUADRATURE COMPONENTS

X = ADC(1)
Y = ADC(2)
TEMP = (Y**2 - X**2) *SIN (2.*X1)/(X**2 + Y**2)/8.
       + X*Y*COS(2.*X1 /(X**2 +Y**2)/4.
X1 = X1 + H**2 + TEMP*DK
X2 = X2 + TEMP*CK
```

A graph showing the output phase variance as a function of the input noise spectral density for the Costas loop with, and without, a limiter is shown in Figure 61. This curve shows that the phase variance is

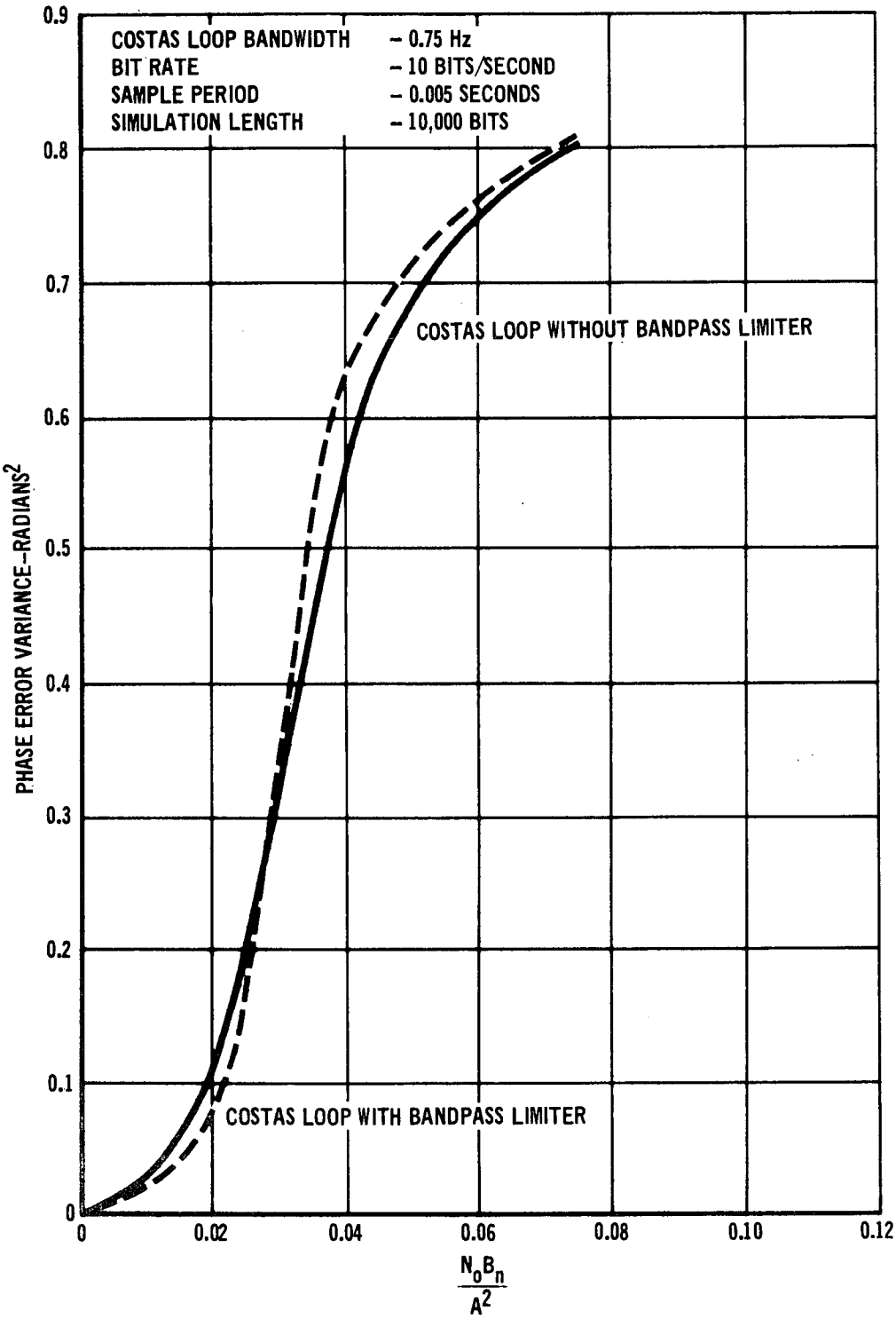
COSTAS LOOP BANDWIDTH – 0.75 Hz
BIT RATE – 10 BITS/SECOND
SAMPLE PERIOD – 0.005 SECONDS
SIMULATION LENGTH – 10,000 BITS
COSTAS LOOP WITHOUT BANDPASS LIMITER
COSTAS LOOP WITH BANDPASS LIMITER
PHASE ERROR VARIANCE–RADIANS^2
0.9
0.8
0.7
0.6
0.5
0.4
0.3
0.2
0.1
0
0
0.02
0.04
0.06
0.08
0.10
0.12
$\frac{N_0 B_n}{A^2}$
PHASE ERROR VARIANCE

Figure 61

nearly identical for both cases. Addition of the bandpass limiter does not degrade Costas loop operation, and allows the bandwidth of the Costas loop to be set independently of the input signal amplitude.

3.1.7 Study of Bit Synchronization

One of the objectives of this study is to determine an "optimum" bit synchronizer for use with the MDAC digital receiver. This bit synchronizer must also be "easily realizable" on a digital computer and must adapt to relatively large bit rate variations.

To develop an "optimum" bit synchronizer, a model of the input data stream and a criterion of optimality is required. The model of the input data stream must specify the symbol waveforms, the symbol occurrence statistics and the statistics of the timing jitter. Previously, using nonlinear filter theory, we [11, 12, 13] synthesized a bit synchronizer and detector which was optimum in the sense of minimum bit error probability for the case of a constant known bit rate, but an unknown phase. Other authors [14, 15, 16] have considered slightly less general situations using Bayesian or maximum likelihood estimation and have obtained somewhat similar results. Although none of these authors directly consider the case of varying or unknown bit rate, this case can also be treated by a conceptually straightforward generalization of the previous results.

The second constraint on our bit synchronizer is that it be "easily realizable" on the digital computer. In a certain sense, any system which can be mathematically defined can be implemented essentially exactly using a digital computer and at least approximately using analog hardware. The optimum bit synchronizer defined in reference 11 is certainly physically realizable in the classical mathematical sense in that it does not require operations on data

from future time. However, from a practical hardware implementation viewpoint it is not realizable for normal bit rates. Even assuming a known bit rate of 1/T bits/seconds, the implementation of the optimum bit synchronizer would require a bank of 4M correlators (i.e., matched filters) to achieve a minimum timing error of T/M seconds. If the bit rate is also unknown, the number of correlators required is increased by another factor which is related to the uncertainty in bit rate.

A normal analog bit synchronizer at high signal-to-noise ratios will operate with a timing error of less than 5% which would require that M be greater than 20 to get equivalent performance. Thus with no uncertainty in bit rate, at least 80 correlators are required for the bit sync alone. Section 4 discusses this approach in detail and presents experimental performance data.

Suppose we now attempt to synthesize the "optimum realizable" bit synchronizer directly. What really do we mean by "realizable"? We propose that by "realizable", we really mean practically implementable at reasonable bit rates. Since this definition of "realizable" is not a mathematically precise definition, the "optimum realizable" solution cannot be determined directly from a mathematical argument. However, there is an analytical approach which leads to physically meaningful results and this approach will now be outlined.

If we look at the various bit synchronizers that have been implemented, we find that they all resemble phase-locked loops in the sense that they all make an estimate of the phase difference or error between the incoming bit stream and some internally generated reference, filter this error estimate, and then update the internal reference based on the filtered error value. In fact, the optimum bit synchronizers discussed earlier can also be thought of in this way

if the idea of a phase detector and filter are each generalized somewhat. Therefore, we have investigated two approaches to bit synchronization which utilize a phase detector and loop filter combination. The first type utilizes a nonlinearity to generate a frequency component at the bit rate and tracks this component with a phase-locked loop. The second approach utilizes an early and late gate to generate an error signal which is used in a feedback loop to center the gates on the transition. In the following sections we will discuss two implementations of each type of bit synchronizer and compare them by determining timing jitter as a function of signal-to-noise ratio and mean acquisition time as a function of frequency offset.

Nonlinear Bit Synchronization

We will investigate two types of bit synchronizers which fall into this category. The first technique, which was considered by Wintz and Luecke [14], consists of filtering, squaring, and bandpass filtering the bit stream and utilizing positive zero crossing of the resultant signal. In general for the case where the bit rate is unknown, the bandpass filter would be replaced by a phase-locked loop as shown in Figure 62.

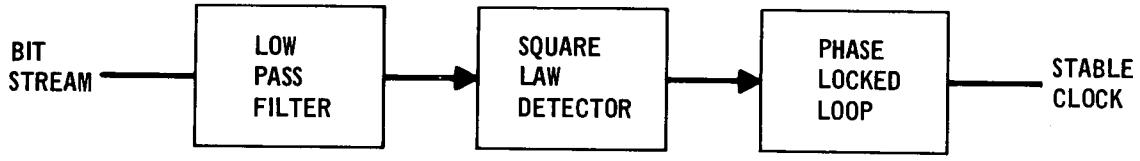

SQUARE LAW BIT SYNCHRONIZER

Figure 62

The input low pass filter is used to obtain a maximum signal-to-noise ratio at the input to the square law detector. The square law detector generates a frequency component at the bit rate which is tracked by the phase-locked loop.

In order to analyze this technique we must first determine the amplitude of the harmonic generated at the bit rate. This amplitude can be determined by computing a Fourier series of the square law detector output. For the specified square pulse shape with either NRZ or Manchester coded input data, the amplitude of this component is zero. However, this does not negate the use of this approach, since if the input signal is first differentiated and then squared, a frequency component at the bit rate will be generated. The performance of this approach is then determined by computing the amplitude of the fundamental component using Fourier analysis. The ratio between the power at the bit rate and the total power in the bit train is a measure of power penalty with this approach. This technique also has the disadvantage that the amplitude of the frequency component at the bit rate is a function of the input bit sequence. A string of ones or zeros will reduce this amplitude to zero for short intervals of time. This effect reduces the tracking capability of the loop and increases the output phase variance. To illustrate the operation of this technique, we assume for the moment that a one is represented by a positive half sinusoid and a zero by a negative half sinusoid. If we assume that the low pass filter does not alter the shape of the input pulse, the output of the square law detector is

$$V(t) = A^2 \sin^2 wt = \frac{1}{2} A^2 (1 - \cos 2wt) \qquad (146)$$

A = peak bit amplitude

$w = \frac{\pi}{T}$

T = bit period

The phase-locked loop following the square law detector tracks the frequency component at the bit rate $(2\frac{W}{\pi})$ (amplitude $A^2/2$) to obtain the bit timing reference.

The second approach we investigated generates a frequency component at the bit rate by multiplying the input signal by itself delayed by one half of the bit period. A block diagram of this method is given in Figure 63. In contrast to the previous technique, this approach will generate a harmonic at the bit rate for square input pulses with either the NRZ or Manchester format. If the input bits have amplitude A and ones and zeros are equiprobable, it can be shown that the average autocorrelation function has the form shown in Figure 64.

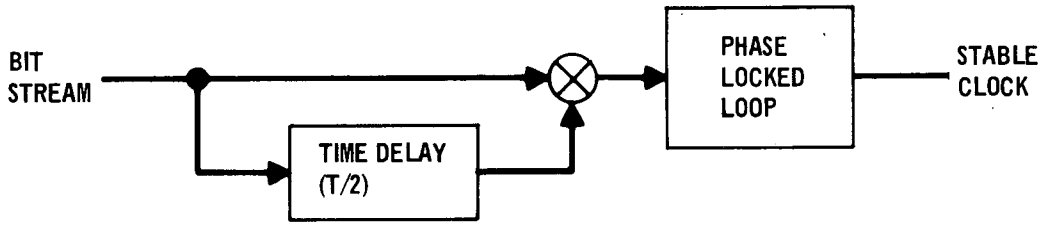

DELAY AND MULTIPLY BIT SYNCHRONIZER

Figure 63

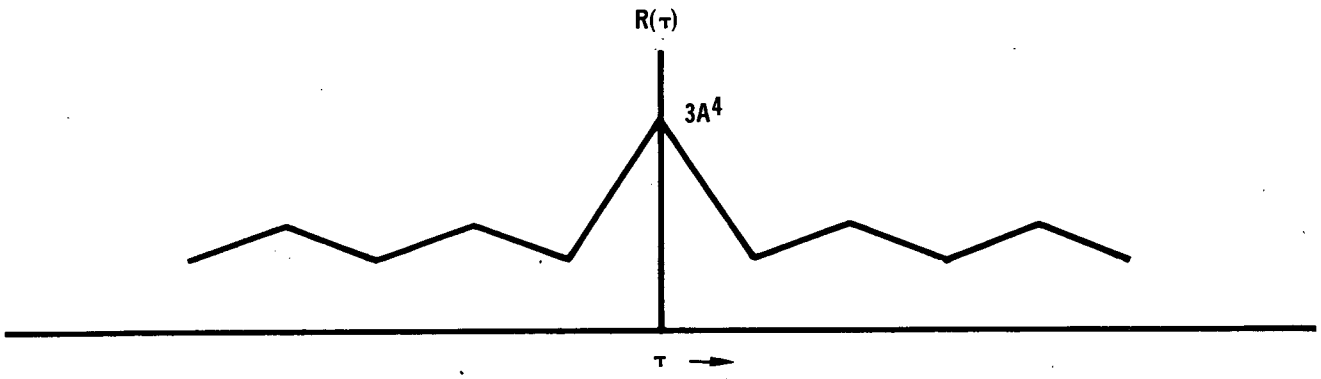

AUTOCORRELATION FUNCTION FOR OUTPUT OF DELAY AND MULTIPLY BIT SYNCHRONIZER

Figure 64

The average time waveform associated with the periodic component of this autocorrelation function is

$$V(t) = \frac{2A^2}{\pi} \sum_{n=1,3,5,\ldots} \frac{1}{n} \sin\left(\frac{2n\pi t}{T}\right) \qquad (147)$$

The phase-locked loop following the multiplier will track the frequency component at the bit rate to obtain the clock signal. For NRZ data the amplitude of this component is time varying because it depends on the bit sequence. For extremely low loop bandwidths this effect will be negligible since the variance in amplitude will be averaged. As with the square law implementation, for wider loop bandwidths the tracking effectiveness of the loop will be decreased and the output phase variance will be increased.

Gated Bit Synchronization

The final type of bit synchronizer which we investigated in this section is a gated phase-locked loop. This technique uses two overlapped gates around the transition as shown in Figure 65.

The first gated technique that we considered was developed by Layland [17] and is shown in Figure 66. In this technique the signal in the early and late gates is integrated, squared, and subtracted to determine the error signal, which is then filtered and used to drive the VCO.

We also investigated a second gated approach, which was suggested by Simon [18], that determines the error signal by subtracting the absolute values of the early and late gates outputs. Both of these approaches can be used with either NRZ or Manchester coded input data. Since the gate width must be reduced to one half of the bit period for the latter type data, the possibility of locking-up on the wrong transition exists, and the linear region of the error curve will be reduced.

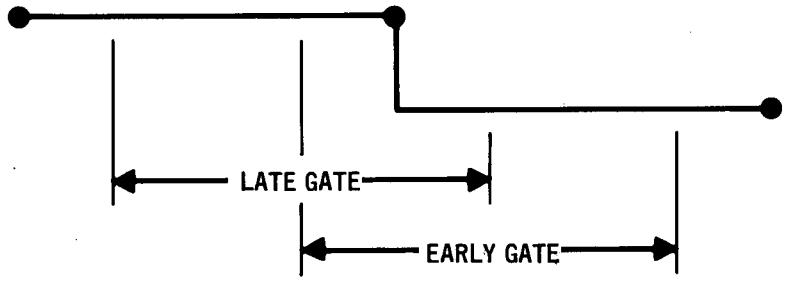

GATE LOCATION

Figure 65

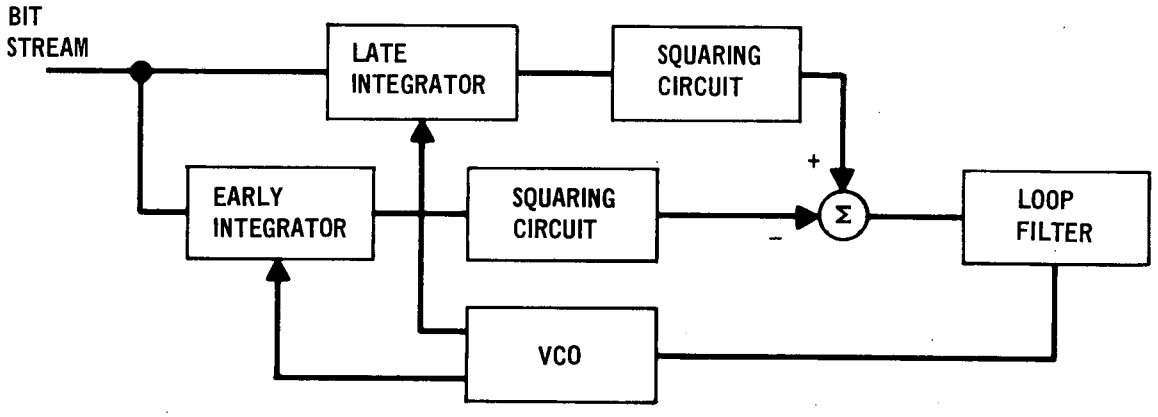

GATED BIT SYNCHRONIZER

Figure 66

Comparison of Techniques

We first determined the rms bit jitter as a function of the signal-to-noise ratio for the square law and absolute value gated bit synchronizers and the delay and multiply nonlinear synchronizer. The square law nonlinear implementation was omitted because its operation is essentially the same as the delay and multiply approach. The resulting data, which is shown in Figure 67, was obtained using 20 samples per bit and an equivalent loop time constant of 10 bit periods. This data shows that there is very little difference between any of the three approaches. The absolute value method has lower rms tracking error over the total range of signal-to-noise ratios. For high signal-to-noise ratios the delay and multiply method ranks second, while at the low signal-to-noise ratios the square law implementation is second best.

We next determined the acquisition time as a function of the percent uncertainty in bit rate. The main problem in obtaining this data is defining when acquisition has occurred. In our digital simulation, we utilized 80 samples per bit and defined acquisition as having occurred when the absolute error remained less than 2 samples ($\frac{1}{40}$ of the bit period) for a total of 10 bits (i.e., one loop time constant). We then designed each of the bit synchronization loops to operate with a nominal bit period of 80 samples and a time constant of 10 bit periods. Figure 68 shows a graph of the pull-in time in bit periods as a function of the bit period increase in percent. These results were obtained using a noise free random bit sequence of equally probable ones and zeros. This data indicates that the square law gated implementation gives the best acquisition time. The other two approaches are approximately equivalent.

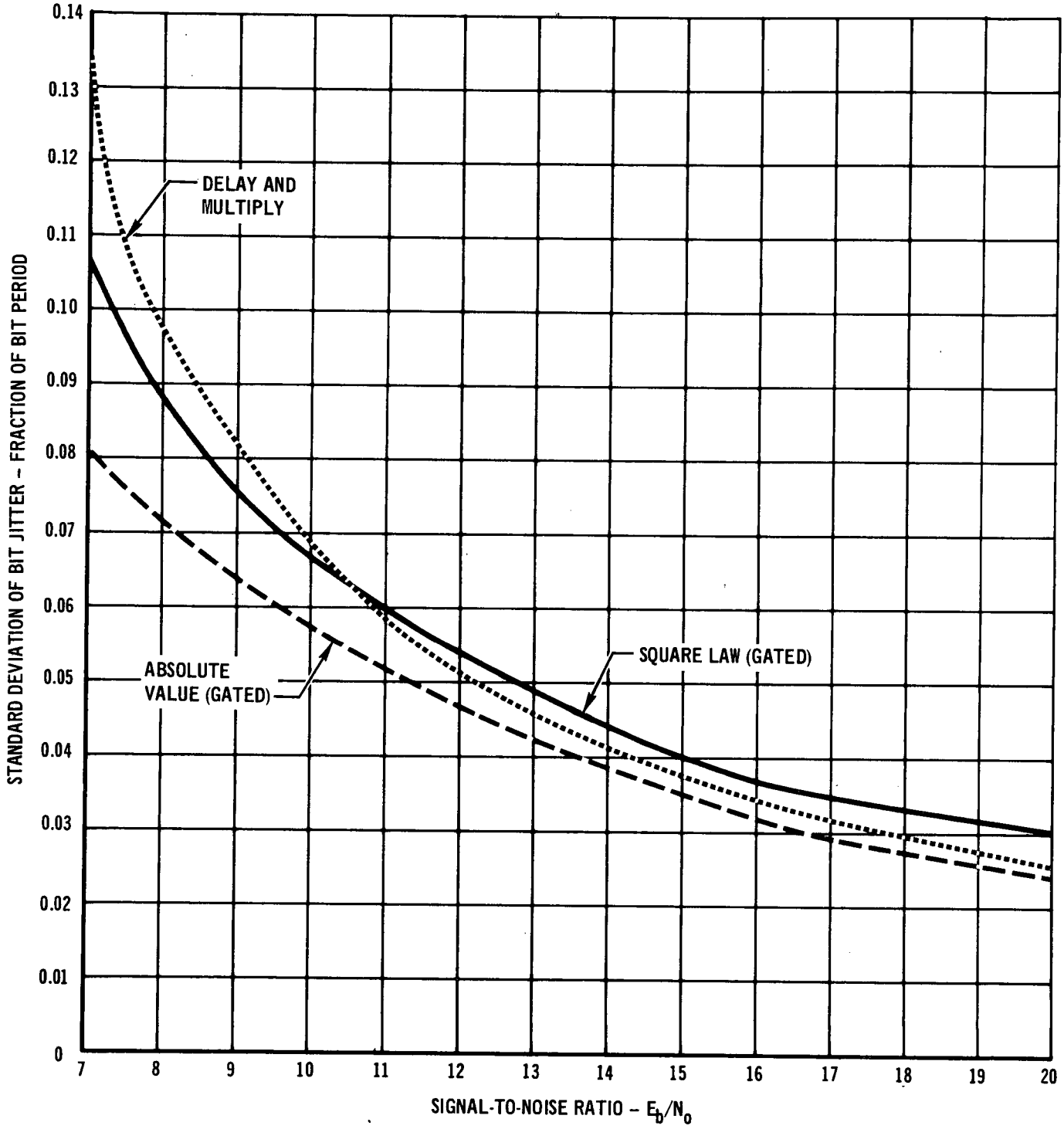

COMPARISON OF BIT SYNCHRONIZERS
LOOP TIME CONSTANT = 10 BIT PERIODS

Figure 67

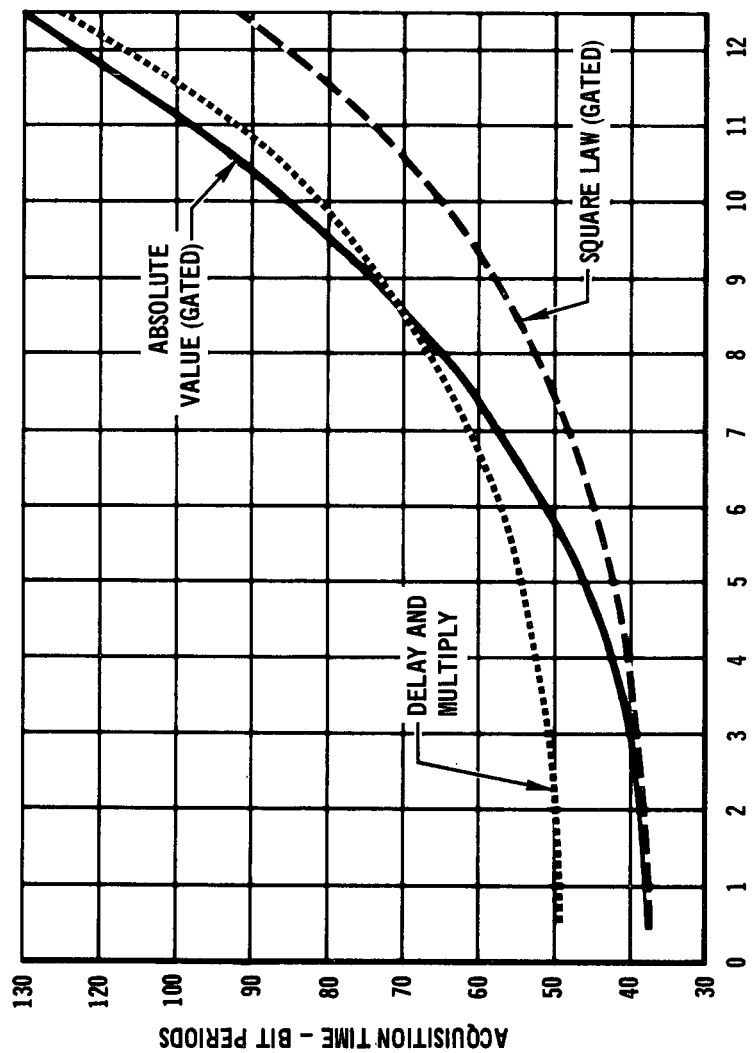
ACQUISITION TIME – BIT PERIODS
130
120
100
90
80
70
60
50
40
30
0
1
2
3
4
5
6
7
8
9
10
11
12
BIT PERIOD INCREASE – PERCENT
ABSOLUTE VALUE (GATED)
SQUARE LAW (GATED)
DELAY AND MULTIPLY
BIT SYNCHRONIZER ACQUISITION TIME
LOOP TIME CONSTANT = 10 BIT PERIODS

Figure 68

In determining the best approach to use for the MDAC Digital PSK receiver, we rated pull-in time as an important performance criterion. The rms bit jitter for each of the techniques can be equalized by increasing the signal-to-noise ratio, but the acquisition times which were shown in Figure 68 were taken for the noise free case and thus cannot be further improved. With this in mind, we selected the square law gated implementation since it gives the optimum pull-in time and is only slightly worse than the absolute value implementation with respect to bit jitter.

Synthesis of Bit Synchronization Algorithm

In this section we derive the algorithms for the bit synchronization loop. We first derive an algorithm for NRZ data, and then, using a similar approach, derive an algorithm for split-phase data.

Synthesis of Bit Synchronization Algorithm - NRZ Data

A functional diagram of the MDAC Digital PSK bit snychronization loop, as modeled after the telemetry bit synchronization loop developed by JPL [17], is shown in Figure 69. The bit synchronization loop operates by sampling the early and late integrals of the input NRZ data stream; squaring the two integrals; differencing and filtering the two squared values to obtain a phase-error correction; and then generating the early gate, late gate, and bit timing commands.

The early integral is the integration of the input data stream from one quarter of a bit period before the local estimate of the data transition time, $\hat{t}_i$, to three quarters of a bit period after the estimated data transition time. The late integral is the integration of the data stream from three quarters of a bit period before the estimated data transition time to one quarter of a bit period after the estimated data transition time. The sign

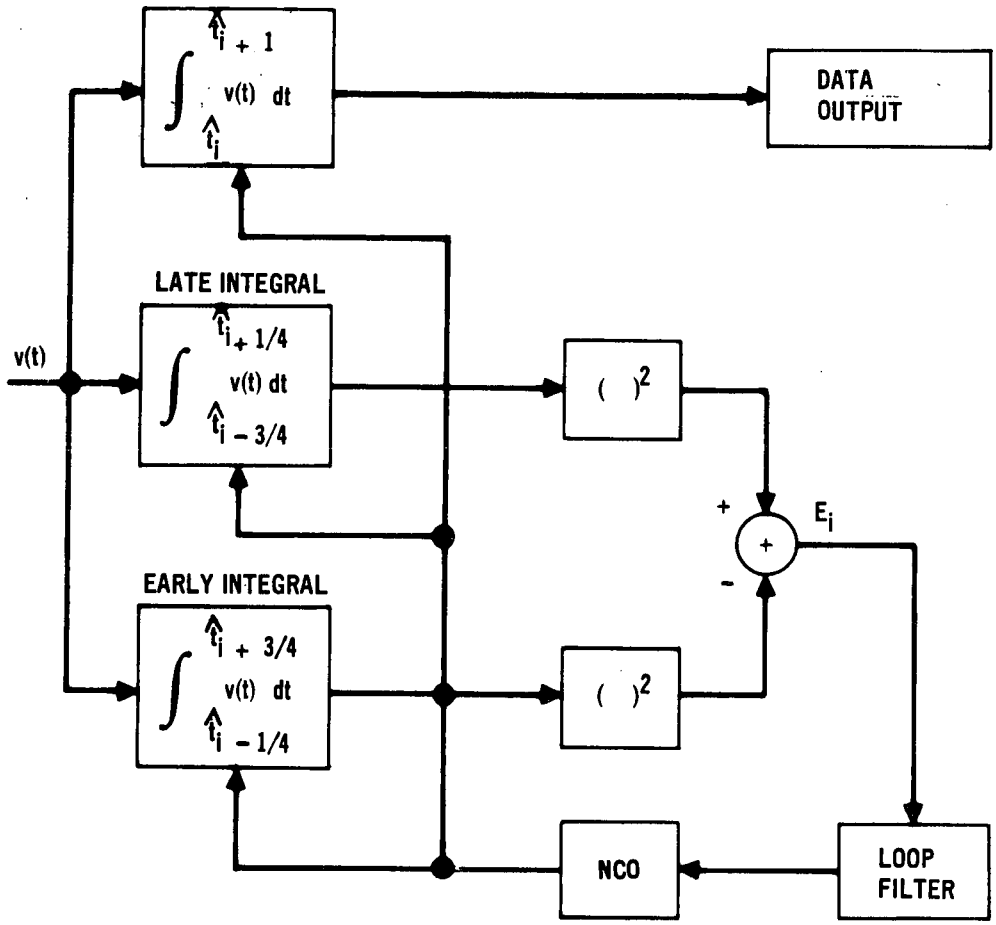

BIT SYNCHRONIZATION LOOP

Figure 69

of the two integrals is removed by squaring so that the bit sync loop error signal is independent of the polarity of the data transitions. E_i, the loop phase error signal, is generated by differencing the squares of the two integrals. The value of this difference will be zero (for the noise free case) when no data transitions have occurred during the early and late integrals, or when a data transition occurred at the same time as the local estimate of the transition time. When the difference of the two squares is not zero, there is a phase error in the local estimate of the transition time. The sign of the difference indicates the direction to shift the phase of the local estimate of the transition time to correct the phase error.

The magnitude of the difference is proportional to the amount of phase shift necessary to correct the phase error.

For example consider the case where the local estimate of t_i is off by one quarter of a bit period. Let t_i denote the actual transition time and T denote the bit period. Then $\hat{t}_i + \frac{1}{4} = t_i$. Define $v(t) = +1$ for $t \leq t_i$ and $v(t) = -1$ for $t > t_i$. Thus the late integral is +T and the early integral is zero. The error signal, E_i, is then $+T^2$. If $v(t) = -1$ for $t \leq t_i$ and $v(t) = 1$ for $t > t_i$, the same error signal is obtained; thus the error signal is data independent. Now let the local estimate of t_i be off by one quarter of a bit period in the opposite direction so that $\hat{t}_i - \frac{1}{4} = t_i$. Let $v(t) = +1$ for $t \leq t_i$ and $v(t) = -1$ for $t > t_i$. The late integral is now zero and the early integral is -T resulting in $E_i = -T^2$. Changing the sign on the transition as before does not change the error signal. When $\hat{t}_i = t_i$ the difference of squares error signal is zero regardless of the sign of the transition. Similarly the error signal is zero if v(t) has no transition between $\hat{t}_i - 3/4$ and $\hat{t}_i + 3/4$.

The error signal, E_i, computed in this manner is linear for $\hat{t}_i - 1/4 \leq t_i \leq \hat{t}_i + 1/4$ as shown in Figure 70. Outside this region the sign of the error signal corresponds to the direction to shift the estimate of the transition time to correct the phase error in a minimum number of steps. Had the integration windows been chosen so that the early and late integrals were computed over an interval of less than one bit period each, the error signal would have a smaller linear range.

For computer implementation the phase error signal, E_i, is scaled to an equivalent number of discrete phase steps. This number is added to the number of samples in the basic bit period which must be applied apriori to the computer program. The phase shifter accepts this output consisting of

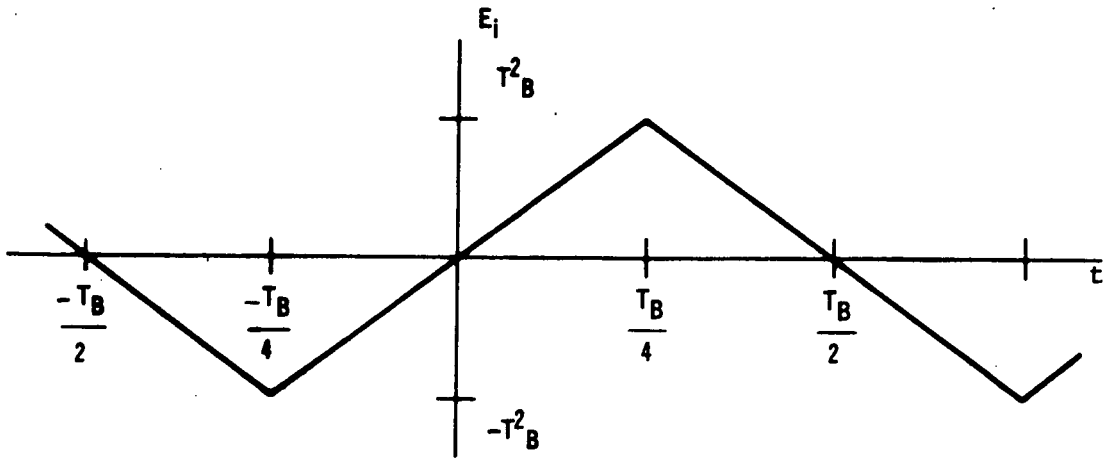

LOOP ERROR SIGNAL

Figure 70

the number of samples in the basic bit period combined with the number of samples of phase correction necessary to synchronize the local data clock with the actual data. This value is counted down to zero and the phase shifter is again ready to accept new timing information. When no phase correction is indicated the phase shifter merely counts down the number of samples in the basic bit period and outputs the timing commands for the early gate, late gate, and data integrals. We considered two different procedures when a phase correction is necessary. In the first case we reduce computation time by not storing any samples of the input signal. To operate without storing input samples, a computation of the error signal must be omitted each time the gates are moved while new samples are read into the gates. The phase shifter outputs only the data timing commands, and no error signal is computed during that data interval. This approach may degrade tracking an unknown bit rate since for a large bit rate offset the gate center is constantly being slewed. If the offset is large enough, the gate center is moved on each sample. With this implementation the gate can only move on every other sample since an error calculation is skipped after a move occurs.

In the second approach, this problem is eliminated by a more complex technique in which input samples are stored and an error signal is computed on each bit. All the input samples are stored from the bit period prior to an error signal calculation. When a phase correction is necessary, the phase shifter uses the stored samples and the new value of $\hat{t}_i$ to update the gate values. The phase shifter outputs the data timing commands and gate timing commands for the next error signal. We developed computer algorithms for both approaches and have compared their performance in this section. We will first develop the algorithm which does not store samples. The relative positions of timing marks for the early, late, and data integrations are shown in Figure 71 for perfect synchronization.

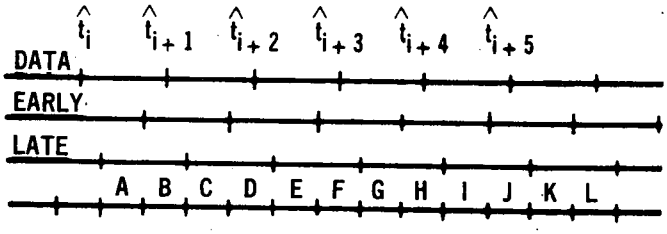

TIME POINTS DEFINING EARLY, LATE, AND DATA INTEGRALS

Figure 71

Some simplification in computer implementation may be obtained from Figure 71. The late integral in the vicinity of $t_i + 1$ is the sum of the integrals A and B. The early integral is B + C. The error signals at $t_i + 1$ and $t_i + 2$ are given by Equations (148) and (149) respectively.

$$E_{i+1} = (A + B)^2 - (B + C)^2 \tag{148}$$

$$E_{i+2} = (C + D)^2 - (D + E)^2 \tag{149}$$

Figure 71 shows that the early and late integrals overlap by one half of a bit period.

In order to reduce computations the overlapping integration can be removed by generating bit timing commands so that there are three integration windows each one half bit period long as shown in Figure 72.

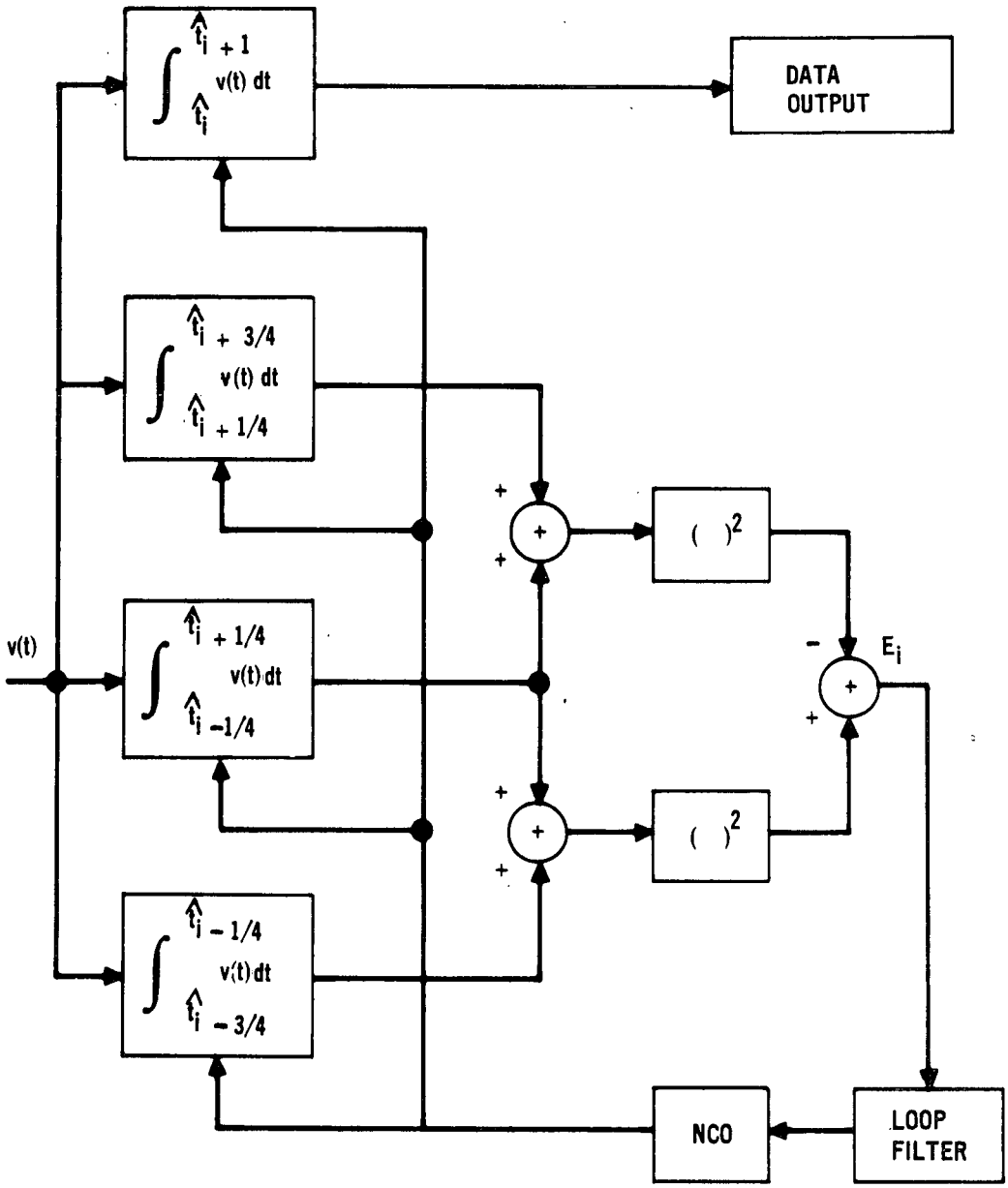

REDUCED BIT SYNCHRONIZATION LOOP Figure 72

The early and late integrals are then determined by Equations (150) and (151) where the overlapping integrations have been removed.

$$\int_{\hat{t}_i-1/4}^{\hat{t}_i+3/4} v(t)\,dt = \int_{\hat{t}_i-1/4}^{\hat{t}_i+1/4} v(t)\,dt + \int_{\hat{t}_i+1/4}^{\hat{t}_i+3/4} v(t)\,dt \qquad (150)$$

$$\int_{\hat{t}_i - 3/4}^{\hat{t}_i + 1/4} v(t)\,dt = \int_{\hat{t}_i - 3/4}^{\hat{t}_i - 1/4} v(t)\,dt + \int_{\hat{t}_i - 1/4}^{\hat{t}_i + 1/4} v(t)\,dt \qquad (151)$$

Let A_i, B_i, and C_i be defined by Equations (151), (152), and (153).

$$A_i = \int_{\hat{t}_i - 3/4}^{\hat{t}_i - 1/4} v(t)\,dt \qquad (152)$$

$$B_i = \int_{\hat{t}_i - 1/4}^{\hat{t}_i + 1/4} v(t)\,dt \qquad (153)$$

$$C_i = \int_{\hat{t}_i + 1/4}^{\hat{t}_i + 3/4} v(t)\,dt \qquad (154)$$

The A integral on the i + 1 data bit is identical to the C integral on the i^{th} data bit. Therefore additional computation time may be saved by updating the A integral as shown in Equation (155).

$$A_i + 1 = C_i \qquad (155)$$

The video input, v(t), for the bit synchronization loop is generated from quadrature components, x and y, and the Costas loop phase output,

$$v(t) = x \cos \hat{\theta} + y \sin \hat{\theta} \qquad (156)$$

Using this expression for v(t) the A_i, B_i, and C_i integrals may be evaluated by rectangular integration. The A_i, B_i and C_1 integrals can be defined in terms of notation previously employed.

$$A_n = A_{n-1} + H\,[x_{n-1} \cos X1_{n-1} + y_{n-1} \cos X1_{n-1}]$$

$$B_n = B_{n-1} + H\,[x_{n-1} \cos X1_{n-1} + y_{n-1} \cos X1_{n-1}] \qquad (157)$$

$$C_n = C_{n-1} + H\,[x_{n-1} \cos X1_{n-1} + y_{n-1} \cos X1_{n-1}]$$

It is required that the bit synchronization loop be able to acquire and track a ramp input. Thus, the bit synchronization loop must use a second order filter. Choose the loop filter of Figure 72 as $F(s) = \frac{s+a}{s} = 1 + \frac{a}{s}$ Then the feedback loop of Figure 72 can be represented as shown in Figure 73. where the gain G is chosen to scale the error signal to an integer number of discrete phase steps. G is then $\frac{SR}{4T^2}$ where SR is the number of samples per bit.

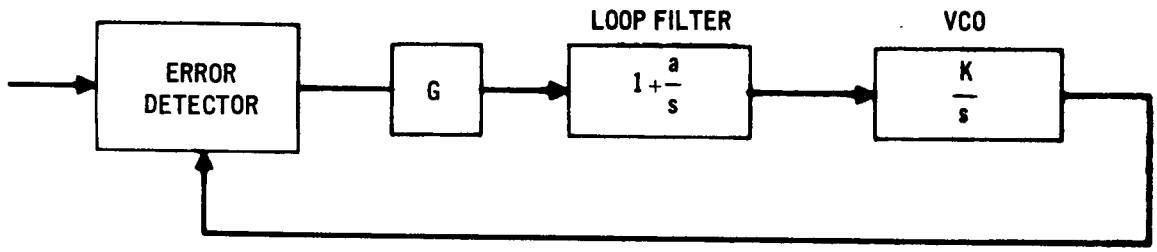

BIT SYNCHRONIZATION FEEDBACK LOOP Figure 73

The loop transfer function of Figure 73 is given by Equation (158).

$$H(s) = \frac{Gk(s+a)}{s^2 + Gks + GKA} \qquad (158)$$

Equation (158) is in the standard second order form given in Equation (159)

$$H(s) = \frac{2\zeta\omega_{os} + \omega_o^2}{s^2 + 2\zeta\omega_{os} + s^2} \qquad (159)$$

The loop time constant, TCON, is approximately $\frac{1}{\zeta\omega_o}$.

Equation (160) follows from Equation (158) and (159).

$$k = \frac{2\zeta\omega_o}{G}$$

$$a = \frac{\omega_o}{Gk} \qquad (160)$$

Since E_i is zero one half the time due to no transitions in the data stream, the integrator gain k is doubled to compensate for the loss of error signal. Thus,

$$k = \frac{4\zeta\omega_o}{G} \qquad (161)$$

The digital bit synchronization algorithm can be derived as follows. Let E_i be the input to the loop filter. Since the $\frac{a}{s}$ term in the loop filter and the $\frac{k}{s}$ term in the VCO represent integrations in the time domain, the algorithm for the bit synchronization loop, using rectangular integration, can be shown to be given by Equation (162).

```
E = ERR + EI*T
ERR = E                                    (162)
ERRR = k*a*E + k*EI
THAT = THAT + ERRR *T
```

where EI = E_i, k and a are defined as before, T is the bit period, and THAT is the final filtered output.

The input for the phase shifter is formed by first converting THAT to the nearest whole number of samples NTHAT, and computing the difference $IR = NTHAT_n - NTHAT_{n-1}$. This integer number is the estimated number of samples of phase shift required to align the transition times. It is the

change in NTHAT from the n-1 error signal to the nth error signal that represents the phase correction, because the phase shifter uses its present estimate of the transition time as a reference and can move only in integer steps away from this position to correct its estimate of the transition time. The phase shifter adds or subtracts this difference, IR, to the number of samples in the basic bit period and counts down this number to correct the local estimate of the transition time. Therefore, if there is a ramp input caused by incorrect knowledge of the bit period, the phase shifter tracks the ramp by changing the basic bit period by IR samples.

To generate the timing commands, the phase shifter relies on a knowledge of the number of samples per bit and the integration intervals for the A_i, B_i, and C_i integrals. Reference to Equations (152), (153), and (154) and Figure 71 shows that the integration window for the early and late integrals is 1.5 bit periods long. Each integral, A_i, B_i, and C_i, is over half of a bit period and thus contains .5 SR samples. The phase shifter has a counter, I, that begins at $\hat{t}_i$ -3/4, counts 1.5 SR samples, and then is reset to zero. The A_i integral is computed from $\hat{t}_i$ -3/4 to $\hat{t}_i$ - 1/4 over the first .5 SR samples; the B_i integral is computed from $\hat{t}_i$ - 1/4 to $\hat{t}_i$ + 1/4 while C_i is computed from $\hat{t}_i$ + 1/4 to $\hat{t}_i$ + 3/4 over the last .5 SR samples

E_i is then computed, filtered, and a decision is made on IR to correct the phase. If IR = 0, A_{i+1} is set equal to C_i and the counter I is advanced so that B_{i+1} and C_{i+1} are computed. If it is necessary to correct the local estimate of the transition time, then a slightly different procedure is followed. E_i is computed at t_i + 3/4 following calculation of C_i as shown in Figure 71. The phase shifter corrects by increasing or decreasing the number of samples between t_i + 3/4 and t_i + 1. No error signal E_{i+1}

is calculated because it would have been necessary to save and order the samples received while the phase correction was being made to obtain the correct A_{i+1} and B_{i+1} integrals. Therefore the phase shifter waits until the A_{i+2} integral is to be computed and again begins outputting timing commands.

The phase shifter has a second counter IDUM that generates the timing command for the correlator integral by counting the number of samples in the basic bit period starting at $\hat{t}_i$. When SR samples are counted the bit decision is made and the correlator integrator reset. When a phase correction is necessary IDUM is advanced or retarded so that the correlation integrates over less than or more than a bit period as indicated by the error signal. In this manner the bit synchronization loop is able to adjust the timing commands of the data, early, and late integrals to correct the phase estimate of the local clock without storing input samples.

The sample storage approach for bit synchronization is identical to the approach just described except the action taken when a phase correction is necessary. In the second approach all the input samples from the bit period prior to an error signal calculation (from $\hat{t}_i$ -1/4 to $\hat{t}_i$ +3/4) are stored and ordered in the computer. After the error signal, E_i, is computed at $\hat{t}_i + 3/4$, the phase shifter uses the new value of $\hat{t}_i$ to update the gate integrals for calculating E_{i+1}. Depending on the sign and the magnitude of E_i, all or portions of A_{i+1} and B_{i+1} integrals are calculated from the stored samples. The counter, I, is advanced so that the next input sample goes to the proper gate A or B. The correlator timing signal IDUM is set to the proper value from the new value of $\hat{t}_i$, and a bit decision is made as indicated by the corrected value of IDUM. IDUM is advanced or retarded

so that the correlator integrates over less than or more than a bit period as indicated by the error signal.

In this manner the bit synchronization loop is able to adjust the timing commands of the data, early, and late integrals to correct the phase estimate of the local clock. By using the stored input samples, the bit synchronizer updates the gate integrals after an error signal calculation, and, thus, an error signal is calculated on every bit.

A curve of bit error rate for the digital receiver with both bit synchronization techniques is shown in Figure 74. The bit error rate is slightly lower when using the bit synchronizer with sample storage. A curve of standard deviation of bit jitter is shown in Figure 75. Bit jitter is also lower when using the sample storage bit synchronization algorithm. We investigated tracking performance of the bit synchronization loops for cases having a large uncertainty in bit rate. We found that without sample storage, the bit synchronization loop time constant must be 5 bit periods or less for the loop to track a 5% uncertainty in bit rate. The bit synchronization loop with sample storage will track the 5% uncertainty in bit rate with a loop time constant of 10 bit periods or less, and will track a 10% uncertainty in bit rate with a loop time constant of 8 bit periods or less. Without sample storage, the bit synchronization loop will not track a 10% uncertainty in bit rate because of the one and a half bit delay after each correction of the bit timing reference before a new error signal can be computed. Sample storage allows the digital receiver to operate over a larger uncertainty in bit rate than was possible previously and significantly reduces bit tracking error (Figure 76).

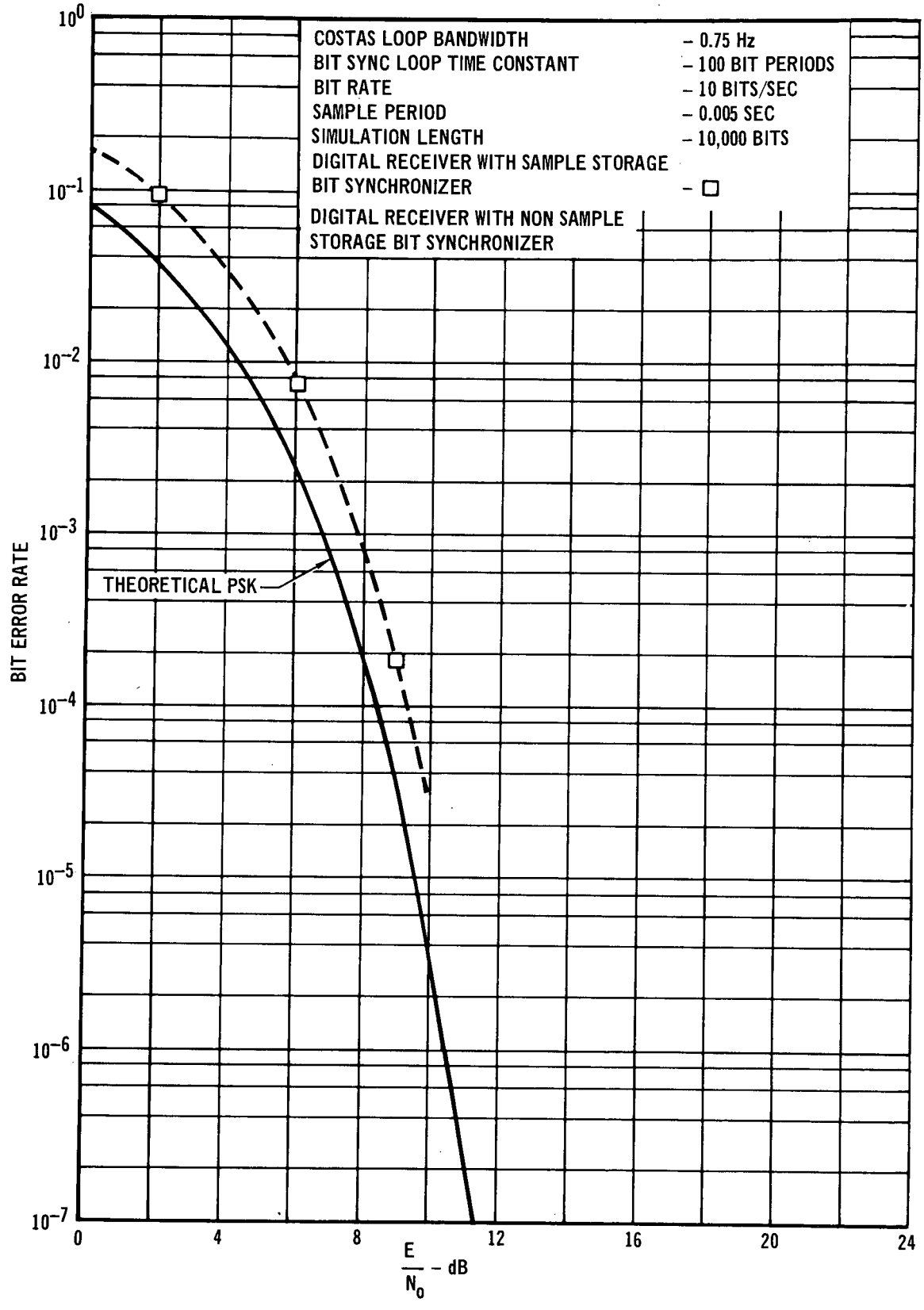

BIT ERROR RATE FOR DIGITAL RECEIVER WITH AND WITHOUT SAMPLE STORAGE BIT SYNCHRONIZER

Figure 74

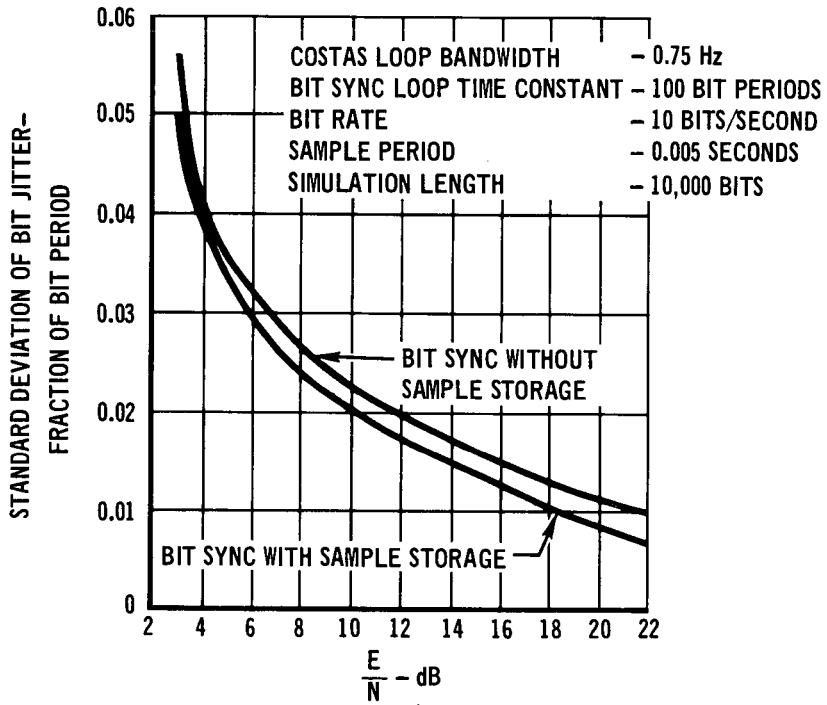

STANDARD DEVIATION OF BIT JITTER

Figure 75

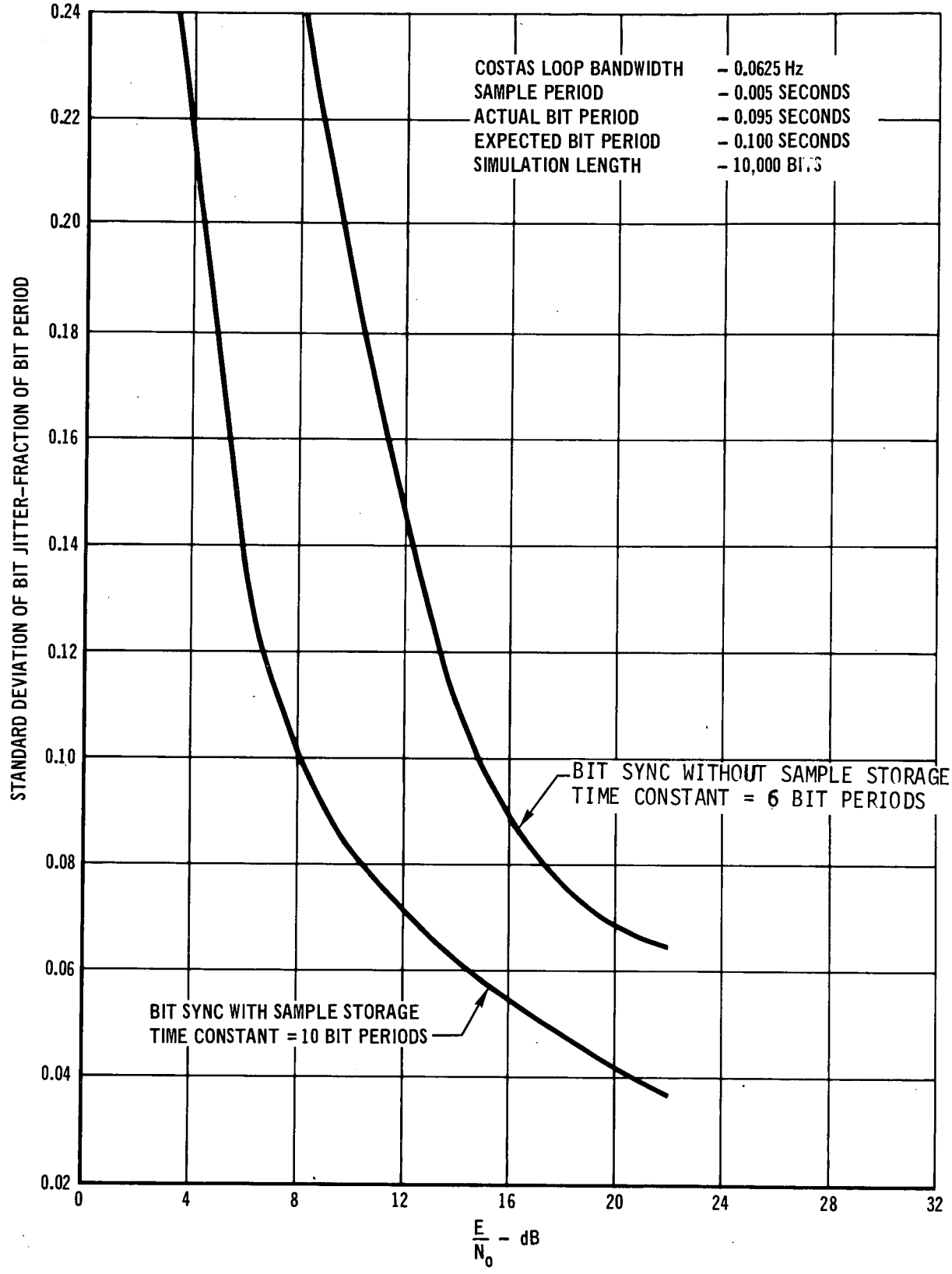

STANDARD DEVIATION OF BIT JITTER – 5% TIMING ERROR Figure 76

Synthesis of Bit Synchronization Algorithm Split-Phase Data

We modified our (NRZ) sample storage bit synchronization algorithm to operate with split-phase data by adding an "M-out-of-N" detector to determine correct phase. Split-phase data has a transition in the middle of each bit. The bit synchronizer must center the bit timing on this transition and not on a transition which may or may not occur at the end of the bit.

For split-phase data, we operate our bit synchronizer at twice the split-phase bit rate. Each half of the information bit is detected, and thus an error signal, E_i, is generated on each half bit. The phase shifter generates timing commands in exactly the same manner as for NRZ data for the early, late, and data integrals on each one half data bit. The phase shifter also controls a correlator integral over the entire information bit; and if necessary, corrects timing for this integral after each error signal is computed.

To center the bit timing correctly a counter is used to determine the number of mid-bit transitions in N bit periods. If this number is above the threshold setting after N bit periods, correct bit timing is assumed. When the number of transition is less than the threshold setting, the phase shifter changes its estimate of the mid-bit transition by 180° and initializes all counters.

With an "M-out-of-N" detector the probability of false acquisition and the probability of acquisition are defined in Equations (163) and (164).

$$P\{\text{false acquisition}\} = P\{\text{M or greater transitions out of N} \mid \text{incorrect phase}\}$$
$$= \sum_{K=M}^{N} \binom{N}{K} (.5)^N \qquad (163)$$

$$P\{\text{acquisition}\} = P\{\text{M or greater transitions out of N} \mid \text{correct phase}\}$$
$$= \sum_{K=M}^{N} \binom{N}{K} (1-P_e)^K P_e^{N-K} \qquad (164)$$

where P_e is the error probability for the one half bit detections made for the "M-out-of-N" detector. For any value of P_e, a value of M and N can be calculated to insure a high probability of acquisition and a low probability of false acquisition. Note that these results assume that bit errors occur independently.

We first simulated the performance of the digital receiver with split-phase data using a "11-out-of-14" detector and compared the results to the performance of the digital receiver with NRZ data (Figure 77 and Figure 78). For $P_e = .1$, this threshold setting resulted in $P\{\text{acquisition}\} = 0.9559$ and $P\{\text{false acquisition}\} = 0.0288$. The standard deviation of bit jitter was almost identical except for low signal-to-noise ratios where the bit jitter is lower for split-phase data. Intuitively the bit synchronization algorithm should perform better for split-phase data because there are more transitions in the split-phase data.

The bit error rate is significantly higher at low signal-to-noise ratios for split-phase data. This effect is caused by the phase indicator slipping 180° out of phase which in turn causes bursts of bit errors. On the average the phase indicator would slip 180° out of phase once in 315 bits. To reduce the likelihood of phase slips it was decided to use a larger number of bits (i.e., larger N) in the decision algorithm. With $P_e = 0.1$, a threshold setting of "66-out-of-90" results in $P\{\text{acquisition}\} = 9.99998 \times 10^{-1}$ and $P\{\text{false acquisition}\} = 5.451 \times 10^{-6}$. On the average, the phase indicator would slip 180° out of phase once in 9×10^7 bits. We simulated the performance of the

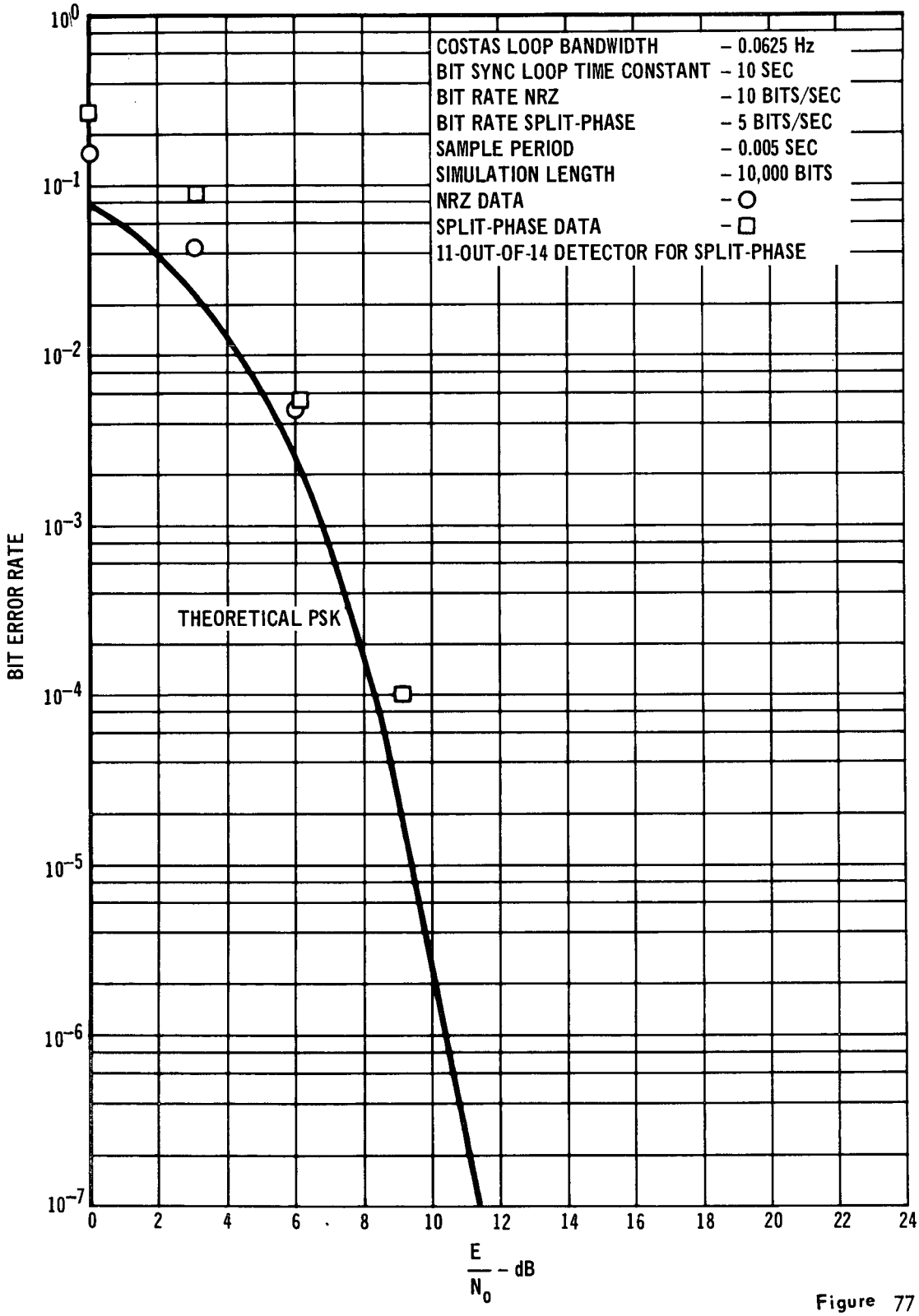

Figure 77

BIT ERROR RATE – NRZ AND SPLIT-PHASE

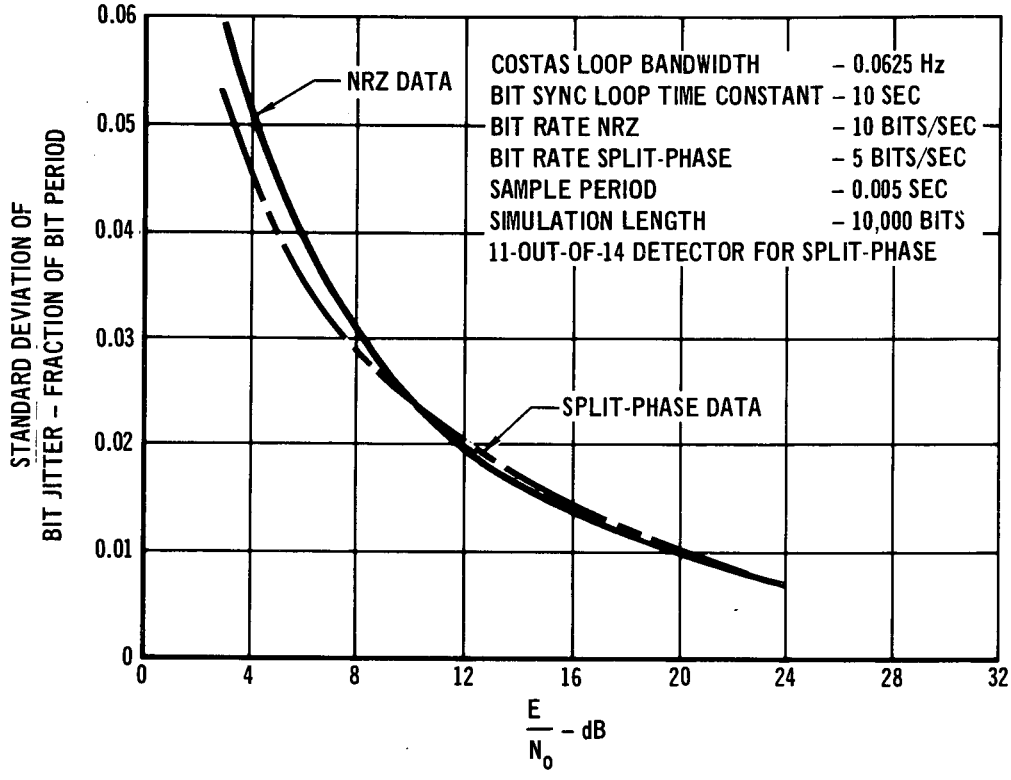

STANDARD DEVIATION OF BIT JITTER – NRZ AND SPLIT-PHASE Figure 78

digital receiver with this decision criterion and compared the results to the performance of the receiver with NRZ data (Figure 79 and Figure 80). The rms bit jitter for both cases is nearly identical. The bit error rate for split-phase data is slightly lower except at 0 dB. We observed that the bit synchronizer slipped 180° out of phase causing bursts of bit errors much more often than Equations (163) and (164) predict. This apparently results from the bit errors not being independent. When the carrier or bit synchronization error is large, the digital receiver makes a sequence of bit errors. The bit errors are dependent, and thus Equations (163) and (164) do not hold. However, for signal-to-noise ratios greater than 3 dB, Equations (163) and (164) do accurately describe receiver performance. The conclusion is that, with split-phase data, large values of M must be used to get near optimum performance. The only bad effect of increasing M is that it increases acquisition time.

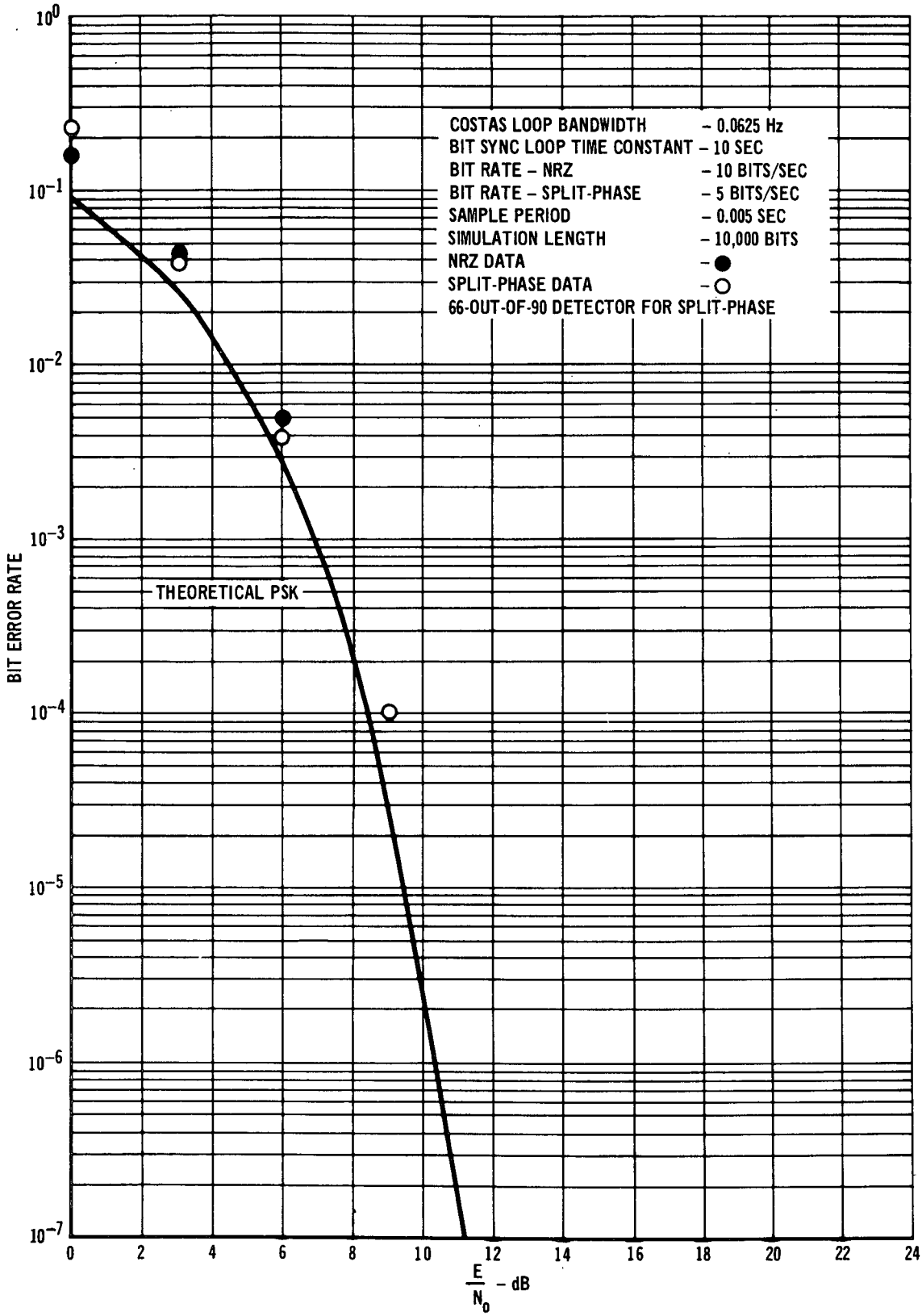

BIT ERROR RATE – NRZ AND SPLIT-PHASE Figure 79

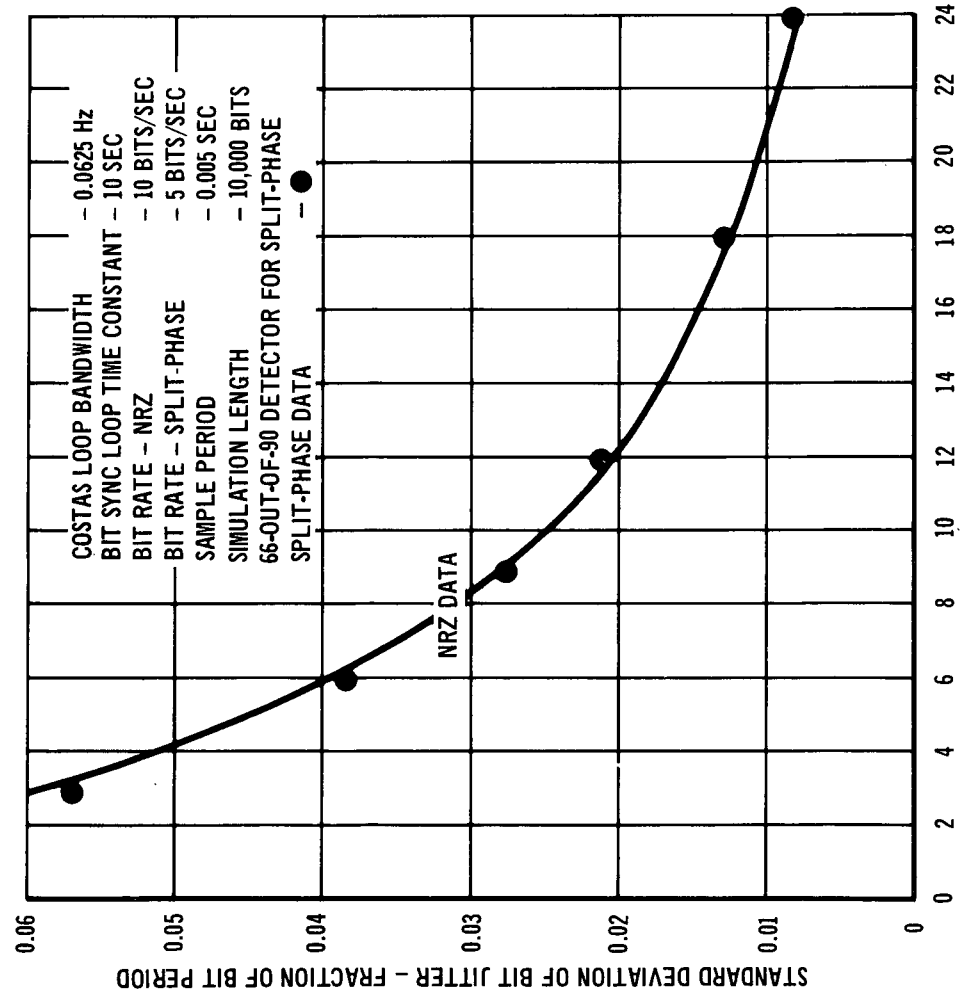

STANDARD DEVIATION OF BIT JITTER - NRZ AND SPLIT-PHASE

Figure 80

Automatic Gain Control - Bit Synchronizer

In Section 2.5 we investigated several techniques for automatic gain control. We determined that the bandpass limiter was the preferred technique for use with a phase-locked loop, and in Section 3.1.6 we applied this technique to the Costas loop. In this section we develop an AGC technique for the bit synchronization loop.

The input sample to the bit synchronization loop is described by Equation (165) in terms of the quadrature components and the Costas loop phase estimate.

$$V = x \cos \hat{\theta} + y \sin \hat{\theta} \tag{165}$$

By applying the techniques developed in Section 2.5, the equation for the input signal with a bandpass limiter may be written as Equation (166).

$$V = \frac{x}{\sqrt{x^2 + y^2}} \cos \hat{\theta} + \frac{y}{\sqrt{x^2 + y^2}} \sin \hat{\theta} \tag{166}$$

Equation (166) should be evaluated using integer arithmetic to reduce computation time. However, there is no integer square root function available on the CDC 3200. The bandpass limiter, therefore, cannot be used for AGC in the bit synchronization loop.

Since we could not use a bandpass limiter, we determined that the most efficient technique for AGC would be a hard limiter at the input of the bit synchronizer. The input samples, V, are hard limited to $\pm$ A volts. A curve of standard deviation of bit jitter for the sample storage bit synchronizer with and without AGC is given in Figure 81. Addition of AGC has significantly reduced bit jitter. A curve comparing bit error rates for the original digital receiver and the digital receiver with sample storage bit synchronizer and AGC in both the Costas loop and bit synchronization loop is given in Figure 82. Note that digital receiver performance is slightly better with the improved bit synchronization technique and AGC.

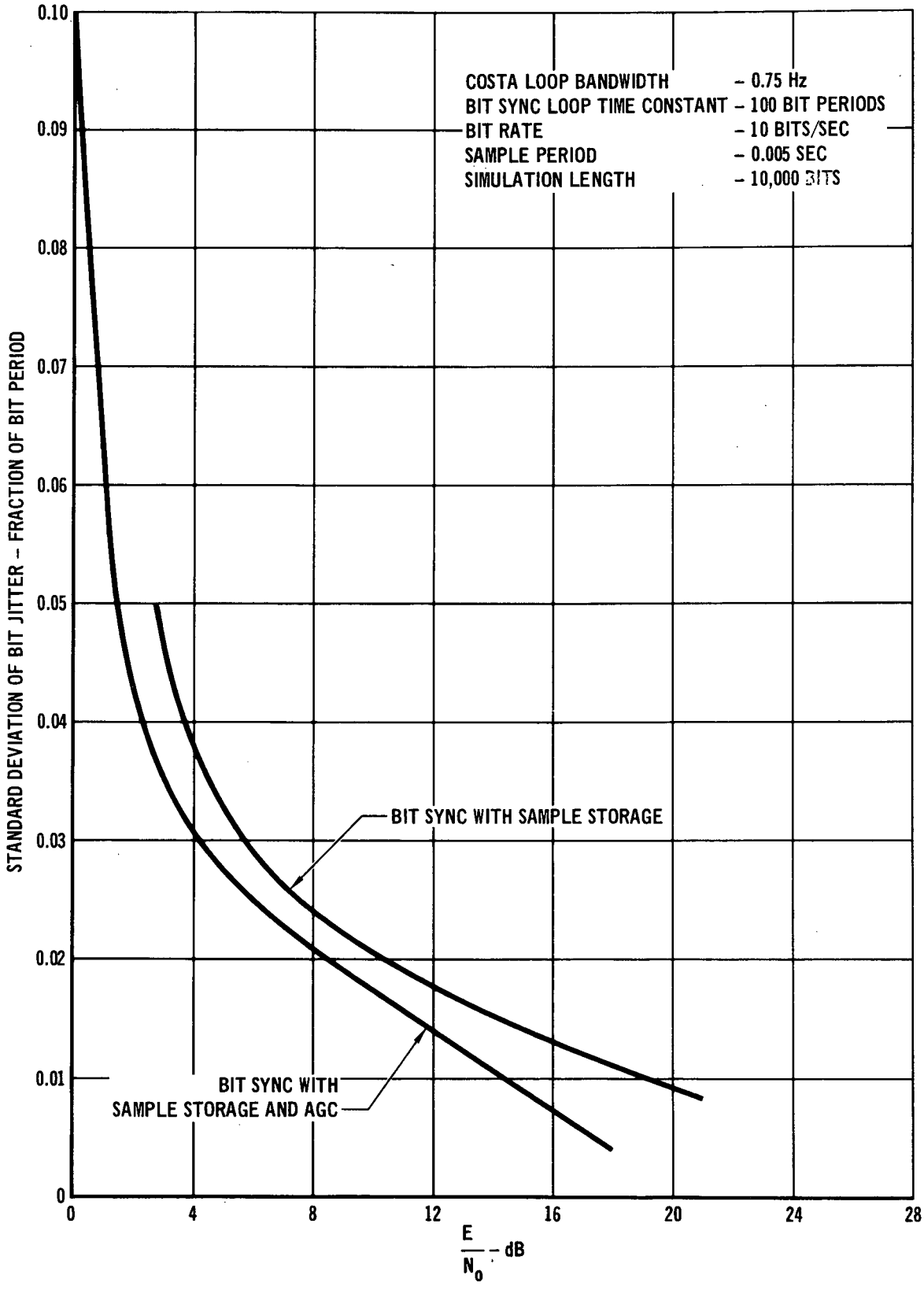

STANDARD DEVIATION OF BIT JITTER; AGC AND NO AGC Figure 81

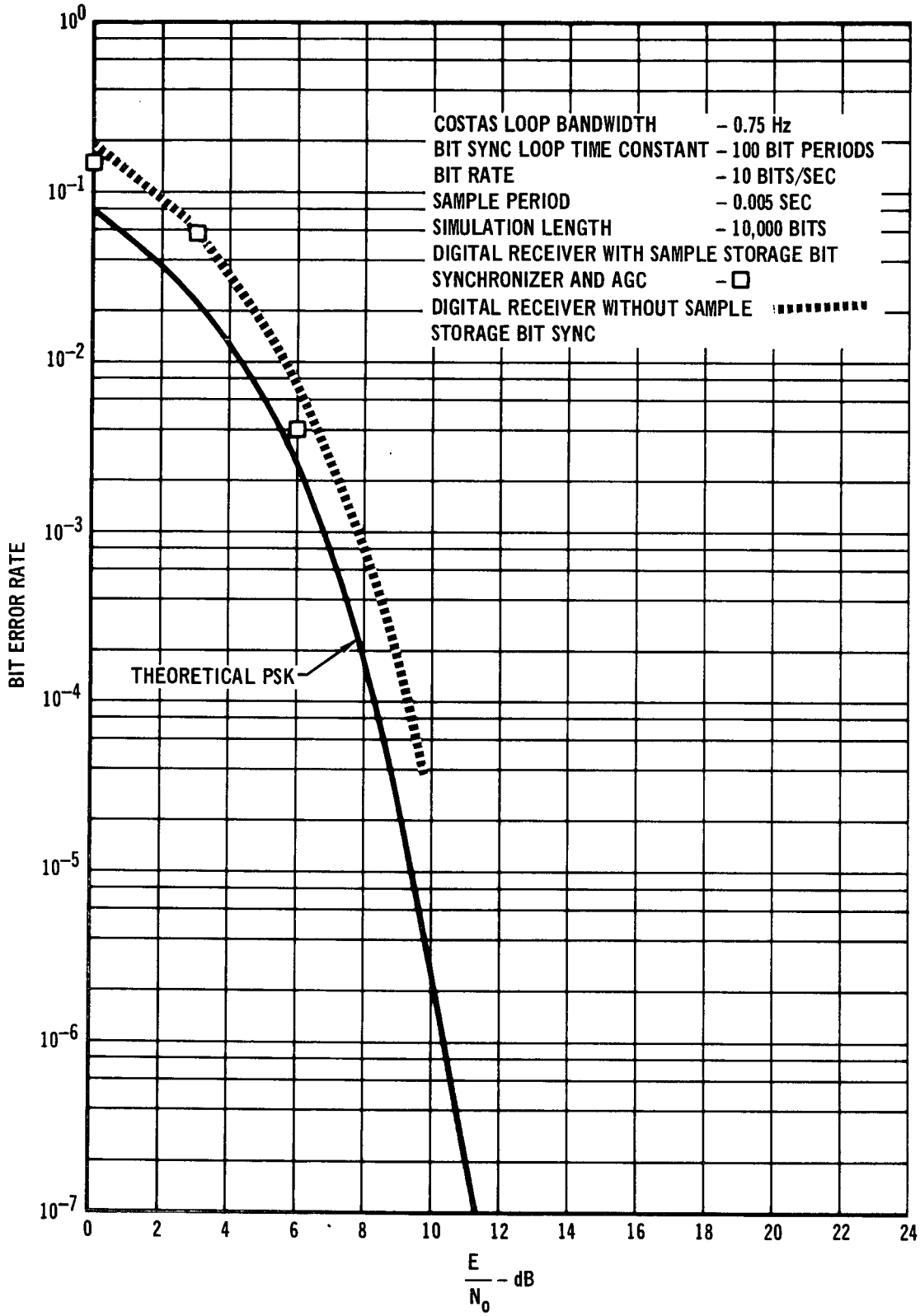

DIGITAL RECEIVER WITH SAMPLE STORAGE BIT SYNCHRONIZER AND AGC

Figure 82

3.1.8 Development of Integrated Program

In this section we describe the various computer programs developed for demodulating PSK data. We describe the philosophy used in developing the programs, and give instructions for using the programs.

NRZ Data with Hard Line Bit Synchronization

We developed an algorithm for demodulating PSK signals with an NRZ data format for use on the MDAC CDC 6600 hybrid computer facilities. This program was optimized for use with a signal that has hard line bit synchronization available. The hard line bit synchronization signal changes state from 0 to 10 volts to indicate the end of a bit period. All operations are done with floating point arithmetic. The computer program for hard line bit synchronization is shown in Figure 83 . The program variables are defined as follows:

SR = number of samples per bit

BR = number of bits per second

H = interval between samples

BWN3DB = noise bandwidth of Costas loop

BW = ω_o of Costas loop

AMP = A is the peak input signal amplitude without noise

ZETA = ζ

AK = K from Costas loop

BK = a from Costas loop

TX = the correlator output

IOUT = bit stream, 0 to 1

X and Y are the input quadrature components

AJ = the hard line bit sync signal 0 to 10 volts

Y1 = the Costas loop phase output range $\pm \pi/2$

ADC = output of analog to digital converter

```
      PI = 3.14159
      P12 = 2 * PI
      SR = 20
      BR = 10
      H = 1/(BR * SR)
      HI = .5 * H
      BWN3DB = .5
      BW = (4* BWN3DB)/(2 * ZETA + 1/(2 * ZETA))
      AMP = 1
      ZETA = SQRT (2)/(2)
      AK = 8 * ZETA * BW/AMP ** 2
      BK = BW/(2 * ZETA)
      DK = H * AK
      CK = H* BK * AK
      TX = 0
      X1 = 0
      X2 = 0
      IOUT = 0
101   X = ADC (01)
      Y = ADC (02)
      AJ = ADC (03)
      TEMP = (X ** 2 - Y ** 2) * SIN (2 * X1)/8 + X * Y * COS (2 * X1)/4
      X1 = X1 + H * X2 - TEMP * DK
      X2 = X2 - TEMP * CK
      RJN = X1/PI + SIGN (.5, X1)
      NNN = RJN
      QB = NNN
      Y1 = X1 - QB * PI
      TX = TX + HI * (X * COS (X1) - Y * SIN (X1))
      IF = (AJ. LT. 5) GO TO 60
      IOUT = 0
      IF (TX. GT. 0.0) IOUT = 1
      TX = 0
 60   DAC (01) = Y1
      DAC (02) = IOUT
      GO TO 101
```

COSTAS LOOP WITH
HARD LINE SYNC

Figure 83

DAC = output of digital to analog converter

The program inputs are X and Y, the quadrature components, and AJ, the hard line bit sync signal. X and Y must be normalized to an input amplitude of 1 volt in the absence of noise. Y1, the Costas loop phase, with a range of $\pm\frac{\pi}{2}$, and the detected bit IOUT, 0 or 1, are the outputs from the program.

NRZ Data with Data Derived Bit Synchronization

We developed a digital receiver optimized for use with the Goddard CDC 3200 computer. The digital receiver uses two GSFC subroutines for input and output of data on the CDC 3200 hybrid computer facilities. The subroutine for data input is INDATA (INT, NPTS). INT is an array dimensioned NPTS + 2. NPTS is the number of input samples buffered into the computer between computations. NPTS is used to establish the sampling rate. The first two elements of INT are the quadrature component samples. The subroutine for data output is DISTWO (NOUT). NOUT is a 2 dimensional array whose contents are displayed on the brush recorder. The contents of NOUT must be positive with a range of 0 - 1000. A generalized flow chart for the digital receiver is shown in Figure 84. Because integer operations on the Goddard CDC 3200 computer are executed much faster than floating point operations, the MDAC Digital PSK Receiver was implemented using integer logic and arithmetic. The receiver will accept input samples generated form the IF Sampling technique or the quadrature component sampling technique. However, the programs discussed in this section assume IF Sampling.

Because the digital receiver was implemented using integer arithmetic, it was necessary to scale the program variables and constants to keep as many significant figures as possible without danger of integer overflow. (The range

FLOW CHART OF DIGITAL PSK RECEIVER WITH DATA DERIVED SYNC

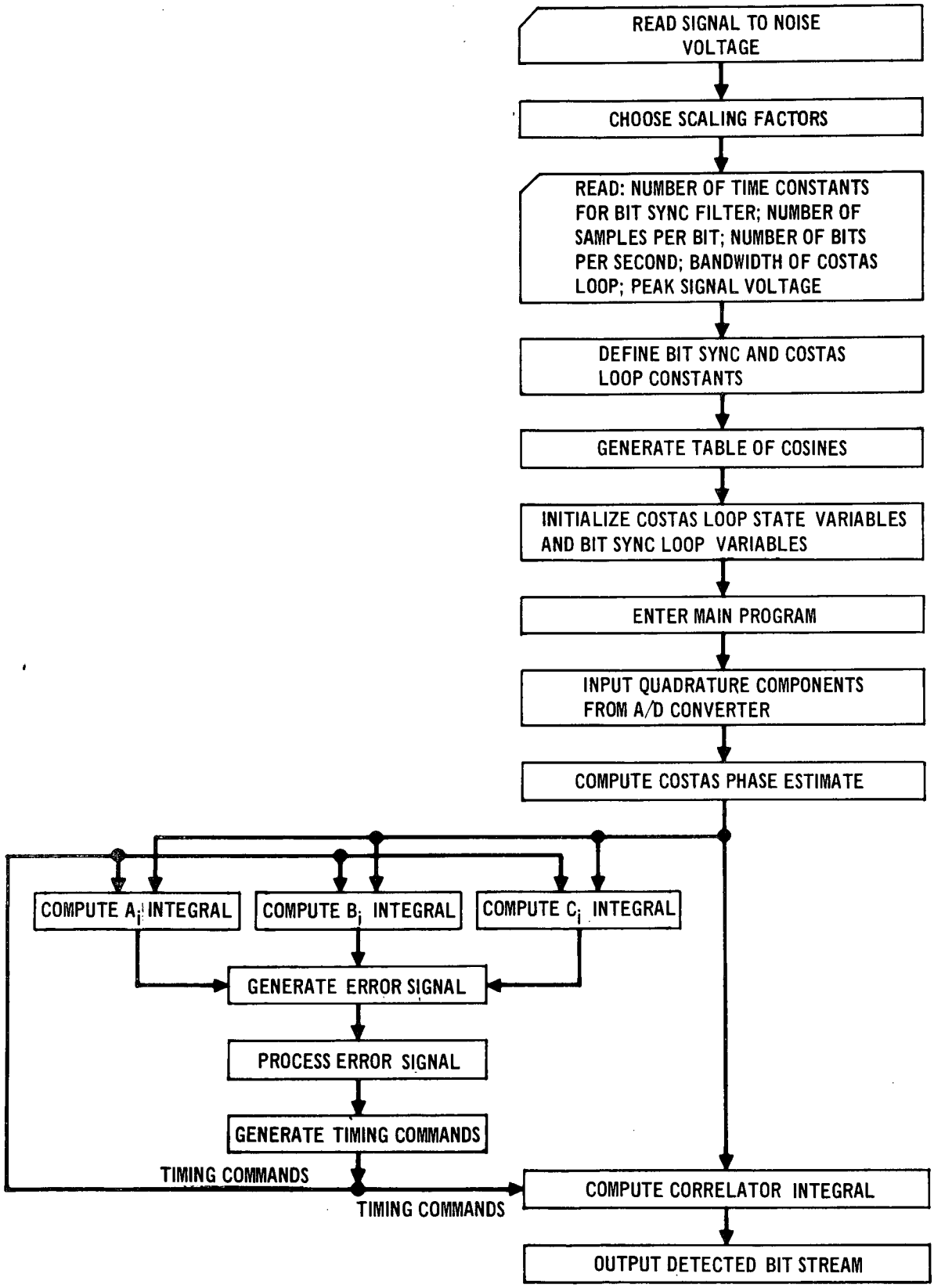

Figure 84

of integers is from -8,388,607 to +8,388,607.) Sine and cosine terms for the Costas loop equations are computed by a table look up. A table of cosine values is stored, and sine values are calculated from the identity $\sin\theta=-\cos(\theta+90°)$.

Digital Receiver without Sample Storage Bit Synchronization

A listing of the digital receiver without sample storage bit synchronization but with the DC bias remover is given in Appendix IV. This receiver is the least complex version of those developed under this contract. The receiver has no AGC in either the Costas or bit synchronization loops, but does have acquisition and tracking modes which are chosen by sense switch 3. Sense switch 3 must be turned on for tracking and turned off for acquisition.

This receiver is designed to operate with the IF sampler at 244 Hz IF and the bit rate at 12.2 bits/seconds and uses the subroutine INDATA. For the subroutine INDATA,NPTS must be set to 4. The first two samples from INDATA are the signal quadrature components as described in Section 3.1.1.

For the receiver to operate efficiently without hard limiting, an estimate the expected signal-to-noise ratio in the information bandwidth must be obtained for input scaling. This value in dB, SNR, should be a conservative estimate of the signal-to-noise ratio. Using an estimate lower than the actual signal-to-noise ratio will not significantly effect performance of the receiver. On the hand, too high an estimate may result in an integer overflow causing program interrupts. The value of SNR along with the time constant, τ, of the low pass filter expressed in bit periods for the DC bias remover are input on the same card in (F20.6, I10) format. τ is normally set at 200 bit periods.

The next five parameters are all read from one card in (2I10, 3F20.6) format. They are: N, the time constant of the bit synchronization loop for acquisition expressed in bit periods; ISR, the number of samples per bit; BR, the number of bits per second; BWN3DB, the noise bandwidth of the Costas loop for acquisition; and SP, the peak signal voltage input to the A/D converter. N is a positive integer greater than zero. N must be less than 280 or an integer overflow will result due to scaling in the program. ISR must be an integer multiple of 4. The maximum Costas loop noise bandwidth is limited by sampling theorem requirements; that is, the sampling rate must be 2 to 10 times greater than the reciprocal of the loop noise bandwidth. Setting the sampling rate a factor of 5 times the reciprocal of the noise bandwidth will prevent Costas loop stability problems. BR is set equal to the number of bits per second. SP is used to scale the quadrature components IX and IY, and should be set to the peak-to-peak signal input voltage to the A/D converter in the absence of noise. The parameters for the tracking mode are both input from one data card in (I10, F20.6) format. NB is the time constant of the bit synchronization loop in bit periods, and BWA is the Costas loop noise bandwidth. Typical parameters for the receiver operating with the IF sampler at 244 Hz IF and with a bit rate of 12.2 bits/second are listed here.

N = 10 bit periods

ISR = 20 samples/bit

BR = 12.2 bits/second

BWN3DB = 1.0 Hz

SP = 1.0 volts

NB = 280 bit periods

BWA = 0.0625 Hz

The receiver has multiple outputs which are controlled by sense switches 1 and 2. The program outputs are: the detected bit, IOBIT; the Costas loop phase estimate, IXX; one input quadrature component, INT(1); the bit synchronization error signal, IR; and the correlator integral, ITX. IOBIT is a binary signal, 0 or 1, and is scaled to 0 or 1000 for display on the brush recorder. IXX has a range of $-\frac{\pi}{2}$ to $+\frac{\pi}{2}$ and is scaled to a range of 0 to 785 for display. For INT(1), 512 on the brush recorder corresponds to 0 volts. IR is the number of samples of bit timing correction, for which 600 on the brush recorder corresponds to 0 correction. One sample of correction is an increment of 40 on the brush recorder. For ITX, ISR*15 on the brush recorder corresponds to 0 volts. Sense switch 1 must be turned off to display IOBIT and INT(1). Sense switch 1 must be turned on, and sense switch 2 must be turned off to display IOBIT and IXX. Both sense switch 1 and 2 must be turned on to display ITX and IR.

Nine input parameters together define the scaling constants, the sampling period, and the Costas and bit synchronization loop parameters for acquisition and tracking. From these parameters all scaling and input-output parameters are computed.

A listing of the digital receiver with sample storage bit synchronization and the DC bias remover is given in Appendix V. This receiver has AGC in both the Costas and bit synchronization loops, and also has acquisition and tracking modes which are chosen by sense switch 3. Sense switch 3 must be turned on for tracking and turned off for acquisition. This listing is for the receiver set to operate with the IF sampler at 244 Hz IF and the bit rate at 12.2 bits/second. The receiver uses the subroutine INDATA with NPTS set to 4. The first two samples from INDATA are the signal quadrature components

as described earlier.

In developing this receiver we devoted considerable efforts to the scaling problems encountered in converting the Costas loop and bit synchronization loop equations from floating point to integer arithmetic. We scaled the Costas loop equations from floating point to integer arithmetic. We scaled the Costas loop equations for operation over a wide range of loop noise bandwidths from 1.18×10^{-2} to 1.18×10^{1} Hz. A wide range of bandwidths is necessary for the Costas loop to acquire large offset frequencies rapidly before switching to a tracking mode. The loop bandwidth changes three orders of magnitude, but one of the bandwidth related parameters changes from 10^{-6} to 10^{3} - nine orders of magnitude. In order to keep as many significant figures as possible without danger of integer overflows, we divided this bandwidth range into nine divisions.
Then we scaled the bandwidth related parameters and the Costas loop equations to keep either two or three significant figures for each of these divisions. Three significant figures are used for SNR greater than 5 dB, and two significant figures are used for SNR less than 5 dB.

The digital receiver with sample storage bit synchronization uses the same input parameters as the digital receiver without sample storage bit synchronization. Because this version of the digital receiver has AGC, the receiver does not depend on SP, the peak signal amplitude, for correct loop again. The input peak signal voltage must only be large enough to prevent A/D converter quantization problems. The AGC removes receiver dependence on the input signal amplitude. The receiver outputs are the same as those described for the digital receiver without sample storage bit synchronization.

Split-Phase Data with Data Derived Bit Synchronization

We developed a digital receiver for use with split-phase data format. This receiver is identical to the NRZ receiver except an "N-out-of-M" detector has been added to determine phase for bit synchronization (N=66 and M=90).

A listing of the digital receiver for split-phase data format is given in Appendix VI. This receiver has the DC bias remover and AGC in both the COS-tas and bit synchronization loops. The receiver has acquisition and tracking modes which are controlled as before by sense switch 3. This listing is for the receiver set to operate with the IF Sampler at 244 Hz IF and the bit rate at 6.1 bits/second. The receiver uses the subroutine INDATA with NPTS set to 4. The first two samples are the signal quadrature components as described in Section 3.1.1.

The digital receiver uses the same input parameters that are used in the NRZ case. However, the time constant of the bit synchronization loop is limited to 140 bit periods, and the number of samples per bit, ISR, must be an integer of multiple of 8.

The receiver has multiple outputs which are controlled by sense switches 1 and 2. The program outputs are: the demodulated bit stream, IOUTT; the Costas loop phase, IXX; the coded split-phase signal before demodulation, IOBIT; one input quadrature component, INT(2); and the bit synchronization error signal, IR. IOUTT is a binary signal, 0 or 1, and is scaled to 0 or 1000 for display on the brush recorder. All the other outputs are scaled as described for the receiver without sample storage bit synchronization. Sense switch 1 must be turned off to display IOUTT and IXX. Sense switch 1 must be turned on, and sense switch 2 must be turned off to display IOBIT and INT(2). Both sense switch 1 and 2 must be turned on to display IOUTT and IR.

Baseband Digital Receiver with Data Dervied Bit Synchronization

We developed a digital receiver for use with NRZ data that has already been converted to baseband. This receiver was developed from our digital PSK receiver. Since the data is at baseband there is no need for a carrier tracking loop in the receiver. Only a bit synchronization loop and a correlator are necessary for the baseband receiver. To develop the baseband receiver we modified our digital PSK receiver by removing the Costas loop equations. The remaining receiver functions are unchanged.

A listing of the baseband digital receiver for NRZ data is given in Appendix VII. The receiver has AGC, the DC bias removes, and acquisition and tracking modes controlled as before by sense switch 3. The listing is for the baseband receiver operated with a bit rate of 12.2 bit/seconds. The input bit stream was sampled directly by the A/D converter with a sampling frequency of 976 Hz. The baseband receiver uses every fourth sample from the A/D converter effectively reducing the sampling frequency to 244 Hz (20 samples/bit).

The expected signal-to-noise ratio, and the time constant of the low pass filter in the DC bias remover are input as described previously. The next four input parameters are all read from one card in (2I10, 2F20.6) format. They are: N, the number of bit periods in the time constant of the bit synchronization loop for acquisition; ISR, the number of samples per bit; BR, the number of bits per second; and SR, the peak signal input voltage. The number of bit periods in the time constant of the bit synchronization loop for tracking, NB, is read from one card in (I10) format.

The receiver has multiple outputs which are controlled by sense switches 1 and 2. The receiver outputs are: the detected bit, IOBIT; the correlator integral, ITX; the bit synchronization loop error signal, IR: and the input baseband NRZ data, INT(2). All these outputs are scaled as described earlier in this section. Sense switch 1 must be turned off to display IOBIT and INT(2). Sense switch 1 must be turned on, and sense switch 2 must be turned off to display IOBIT and IR. Both sense switch 1 and 2 must be turned on to display IOBIT and ITX.

3.1.9 Study of Acquisition Techniques

We designed the Digital PSK Receiver with the philosophy that receiver operation be totally "hands off" once the computer program is compiled. To that end, all scaling, parameter definitions, and input-output operations are performed automatically after the user inputs nine parameters on data cards. In free running acquisition, the user must decide when the receiver has locked on to the noisy signal and then switch the receiver to the tracking mode. The user must also ascertain when the receiver loses lock while tracking and then switch the receiver to the acquisition mode. To make receiver operation fully "hands off", we designed logic to indicate when the receiver is in lock and studied two automatic acquisition techniques.

Acquisition Indicator

In practical applications of phase-locked loops, an indication of lock is obtained by beating a 90° phase shifted version of the VCO output with the input signal, low pass filtering this result, and then thresholding the low pass filter output. Unfortunately, this simple technique is not applicable to the Costas loop because of the phase modulation of the input signal. This technique, if it could be applied to the Costas loop, would also only indicate

that the carrier tracking loop is in lock. For the digital receiver, a technique is needed that will indicate when both the carrier synchronization and bit synchronization loops are in lock. Intuitively, the correlator output from the digital receiver is a good indicator of lock. For the correlator output to be correct, both good carrier synchronization and good bit synchronization are required. In lock with no noise, the correlator output will be either + AT or - AT. To use the correlator output as an indication of lock, it is necessary to remove the data dependent sign changes since the magnitude of the correlator output is the parameter of interest.

Using this philosophy, we designed an acquisition indicator. The correlator output is passed through an absolute value nonlinearity, low pass filtered, and thresholded to determine acquisition status. We determined the mean and variance of the correlator output in both the in-lock and out-of-lock cases. For the out-of-lock case, we assume that the bit timing error (no noise) was uniformly distributed between -0.5 T and +0.5 T, and that the Costas loop phase error was uniformly distributed between $-\pi$ and $+\pi$. The mean correlator output due to signal alone is then 0 and the variance is $5(AT)^2/12$. For the in-lock case, the mean correlator output is AT, and the variance is zero. We computed the mean, $\bar{z}$, and the variance, σ_z^2, of the signal at the output of the absolute value nonlinearity from Equations (167) and (168) where μ and σ^2 are the mean and variance of the correlator output.

$$\bar{z} = \frac{2\sigma}{\sqrt{2\pi}} e^{-\frac{\mu^2}{2\sigma^2}} + \mu \operatorname{erf}\left[\frac{\sqrt{2}\mu}{2\sigma}\right] \qquad (167)$$

$$\sigma_z^2 = \sigma^2 + \mu^2 - z^2 \qquad (168)$$

For the in-lock case, at 0.0 dB our analysis predicted the mean and variance of the signal at the output of the absolute value nonlinearity to be 1.05 and

0.39 respectively (the correlator output has been normalized to 1.0). A digital simulation at 0.0 dB showed a mean of 0.97 and a variance of 0.38. For the out-of lock case, at 0.0 dB we predicted a mean of 0.76 and variance of 0.33. A digital simulation of the out-of-lock case showed a mean of 0.75 and a variance of 0.29. These results validate our analysis of the acquisition indicator performance. To decrease the variance we passed the output of the absolute value through a low pass filter with a time constant of ten bit periods. Our analysis and simulation show that the threshold should be set between .9 and .99 to insure a high probability of acquisition. Typical performance of the acquisition indicator in the absence of noise is shown in Figure 85 along with the bit tracking and phase tracking errors. The output fluctuates around the mean out-of-lock value (0.5) until the bit tracking error is less than 0.1 T and the phase tracking error is less than 0.5 radians. The output then charges up to the mean in-lock value (1.0) as the tracking errors go to zero. A strip chart recording made at NASA Goddard with the Digital PSK receiver showing the acquisition indicator and the Costas loop phase is given in Figure 86 . These results indicate that this technique generates a valid indication of lock.

Stepped Bandwidth Acquisition

One simple approach for automatic acquisition is to operate the receiver with a wide bandwidth initially and then narrow the loop bandwidths in steps as the acquisition indicator crosses successively higher threshold values. When the acquisition indicator drops below preset threshold values, the loop bandwidths are widened automatically to reacquire. This technique requires that any initial offset frequency be within the pull-in range of the widest loop bandwidth used.

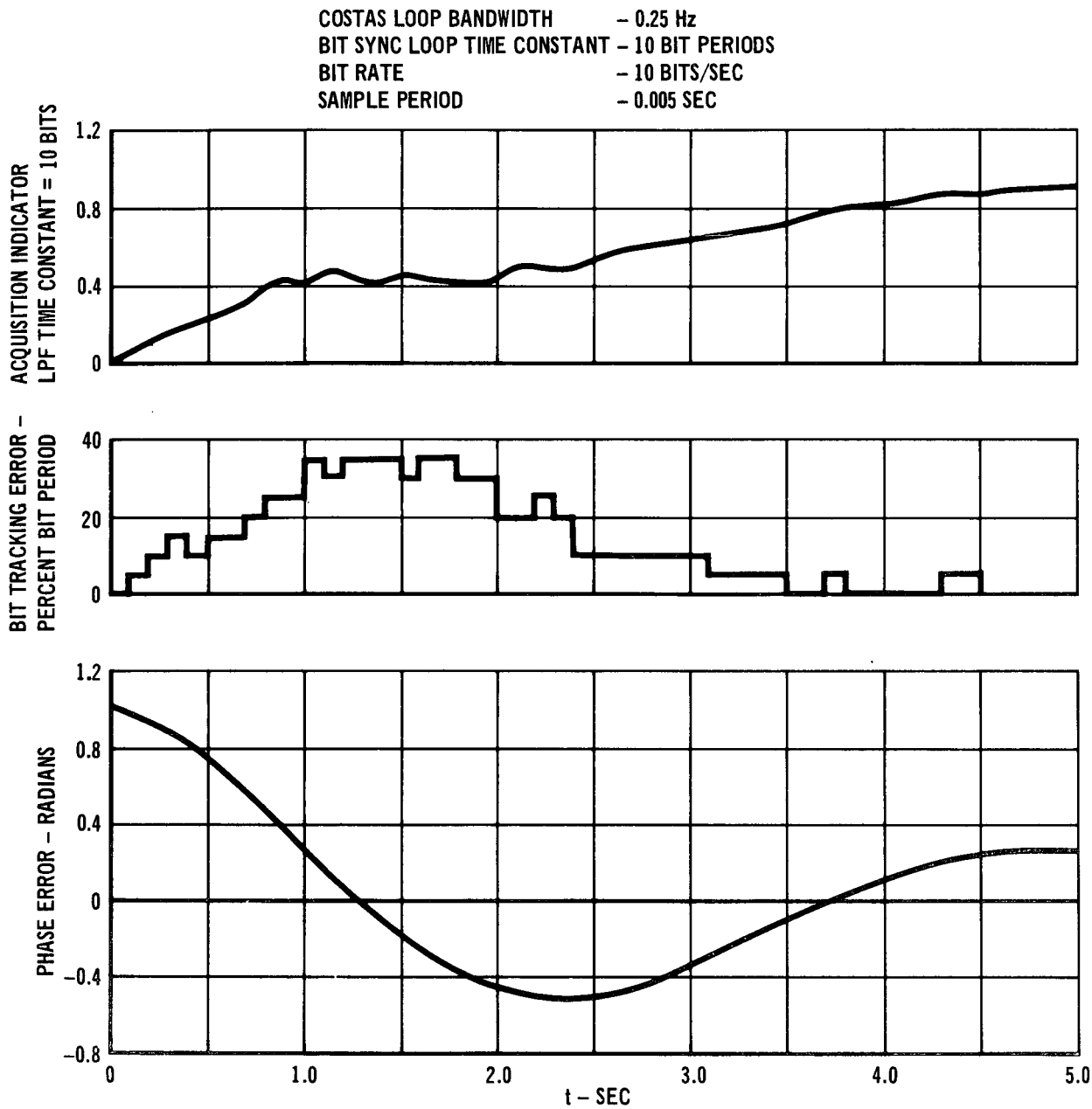

ACQUISITION INDICATOR – SIMULATION

Figure 85

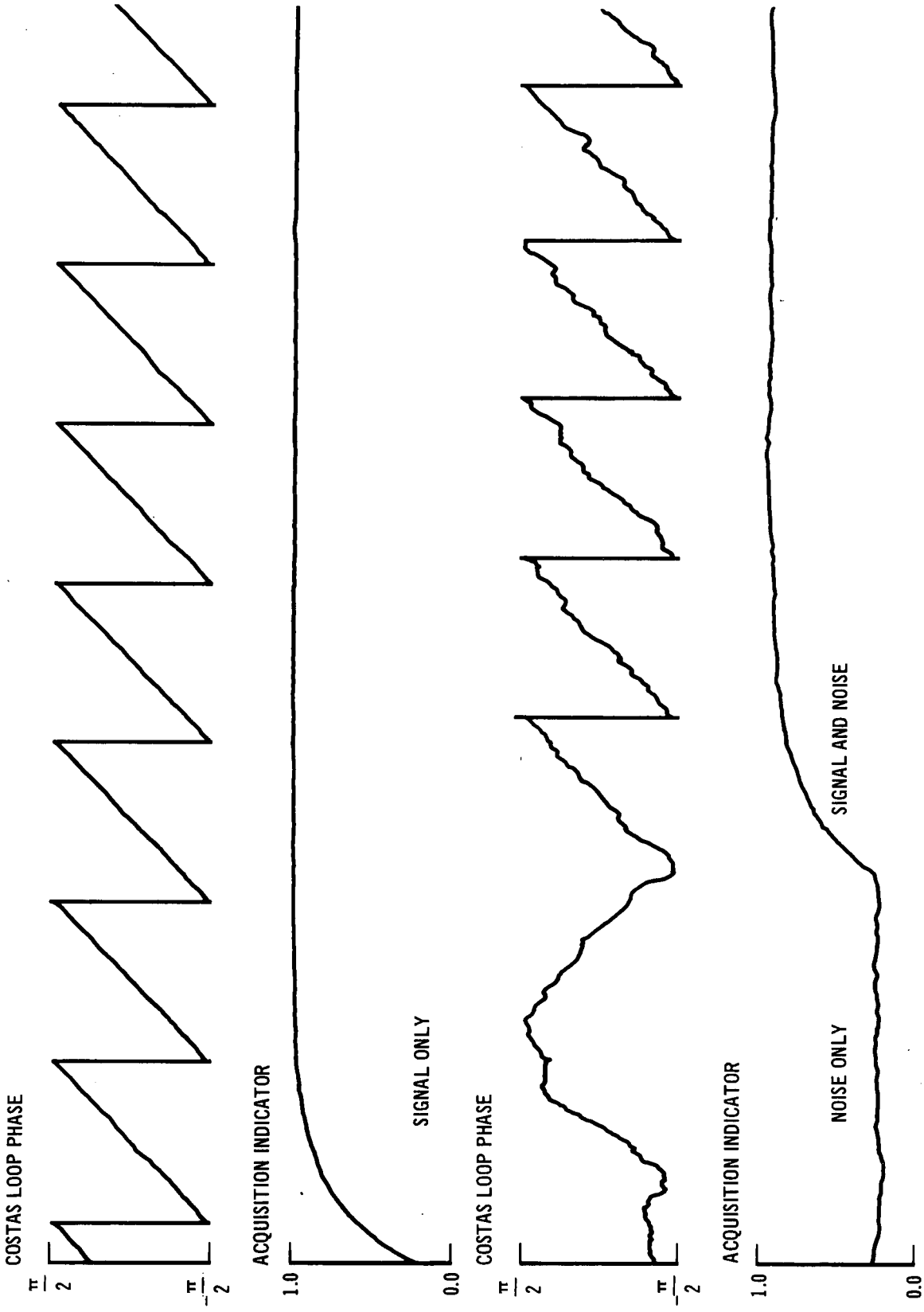

ACQUISITION INDICATOR – EXPERIMENTAL

COSTAS LOOP BANDWIDTH - 2.0 Hz

Figure 86

We experimentally investigated acquisition with this technique using a Costas loop with three bandwidths 1.0 Hz, 0.25 Hz, and 0.0625 Hz. The initial bandwidth of 1.0 Hz is reduced by a factor of 4 when a threshold of 0.90 is crossed, and is again reduced by a factor of 4 when a threshold of 0.95 is crossed. With no noise and with offset frequencies within the pull-in range of the loop, the bandwidths are reduced as desired and the receiver acquires without difficulty. However, for any acquisition technique to be practical, it must result in receiver acquisition at low signal-to-noise ratios; i.e., 0.0 to 3.0 dB. We were unable to acquire using this technique at less than $\frac{E}{N_o} = 3$ dB. The acquisition indicator would cross one threshold for a few seconds, but would then go below threshold again. At low signal-to-noise ratios the acquisition indicator caused instabilities with this technique. We investigated receiver acquisition with other loop bandwidths and threshold levels, and had similar results. Although this technique is very simple to implement, its performance at low signal-to-noise ratios was unsatisfactory.

Swept Frequency Acquisition

A common approach for acquisition in phase-locked loops is the swept frequency method discussed in Section 2.6.1 and Section 2.8.3. This approach was applied to the digital receiver for automatic acquisition. The VCO frequency of a very narrow bandwidth Costas loop is swept until the acquisition indicator crosses threshold. The frequency of the sweep when the threshold is crossed is used as the initial condition on the VCO frequency of the Costas loop in the tracking mode. If this frequency is within the pull-in range of the Costas loop, the loop will rapidly acquire. Once an accurate phase reference is established, the bit synchronization loop will also pull-in rapidly.

The swept VCO output is $\cos [\omega_o t + \hat{\theta}(t) + \phi(t)]$ where $\phi(t) = \omega_i t + \frac{1}{2} \alpha t^2$. The initial sweep frequency is ω_i rad/sec, and the sweep rate is α rad/sec/sec. Because the frequency offsets encountered in practice at NASA Goddard are less than 1.0 Hz, the initial frequency is usually set at -2π or $-\pi$ rad/sec. The frequency is then swept to the final frequency, ω_f, either at $+2\pi$ or $+\pi$ rad/sec. If the Costas loop has not acquired by this time, the sweep is initialized to ω_i and swept again to ω_f. When the threshold is crossed at t_a, VCO frequency is computed, $\omega_a = \omega_i + \alpha t_a$. ω_a is then used as an initial condition on the frequency of the Costas loop. If the acquisition indicator falls below frequency threshold at any time, the Costas loop is automatically swept again.

Because the Costas loop is operating in a non-linear mode during acquisition, it is impossible to analytically determine the sweep rate to insure a high probability of acquisition. For this reason a digital simulation must be used to determine the sweep rate. In Sections 2.6 and 2.8.3 we investigated probability of acquisition for a phase-locked loop with various sweep rates using a digital simulation and compared these results to those obtained by Frazier and Page[9]. We then investigated probability of acquisition for the digital receiver using a digital simulation. For the noise free case we found that the Costas loop would not acquire with a sweep rate which insured a probability of acquisition of 1.0 for a phase-locked loop. Both loops were operated under the same conditions; i.e., identical loop noise bandwidths and identical sample rates, with no noise. In general we found that the Costas loop must be swept almost an order of magnitude slower than a phase-locked loop to acquire. This may be attributed to basic differences in the Costas loop and the phase-locked loop. First, the Costas loop has a smaller linear range than the phase-locked loop. This is because the error signal for the linearized

Costas loop is proportional to sin $[2(\theta - \hat{\theta})]$ whereas the error signal for the linearized phase-locked loop is proportional to $\sin[\theta - \hat{\theta}]$. Second, the phase error variance for the Costas loop (Equation 169) is greater than the phase error variance for the phase-locked loop for the same loop noise bandwidth, B, (Equation 170).

$$\sigma_\phi^2 = \frac{N_o B}{A^2} \left[1 + \frac{N_o W}{2A^2}\right] \tag{169}$$

$$\sigma^2\phi = \frac{N_o B}{A^2} \tag{170}$$

W = bandwidth of low pass filters in Costas loop

$\frac{A^2}{N_o}$ = signal-to-noise density ratio

The Costas loop generates cross terms between the signal and noise as well as squared terms. These factors account for the differences in acquisition for the Costas and phase-locked loops.

The swept frequency technique can be used for automatic acquisition, but the Costas loop VCO frequency must be swept slowly. However, for the small uncertainty expected in frequency, the low sweep rates are not restrictive.

Variable Sampling Rate for Acquisition

In the phase-locked loop study, we sampled at a rate consistent with the maximum expected offset frequency. However, during normal tracking operation, the frequency at the output of the loop phase detector is much less than the offset frequency. After acquisition has occurred, the sampling rate required for tracking (at high signal-to-noise ratios) need only be consistent with the bandwidth of the tracking loop. In order to increase the efficiency of our PSK demodulator, we investigated the use of a variable sampling rate acquisition technique.

There are several problems associated with mechanizing this approach. For high sampling rates, there is insufficient time to perform all calculations between samples. Since a good phase reference is basic for all receiver functions, the Costas loop is operated alone at a high sampling rate until the signal is acquired. Then the sampling rate is lowered so that all receiver functions can be executed.

The most difficult problem with this technique is that of controlling the sampling rate from the digital computer. With the quadrature component sampling technique, it is necessary to physically change the rate at which the A/D converter samples the quadrature components. This must be done by changing the sampling frequency of the A/D converter. Thus, operation of the digital receiver is interrupted while the sampling frequency is manually reduced. This method is not attractive since it requires a special A/D converter.

The problem of controlling the sampling rate from the digital computer is easily solved using the IF sampling technique. Section 3.1.1 discussed the IF sampling technique. We showed that the digital processor can change the effective sampling rate by discarding certain samples. For example, the first two samples from S/H 1 in Figure 52 are quadrature samples of 0.97 KHz IF. The digital processor can fix the interval between samples of the quadrature components at 1.024 msec by discarding the next two samples from S/H 1 before accepting the fifth and sixth samples as the next pair of quadrature samples. The digital receiver could operate the Costas loop alone with a 1.024 msec interval between samples of the quadrature components. After the Costas loop acquires, the interval between samples of the quadrature components is lengthened to 2.048 msec

F

by discarding six samples between pairs of quadrature component samples. After reducing sampling rate, all receiver functions are executed. In order to reduce the sampling rate it is necessary to change the variable NPTS in the subroutine INDATA from 4 to 8 using a sense switch. The sampling rates 1.024 msec and 2.048 msec were only used for an example of variable sampling rates at .97 KHz IF. Following the method outlined here, the user defines the sampling rates to be compatible with the IF frequency being used.

Thus, variable sampling rate acquisition appears to be an attractive technique for acquiring over wider frequency uncertainities than would normally be possible.

3.2 Digital PSK System Performance Analysis

The Digital PSK program was developed and optimized especially for the NASA Goddard CDC 3200 computer. For instance, the program was written with all integer operations to get minimum computation time with no floating point hardware on the NASA Goddard CDC 3200. It was scaled to get the maximum possible resolution (i.e. minimum quantization) without danger of a variable overflow. The program in its Fortran version has a maximum bit rate (at four samples per bit) of approximately 80 bits/second. Rewriting this program in machine language would considerably increase the maximum bit rate.

The basic parameter in the PSK system evaluation is bit error rate, however the statistics of the phase error and bit timing error are also of interest for complete system optimization and analysis. Although the optimum possible performance of a PSK demodulator is well known and presented in Equation (171) in terms of the signal power to noise density ratio, $\frac{E}{N_o}$, this is not really sufficient for comparisons since

it ignores the effect of non-perfect synchronization.

$$P_e = \frac{1}{2}\left(1 - \text{erf}\sqrt{\frac{E}{N_o}}\right) \qquad (171)$$

Most systems will approach this bound as the bit sync and carrier tracking bandwidths go to zero; however no system can achieve this performance for wideband carrier phase and bit rate variations. We obtain expressions which relate phase error and bit timing statistics to our system parameters. These are then related to the bit error probability of the total system. These results can then be compared with the bit error probability achieved with perfect phase and bit timing and the error probability achieved with other non-ideal systems.

3.2.1 Sampling Losses

The first E/N_o loss in a digital system comes from the finite sampling rate. The low-pass filters (or bandpass filters for IF sampling) which precede the A/D converter must be wide enough to pass the uncertainty or variations in carrier frequency. Normally it might be supposed that the bandwidths of these filters were not very critical since if they were too wide the extra noise could be filtered out digitally within the computer. However this is not completely true for two reasons. First, the limited dynamic range of an A/D converter makes the quantization error of the digital processor dependent on dynamic range and thus bandwidth of the noisy input. Second, the finite sampling rate of the A/D converter limits the degree to which the noise can be filtered out. Aliasing or spectral fold-over causes an effective increase in the input noise density. This effect is decreased by increasing the sampling frequency to several times the low-pass filter bandwidth.

The loss in E/N_o due to aliasing of the noise spectrum is shown in Figure 87 for the case of a single break RC filter. This figure assumes that the bandwidth of the signal is such that it is unaffected by the filtering before A/D conversion. Note that the losses shown in Figure 87 could be reduced by using sharper cut-off filters or completely eliminated by using a perfect integrate and dump filter.

Another consideration in choosing the low pass filter bandwidth is the degradation due to intersymbol interference. Figure 88 shows the degradation in signal-to-noise ratio from intersymbol interference as a function of bandwidth and bit error rate. The best choice of low pass filter bandwidth corresponds roughly to the value for which the loss due to intersymbol interference is equal to the sampling loss. Figure 89 shows a plot of the combined intersymbol interference and sampling loss as a function of bandwidth for a probability of error of 10^{-6} and 20 samples/bit. This indicates that a good choice of bandwidth (for low probabilities of error and 20 samples per bit) is three to three and one half times the bit rate.

The loss in performance due to quantization error is determined by the sample S/N (i.e. the S/N in the low-pass filter bandwidth). Let 2A be the total spread of the quantization levels, σ^2 the variance of the input noise samples, and S the amplitude of the input signal.

Let $A = S + 3\sigma$ (172)

so that each sample lies within the quantization levels $\pm A$ with high probability. The distribution of the quantization noise, n_q, will be approximately uniform,

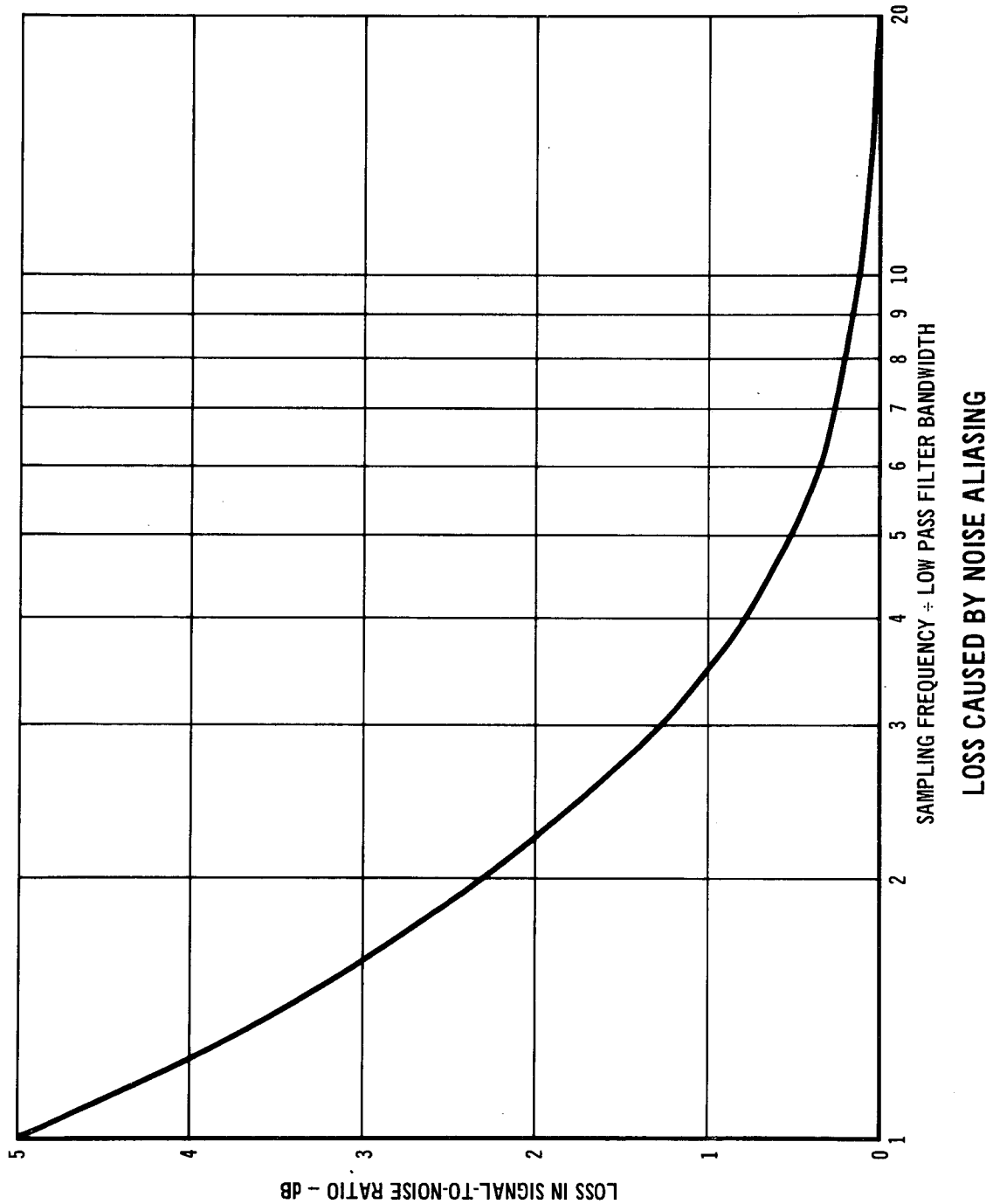
LOSS CAUSED BY NOISE ALIASING
SAMPLING FREQUENCY ÷ LOW PASS FILTER BANDWIDTH
1
2
3
4
5
6
7
8
9
10
20
LOSS IN SIGNAL-TO-NOISE RATIO – dB
0
1
2
3
4
5

Figure 87

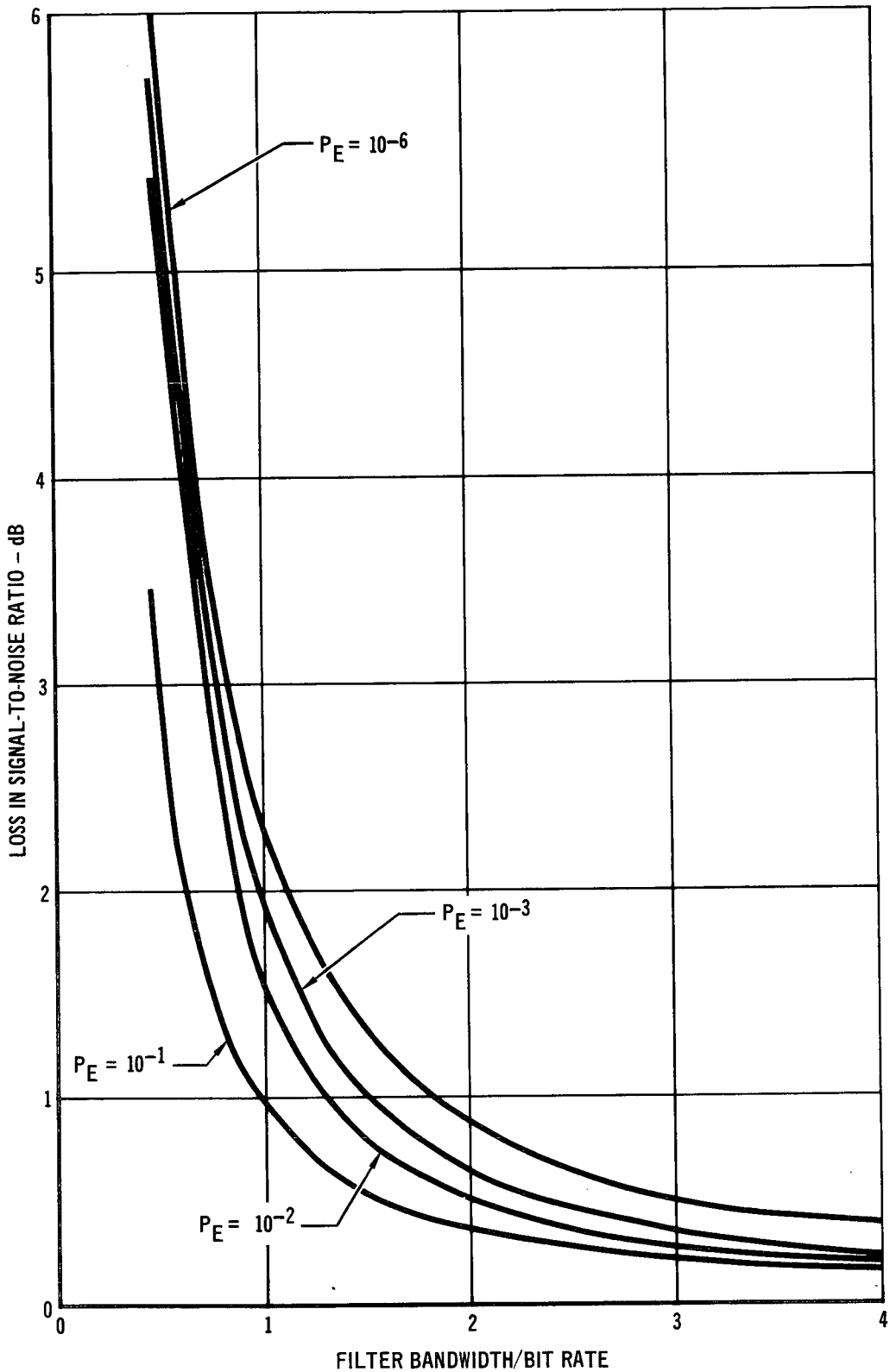

LOSS CAUSED BY INTERSYMBOL INTERFERENCE

Figure 88

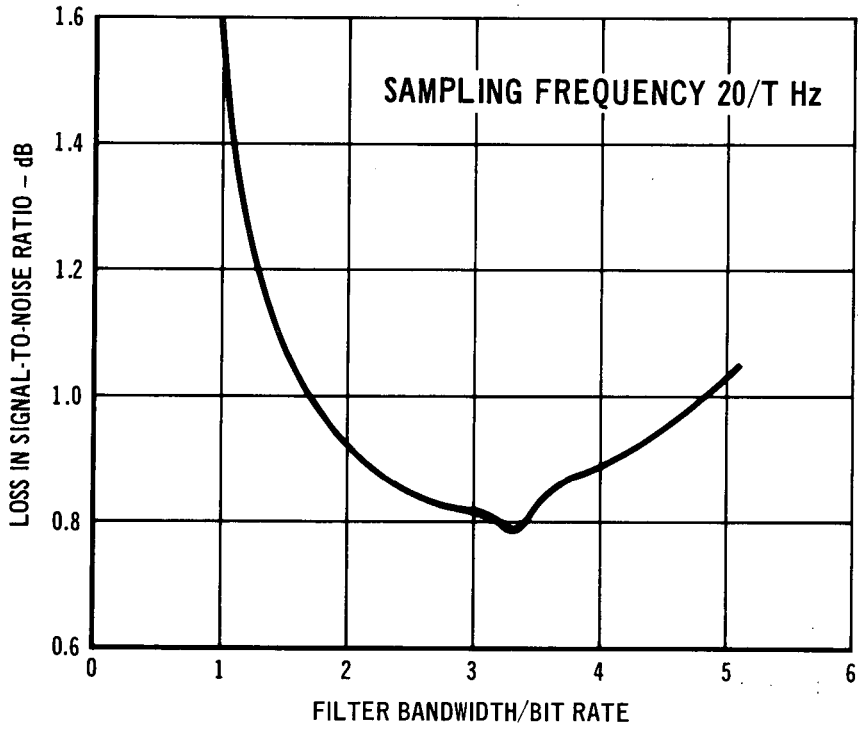

TOTAL SAMPLING LOSS

Figure 89

$$P(n_q) = \begin{cases} Q/2A \text{ for } -A/Q \leq n_q \leq A/Q \\ 0 \text{ for } |n_q| \geq A/Q \end{cases} \tag{173}$$

where Q is the number of quantization levels. Thus the variance of the quantization noise (σ_{n_q}) is given by Equation (174).

$$\sigma_{n_q} = \frac{A^2}{3Q^2} = [\ s + 3\sigma]^2/3Q^2 \tag{174}$$

With a frequency offset, the quantization noise samples will be approximately independent, sample to sample. Thus, the bandwidth of the quantization noise will be approximately a factor of 10 greater than the signal bandwidth. This implies that effective quantization noise power (in the signal bandwidth) is actually about 1/5 σ_{n_q}. We will ignore the improvements due to filtering of quantization noise and obtain an approximate expression for the total system signal-to-noise ratio $(S/N)_t$.

$$(S/N)_t = \frac{s^2}{\sigma^2(1 + \frac{(s/\sigma + 3)^2}{3Q^2})} \tag{175}$$

For $\frac{s^2}{\sigma^2} = 100$ and Q = 32 levels, the increase in noise is only on the order of 10% and the effect decreases with increasing s/σ. Thus the effect of quantization is not expected to be significant for the Goddard CDC 3200 ($Q = 2^{12}$), although quantization noise may be significant in a special purpose hardware implementation.

Low Resolution Sampling and Processing

We experimentally investigated the effect of reducing the number of bits/word both in the A/D converter and in the digital processor. We were particularly interested in whether reducing the number of bits from 12 (the word length of the A/D converter used with the GSFC CDC 3200) to 8 would significantly degrade performance. 8 bits is particularly convenient for a hardward implementation in that 8 bit read-only memories for the sine table look-up routine are readily available. Section 5 discusses the advantage of using an 8 bit word length. Reducing the word length from 12 bits to 8 bits caused no measurable change in the probability of bit error or the phase error variance at $\frac{E}{N_o}$ = 3 db. The timing error variance increased from .293 to .269 (measured in terms of time between input samples). At $\frac{E}{N_o}$ = 9 db there was still no measurable degradation in bit error probability, although the phase error variance increased from 2.0×10^{-4} to 2.1×10^{-4} radians and the timing error variance increased from .158 to .160 sample periods.

The A/D converter can operate with fewer bits/word than the digital processor when angle modulated signals are demodulated. Experimental results indicate that hard-limiting the PSK before sampling results in approximately 1.0 db loss in output E/N_o. However, since A/D converter speed is not really a problem in increasing bit rate, there does not appear to be any reason for looking at low-resolution, high speed, A/D converters.

Analytical results discussed earlier in this report indicate that decreasing the number of bits/word below 6 causes a degradation in performance especially for large values of E/N_o.

3.2.2 Losses Due to Imperfect Phase Synchronization

The loss in E/N_o due to imperfect bit and carrier synchronization cannot be easily predicted or even tightly bounded without several very restrictive assumptions. This section will present techniques for predicting losses due to imperfect synchronization and compare these results with experimentally determined data.

The first step in determining the effect of phase reference error is to define the statistics of the phase error. We will assume that the sampling rate is sufficient to make the dynamics of the digital Costas loop appear continuous. The effect of sampling is accounted for by using the sample signal-to-noise ratio as the continuous loop input signal-to-noise ratio. The phase error distribution function has been shown 19 to be approximated by the right-hand side of Equation (176). α and B are functions of the Costas

$$P(\phi) = \frac{e^{(\alpha\cos\phi + B\phi)}}{4\pi^2\, e^{-B\pi}\, |I_{jB}(\alpha)|^2} \int_{\phi}^{\phi + 2\pi} e^{-Bx - \alpha\cos x}\, dx \qquad (176)$$

loop parameters and the input signal-to-noise ratio, and $I_{JB}(x)$ is the modified Bessel function of imaginary order and of argument x. For high loop signal-to-noise ratios, Equation (176) is approximately Gaussian, whereas for low signal-to-noise ratios, it approaches a uniform distribution. The probability of bit error for imperfect phase synchronization can then be expressed as in Equation (177) for the case where the Costas loop bandwidth is much less than the bit rate frequency.

$$Pe = \int_{-\infty}^{\infty} [1 - \text{erf} (\sqrt{\frac{E}{n_o}} \cos (\phi))] P(\phi) \, d\phi \qquad (177)$$

For large loop signal-to-noise ratios the Costas loop is nearly linear; thus, the phase error variance can be approximated as shown in Equation (178).

$$\sigma_\phi^2 = \frac{N_o B}{A^2} \left[1 + \frac{N_o W}{2A^2} \right] \qquad (178)$$

W is the bandwidth of the low-pass filters G(s). If G(s) are integrate-and-dump filters, then $W = \frac{1}{2T}$ where T is the integrate time. B is the bandwidth of F(s), and $\frac{A^2}{N_o}$ the signal-to-noise density ratio. Equation (178) indicates an objectionable property of the Costas loop. The Costas Loop generates cross terms between the signal and noise as well as squared noise terms. These terms cause loop performance to be directly dependent on both the bandwidth of the two low-pass filters G(s) and the loop filter F(s) (Figure 57). As our Digital PSK software is presently configured, the bandwidth of the two low-pass filters labeled G(s) is assumed to be the same as the bandwidth of the analog low-pass filters used in the quadrature component generation. By proper manipulation this allows the digital filtering operation. This simplifies the digital Costas loop implementation, but it also makes the bandwidth of the external analog filters more critical. If the low-pass filter bandwidths are too wide, the extra noise will cause signal suppression when the outputs of the low-pass filters are multiplied together. This will increase the phase variance σ_ϕ^2 as indicated in Equation (178). Figure 90 is a plot comparing the phase variance from the Digital PSK program and the linear theoretical value given by

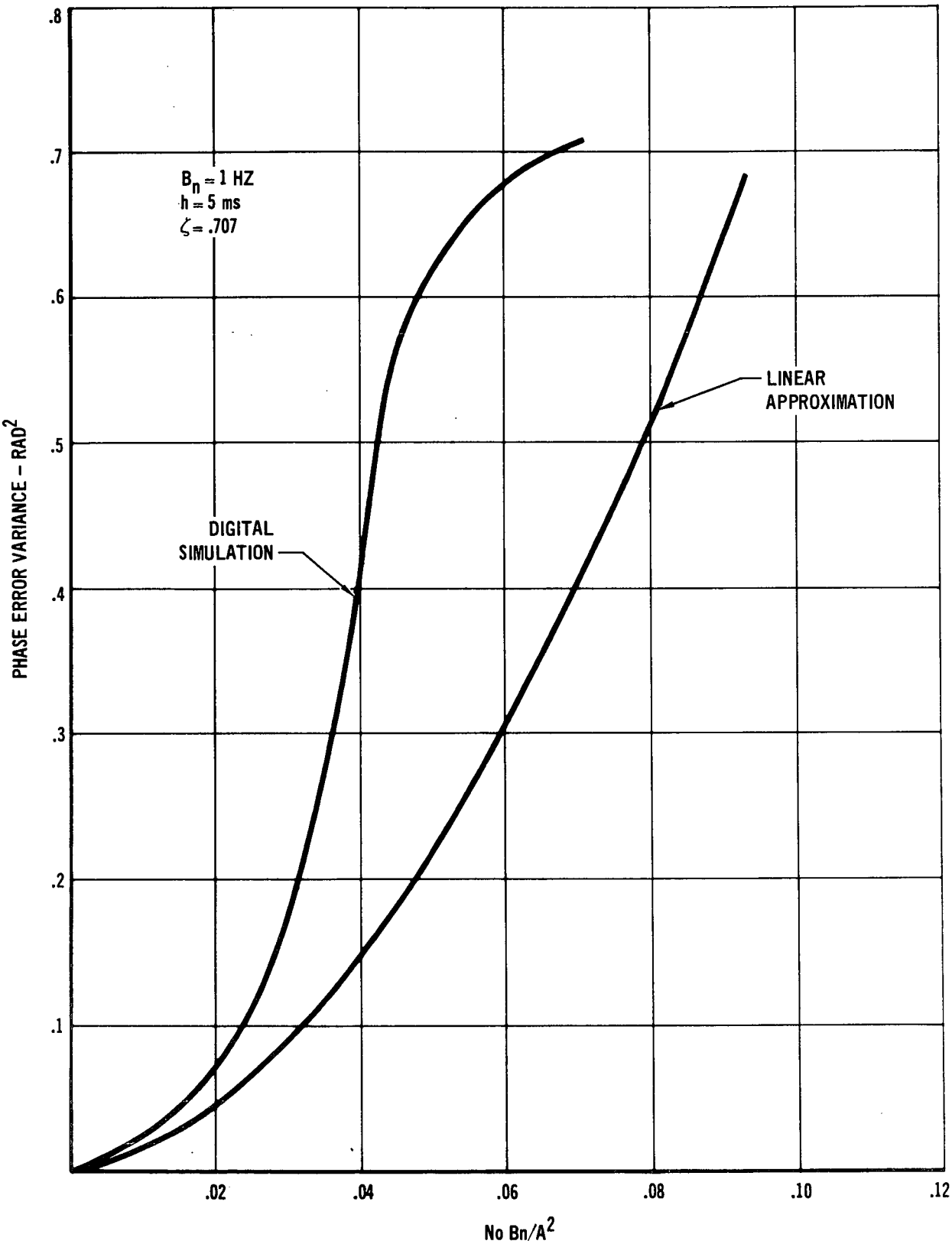

COSTAS LOOP PHASE ERROR VARIANCE

Figure 90

Equation (178) The linear theoretical values for phase variance are only accurate when the signal-to-noise ratio in the bandwidth of the G(s) filters is high. Figure 91 is a plot of probability of error as a function of signal-to-noise ratio with the phase reference supplied by a Costas loop. This figure assumes Gaussian phase error with a variance given by Equation (178). To simplify analysis of losses due to imperfect phase reference, Figure 91 shows the probability of error as a function of $\frac{E}{N_o}$ and the phase filter σ_ϕ^2 (assuming Gaussian phase error). Thus to determine the loss in signal-to-noise ratio, the designer first determines the phase variance either by simulation or by Equation (178) and then uses Figure 91 to determine the loss in error rate performance.

3.2.3 Losses Due To Imperfect Bit Synchronization

The analysis of bit synchronization errors is somewhat more difficult since the bit synchronization estimate is limited to one of N discrete values (where N is the number of samples/bit). It has been shown that the mean absolute value of the bit timing error is inversely proportional to the square root of the signal-to-noise ratio (in the information bandwidth) and the square-root of the time constant of the averaging filter in bit tracking loop. Although these results were obtained for analog bit synchronizers, they also hold approximately for digitally implemented bit synchronizers.

Appendix III presents an analysis of mean square timing jitter for the bit synchronization technique used in the Digital PSK program. Figure 92 compares the theoretical timing jitter rms value with that measured in the Digital PSK program for a bit synchronization loop time constant of 10 bit periods and 80 samples/bit. Figure 93 shows

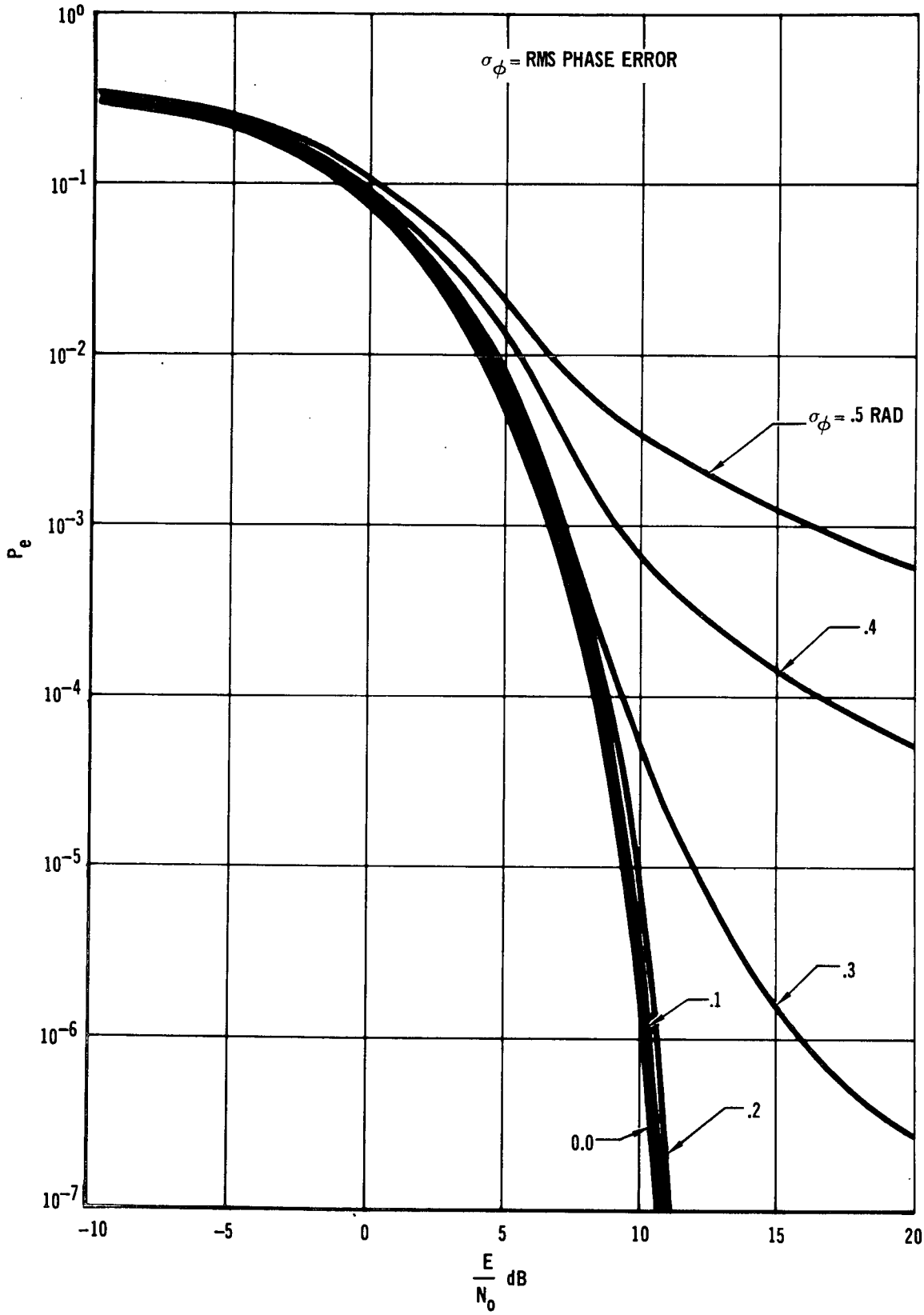

PROBABILITY OF ERROR WITH A NOISY PHASE REFERENCE

Figure 91

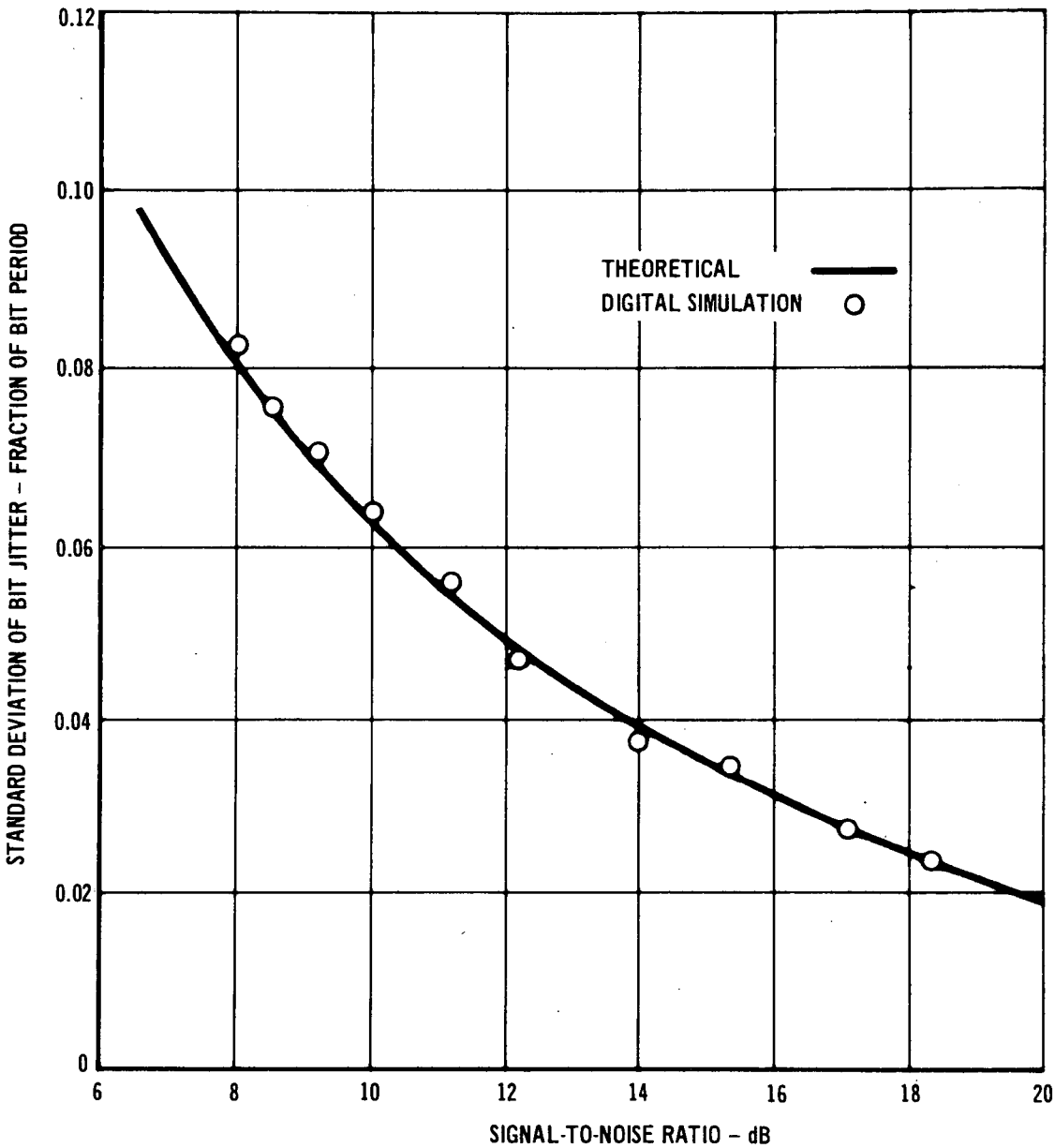

STANDARD DEVIATION OF BIT JITTER VERSUS SIGNAL-TO-NOISE RATIO Figure 92

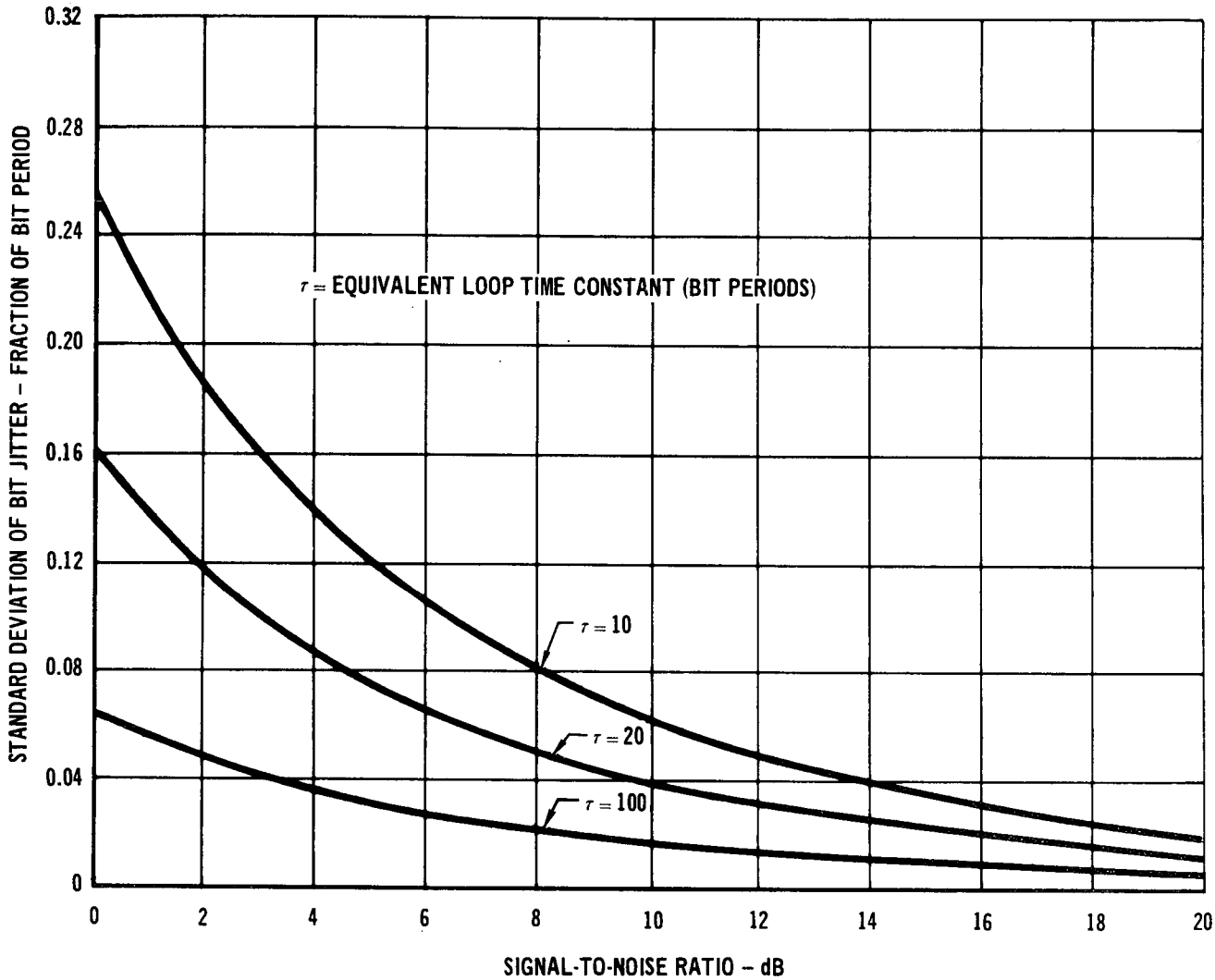

BIT SYNCH ERROR VERSUS SIGNAL-TO-NOISE RATIO (THEORETICAL)

Figure 93

the effect of the bit tracking loop bandwidth (or time constant) on rms timing jitter σ_T. The rms timing jitter can then be approximately related to the average loss in signal-to-noise ratio as shown in Equation (179) for the high signal-to-noise ratio case. This result assumes Gaussian distributed phase error and a bit width T. The effect of

$$(S/N)_{Loss} = 10 \log \left[1 - \frac{4\sigma_T}{T\sqrt{2\pi}} + \frac{\sigma_T^2}{T^2}\right] \qquad (179)$$

sampling rate on rms timing jitter is shown in Figure 94 which was determined by simulation. Thus, the increase in probability of error due to imperfect bit synchronization is determined by first calculating the rms value of the bit timing error using the loop parameters and then calculating the increase in probability of error.

3.2.4 Performance Evaluation

The past sections have compared theoretical predictions and experimental measurements of various subsystem output statistics such as the phase error and bit timing error variance. This section will look at the total system and will compare theoretical predictions and experimental measurements of probability of error for the entire MDAC Digital PSK receiver. Since demodulation of deep space telemetry is one of the chief applications of interest, it is especially important that the MDAC Digital Receiver operate as close to the theoretical optimum as the bit timing and frequency stability will allow. It is also important that the receiver be flexible and versatile without sacrificing error rate performance.

Figure 95 is a comparison of optimum theoretical error rate performance with experimental data taken using the NASA GSFC CDC 3200

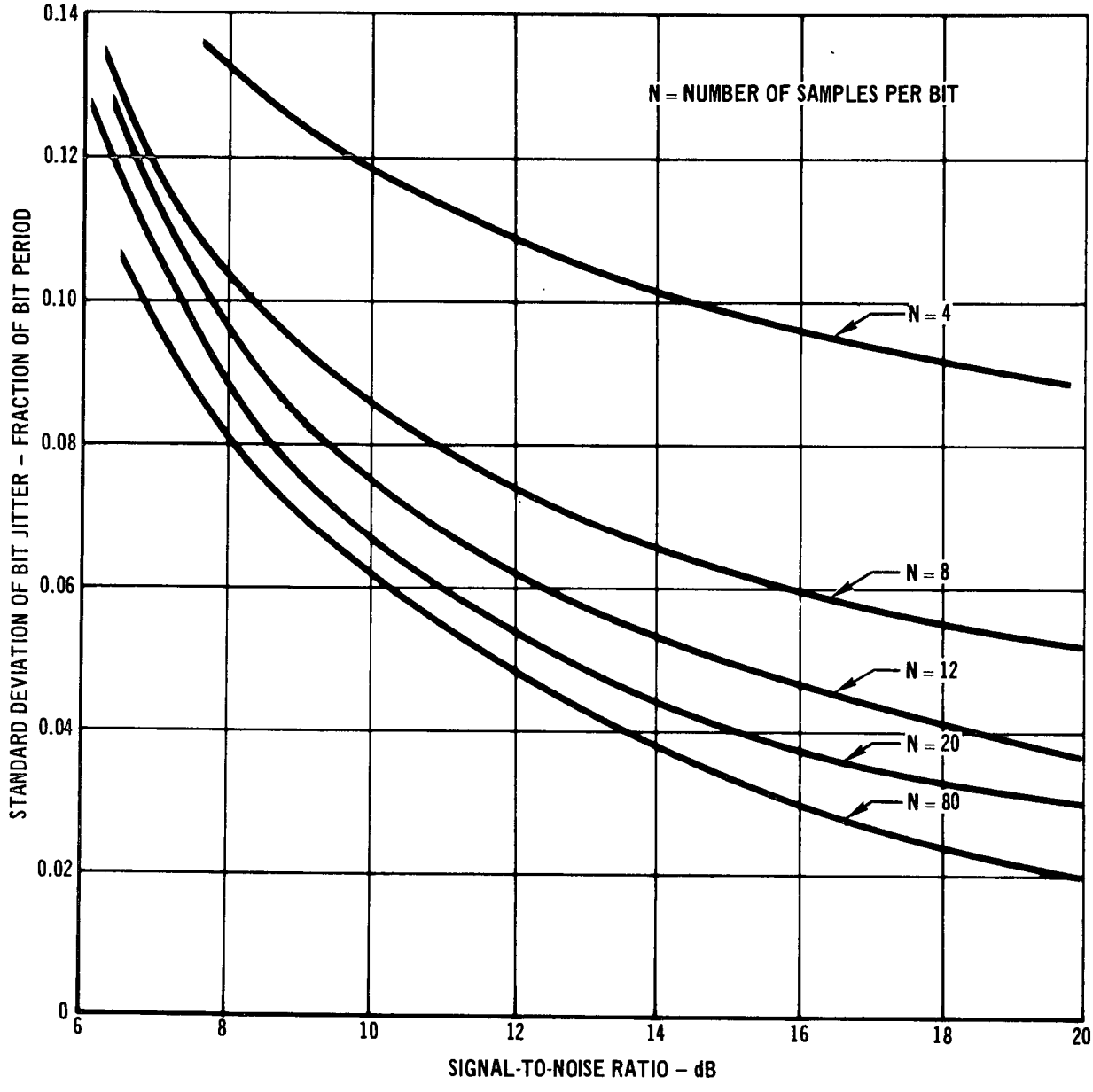

EFFECT OF SAMPLE RATE ON BIT SYNC ERROR

Figure 94

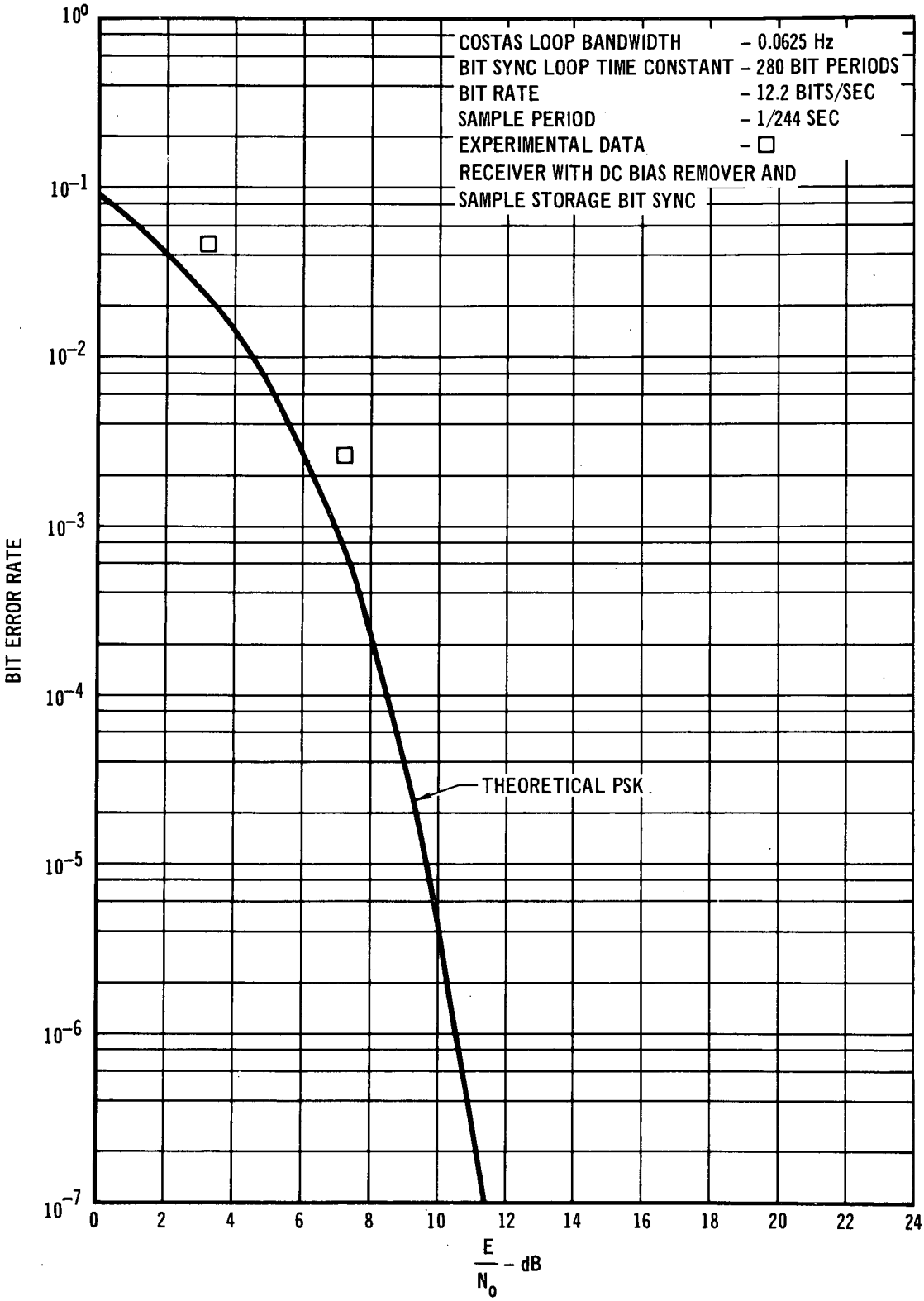

BIT ERROR RATE – SAMPLE STORAGE BIT SYNC Figure 95

computer. This data was taken using the sample storage bit synchronizer and NRZ data. Figure 96 presents a similar comparison except that AGC was added for this set of measurements. Comparison of Figure 95 and Figure 96 indicates that AGC does not cause a perceptable degradation in error rate performance. Note that the MDAC Digital receiver is operating within less than 2dB of theoretical. This data was taken without optimizing the pre-sampling IF filter bandwidth. The very low IF frequency (244 Hz) was chosen to simplify obtaining IF bandwidths on the order of 100 Hz or less. The pre-sampling bandpass filter was constructed using low-pass and high-pass filters with overlapping passbands. Figure 97 shows the transfer function of the optimized IF filter used to obtain the experimental data shown in Figure 98 . Note that the experimental data taken with this IF filter is within 0.5 dB of the theoretical optimum. This is within the measurement error of the experiment since E/N_o can generally not be measured more accurately than 0.5 dB with standard Gaussian noise sources.

Figure 99 shows a plot of experimental error rate performance with split phase data using a "66 out of 90" phase detector algorithm. Even though this data was taken without optimizing the pre-sampling IF filter, the experimental data is within 1.0 dB of the theoretical optimum.

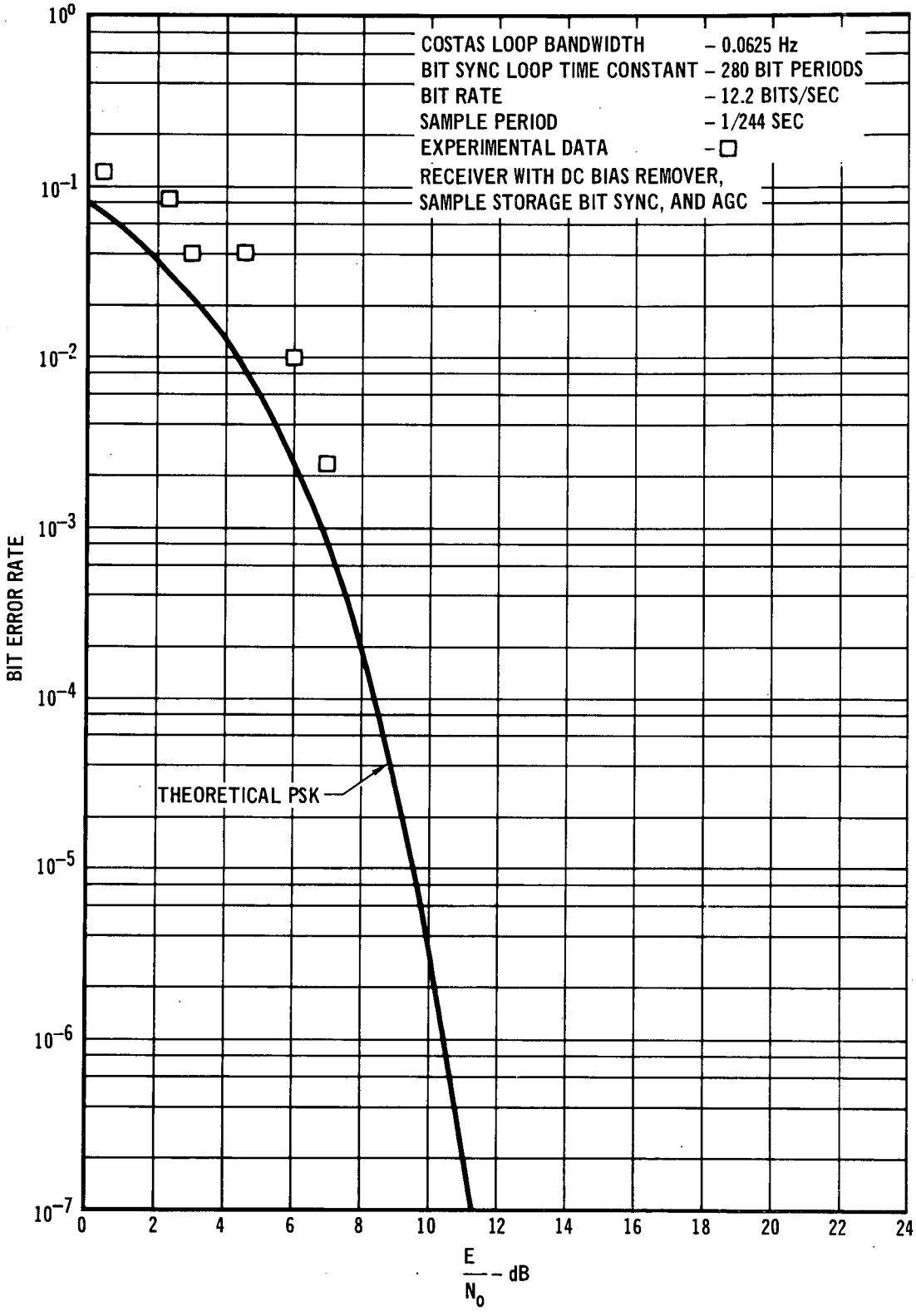

BIT ERROR RATE – AGC

Figure 96

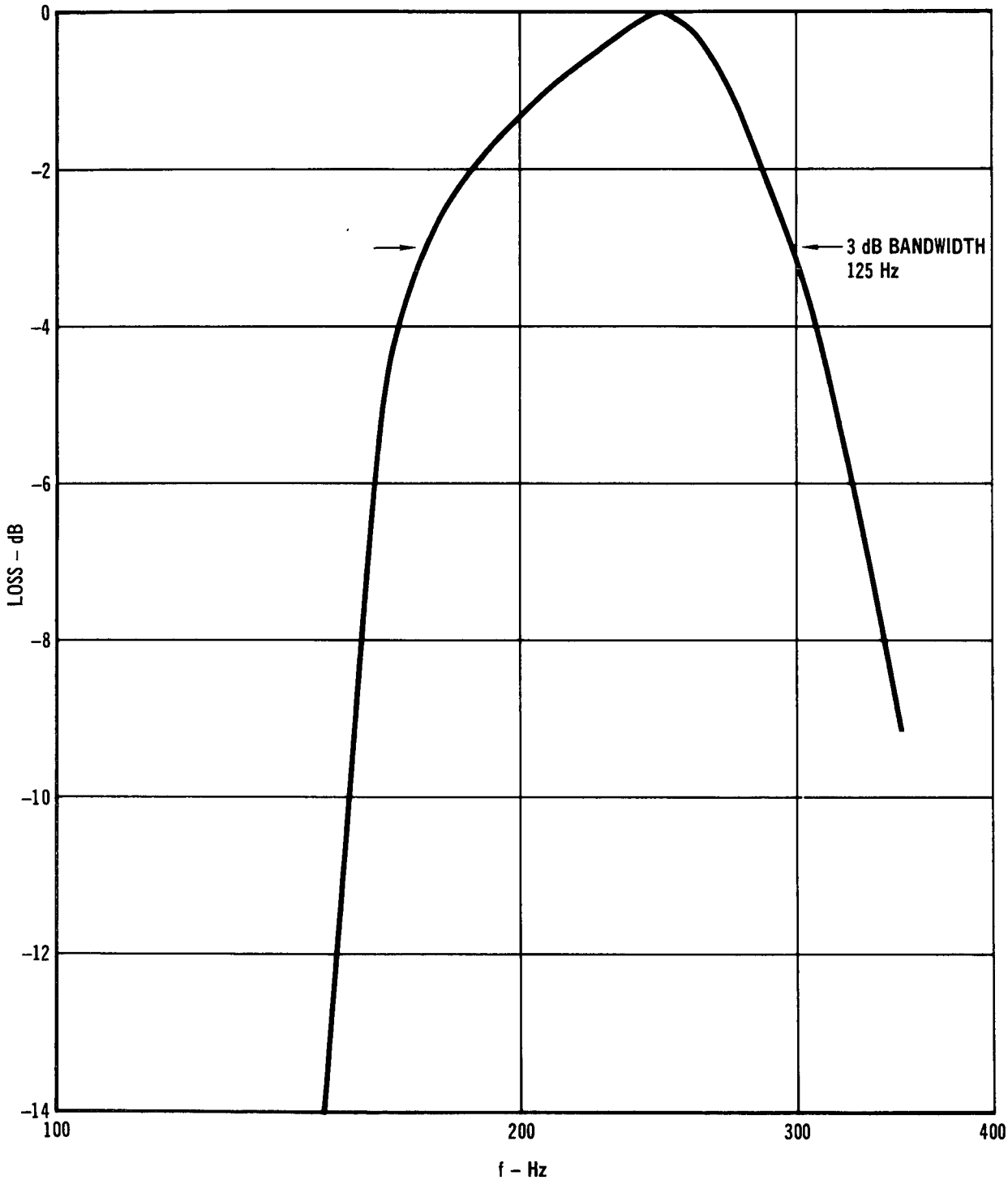

BANDPASS FILTER

Figure 97

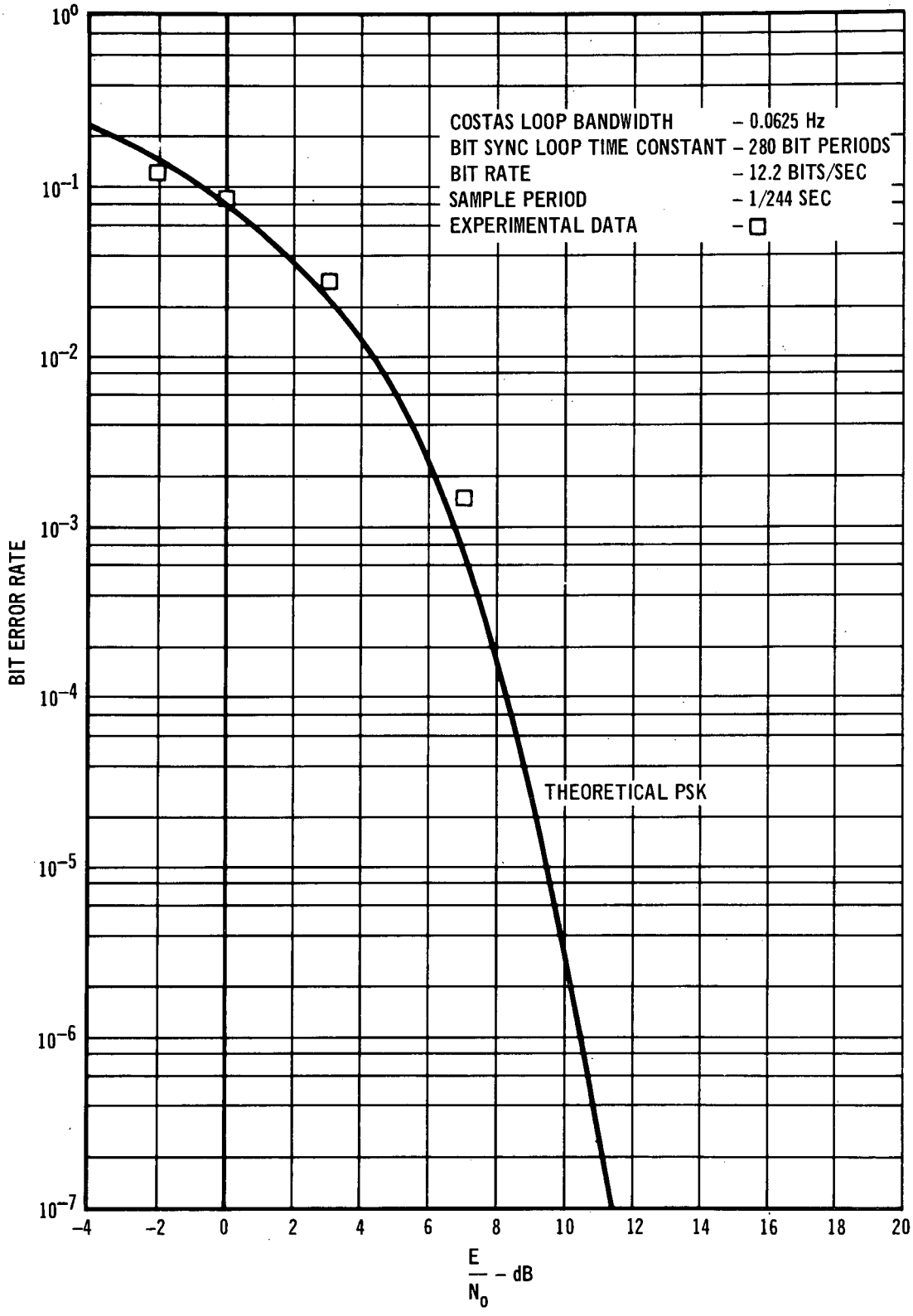

BIT ERROR RATE – OPTIMIZED IF FILTER

Figure 98

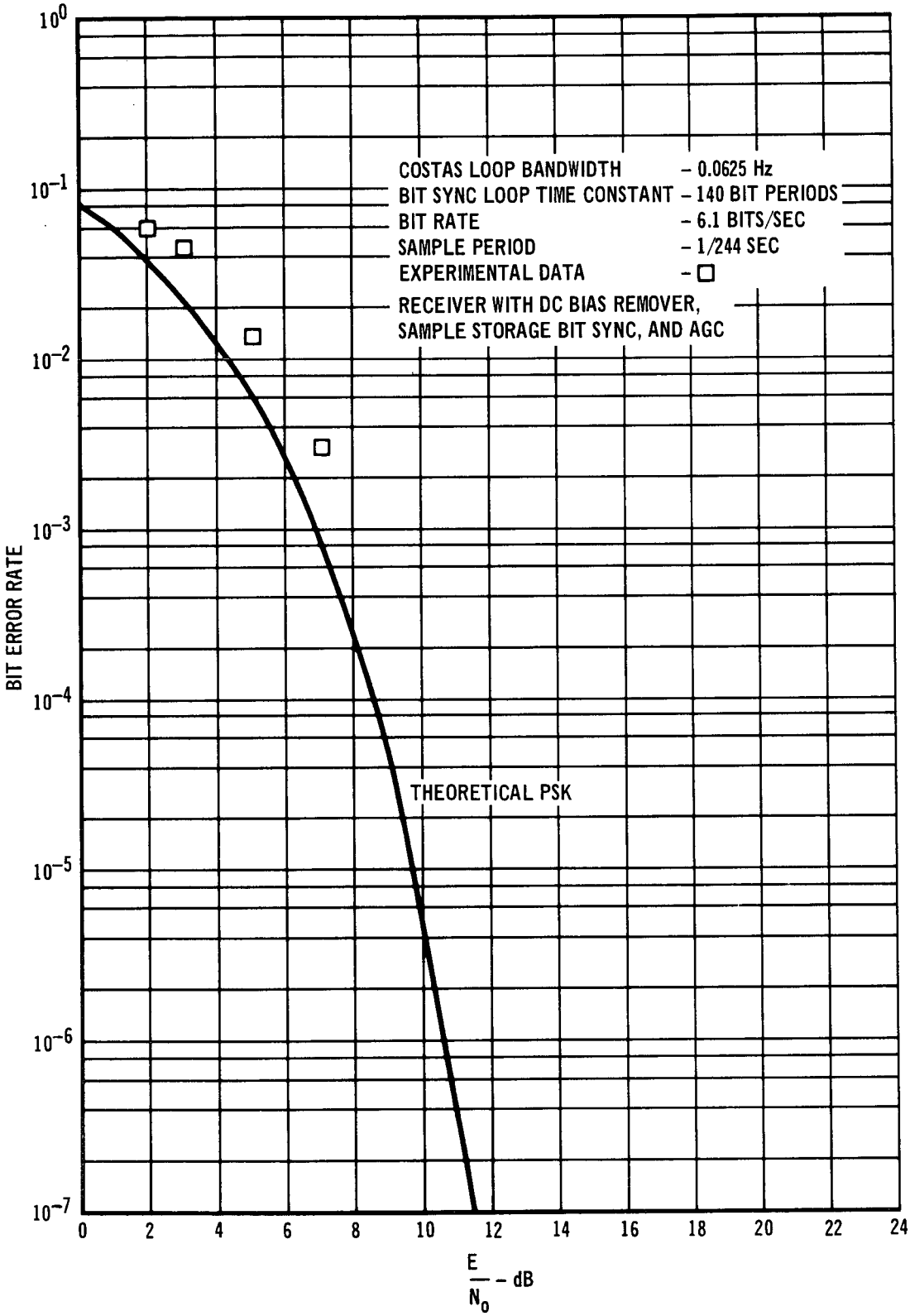

BIT ERROR RATE SPLIT – PHASE DATA

Figure 99

4. STUDY OF NON-ANALOG SYNTHESIS TECHNIQUES

One of the reasons for studying digital signal processing is that it provides a capability for implementing certain processing techniques which would be difficult or impossible with analog techniques. In particular, techniques which cannot be represented in terms of lumped parameter elements (for example, ideal time delays, two-dimensional processing algorithms, etc.) are difficult to implement with analog hardware. The restriction to one-dimensional processing prevents the development of optimum detection and estimation algorithms with analog hardware for many cases of practical interest. This follows by noting that, in the general case, an optimal detection or estimation algorithm generates and uses a conditional probability density of the state variable. Since this density changes with time, it is at least two-dimensional and may be considerable larger if other so-called "nuisance" state variables are involved. For sampled data inputs, the conditional probability density of the state vector is determined using Bayes law.

4.1 Bayesian Estimation

We assume that at any time t_{k+1} the system equation governing the evolution of the state are of the following form.

$$\underline{X}_{k+1} = \underline{f}(\underline{X}_k, \underline{W}_k) \tag{180}$$

$$\underline{Z}_{k+1} = \underline{h}(\underline{X}_{k+1}, \underline{V}_{k+1}) \tag{181}$$

where $\underline{X}_k$ is the state vector, $\underline{V}_k$ the measurement noise, $\underline{Z}_k$ the measurement, and $\underline{W}_k$ the state disturbance, all at k.

Let $\underline{z}_{k+1} = (\underline{Z}_1, \cdots, \underline{Z}_{k+1})$ be the set of previous observations. Then by definition

$$P(\underline{X}_{k+1}, \underline{Z}_{k+1} \mid \underline{z}_k) = P(\underline{Z}_{k+1} \mid \underline{z}_k, \underline{X}_{k+1})\, P(\underline{X}_{k+1} \mid \underline{z}_k) \tag{182}$$

$$= \int P(\underline{Z}_{k+1} \mid \underline{z}_k, \underline{X}_{k+1})\, P(\underline{X}_{k+1} \mid \underline{z}_k, \underline{X}_k)\, P(\underline{X}_k \mid \underline{z}_k)\, d\underline{X}_k \tag{183}$$

From Equation (180) and Equation (181), we note that

$$P(\underline{X}_{k+1} \mid \underline{z}_k, \underline{X}_k) = P(\underline{X}_{k+1} \mid \underline{X}_k) \tag{184}$$

$$P(\underline{Z}_{k+1} \mid \underline{z}_k, \underline{X}_{k+1}) = P(\underline{Z}_{k+1} \mid \underline{X}_{k+1}) \tag{185}$$

Therefore

$$P(\underline{X}_{k+1}, \underline{Z}_{k+1} \mid \underline{z}_k) = \int P(\underline{Z}_{k+1} \mid \underline{X}_{k+1})\, P(\underline{X}_{k+1} \mid \underline{X}_k)\, P(\underline{X}_k \mid \underline{z}_k)\, d\underline{X}_k \tag{186}$$

Finally, we obtain the solution for $P(\underline{X}_{k+1} \mid \underline{z}_{k+1})$ by noting that by definition

$$P(\underline{X}_{k+1} \mid \underline{z}_{k+1}) = \frac{P(\underline{X}_{k+1}, \underline{Z}_{k+1} \mid \underline{z}_k)}{P(\underline{Z}_{k+1} \mid \underline{z}_k)} \tag{187}$$

Given $P(\underline{X}_{k+1} \mid \underline{z}_{k+1})$, we can compute the optimal estimate of $\underline{X}_{k+1}$ using any criterion of optimality we desire. For instance, the maximum likelihood estimate would be the value of X_{k+1} which maximizes $P(\underline{X}_{k+1} \mid \underline{z}_{k+1})$.

To illustrate the use of this approach, we consider the problem of tracking the phase of a sine wave in noise. For this case the state vector $\underline{X}_k$ contains the phase and frequency of the sine wave, that is

$$\underline{X}_{k+1} = \begin{bmatrix} a & o \\ o & b \end{bmatrix} \underline{X}_k + \underline{W}_k \tag{188}$$

where

$$\underline{X}_k = \begin{bmatrix} f_k \\ \theta_k \end{bmatrix} \tag{189}$$

f_k is the frequency offset at time k and θ_k is the phase offset at time k.

The measurement vector is given by

$$\underline{Z}_k = \begin{bmatrix} \cos(\theta_k + k\Delta T f_k) \\ -\sin(\theta_k + k\Delta T f_k) \end{bmatrix} + \underline{V}_k \tag{190}$$

ΔT is the time between samples and $\underline{Z}_k = \begin{bmatrix} a_k \\ b_k \end{bmatrix}$.

The measurement noise and the state disturbances are modeled as bivariate gaussian random variables with zero mean and covariance matrices given by $\text{cov}(W_k) = Q$ and $\text{cov}(V_k) = R$.

$$P(\underline{X}_{k+1} \mid \underline{X}_k) = \left[2\pi \, |Q|^{1/2}\right]^{-1} e \left[-\frac{1}{2} \begin{pmatrix} f_{k+1} - af_k \\ \theta_{k+1} - b\theta_k \end{pmatrix}^T Q^{-1} \begin{pmatrix} f_{k+1} - af_k \\ \theta_{k+1} - b\theta_k \end{pmatrix} \right] \tag{191}$$

$$P(\underline{Z}_{k+1} \mid \underline{X}_{k+1}) = \left[2\pi \, |R|^{1/2} \right]^{-1} e \left[-\frac{1}{2} \begin{pmatrix} a_{k+1} - \cos(\theta_{k+1} + k\Delta T f_{k+1}) \\ b_{k+1} + \sin(\theta_{k+1} + k\Delta T f_{k+1}) \end{pmatrix} R^{-1} \right. \tag{192}$$

$$\left. \begin{pmatrix} a_{k+1} - \cos(\theta_{k+1} + k\Delta T f_{k+1}) \\ b_{k+1} + \sin(\theta_{k+1} + k\Delta T f_{k+1}) \end{pmatrix} \right]$$

$P(\underline{X}_k \mid \underline{Z}_k)$ is available from the previous step. $P(\underline{Z}_{k+1} \mid \underline{Z}_k)$ is independent of $\underline{X}_k$ and thus can be easily determined by noting that

$$P(\underline{X}_{k+1} \mid \underline{Z}_{k+1})\, P(\underline{Z}_{k+1} \mid \underline{Z}_k) = P(\underline{X}_{k+1}, \underline{Z}_{k+1} \mid \underline{Z}_k) \tag{193}$$

and integrating both sides with respect to $\underline{X}_k$

$$P(\underline{Z}_{k+1} \mid \underline{Z}_k) = \int P(\underline{X}_{k+1}, \underline{Z}_{k+1} \mid \underline{Z}_k)\, d\underline{X}_{k+1} \tag{194}$$

Thus $P(\underline{Z}_{k+1} \mid \underline{Z}_k)$ is a constant (i.e. independent of $\underline{X}_k$) picked to normalize $P(\underline{X}_{k+1}, \underline{Z}_k \mid \underline{Z}_k)$. Note that for computer implementation $P(\underline{X}_{k+1} \mid \underline{Z}_k)$ is only evaluated at a finite set of values of $\underline{X}_{k+1}$. Thus the integration shown in Equations(186) and(194) reduces to a double summation over the possible values of θ_k and f_k. Thus combining the results of Equations (186), (191), (192), and (194), we note that $P(\underline{X}_k \mid \underline{Z}_k)$ is completely specified.

To obtain the optimum Bayesian estimator for a PSK system, the state vector $\underline{X}_k$ should contain the phase offset and frequency offset, the bit timing and the data bits. This would require a four dimensional state vector. In order to reduce the dimensionality of the Bayesian estimator, carrier and bit synchronization are performed separately as is shown in Figure 100 . This is not an optimum Bayesian estimator since the carrier synchronization is only optimum for the leading edge of the bit, τ, and the value of the bit, S, known exactly, and the bit synchronization is only optimum for the phase offset, θ, and the frequency offset, f, known exactly. But, it approaches the optimum as better estimates of $\hat{\tau}$, $\hat{\theta}$, $\hat{f}$, and $\hat{S}$ are obtained.

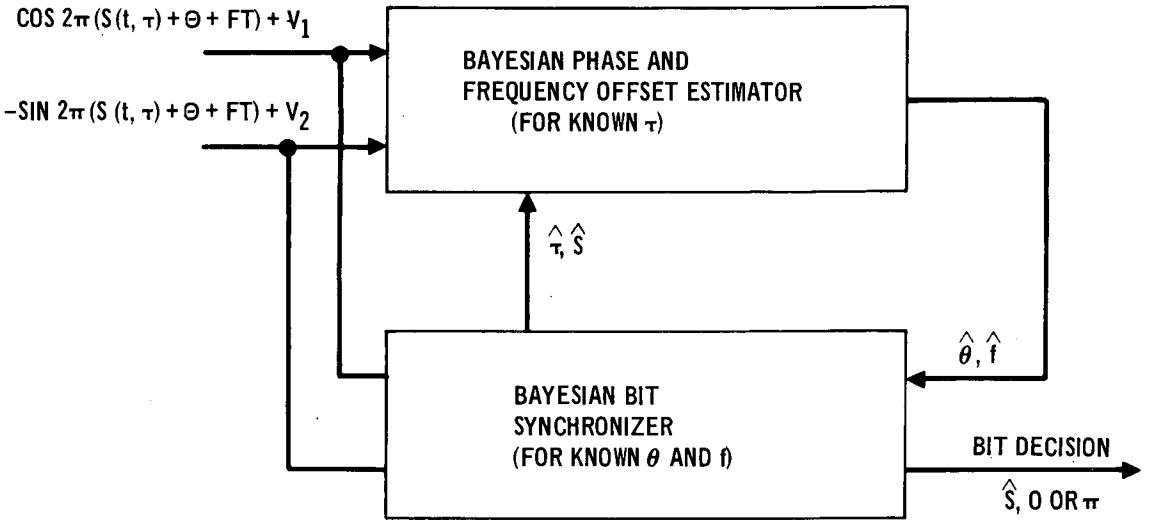

REDUCTION OF DIMENSIONALITY

Figure 100

The Bayesian carrier estimator, assuming perfect bit synchronization, is given by Equations (186) and (187) with the state vector of Equation (188) the measurement vector of Equation (190), and the conditional densities of Equations (191) and (192)

Now, the Bayesian bit estimator, assuming perfect carrier synchronization, is given by

$$P(\tau_{k+1},\ S_{k+1} \mid \underline{z}_{k+1}) = \frac{P(\tau_{k+1},\ S_{k+1},\ \underline{Z}_{k+1} \mid \underline{z}_k)}{P(\underline{Z}_{k+1} \mid \underline{z}_k)} \tag{195}$$

and

$$P(\tau_{k+1},\ S_{k+1},\ \underline{Z}_{k+1} \mid \underline{z}_k) = P(\underline{Z}_{k+1} \mid \tau_{k+1},\ S_{k+1}) \int P(\tau_{k+1} \mid \tau_k)\ P(\tau_k,\ S_{k+1} \mid \underline{z}_k)\ d\tau_k \tag{196}$$

C3

with the state equation for the bit edge of

$$\tau_{k+1} = c\ \tau_k + u_k \tag{197}$$

where again t_k denotes the time and S_k is the value of the bit at time t_k.

The state disturbance is modeled as a Gaussian random variable with zero mean and variance σ_τ^2 which yields

$$P(\tau_{k+1} \mid \tau_k) = \left[2\pi\ \sigma_\tau^2\right]^{-1/2} e \left[- \frac{1}{2\sigma_\tau^2}(\tau_{k+1} - c\tau_k)^2 \right] \tag{198}$$

For bit synchronization the measurement vector is given by

$$\underline{Z}_k = \begin{bmatrix} \cos\ (S_k(t,\tau_k)) \\ -\sin\ (S_k(t,\tau_k)) \end{bmatrix} + \underline{V}_k \tag{199}$$

and the measurement noise takes the form

$$P(\underline{Z}_{k+1} \mid \tau_{k+1},\ S_{k+1}) = \left[2\pi \mid R \mid^{1/2}\right]^{-1} e \left[- \frac{1}{2} \begin{pmatrix} a_{k+1} - \cos(S_{k+1}(t,\ \tau_{k+1})) \\ b_{k+1} + \sin(S_{k+1}(t,\ \tau_{k+1})) \end{pmatrix}^T R^{-1} \right.$$

$$\left. \begin{pmatrix} a_{k+1} - \cos(S_{k+1}(t,\ \tau_{k+1})) \\ b_{k+1} + \sin(S_{k+1}(t,\ \tau_{k+1})) \end{pmatrix} \right] \tag{200}$$

The desired output, the estimate of S_{k+1}, is obtained from Equation (195) by choosing the maximum of

$$P(S_{k+1} \mid \underline{z}_{k+1}) = \int P(\tau_{k+1},\ S_{k+1} \mid \underline{z}_{k+1})\ d\tau_{k+1} \tag{201}$$

The above formulation will yield near optimum Bayesian carrier and bit synchronization. The only thing left is to determine the parameters of the state equations, a, b, and c. These are obtained by specification of the bandwidths of the processes described by the state equations. Given the following form of the state equations

$$Y_{k+1} = \alpha\, Y_k + W_k \tag{202}$$

and taking the Z transform we obtain

$$z\, Y(z) = \alpha\, Y(z) + W(z) \tag{203}$$

or

$$Y(z) = \frac{1}{(z - \alpha)}\, W(z) \tag{204}$$

Then the power spectral density is given by

$$S_Y(z) = \frac{1}{(z - \alpha)}\,\frac{1}{(z^{-1} - \alpha)}\; S_W(z) = \frac{1}{(z - \alpha)}\;\frac{1}{(z^{-1} - \alpha)}\;\sigma_W^{\,2} \tag{205}$$

where $\sigma_W^{\,2}$ is the sampled power spectral density. The mean square value of Y is given as

$$\overline{Y^2(kT)} = \frac{1}{2\pi j}\int S_Y(z)\,\frac{dz}{z} \tag{206}$$

Making the change of variables $z = \frac{1 + W}{1 - W}$ we obtain

$$\overline{Y^2(kT)} = \frac{1}{2\pi j}\int S_Y(W)\,\frac{2\,dW}{(1 - W^2)} = \frac{1}{2\pi j}\int \frac{2\sigma_n^{\,2}\,dW}{[1 - \alpha + (1 + \alpha)\,W]\,[1 - \alpha - (1 + \alpha)\,W]} \tag{207}$$

This is evaluated as

$$\overline{Y^2(kT)} = \frac{\sigma_n^2}{(1-\alpha)(1+\alpha)} \tag{208}$$

The maximum of $S_Y(z)$ is evaluated at $z = 1$ to yield

$$S_Y(z)\,\Big|_{max} = S_Y(z=1) = \frac{\sigma_n^2}{(1-\alpha)^2} \tag{209}$$

and the bandwidth is obtained from

$$(BW)\ (S_Y(z=1)) = \overline{Y^2(kT)}$$

to be

$$BW = \frac{1-\alpha}{1+\alpha} \tag{210}$$

$$\alpha = \frac{1-BW}{1+BW} \tag{211}$$

4.2 Performance Evaluation

A computer simulation of the previously derived PSK synchronization algorithms utilizing separate carrier and bit synchronization was performed to determine probability of bit error. Since the conditional densities of the phase and frequency offset in Equation (187) and of the bit edge in Equation (195) are not calculatable in closed form, we compute the conditional probabilities only for a finite set of phase, frequency offset, and the bit edge values which in turn reduces the conditional densities to discrete densities. We let the phase offset, frequency offset, and bit edge each have 10 possible values. For these divisions of the state parameters the carrier tracking conditional density of Equation (187) reduces to

$$P(f_{k+1}, \theta_{k+1} \mid \underline{z}_{k+1}) = \frac{P(\underline{Z}_{k+1} \mid f_{k+1}, \theta_{k+1}) \sum_{\theta_k} \sum_{f_k} P(f_{k+1}, \theta_{k+1} \mid f_k, \theta_k)\, P(f_k, \theta_k \mid \underline{z}_k)}{P(\underline{Z}_{k+1} \mid \underline{z}_k)} \tag{212}$$

where $P(\underline{Z}_{k+1} \mid \underline{z}_k)$ is a normalizing constant given by the double summation over f_{k+1} and θ_{k+1} of the numerator. The summations over f_k, θ_k, f_{k+1}, and θ_{k+1} consist of the 10 possible values of each of these parameters.

Also, for these values of the state parameters the bit tracking conditional density of Equation (195) is

$$P(\tau_{k+1}, S_{k+1} \mid \underline{z}_{k+1}) = \frac{P(\underline{Z}_{k+1} \mid \tau_{k+1}, S_{k+1}) \sum_{\tau_k} P(\tau_{k+1} \mid \tau_k)\, P(\tau_k, S_{k+1} \mid \underline{z}_k)}{P(\underline{Z}_{k+1} \mid \underline{z}_k)} \tag{213}$$

and $P(\underline{Z}_{k+1} \mid \underline{z}_k)$ is the summation over τ_{k+1} of the numerator. Using Equation (212) involves knowledge of τ_{k+1} and S_{k+1} and using Equation (213) involves knowledge of f_{k+1} and θ_{k+1} as is shown in Figure 100. In the simulation bit synchronization is physically done first, then the estimates $\hat{\tau}$ and $\hat{S}$ calculated and finally $\hat{\tau}$ and $\hat{S}$ are fed back for carrier synchronization. The estimates $\hat{\theta}$ and $\hat{f}$ are then calculated and fed back for bit synchronization. Since these estimates are updated with every sample, there is a one sample delay of the estimates $\hat{\theta}$ and $\hat{f}$. This introduces very little error because the phase and frequency offset change slowly with respect to the sampling time.

Since it is not known beforehand where the bit edge is, observation intervals, each the length of a bit period, are formed. There are parts of two bits in each observation interval and four possible combinations, $B(t,\tau)$, of these two bits $(0,0)$, $(0,\pi)$, $(\pi,0)$, or (π,π). Let

$$P_{i,j}^{n+1}(t,\tau) = \text{Prob}\left\{B(t,\tau) = i\pi \text{ for } nT \le t \le nT + \tau;\ B(t,\tau) = j\pi \text{ for } nT + \tau < t \le (n+1)T\right\} \quad i,j = 0,1 \tag{214}$$

be the joint probabilities of τ and B in the $(n+1)^{\underline{st}}$ observation interval, then

$$P_{i,j}^{n+1}(t) = \sum_{\tau_k} P_{i,j}^{n+1}(t,\tau_k) \tag{215}$$

is the probability of the bit sequence (πi, πj) in this interval. The estimate of the data bit at time t_{k+1}, S_{k+1}, (for $nT \le t_{k+1} \le (n+1)T$) that is used for carrier synchronization is given by

$$\hat{S}_{k+1} = \begin{cases} 0 & \text{if } P_{0,0}^{n+1}(t_{k+1}) + P_{0,1}^{n+1}(t_{k+1}) \ge \frac{1}{2} \\ \pi & \text{otherwise} \end{cases} \tag{216}$$

if $t_{k+1} \le nT + \hat{\tau}$ and

$$\hat{S}_{k+1} = \begin{cases} 0 & \text{if } P_{0,0}^{n+1}(t_{k+1}) + P_{1,0}^{n+1}(t_{k+1}) \ge \frac{1}{2} \\ \pi & \text{otherwise} \end{cases} \tag{217}$$

if $t_{k+1} > nT + \hat{\tau}$. At the end of each observation interval an estimate of the bit is made. This estimate at the end of the $(n+1)^{\underline{st}}$ interval is given by

$$\hat{S}_{(n+1)T} = \begin{cases} 0 & \text{if } P_{0,0}^{n+1}((n+1)T) + P_{0,1}^{n+1}((n+1)T) \ge \frac{1}{2} \\ \pi & \text{otherwise} \end{cases} \tag{218}$$

since this expression contains all the observations of the $(n+1)^{\underline{st}}$ bit.

At the end of each observation interval the probabilities are reinitialized as

$$P_{0,0}^{n+1}(nT,\tau) = P_{0,1}^{n+1}(nT,\tau) = \frac{1}{2}\left[P_{0,0}^{n}(nT,\tau) + P_{1,0}^{n}(nT,\tau)\right]$$
$$P_{1,0}^{n+1}(nT,\tau) = P_{1,1}^{n+1}(nT,\tau) = \frac{1}{2}\left[P_{0,1}^{n}(nT,\tau) + P_{1,1}^{n}(nT,\tau)\right] \quad (219)$$

The estimate for τ_{k+1} that is fed back for carrier synchronization is, from Equation (213),

$$\hat{\tau}_{k+1} = \text{maximum}\left\{P(\tau_{k+1} \mid z_{k+1})\right\} = \text{maximum}\left\{\sum_{S_{k+1}} P(\tau_{k+1}, S_{k+1} \mid z_{k+1})\right\} \quad (220)$$

The estimates of f_{k+1} and θ_{k+1} used for bit synchronization are obtained jointly as, from Equation (212),

$$\left\{\hat{f}_{k+1}, \hat{\theta}_{k+1}\right\} = \text{maximum}\left\{P(f_{k+1}, \theta_{k+1} \mid z_{k+1})\right\} \quad (221)$$

In the simulation we let the phase offset vary from 0 to 2π, the frequency offset from -1 to +1 Hz, and the bit timing from 0 to T, the bit period. The variances and the bandwidths of the frequency and phase offsets were set to obtain a fairly rapid acquisition time. For the frequency offset and phase offset the variances were picked to be 0.04 Hz^2 and $(0.02)_x(2\pi)^2$ $radians^2$ respectively and the bandwidths 0.001 Hz and $(0.0025)_x(2\pi)$ radians

respectively. The variance and bandwidth on the bit timing were set at essentially zero. The probability of bit error for these parameters is given in Figure 101. A typical learning curve for the bit synchronization is shown in Figure 102.

Although we have shown that this approach can be implemented at very low bit rates, the small performance gains which were obtained do not justify the difficulty involved in the implementation. Note that the regular MDAC Digital PSK receiver operates within 0.5 dB of theoretical for practical tracking bandwidths and thus the maximum possible performance gain for the Bayesian approach is less than 0.5 dB.

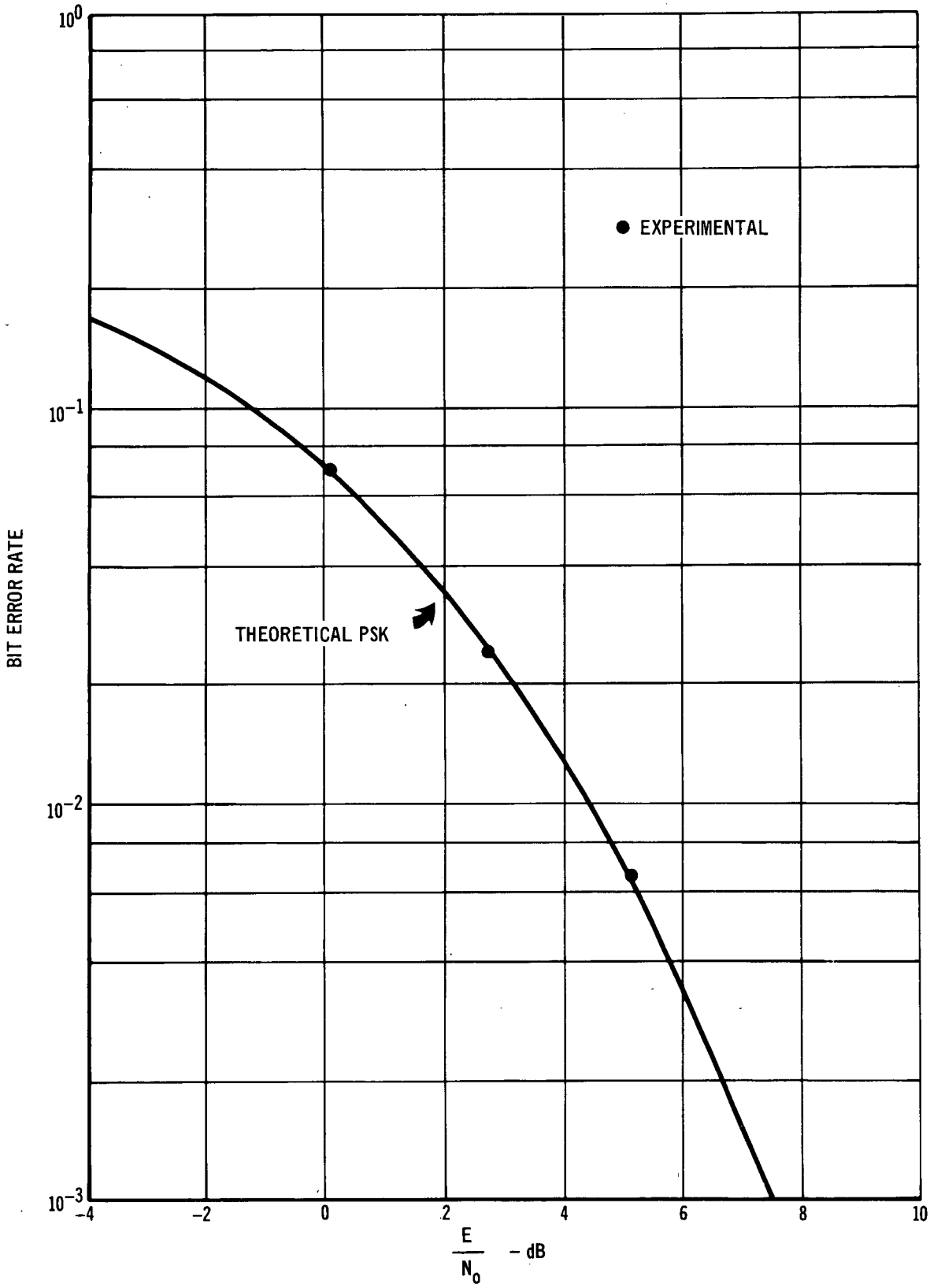

PROBABILITY OF BIT ERROR WITH BAYESIAN ESTIMATION

Figure 101

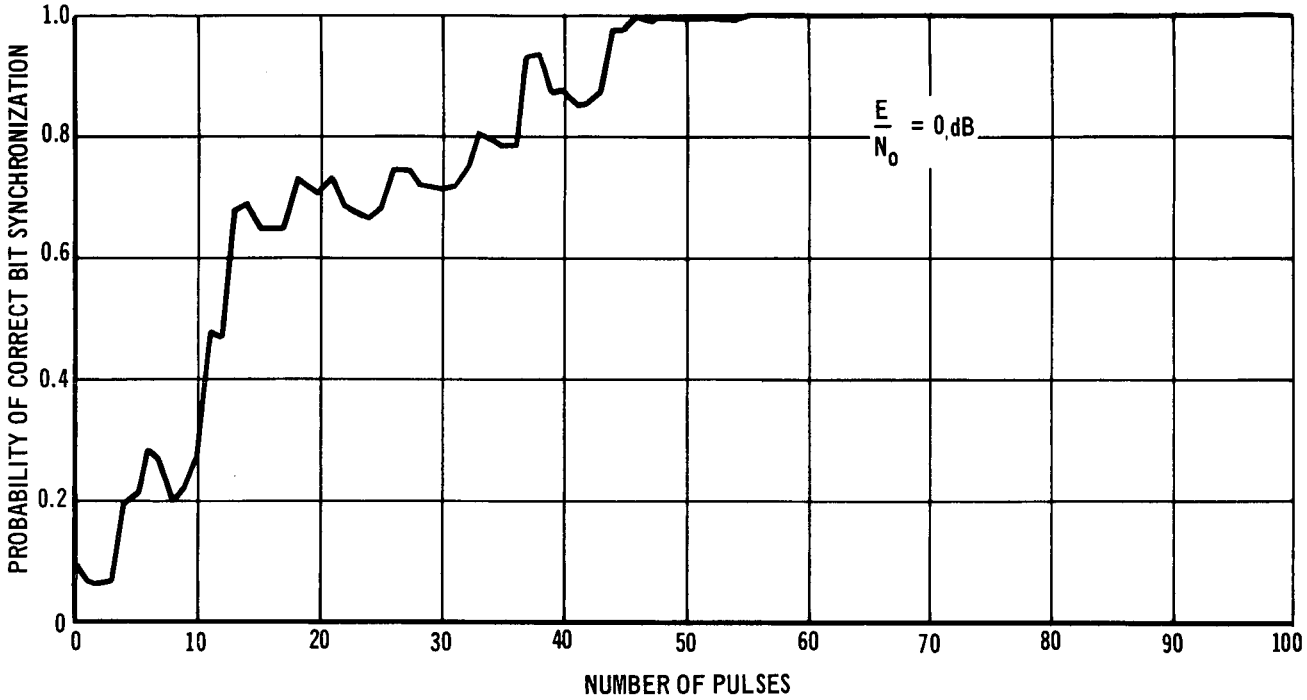

TYPICAL LEARNING CURVE FOR BIT SYNCHRONIZATION

Figure 102

5. HARDWARE IMPLEMENTATION

One of the primary reasons for this study of digital signal processing was to develop computer software that would enable any NASA ground station with computer facilities to demodulate low data rate telemetry without the purchase of any additional hardware. The use of digital signal processing for very low data rates (i.e. less than 10 bits/second) was also of special interest due to the difficulty of constructing very low bandwidth circuits with analog hardware.

Since digital signal processing also has considerable utility in higher bandwidth applications, it was decided to investigate the upper data rate capability of the MDAC digital PSK receiver. To significantly increase data rate, it is necessary to use special purpose digital logic rather than a general purpose computer.

A complete hardware design of the entire MDAC PSK receiver was beyond the scope of this study and not really necessary to determine the upper bit rate capability. Thus we decided to concentrate our design effort on the phase-tracking part of the receiver. The Costas loop, rather than the bit synchronizer, was chosen for hardware design because it appeared to be the more time consuming of the two calculations. Note that the phase and bit tracking loops are essentially separate algorithms which can be performed in parallel.

This section presents results of a study to determine the best hardware realization of the digital Costas phase-locked loop depicted in block diagram form in Figure 103.

Section 5.1 describes different machine organizations for the accomplishment of the task. Section 5.2 is a detailed description of one of these

DIGITAL COSTAS LOOP

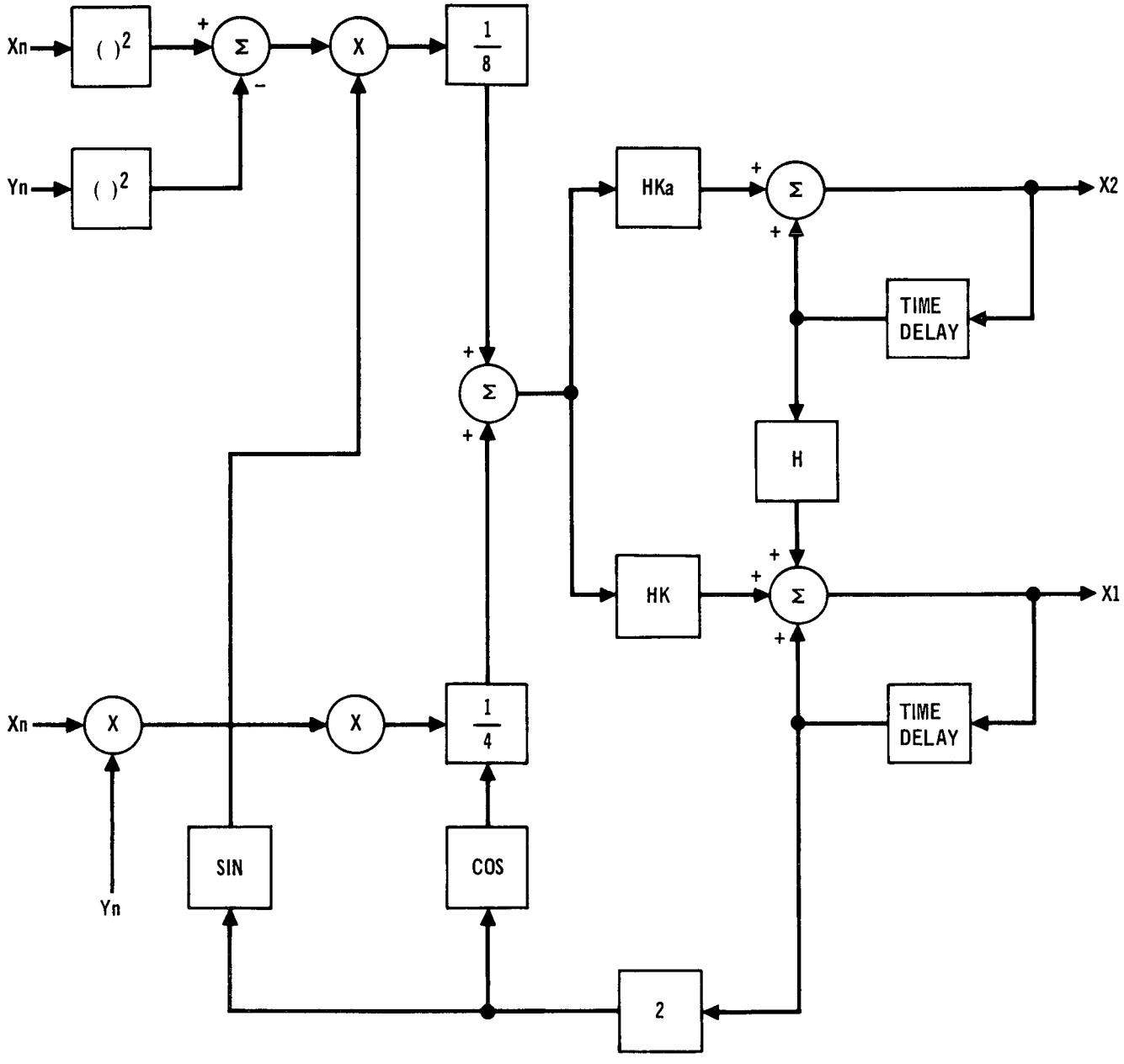

Figure 103

methods. Section 5.3 describes additional effort required to complete trade-off studies between the various methods.

5.1 Machine Organizations

The required computations can be accomplished using a single time shared arithmetic logic unit (ALU). This unit is capable of addition and subtraction. With one ALU multiplication is performed by a process of shift and add and re-requires as many clocks as there are bits in the multiplier.

The computations may be performed in a shorter elapsed time if two arithmetic logic units share the computation load and even faster with three arithmetic logic units. However, no further increase in speed can be obtained by addition of a fourth ALU, because it would have to wait for results from previous ALU's.

A further increase in speed can be obtained by speeding up the multiplication process through the use of look-up table multipliers which can function in an add time. Such devices are now available.

Figure 104 lists these candidate machine organizations and their operating speeds assuming Transistor-Transistor-Logic (TTL). These speeds are the rate at which a pair of samples, x_n and y_n, can be processed.

Note that with 20 samples/bit, we could go up to 100 K bits/sec using 12 bit accuracy for the calculations and look-up table multipliers. Section 3.2.1 shows that 12 bit accuracy does not cause significant performance degradation.

The following section of this document describes the logic required for the three ALU case and describes its operation.

5.2 Parallel, 3 Arithmetic Logic Unit (ALU) Design

CANDIDATE SYSTEMS VERSUS SPEED

	(TTL ALU'S)	
	24 BIT	12 BIT
SERIAL (1 ARITHMETIC UNIT)	100 KHz	170 KHz
SERIAL-PARALLEL (2 ARITHMETIC UNITS)	170 KHz	290 KHz
PARRALLEL (3 ARITHMETIC UNITS)	210 KHz	360 KHz
LOOK-UP TABLE MULTIPLIERS	–	2000 KHz

Figure 104

TIME SLOT – OPERATIONS

SLOT	ALU A	ALU B	ALU C
000	Xn^2	$X_nY_n = M$	Y_n^2
001		$X_n^2 - Y_n^2 = N$	
010	N Sin 2X1		MCos 2X1
011		$N \sin 2X_1 + M \cos 2X_1 = L$	
100	LHKa	HX2	LHK
101		$HX2 + X_1 = R$	
110		$R + LHK = X_1$	
111		$X2_i + LHKa = X2_{i+1}$	

Figure 105

5.2.1 General Description

Eight (8) time slots are used to complete one iteration of computations (Reference Figure 103) using the parallel (3 ALU) processor design. Figure 105 identifies the computations performed in each time slot. Two clocks are required for an addition or subtraction operation. The number of clocks required for each multiplication is 2 times the length of the multiplier. The following lists the number of clocks required during each slot:

SLOT	NUMBER OF CLOCKS
000	22
001	2
010	22 or 28*
011	2
100	22
101	2
110	2
111	2
Total	76 or 82

* 22 clocks using ROM Method A and 28 clocks using ROM Method B.

The maximum clock rate is limited by the time required to perform an addition. Addition time varies with word length and adder configuration. For the configuration used in this design; the typical addition time is 36 ns. with maximum value of 48 ns. If the word lengths to be added were increased to 24 bits; this addition time increases to typically 60 ns. If the clock period is chosen as 36 ns; then the time required to process one pair of samples, x_n and y_n, is 36 ns/clock x 76 clocks = 2736 ns using ROM Method A. These conditions correspond to 360 K Hz operating speed. Using ROM Method B;

a clock period of 60 ns or greater is required to allow 600 ns for accessing the ROM during slots 111 and 000. Using ROM Method B, the time required to process is 4920 ns.

Through this design the following word lengths were selected.

WORD	LENGTH
Xn	11 + sign
Yn	11 + sign
HKa	11
HK	11
H	5

All computed quantities will be rounded off to 11 bits plus sign.

5.2.2 Functional Block Diagram

Major functional entities and their interconnections are identified in Figure 106. A brief functional description of each of these blocks follows:

Operation Sequences and Clock

The logic circuitry required to time order operations is contained within this block. An eight (8) counter and gating to decode each state provides the slot timing signals. The clock oscillator provides the signals for advancing the eight (8) counter when the required feedback signal indicates operations within a given state are complete. The clock output is also used to generate the ØA, ØB, and M signal required to sequence each arithmetic operation.

Arithmetic Logic Units (ALU's)

The logic required to perform multiplications, additions, and subtractions is contained within these blocks. ALU's A and C perform multiplications only whereas ALU B must multiply, add, or accomplish two (2) types of subtraction.

Each ALU uses 3 74181, 4 bit arithmetic logic unit/function generators connected together and with a 74182, Look Ahead Carry Generator to form a 12

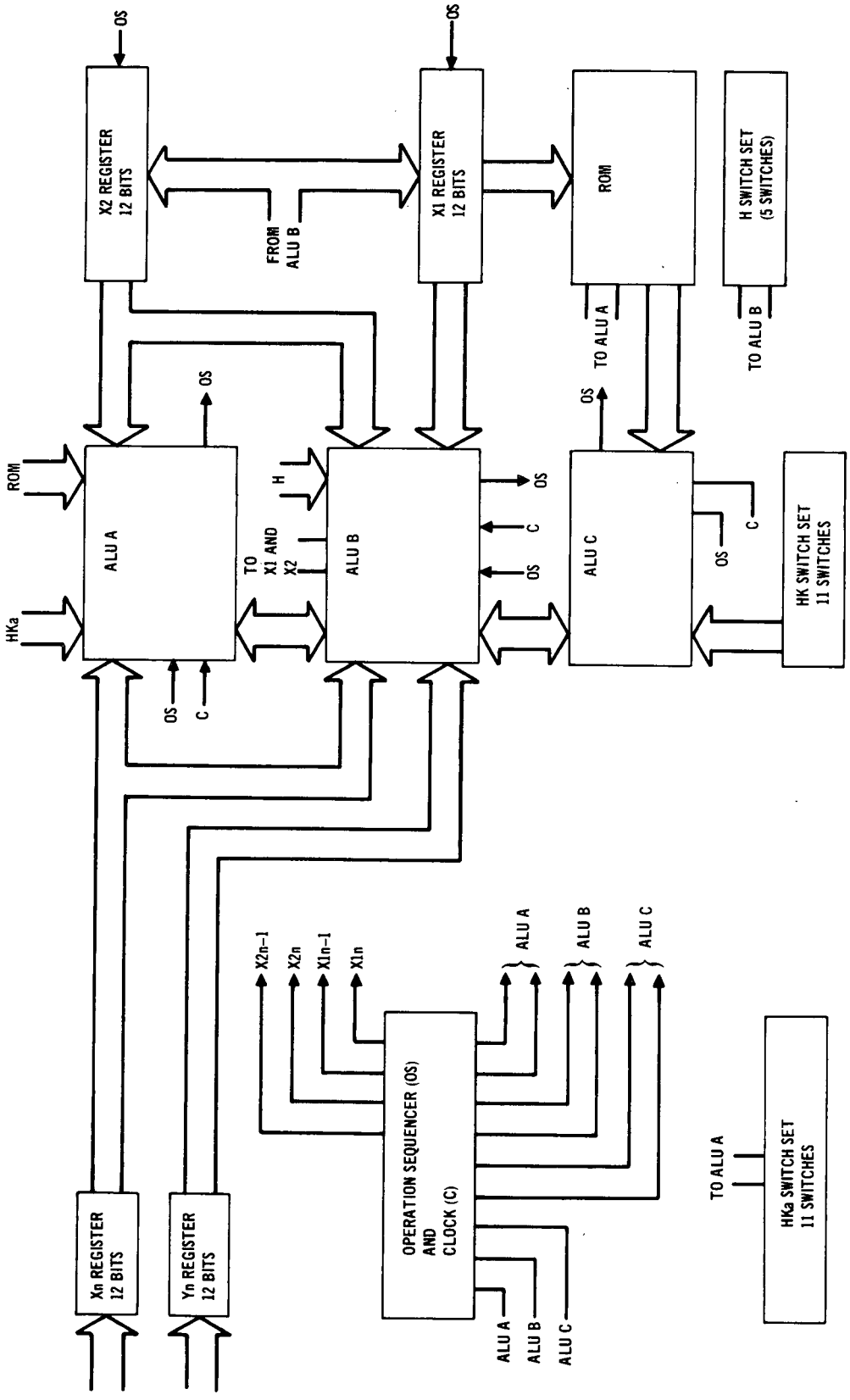

FUNCTIONAL BLOCK DIAGRAM
Phase Estimation Processor

FIGURE 106

bit arithmetic unit capable of performing additions or subtractions in 36 ns. Associated with these arithmetic units are the following registers:

A Register - Stores and inputs the augend or multiplicand to the arithmetic unit. This is a 12 bit latch type register.

B Register - Stores the multiplier. This is a 12 bit parallel in parallel out shift register.

Accumulator - Stores and inputs the addend or partial products to the arithmetic units. Also used to store the arithmetic unit output. This is a 12 bit parallel in, parallel out shift register.

D Register - Stores the number of operations required during multiplication. This is a 4 bit down counter.

In addition to these registers, gating logic is required to input from multiple sources. Both 4 line to 1 line and 2 line to 1 line data selectors are used. Wherever data must be complemented prior to loading (ALU B only); 4 bit True/Complement logic elements are used. The function of all other logic elements is given by their logic symbols.

Read Only Memory (ROM)

Value of the sine and cosine of the angles stored in the X1 Register are stored in ROM's. Two methods of obtaining these values have been devised.

Method A stores 128 values of the sine and cosine in the 0 to 90° quadrant. Each value contains 8 bits plus sign. Two ROM's are used; one for storing sine values and the other containing the cosine values. Addressing is accomplished by connecting the X1 register outputs, $X1_8$ through $X1_2$, to the ROM's via 4 bit True/Complement elements. The $X1_{10}$ and $X1_9$ register outputs which represent the 180° and 90° bits respectively (actually the 90° and 45° bits, since the times 2 multiplication has been accomplished by

shifting each bit one place to left) are used to select whether the true or complement of the input number is used in the addressing and to select the sign bit of the output word. It should be noted that the complemented address is less than the actual angle by the value of the LSB which in this case is 0.7^{o}.

Method B uses a single storage element (made up of 4 ROM's) and can store up to 2048 values of the sine in the first quadrant. Only 512 values are accessible due to input word limitations. The output word using this method has 12 bit accuracy $\pm$ 1 - 5/8 bits, however, only the 11 most significant bits are used along with a sign bit. This method breaks up the sine of the angle, A into two parts. Addressing is accomplished in the same manner as Method A. Use of 3, 4 bit address in the input eliminates the 1 bit address error when complement addresses are required. Since simultaneous addressing to obtain both the sine and cosine values is not possible; this method uses a 12 bit latch to store the sine value while the cosine value is accessed.

Storage Registers

The following registers are used solely for storage:

Xn and Yn - 12 bit latches used to store the input words. Data is strobed into this register by external control.

X_1 and X_2 - 12 bit latches used to store the output words. Data is strobed into these registers by control signals generated within the Operation Sequences.

Switching Bits

A total of 27 single-pole, single-throw switches are used to set in desired values of HK, HKa, and H. One throw of each switch is connected to +V for inputting a "1" and the other to grd. for a "0".

5.2.3 Logic Diagrams

Operation Sequencer and Clock (Reference Figure 107)

Initial turn-on of power clears flip-flops 1A, 1B, and 2A. Gate 3A decodes this 000 state and outputs for use by ALU's as well as enabling the 8A gate. Internally, OR gate 6A is enabled, and it in turn enables gates 7A, 7B, and 7C. Since the initial state of flip-flop 2B is cleared (Q is high), the M output will be high until a ØB output from flip-flop 3A via gate 7A changes flip flop 2B's state. This action allows the ØB output to be gated through 7D. The ØA output is outputted at all times. These 3 outputs, ØA, ØB, and M provide the primary gating signals necessary for sequencing of operations by ALU's A, B, and C.

Following completion of operations in slot 000; the D register of all three ALU's will be decremented to the 000 state. This state is decoded and brought back to the 5C gate. The output of the 5C gate then enables the 8A gate which, via IR gates 11A and 6C, enables gate 10B. Gate 10B then passes the clock pulse to flip-flop 1A causing the 8 bit counter to change to the 001 state. This state is decoded by the 3B gate which outputs the signal for use by the ALU's and enables the 8B gate. Note that the change of slot from 000 to 001 results in the A/S output going high (simultaneously the Mult. goes low). This, along with the ØB signal which is still high, connects the appropriate inputs to the arithmetic unit. The next ØB signal then strobes the adder output into the ALU B unit accumulator and enables gate 8B which enables gates 10B via gates 11A and 6C. Gate 10B passes the clock on to flip-flop 1A which changes state and the counter state becomes 010. This state is decoded by gate 3C, and a sequence identical to that described for slot 000 is underway. All other operations are identical to those described for slots 000 or 001.

OPERATION SEQUENCER AND CLOCK

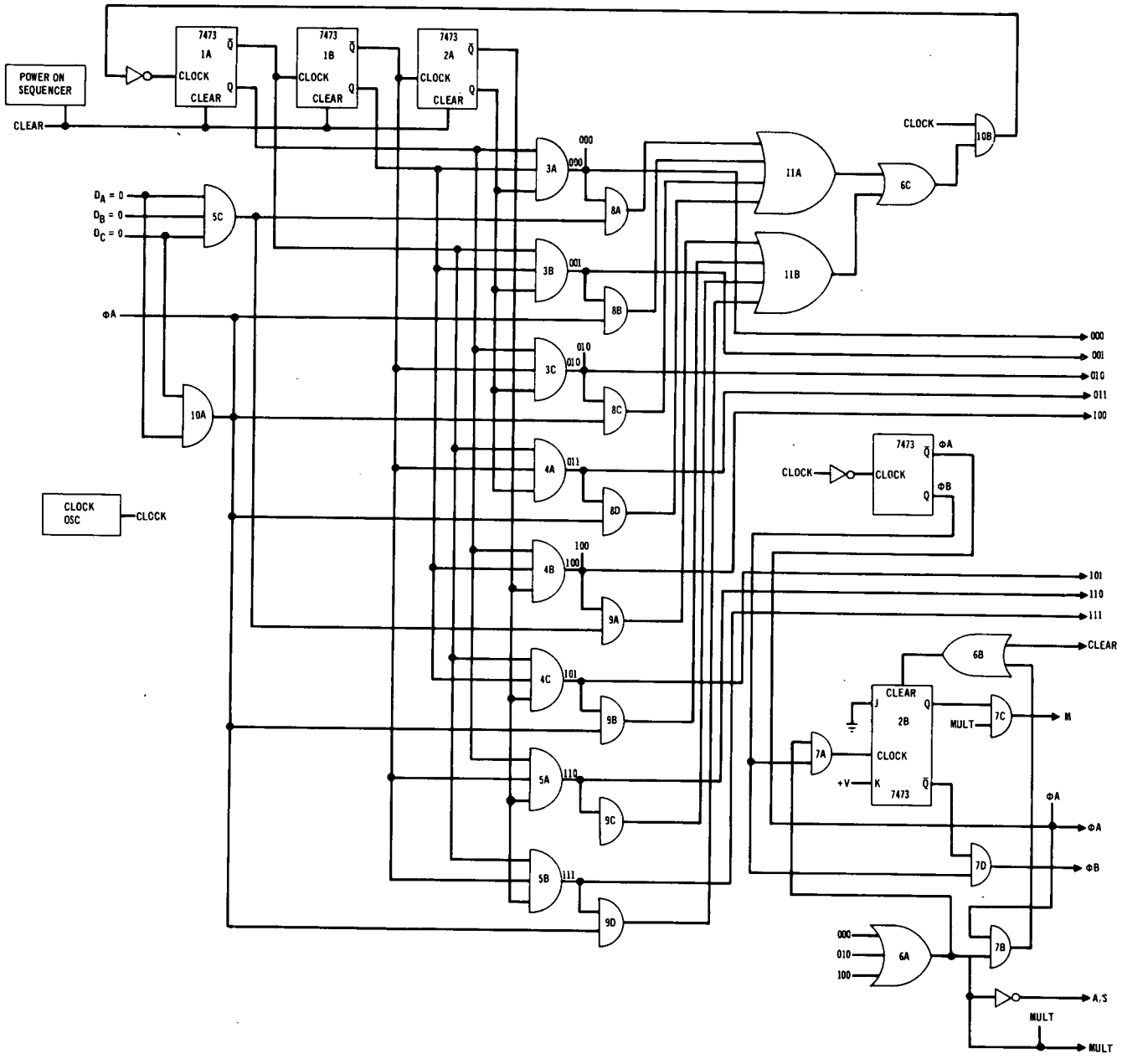

FIGURE 107

Timing diagrams showing the relationship of Operation Sequences Outputs are detailed in Figure (108).

Arithmetic Logic Units A and C (Reference Figure 109)

ALU A and ALU C are used to multiply. During this operation, the arithmetic unit, 6A, 7A, 8A, and 9A performs addition only; therefore the control inputs to the 74181's, 6A, 7A, and 8A are hardwired to the A plus B mode. The outputs of the A Register (4A and 5A) and the Accumulator (10A and 11A) are permanently connected to the 74181 inputs. The output of the 74181 which is the sum of the inputs is strobed into the Accumulator as required by the multiply routine. The operations in the multiply routine are as follows.:

M input - Loads Multiplicand into A Register
Loads Multiplier into B Register
Loads Multiplier length into D Register
Clears the Accumulator

ØA Input - If LSB of B = 1, strobes the Adder output into the Accumulator.

ØB Input - Shifts the contents of Ac and B register on bit to right. Decrements D Register.

When the M input from the Operation Sequence goes high, the clocks to 5A and 4A are gated high via gate 21A. This results in the loading of the data into these latches. The data will be that stored in the Accumulator or ALU B except during time slot 000. Data Selectors, 1A, 2A, and 3A route the selected data to the latches. In addition, the M signal loads the data selected by data selectors 13A, 14A, 15A, 16A, 17A, and 18A into the B register (19A and 20A); clears the Accumulator (10A and 11A); and loads D_o through D_4 into the D register (12A).

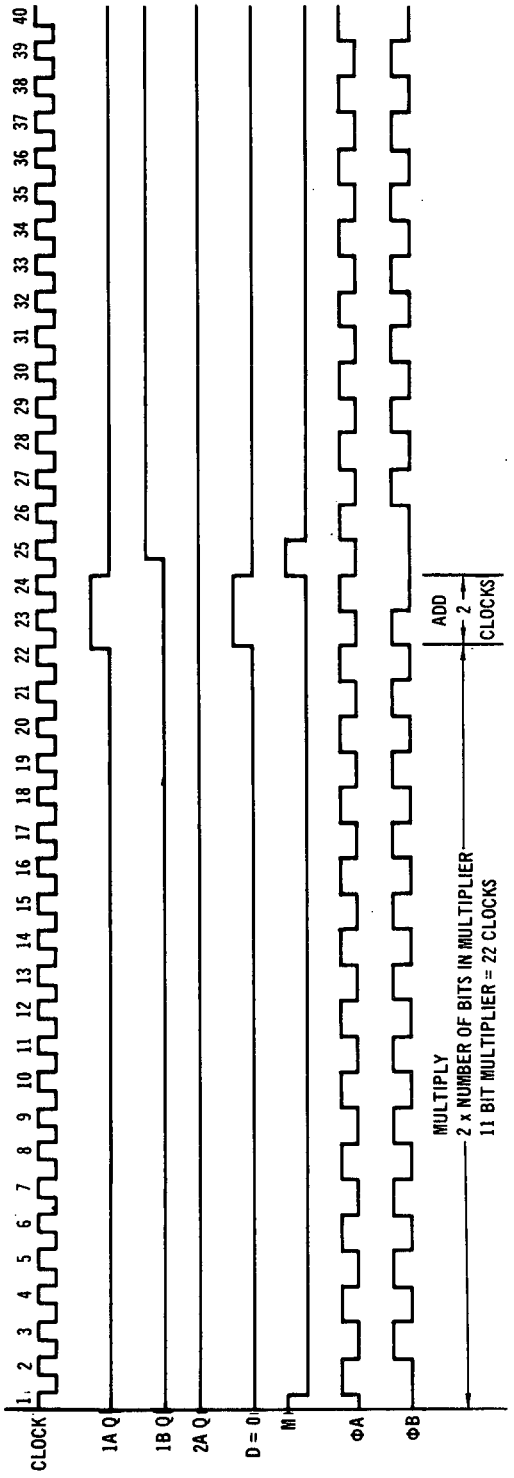

TIMING DIAGRAM

Figure 108

ALU A AND (ALU C)

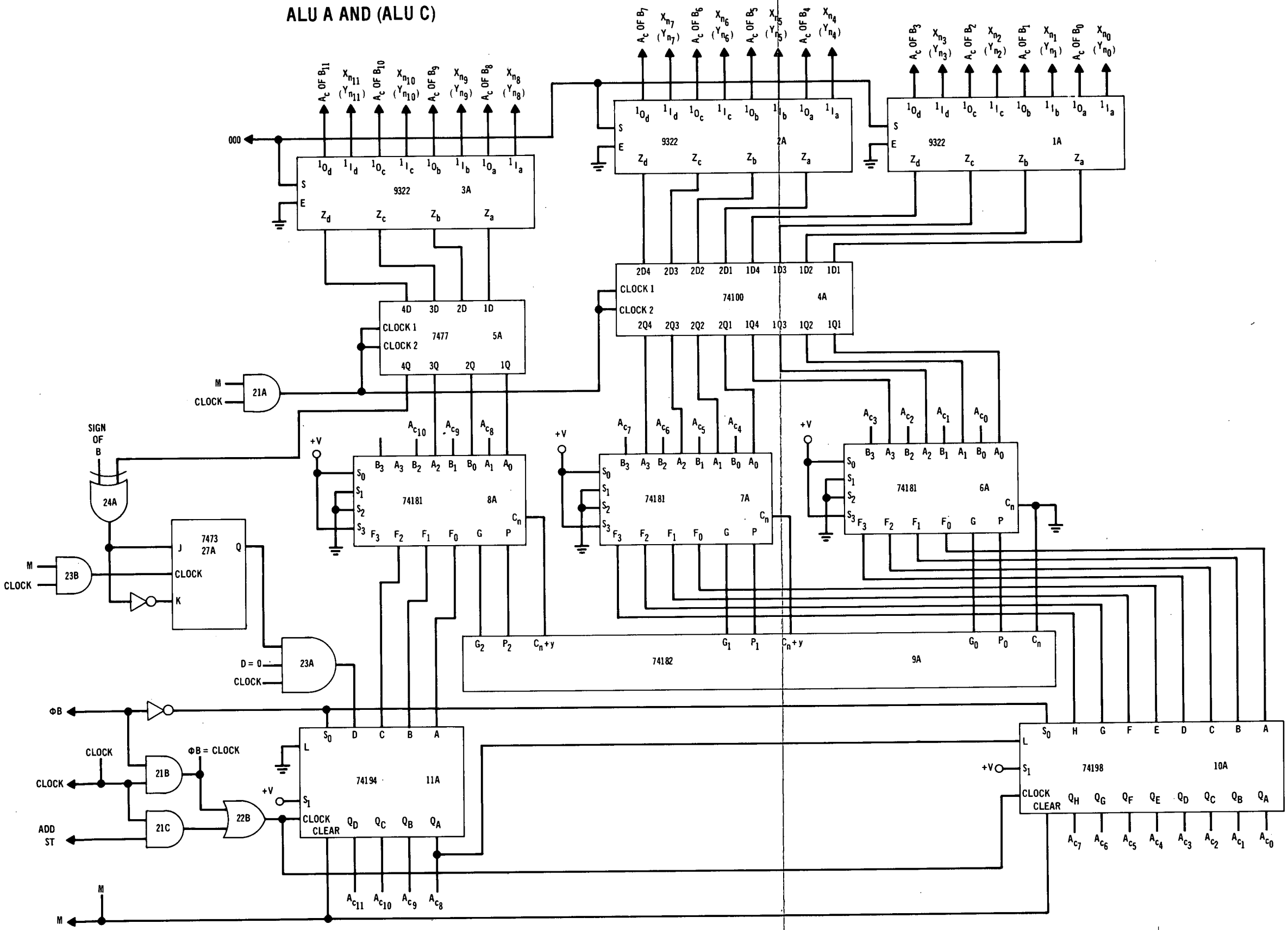

Figure 109

FOLDOUT FRAME 1

ALU A AND (ALU C) (Continued)

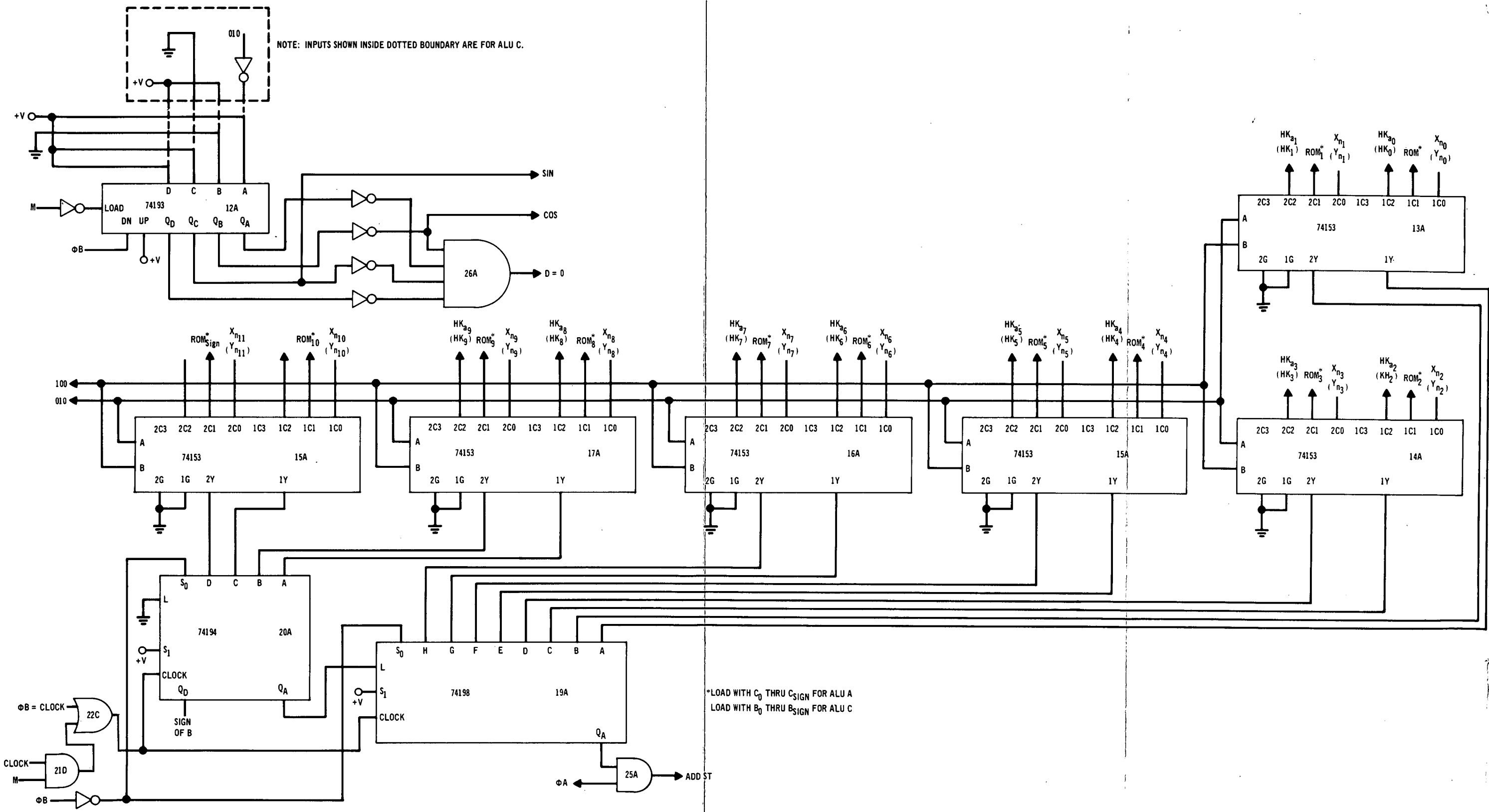

Figure 109 (Continued)

FOLDOUT FRAME 2

The ØA input produces an add st. signal out of gate 25A provided that the LSB of the multiplier stored in the B register (19A and 20A) is a logic one. This add st., via gates 21C and 22B, clocks the sum of the numbers previously stored in the A register and Accumulator (initially all zeros) into the Accumulator.

When the ØA input goes low, the ØB input goes high. This input decrements the D register and raises the S_o input to the Accumulator (10A and 11A) and the B register (19A and 20A). With S_o nnd S_1 to these shift registors at the logic one level, the clock input via gates 21B, 22B, and 22C shifts the contents one place towards Q_A.

The ØA and ØB operations continue until the D register is decremented to 0. This state is detected by gate 26A and the output is fed back to the Operation Sequences. In addition; the D register values of 7 or less is detected and output as Sin and Cos for use in addressing the Method B ROM. The correct sign for the product stored in the Accumulator (10A and 11A) is decoded by Ex=OR gate 24A and gate 23A during the time M input is high. This value is stored in the flip-flop 27A until the D=0 signal goes high. The D=0 signal enables gate 23A which strobes the proper sign into the Accumulator sign bit.

Arithmetic Logic Unit B (Reference Figure 110)

The operation of ALU B is more complex than that of ALU's A and C due to the requirement that the arithmetic unit (3A, 4A, 5A, and 6A) perform additions, subtractions, and comparisons as well as multiplication operations. The outputs of the A register (1A and 2A) and Accumulator (7A and 8A) are hardwired to the arithmetic unit inputs. The arithmetic unit outputs are connected to the Accumulator inputs via True/Complement logic (15A, 16A and 17A) and Data Selectors (13A, 14A and 18A). The Data Selectors allow the

C

ALU B

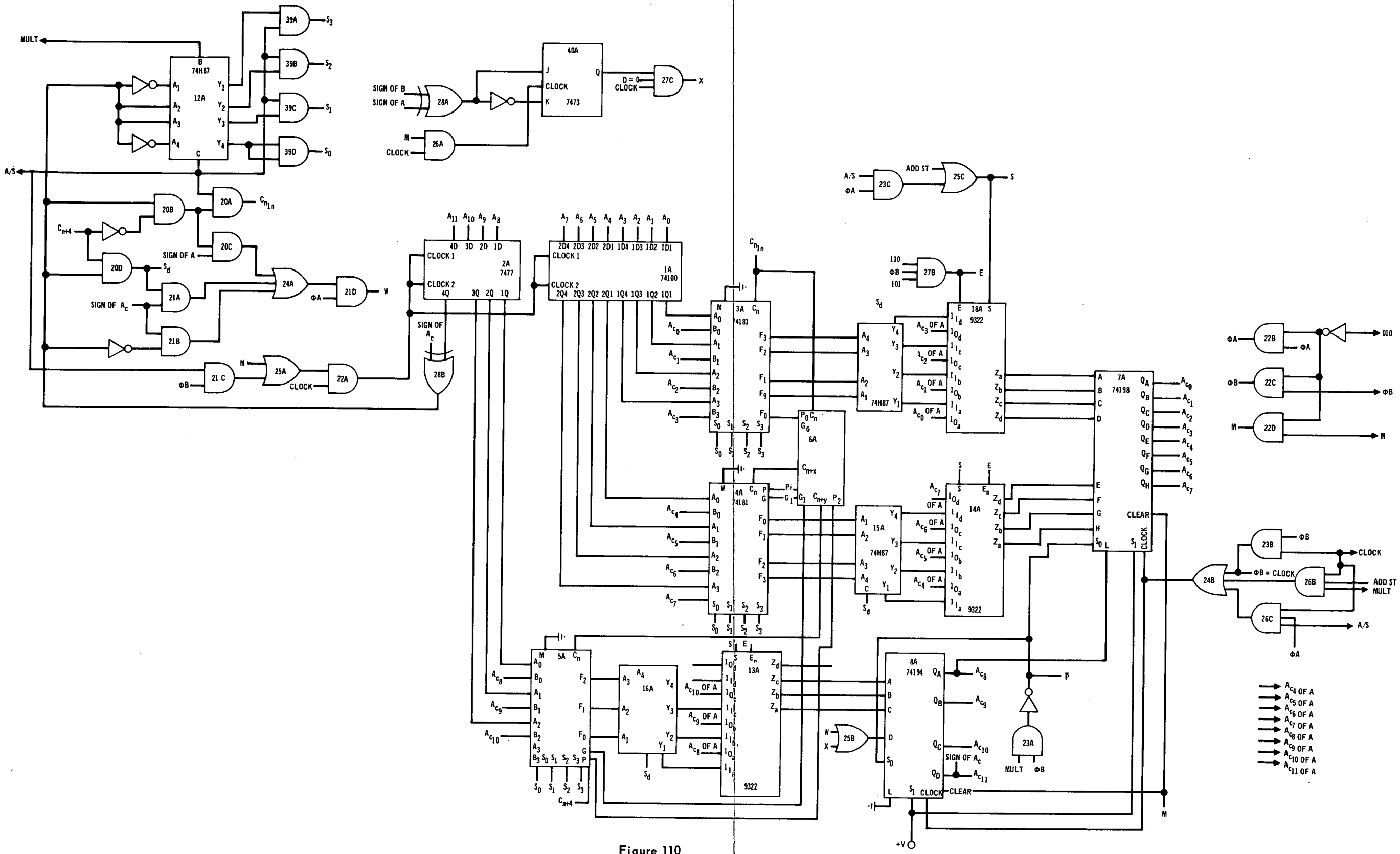

Figure 110

FOLDOUT FRAME 1

ALU B (Continued)

FOLDOUT FRAME 2

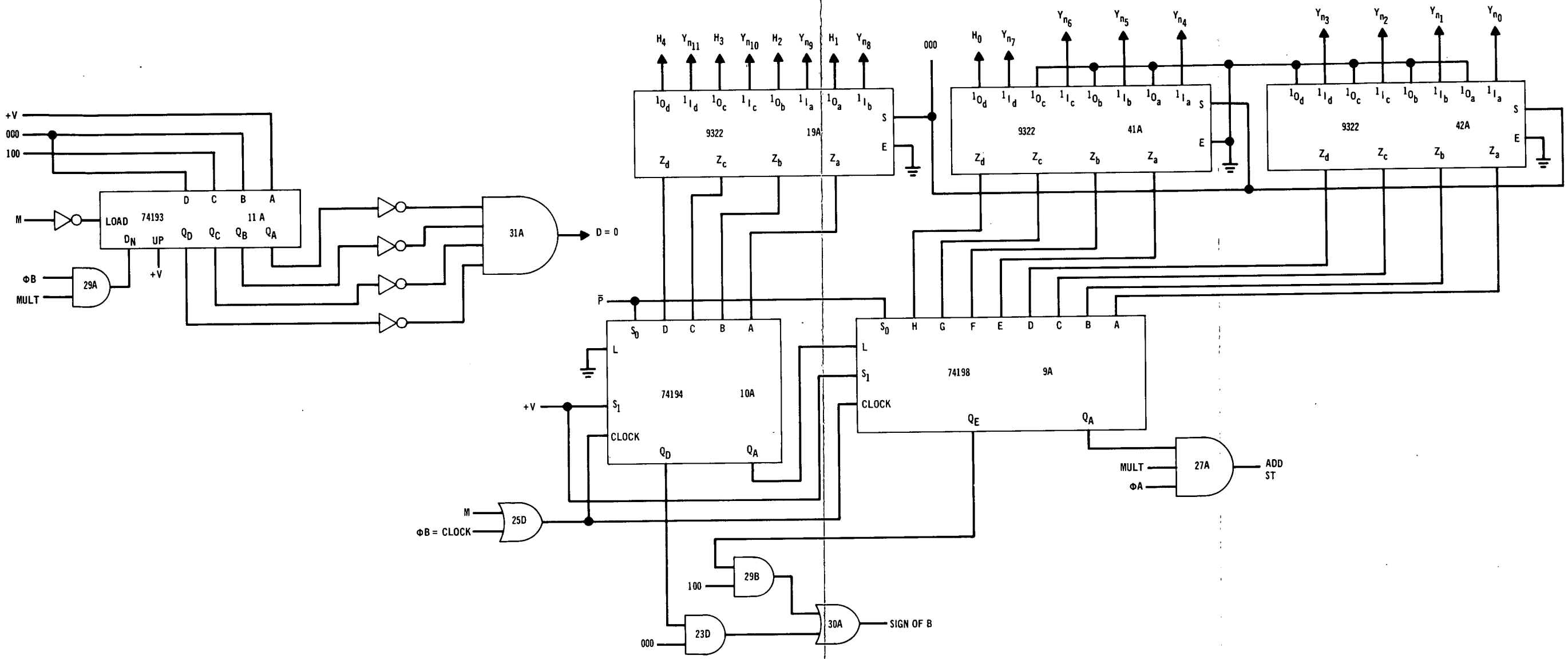

Figure 110 (Continued)

Accumulator to be loaded from the arithmetic unit for all operations and also to be loaded from the Accumulator of ALU A for operations during slots 001, 011, and 111. Selection of the arithmetic unit outputs as inputs to the Accumulator is the function of gates 23C and 25C. Gate 23A selects the shift mode for the Accumulator. This mode is required whenever ØB and a Multi signal occur simultaneously. A clock signal is gated to the clock input of the Accumulator via gates 23B and 24B to produce the shift. Clocks are also supplied to the Accumulator via gates 26B and 24B to load the Accumulator with data from the arithmetic unit during multiply operations when the add st. is high. During other arithmetic operations, ØA loads data into the Accumulator via gates 26C and 24B. Gate 27B inhibits data loading from any source during slots 101 and 110. This is necessary since the addend is already in the Accumulator during this addition as a result of being stored there during the previous slot. During arithmetic operations other than multiply, ØB is used to load the data into the A Register and Accumulator for input to the arithmetic unit.

Control of the arithmetic unit is accomplished by the S_o, S_1, S_2, S_3, and C_n inputs. The following table describes this control:

S_3	S_2	S_1	S_o	C_n	Operation
0	1	1	0	1	A minus B
1	0	0	1	0	A plus B
0	1	1	0	0	A minus B minus 1

During the multiplication operation, the A plus B code must be selected. True/Complementer logic (12A) and gates 39A, 39B, 34C, and 39D provide this code. The outputs of 12A (Y1, Y2, Y3, and Y4) are all ones when there is a logic one on the B input and a logic zero on the A input. This is the case

when multiplication slots are decoded by the Operation Sequencer. These inputs to gates 39A, 39B, 39C, and 39D and the logic zero level on the A1S input provide the proper code for addition.

During other operations, the setup of these signals is controlled by the sign bits stored in the A register (2A) and the Accumulator (8A). When signs are alike, the output of Exclusive OR gate 28B will be a logic zero and the A plus B code will be set up by 12A, gates 39A, 39B, 39C, 39D, 20B and 20A. Gates 25B, 21D, 24A, and 21B provide the proper sign bit into the Accumulator. With unlike signs, the output of 28B is a logic one. True/Complementer (12A) outputs logic zeros for S_3 and S_o and logic ones for S_2 and S_1. Gate 20A outputs a logic one for C_n if the C_n+4 output of 5A is a logic zero. The arithmetic unit C_n+4 is a logic zero when the A register input is larger than the Accumulator input. As a result the arithmetic unit performs the A minus B operation, and the True of the result is loaded into the Accumulator via 15A, 16A, and 17A. Gate 20C enables the sign of A for the sign bit of the Accumulator. If the opposite is true, the C_n input will be a logic zero and the arithmetic unit performs the A minus B minus 1 operation, and the complement of the results is loaded into the Accumulator. Gate 21A via gates 24A, 21D, and 25B loads the sign of Accumulator into the Accumulator.

Exclusive OR gate 28A and gates 26A, 27C, and 25B, and flip-flop 40A provide the proper sign for the Accumulator following completion of multiplication operations.

Inputs to the A Register via data selectors, 32A, 33A, 34A, 35A, 36A, and 37A. The following code is given for the inputs:

Slot	A	B	Input
000/010	0	0	X_n
100/101/111	1	0	A_c of ALU C
001/011/101/110	0	1	X_2
101	1	1	X_1

Gates 24C and 38A set up the required selection codes A and B.

Operation of the B register (9A and 10A) and D Register (11A) is identical to that of the register described for ALU's A and C. Data selectors 19A, 41A and 42A are required to select the proper data for loading into the B register.

Gates 22B, 22C, and 22D inhibit the ϕA, ϕB and M inputs to ALU B during slot 010. This is required to inhibit operations since the ALU is not operated during this time slot.

Sine - Cosine Read Only Memory

The sine and cosine of two times the angle stored in the X1 output are stored in Read Only Memories (ROM's). Standard ROM's storing the sine and cosine are available. These ROM's store values for angles in the 1st quadrant (0 to $\pi/4$). Addressing the ROM is accomplished by hardwiring the X_1 register outputs to ROM inputs. The multiplication by two is accomplished by shifting the wiring one place to left (i.e., X_{10} is wired to ROM, π input position instead of $\pi/2$). Two methods of providing the sine and cosine of the X_1 angles are described in the following:

Method A (Reference Figure 111): -Two 128 word, 8 bit ROM's (1A and cosine counterpart) are used. The X_{10} and X_o inputs, representing the π and $\pi/2$ bits, are connected to gates 5A, 5B, 5C, and 5D. These gates along with OR gates 4A, 4B, 4C, and 4D and True/Complementers 2A and 3A select the True/

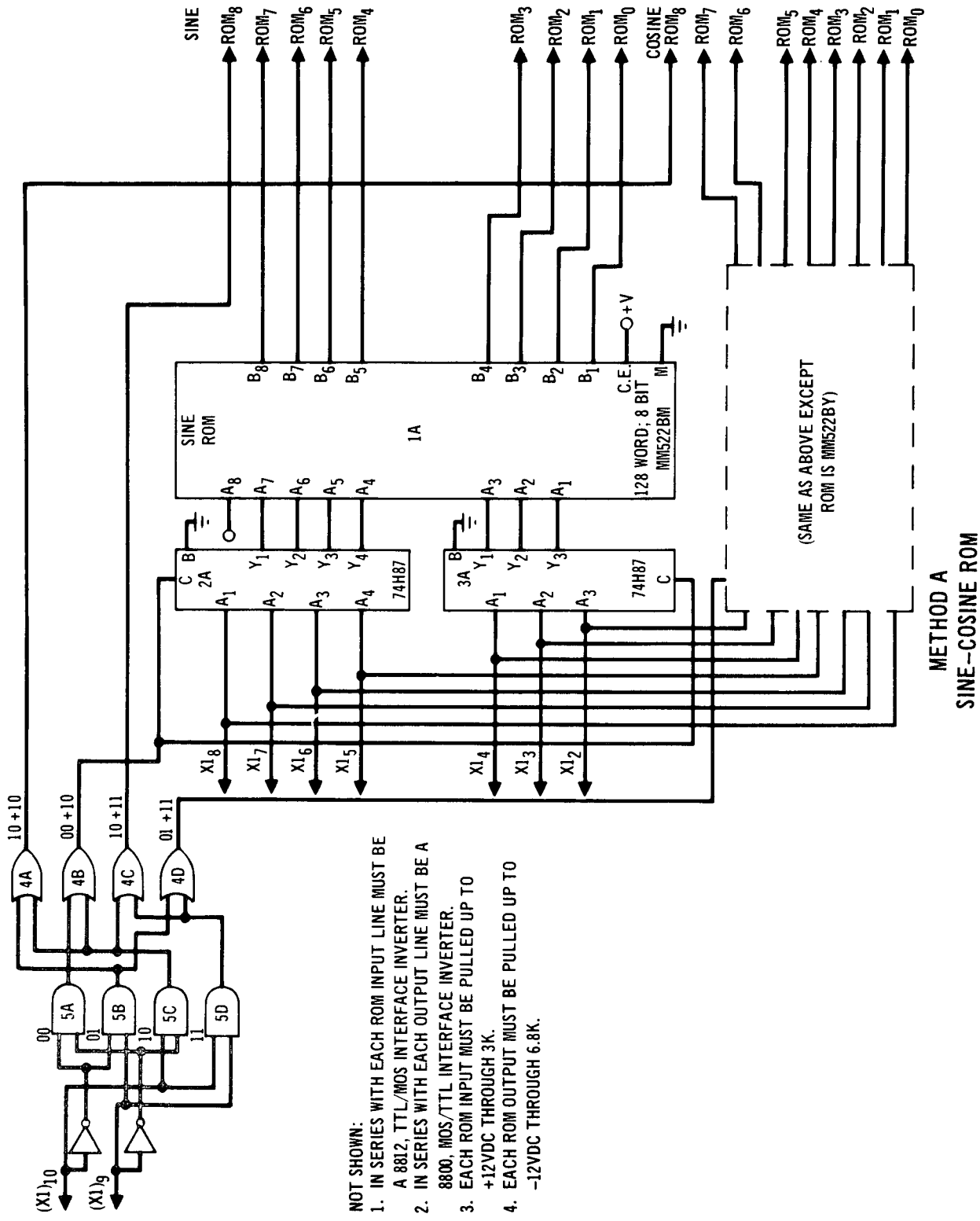
METHOD A
SINE–COSINE ROM
SINE ROM
1A
128 WORD; 8 BIT
MM522BM
(SAME AS ABOVE EXCEPT
ROM IS MM522BY)
74H87
2A
3A
C.E.
+V
NOT SHOWN:
1. IN SERIES WITH EACH ROM INPUT LINE MUST BE A 8812, TTL/MOS INTERFACE INVERTER.
2. IN SERIES WITH EACH OUTPUT LINE MUST BE A 8800, MOS/TTL INTERFACE INVERTER.
3. EACH ROM INPUT MUST BE PULLED UP TO +12VDC THROUGH 3K.
4. EACH ROM OUTPUT MUST BE PULLED UP TO -12VDC THROUGH 6.8K.

Figure 111

Complement of the input angle and decode the output sign bit according to the following:

$X1_{10}$	$X1_9$	Quadrant	Input Sine	Input Cosine	Output Sine	Output Sign Cosine
0	0	1st	True	Complement	0	0
0	1	2nd	Complement	True	0	1
1	0	3rd	True	Complement	1	1
1	1	4th	Complement	True	1	0

Method B (Reference Figure 112) - This method uses 4 ROM's to store 2048 values of the sine in the 1st quadrant. Each value is output as a 12 bit word. The X_1 register which stores the values of the angles has only 12 bits. One bit is lost in the multiplication by two and two bits are required to identify the quadrant. Hence, only 512 values are accessible. Also, the output word resolution is reduced to 10 bits due to B register length limitations. Selecting the correct address for each quadrant for both the sine and cosine is accomplished by gates 18A, 18B, 18C, 18D, 19A, 19B, 19C, 19D, and 20A. When this selection produces an input angle that required complementing (such as sine of 120°) to obtain the proper address; exclusive OR gates, 12A, 13B, 13C, 13D, 14A, 14B, 14C, 14D, 15A, 15B, 15C and adders 5A, 6A, and 7A output the required address. Similarly, adders 8A, 9A, and 10A sum the ROM outputs to produce the 12 bit output. Latches 11A and 12A store the sine value since simultaneous addressing of sine and cosines is not possible when only the sine of an angle is stored. Gates 2A, 12B, and 20B output the correct sign bit. Level converters 16A, 16B, 16C, 16D, 16E, 16F, 17A, 17B, 17C, 17D and 17E are required to interface the TTL address 5A, 6A, and 7A with the MOS ROM's.

Input-Output Registers (Reference Figure 113)

Latches are used to store the X_n (1A and 2A) inputs and the Y_n (3A and 4A)

METHOD B SINE–COSINE ROM

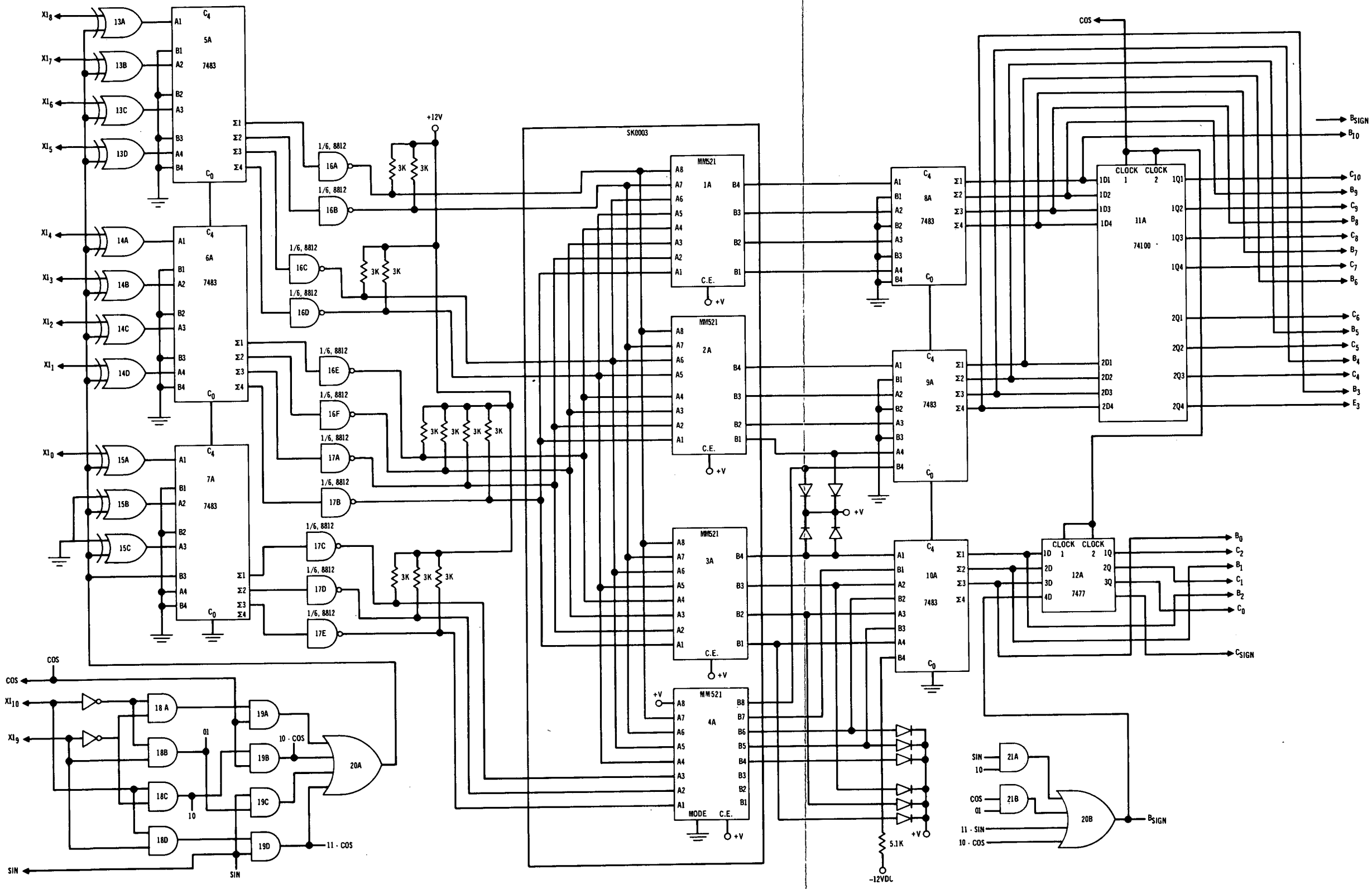

Figure 112

FOLDOUT FRAME

INPUT–OUTPUT REGISTERS

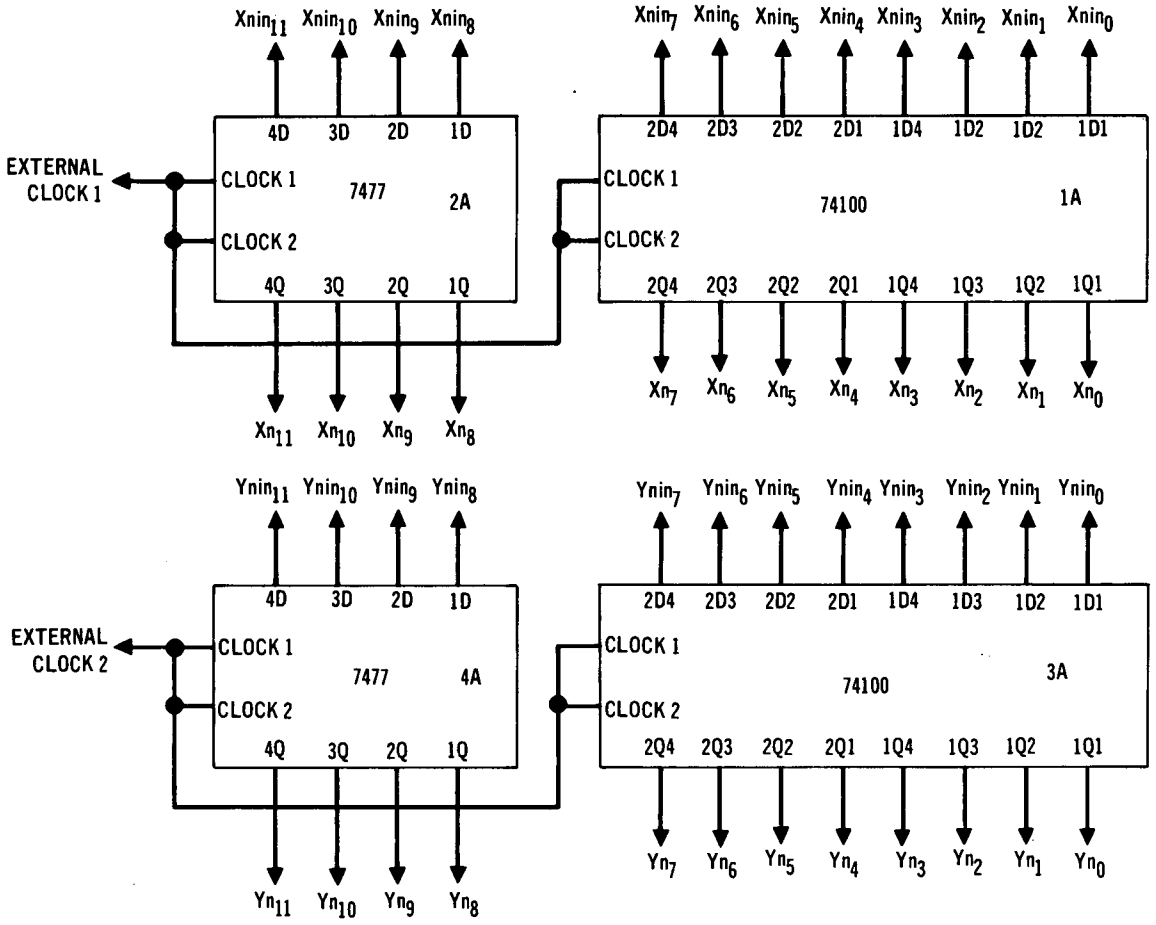

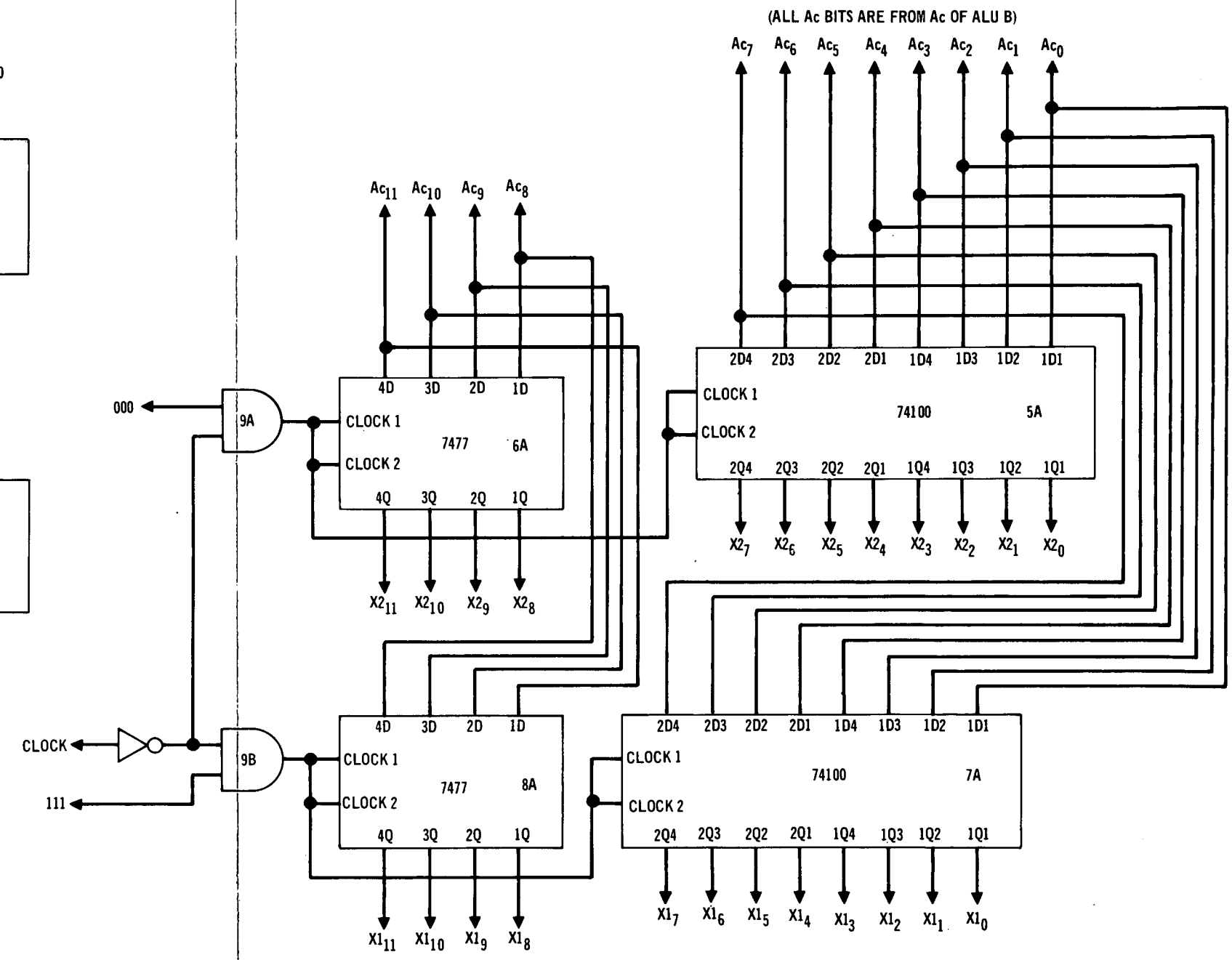

Figure 113

FOLDOUT FRAME 2

inputs. Data is clocked into these latches whenever the respective external clock goes high.

The output registers also use latches for storage. These registers both receive inputs from the Accumulator of ALU B. Gates 9A and 9B are used to enable input clocks during the appropriate time slot.

Parts List

Total Parts Count (exclusive of ROM's)

9	74181
3	74182
6	74198
6	74194
7	74100
7	7477
12	74153
3	74193
6	7473
4	74HB7
12	9322
15	7408
7	7410
3	7420
5	7432
2	7427
1	7425
3	7486
8	7404
27	SPST Switches

Total Parts (Method A ROM)

1	MM522BM
1	MM522BY
4	74H87
1	7408
1	7432
1	7404
3	8812
3	8800
7	3K Resistors
8	6.8K Resistors

Total Parts (Method B ROM)

1	SK003
6	7483
1	74100
1	7477
3	7408
1	7425
3	7486
1	7404
2	8812
11	3K Resistors
10	Diodes
1	5.1K Resistor

5.2.4 Cost Estimate

This design uses 134 or 141 integrated circuits (depending upon the type of ROM used). Packaging and other aspects of the mechanical design of the processor such as thermal considerations have not been completed due to lack of time, however it's estimated that 3 circuit cards will be required. Based on these quantities, the following estimate of cost to produce the processor is given:

Integrated Circuits	$520
Switches	$30
Printed Circuit Costs	$390
Connectors	$15
Labor for Assembly (180 hrs. at $22/hr)	$3,960
Labor for Test and Checkout (120 hrs. at $22/hr)	$2,640
Labor for Design Completion (40 hrs. at $22/hr)	$880
	$8,335

5.3 Future Effort

The design described in Section 5.2 utilizes one of many methods possible. In addition, it is recommended for follow on work that the following designs be completed in the same manner to provide meaningful speed and accuracy vs. cost trade-off data:

a) Serial Processor

b) Serial-parallel processor

c) Maximum speed processor using Look-up Table Multipliers.

References

1. J. B. Scarborough, Numerical Mathematical Analysis, The Johns Hopkins Press, Baltimore, 1966.

2. W. E. Larimore, "Synthesis of Digital Phase-Locked Loops," pp. 14-20, Eascon 1968 Record.

3. D. J. Povejsil, R. S. Raven, and P. Waterman, Airborne Radar , Boston Technical Publishers, Inc., Cambridge, Mass., 1961.

4. J. T. Sterling, "Frequency Acquisition and Pull-in Characteristics of Phase-Locked Loops," General Electric Technical Information Series, No. R63RG01, January 1963.

5. J. A. Develet, Jr., "A Threshold Criterion for Phase-Lock Demodulation," Proceedings of the IRE, pp. 349-356, Vol. 51, No.2, February 1963.

6. A. J. Viterbi,"Phase-Locked Loop Dynamics in the Presence of Noise by Fokker-Planck Techniques,"Technical Report No. 32-427, Jet Propulsion Laboratory, Pasadena, Calif., July 31, 1967.

7. W. C. Lindsey and R C. Tausworthe, "A Survey of Phase-Locked Loop Theory," Jet Propulsion Laboratory Technical Report.

8. A. J. Viterbi, Principles of Communication Theory, McGraw-Hill, New York, 1966.

9. J. P. Frazier and J. Page, "Phase-Lock Loop Frequency Acquisition Study," IRE Transactions on Space Electronics and Telemetry, pp. 210-227, September 1962.

10. S. M. Sussman and G. R. Hicks, Jr., "Direct IF Sampler", Contract NAS5-21168, October 1970.

11. G. M. Lee and J. J. Komo, "Synchronization for PSK Demodulation by Non-Linear Filter Techniques," National Electronics Conference Record, 1969.

12. G. M. Lee and J. J. Komo, "PCM Bit Synchronization and Detection by Non-Linear Filter Theory," IEEE Trans. Commun. Technol., Vol. COM-18, pp. 757-762, December 1970.

13. G. M. Lee, "Non-Linear Filtering with Applications to Communication Theory," D. Sc. Dissertation, Dept. of Elec. Eng., Washington University, St. Louis, Missouri, June 1968.

14. P. A. Wintz and E. J. Luecke, "Performance of Self Bit Synchronizers for the Detection of Anticorrelated Binary Signals," Dept. of Elec. Eng., Purdue University, Lafayette, Ind., Tech. Rep. TR-EE-68-1.

15. J. J. Stiffler, "Maximum Likelihood Symbol Synchronization," Jet Propulsion Lab., California Institute of Technology, Pasadena, Space Program Summary 37-35, Vol. 4, pp 349-357, October 1965.

16. P. Mallory, "A Maximum Likelihood Bit Synchronizer," Proc. 1968 Int. Telem. Conf, pp. 1-16.

17. J. W. Layland, "Telemetry Bit Synchronization," Jet Propulsion Lab., Pasadena, California, Space Programs Summary 37-46, Vol. III, pp. 204-215, July 31, 1967.

18. M. K. Simon, "Non-Linear Analysis of an Absolute Value Type of an Early-Late Gate Bit Synchronizer," IEEE Trans. Commun. Technol., Vol. COM-18, No. 5, pp. 589-596, October 1970.

19. W. C. Lindsey and M. K. Simon, "The Performance of Suppressed Carrier Tracking Loops in the Presence of Frequency Detuning", Proc. of the IEEE, September 1970.

20. W. H. Anderson, R. B. Ball, and J. R. Voss, "A Numerical Method for Solving Differential Equations on Computers," J. ACM, Vol. 7, pp. 61-68, January 1960.

APPENDIX I - ANDERSON, BALL, VOSS METHOD

This appendix develops a set of difference equations which simulate a second order analog filter using the Anderson, Ball, Voss method. Let F(s) be defined as in Equation (I 1).

$$F(s) = \frac{\theta(s)}{e(s)} = \frac{Ks + aK}{s^2} \qquad \text{(I 1)}$$

The differential equation of the loop will have the form given in Equation (I 2).

$$\ddot{\theta} = K\dot{e} + aKe \qquad \text{(I 2)}$$

Following the method developed by Anderson, Ball, and Voss[20], we assume that the output of the filter is known up to time t_n, and approximate both the solution of Equation (I 2) and the input signal in the time interval from t_n to $(t_n + h)$. It is then possible to solve for the coefficients of the polynomial series for $\theta(t)$ and determine the output at time $(t_n + h)$. The input signal is approximated by the polynomial in t given in Equation (I 3).

$$e = B_1 + B_2 (t-t_n) + B_3 (t-t_n)^2 \qquad \text{(I 3)}$$

The coefficients of Equation (I 3) can then be determined as a function of the past, present and future samples of the input signal, e. The results are given in Equations (I 4 - I 6).

$$B_1 = e_n \qquad \text{(I 4)}$$

$$B_2 = \frac{1}{2h} (e_{n+1} - e_{n-1}) \qquad \text{(I 5)}$$

$$B_3 = \frac{1}{2h^2} (e_{n+1} - 2e_n + e_{n-1}) \qquad \text{(I 6)}$$

The solution to Equation (I 2) is approximated by its transient response plus a polynomial in t. Since the transient response of Equation (I 2) is also a polynomial in t, the solution will have the form given in Equation (I 7).

$$\theta = A_1 + A_2 (t-t_n) + A_3 (t-t_n)^2 + A_4 (t-t_n)^3 + A_5 (t-t_n)^4 \qquad \text{(I 7)}$$

Equations (I 3) and (I 7) are now substituted into Equation (I 2).

$$2A_3 + 6A_4 (t-t_n) + 12A_5 (t-t_n)^2 = K \left[B_2 + 2B_3 (t-t_n)\right] + aK \left[B_1 + B_2 (t-t_n) + B_3 (t-t_n)^2\right] \qquad \text{(I 8)}$$

By equating like coefficients, solutions for A_3, A_4, and A_5 can be determined.

$$A_3 = (1/2)KB_2 + (1/2)aKB_1 \qquad \text{(I 9)}$$

$$A_4 = (1/3)KB_3 + (1/6)aKB_2 \qquad \text{(I 10)}$$

$$A_5 = (1/12)aKB_3 \qquad \text{(I 11)}$$

A_1 and A_2 are determined by letting $t = t_n$ and $t = t_{n-1}$ in Equation (I 7).

$$A_1 = \theta_n \qquad \text{(I 12)}$$

$$A_2 = \frac{1}{n}\left[-\theta_{n-1} + \theta_n + A_3h^2 - A_4h^3 + A_5h^4\right] \qquad \text{(I 13)}$$

The final difference equation can be determined by letting $t = t_{n+1}$ and substituting the results from Equations (I 4 - I 6), (I 9 - I 11), (I 12) and (I 13) in Equation (I 7). The difference equation is given in Equation (I 14).

$$\theta_{n+1} = 2\theta_n - \theta_{n-1} + Kh\,(e_{n+1} - e_{n-1})/2 + aKh^2 e_n + aKh^2\,(e_{n+1} - 2e_n + e_{n-1})/12 \qquad \text{(I 14)}$$

Since θ_{n+1} depends on e_{n+1}, a unit delay must be added in the feedback path. The resulting values for e_{n+1}, e_n, and e_{n-1} are given in Equations (I 15 - I 17).

$$e_{n+1} = Y_{n+1} \cos \theta_n - X_{n+1} \sin \theta_n \qquad \text{(I 15)}$$

$$e_n = Y_n \cos \theta_{n-1} - X_n \sin \theta_{n-1} \qquad \text{(I 16)}$$

$$e_{n-1} = Y_{n-1} \cos \theta_{n-2} - X_{n-1} \sin \theta_{n-2} \qquad \text{(I 17)}$$

APPENDIX II - EQUATIONS FOR LINEAR FILTERS

This appendix develops difference equations which simulate the analog filters specified in Equations (II 1) and (II 2). Five numerical methods were examined on the basis of their expected performance and speed.

(1) Runge - Kutta Method

The transfer function of the linear filter $H_1(s)$ is given in Equation (II 1).

$$H_1(s) = \frac{\theta(s)}{E(s)} = \frac{\omega_o^2}{s^2 + 2\zeta\omega_o s + \omega_o^2} \qquad \text{(II 1)}$$

The differential equation can then be written from the above transfer function

$$\ddot{\theta} + 2\zeta\omega_o\dot{\theta} + \omega_o^2\theta = \omega_o^2 E \qquad \text{(II 2)}$$

Using results from Scarborough[1] the numerical solution is determined.

$$F(\dot{\theta}, \theta, E) = -2\zeta\omega_o h\dot{\theta} + \omega_o^2 h\,(E-\theta) \qquad \text{(II 3)}$$

$$A_1 = F(\dot{\theta}_{n-2},\ \theta_{n-2},\ E_{n-2})$$

$$A_2 = F(\dot{\theta}_{n-2} + .5A_1,\ \theta_{n-2} + .5h\dot{\theta}_{n-2} + .125hA_1,\ E_{n-1})$$

$$A_3 = F(\dot{\theta}_{n-2} + .5A_2,\ \theta_{n-2} + .5h\dot{\theta}_{n-2} + .125hA_1,\ E_{n-1})$$

$$A_4 = F(\dot{\theta}_{n-2} + A_3,\ \theta_{n-2} + h\dot{\theta}_{n-2} + .5hA_3,\ E_n)$$

$$\dot{\theta}_n = \dot{\theta}_{n-2} + (A_1 + 2A_2 + 2A_3 + A_4)/6.$$

$$\theta_n = \theta_{n-2} + h\dot{\theta}_{n-2} + h(A_1 + A_2 + A_3)/6.$$

The transfer function for $H_2(s)$ is given in Equation (II 4).

$$H_2(s) = \frac{\theta(s)}{E(s)} = \frac{2\zeta\omega_o s + \omega_o^2}{s^2 + 2\zeta\omega_o s + \omega_o^2} \qquad \text{(II 4)}$$

A corresponding differential Equation (II 5) can be written. To avoid taking the derivative of the input signal, this equation is converted into two first order Equations (II 6) and (II 7) using the dummy variable C.

$$\ddot{\theta} + 2\zeta\omega_b\dot{\theta} + \omega_o^2 = 2\zeta\omega_o\dot{E} + \omega_o^2 E \qquad \text{(II 5)}$$

$$\frac{dc}{dt} = \omega_o^2 (E-\theta) \qquad \text{(II 6)}$$

$$\frac{d\theta}{dt} = C + 2\zeta\omega_o(E-\theta) \qquad \text{(II 7)}$$

Using results from Scarborough [1] for the solution of first order simultaneous differential equations, the difference Equation (II 8) was formulated.

$$F(\theta,E) = 2\zeta\omega_o h(E-\theta) \qquad \text{(II 8)}$$

$$G_1 = F(\theta_{n-2},\ E_{n-2})$$

$$A_1 = hC_{n-2} + G_1$$

$$B_1 = (\omega_o/2\zeta)G_1$$

$$G_2 = F(\theta_{n-2} + A1/2\ \ E_{n-1})$$

$$A_2 = h(C_{n-2} + B1/2) + G_2$$

$$B_2 = (\omega_o/2\zeta)\ G_2$$

$$G_3 = F(\theta_{n-2} + A2/2,\ E_{n-1})$$

$$A_3 = h(C_{n-2} + B2/2) + G_3$$

$$B_3 = (\omega_o/2\zeta)\ G_3$$

$$G_4 = F(\theta_{n-2} + A_3,\ E_n)$$

$$A_4 = h(\theta_{n-2} + B_3) + G_4$$

$$B_4 = (\omega_o/2\zeta)\ G_4$$

$$C_n = C_{n-2} + (B_1 + 2B_2 + 2B_3 + B_4)\ /6.$$

$$\theta_n = \theta_{n-2} + (A_1 + 2A_2 + 2A_3 + A_4)\ /6.$$

(2) Euler's Method

Euler's method for the solution of a n^{th} order differential equation consists of first reducing the equation to n first order simultaneous differential equations and then solving the n equations using rectangular integration. Equation (II 2) can be converted into two first order equations by defining the state variable $\dot{\theta}$ and θ.

$$\dot{\theta} = C \tag{II 9}$$

$$\dot{C} = 2\zeta\omega_o C + \omega_o^2(E-\theta) \tag{II 10}$$

The difference equations for the implementation of Euler's Method can be determined from the above equations and are given in Equations (II 11) and (II 12).

$$\theta_n = \theta_{n-1} + h\,\dot{\theta}_{n-1} \tag{II 11}$$

$$\dot{\theta}_n = h\left[-2\zeta\omega_o\dot{\theta}_{n-1} + \omega_o^2\,(E_{n-1} + \theta_{n-1})\right] + \dot{\theta}_{n-1} \tag{II 12}$$

The difference equations for filter $H_2(s)$ can be determined from Equations (II 6) and (II 7).

$$F = 2\zeta\omega_o h\,(E_{n-1} - \theta_{n-1}) \tag{II 13}$$

$$\theta_n = \theta_{n-1} + hC_{n-1} + F$$

$$C_n = C_{n-1} + (\omega_o/2\zeta)\,F$$

(3) Anderson, Ball, Voss Method

We will now determine the difference equation for filter $H_1(s)$, using the Anderson, Ball, Voss method. We assume that the filter output is known up to time t_n and approximate both the solution to the equation and the input signal in the time interval from t_n to $(t_n + h)$. As was done in Appendix I, the input signal was assumed to have the form shown in Equation(II 14).

$$E = K_1 + K_2 (t-t_n) + K_3 (t-t_n) \qquad \text{(II 14)}$$

The coefficients of this equation can be evaluated as a function of the past, present, and future samples of the input signal, E.

$$K_1 = E_n \qquad \text{(II 15)}$$

$$K_2 = \frac{1}{2h} (E_{n+1} - E_{n-1}) \qquad \text{(II 16)}$$

$$K_3 = \frac{1}{2h^2} (E_{n+1} - 2E_n + E_{n-1}) \qquad \text{(II 17)}$$

The solution to the differential equation of the filter is approximated between time t_n and $t_n + h$ by the sum of its transient response and a polynomial in t.

$$\theta = Ae^{-\zeta\omega_o(t-t_n)} \cos \omega_o \sqrt{1-\zeta^2}(t-t_n) \qquad \text{(II 18)}$$
$$+ Be^{-\zeta\omega_o(t-t_n)} \sin \omega_o \sqrt{1-\zeta^2}(t-t_n) + C_1 + C_2 (t-t_n)$$
$$+ C_3 (t-t_n)^2$$

Equations (II 18) and (II 14) are now substituted into the filter equation (II 2). After equating like coefficients, the results given in Equations (II 19 - II 21) are obtained.

$$C_3 = K_3 \tag{II 19}$$

$$C_2 = K_2 - 4\zeta K_3/\omega_o \tag{II 20}$$

$$C_1 = K_1 - 2(\zeta/\omega_o) K_2 + K_3 (8\zeta^2 - 2)/\omega_o^2 \tag{II 21}$$

The coefficients A and B are determined be letting $t = t_n$ and $t = t_{n-1}$ in Equation (II 18).

$$A = \theta_n - C_1 \tag{II 22}$$

$$B = \left[(\theta_n - C_1)\cos \omega_o h + C_1 e^{-\zeta\omega_o h} - C_2 h e^{-\zeta\omega_o h} + C_3 h^2 e^{-\zeta\omega_o h} - \theta_{n-1} e^{-\zeta\omega_o h}\right] / \sin \omega_o h \tag{II 23}$$

$$\omega = \omega_o \sqrt{1-\zeta^2} \tag{II 24}$$

The resulting difference equation for the loop is given in Equation (II 25).

$$\theta_{n+1} = Ae^{-\zeta\omega_o h} \cos \omega_o \sqrt{1-\zeta^2}\, h + Be^{-\zeta\omega_o h} \sin \omega_o \sqrt{1-\zeta^2}\, h + C_1 + C_2 h + C_3 h^2 \tag{II 25}$$

The difference equation for $H_2(s)$ can also be determined by using the general formula for a second order filter given by Anderson, Ball, and Voss[20]. The results for $H_2(s)$ are given in Equations (II 26 - II 32).

$$A = 2e^{-\zeta\omega_o h} \cos\left(\omega_o h \sqrt{1-\zeta^2}\right) \qquad \text{(II 26)}$$

$$B = -e^{-2\zeta\omega_o h} \qquad \text{(II 27)}$$

$$C = -1/\omega 2_o h^2 \qquad \text{(II 28)}$$

$$D = (1-A-B)\ C + (1+B)/2 + (1-B)/2 \qquad \text{(II 29)}$$

$$F = (1-A-B)\ (1+2C) - (1-B) \qquad \text{(II 30)}$$

$$C = (1-A-B)\ C - .5\ (1+B) + .5\ (1-B) \qquad \text{(II 31)}$$

$$\theta_n = DE_n + FE_{n-1} + GE_{n-2} + A\theta_{n-1} + B\theta_{n-2} \qquad \text{(II 32)}$$

(4) Z - Transform

In order to determine the difference equation using the Z - transform technique, the Z - transform of the transfer function must be determined. However, in order to get meaningful results, a hold circuit must be placed before the filter. A zero order hold was used in order to simplify the implementation. The Z - transform can then be determined as shown in Equations (II 33 - II 39).

$$\frac{\theta(z)}{E(z)} = Z\left[\left(\frac{1-e^{-ST}}{s}\right)\left(\frac{\omega_o^2}{s^2 + 2\zeta\omega_o s + \omega_o^2}\right)\right] \qquad \text{(II 33)}$$

$$\frac{\theta(z)}{E(z)} = (1-z^{-1})\ Z\left[\frac{\omega_o^2}{s(s^2 + 2\zeta\omega_o s + \omega_o^2)}\right] \qquad \text{(II 34)}$$

$$\frac{\theta(z)}{E(z)} = \frac{z(1-B-DA) + C-B+DA}{z^2 - 2Bz + C} \qquad \text{(II 35)}$$

$$A = e^{-\zeta\omega_o h} \sin \omega_o h \sqrt{1-\zeta^2} \qquad \text{(II 36)}$$

$$B = e^{-\zeta\omega_o h} \cos \omega_o h \sqrt{1-\zeta^2} \qquad \text{(II 37)}$$

$$C = e^{-2\zeta\omega_o h} \qquad \text{(II 38)}$$

$$D = \zeta / \sqrt{1-\zeta^2} \qquad \text{(II 39)}$$

The difference equation for the filter is given in Equation (II 40).

$$\theta_n = 2B\theta_{n-1} - C\theta_{n-2} + (1-B-DA)\, E_{n-1} + (C-B+DA)\, E_{n-2} \qquad \text{(II 40)}$$

The difference equation using the Z - transform method for $H_2(s)$ can be derived in a similar manner.

$$\frac{\theta(z)}{E(z)} = (1-z^{-1})\, Z \left[\frac{2\zeta\omega_o s + \omega_o^2}{s(s^2 + 2\zeta\omega_o s + \omega_o^2)} \right] \qquad \text{(II 41)}$$

$$A = e^{-\zeta\omega_o h} \qquad \text{(II 42)}$$

$$B = \zeta / \sqrt{1-\zeta^2} \qquad \text{(II 43)}$$

$$C = \cos \omega_o h \sqrt{1-\zeta^2} \qquad \text{(II 44)}$$

$$D = \sin \omega_o h \sqrt{1-\zeta^2} \qquad \text{(II 45)}$$

$$\theta_n = (1-AC+BAD)\, E_{n-1} + (A^2 - AC - BAD)\, E_{n-2} + (2AC)\, \theta_{n-1} - A^2\theta_{n-2} \qquad \text{(II 46)}$$

E

(5) Tustin's Method

Tustin's method requires that the filter transfer function $H_1(s)$ be written in terms of (1/s) as shown in Equations (II 47) and (II 48).

$$\frac{\theta}{E} = \frac{\omega_o^2}{s^2 + 2\zeta\omega_o s + \omega_o^2} \qquad \text{(II 47)}$$

$$\theta\left(1 + \frac{2\zeta\omega_o}{s} + \frac{\omega_o^2}{s^2}\right) = \left(\frac{\omega_o^2}{s^2}\right) E \qquad \text{(II 48)}$$

The difference equation for $H_1(s)$ is determined by substituting the operator $\frac{h(1+z^{-1})}{2(1-z^{-1})}$ for (1/s).

$$\theta\left[1 + \frac{2\zeta\omega_o h(1+z^{-1})}{2(1-z^{-1})} + \frac{\omega_o^2 h^2 (1+z^{-1})^2}{4(1-z^{-1})^2}\right] \qquad \text{(II 49)}$$

$$= \left[\frac{\omega_o^2 h^2 (1+z^{-1})^2}{4(1-z^{-1})^2}\right] E$$

$$\theta\left[(1-2z^{-1}+z^{-2}) + \zeta\omega_o h\,(1-z^{-2}) + \omega_o^2 h^2\,(1+2z^{-1}+z^{-2})/4\right] \qquad \text{(II 50)}$$

$$= \omega_o^2 h^2\, E\,(1+2z^{-1}+z^{-2})/4$$

This result can then be converted into the difference Equation (II 52).

$$K = 1 + \omega_o^2 h/4 + \zeta\omega_o h \qquad \text{(II 51)}$$

$$\theta_n = \frac{1}{K}\left[(2 - \omega_o^2 h/2)\ \theta_{n-1} + (\zeta\omega_o h - 1 - \omega_o^2 h/4)\ \theta_{n-2} + \omega_o^2 h\ (E_n + 2E_{n-1} + E_{n-2})/4\right] \quad \text{(II 52)}$$

Similar methods can be used to generate the difference equation for $H_2(s)$. The result is given in Equation (II 54).

$$K = 4 + 4\zeta\omega_o h + \omega_o^2 h^2 \quad \text{(II 53)}$$

$$\theta_n = \frac{1}{K}\left[(4\zeta\omega_o h + \omega_o^2 h^2)\ E_n + 2\omega_o^2 h^2\ E_{n-1} + (\omega_o^2 h^2 - 4\zeta\omega_o h)\ E_{n-2} - (2\omega_o^2 h^2 - 8)\ \theta_{n-1} - (4 - 4\zeta\omega_o h + \omega_o^2 h)\ \theta_{n-2}\right] \quad \text{(II 54)}$$

APPENDIX III - BIT SYNCHRONIZATION ERROR

This appendix presents an analysis of our digital bit synchronization technique and provides expressions for the output timing jitter as a function of signal-to-noise ratio and tracking bandwidth. The technique employed to determine bit synchronization error is similar to that used by Layland[17]. A block diagram of the bit synchronization model is shown in Figure III-1.

BIT SYNCHRONIZATION MODEL

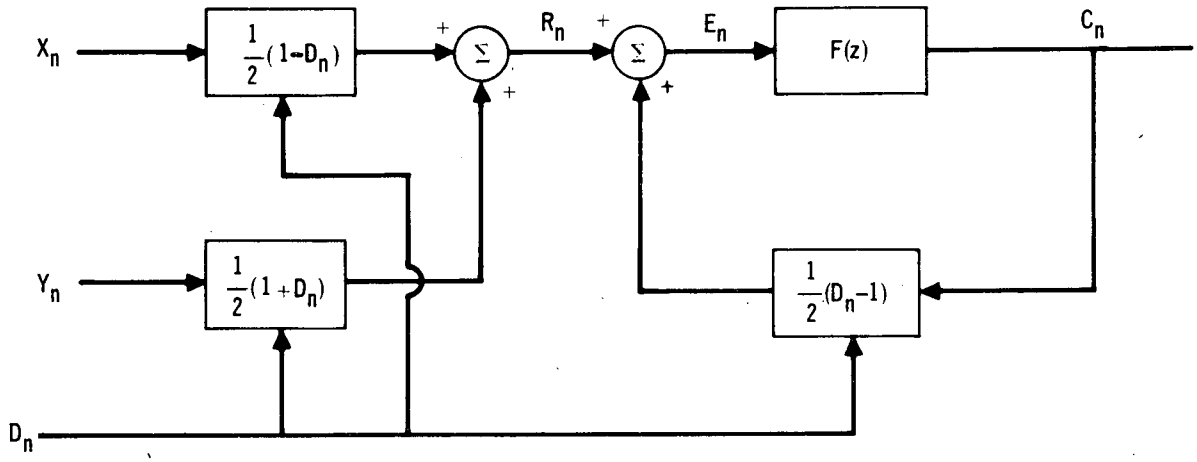

FIGURE III-1

In the above diagram the variable D_n has the value -1 if a bit transition has occurred and has the value +1 if no transition has occurred. For this analysis the two states are assumed to be equally probable, and it is also assumed that there is no correlation between adjacent samples. The above figure also indicates that X_n is the input signal when a transition occurs, and that Y_n is the input signal when no transition occurs. In this analysis we are assuming that the bit synchronization loop is second order. The loop filter F(z) is determined as shown in Equations (III 1) and (III 2).

$$F(z) = Z\left[(1-e^{-sT})\ \frac{K(s+a)}{s^3}\right] \qquad \text{(III 1)}$$

$$F(z) = \frac{Az + B}{z^2 - 2z + 1} \qquad \text{(III 2)}$$

$$A = KT + .5aKT^2$$

$$B = .5\,aKT^2 - KT$$

The difference Equation (III 3) relates C_n to E_n.

$$C_n = 2C_{n-1} - C_{n-2} + AE_{n-1} + BE_{n-2} \qquad \text{(III 3)}$$

Using this result, the difference equation relating the inputs and outputs of the bit synchronizer can be determined. The result is given in Equation (III 4).

$$\begin{aligned} C_n = {} & \left[2 + .5A(D_{n-1} - 1) \right] C_{n-1} + \left[.5B(D_{n-2} - 1) - 1 \right] C_{n-2} \\ & + .5A\,(1 - D_{n-1})\,X_{n-1} + .5A\,(1 + D_{n-1})\,Y_{n-1} \\ & + .5B(1 - D_{n-2})\,X_{n-2} + .5B(1 + D_{n-2})\,Y_{n-2} \end{aligned} \qquad \text{(III 4)}$$

We next square both sides of Equation (III 4) and take the expected value. In order to simplify the results the assumptions given in Equations (III 5 - III 7).

$$\overline{D_n^2} = 1 \qquad \text{(III 5)}$$

$$\overline{D_n} = 0 \qquad \text{(III 6)}$$

$$\overline{D_n D_{n-1}} = 0 \qquad \text{(III 7)}$$

After applying the above operations to Equation (III 4), Equation (III 8) results.

$$\begin{aligned} & (-4 + 2A - .5A^2 - .5B^2 - B)\,\overline{C_n^2} = (A-4)\,\overline{C_n C_{n-1}} \\ & + (2B - .5AB) \left(\overline{C_n X_{n-1} (1 - D_{n-1})} + \overline{C_n Y_{n-1} (1 + D_{n-1})} \right. \\ & \left. + \overline{C_n C_{n-1} (D_{n-1} - 1)} \right) + (2A - B)\,\overline{C_n Y_n} \\ & (2A - B^2 - B^2 - B)\,\overline{C_n X_n} + .5(A^2 + B^2)\,(\overline{X_n^2} + \overline{Y_n^2}) \\ & .5AB(\overline{X_n X_{n-1}} + \overline{Y_n Y_{n-1}}) + AB\,\overline{X_n Y_{n-1}} \end{aligned} \qquad \text{(III 8)}$$

This equation can be further simplified by using Equation (III 4) to solve for the first five terms on the right side of Equation (III 5). This is accomplished by multiplying both sides of Equation (III 4) by the appropriate quantity and averaging. The results are given in Equations (III 9 - III 14).

$$\overline{C_n C_{n-1}(D_{n-1}-1)} = \Big[(3A-4)\,\overline{C_n^2} - 3A\,\overline{C_n X_n} + A\,\overline{C_n Y_n} - B\,\overline{C_n X_{n-1}(1-D_{n-1})} - B\,\overline{C_n Y_{n-1}(1+D_{n-1})} \Big] / (B+4) \quad \text{(III 9)}$$

$$\overline{C_n C_{n-1}} = \Big[(4 - A + .5\,AB)\,\overline{C_n^2} + (A - .5AB)\,\overline{C_n X_n} + (A + .5AB)\,\overline{C_n Y_n} + B\,\overline{C_n X_{n-1}(1 - D_{n-1})} + B\,\overline{C_n Y_{n-1}(1 + D_{n-1})} \Big] / (B+4) \quad \text{(III 10)}$$

$$\overline{C_n X_n} = .5A\,(\overline{X_n X_{n-1}} + \overline{X_n Y_{n-1}}) \quad \text{(III 11)}$$

$$\overline{C_n Y_n} = .5A\,(\overline{Y_n X_{n-1}} + \overline{Y_n Y_{n-1}}) \quad \text{(III 12)}$$

$$\overline{C_n X_{n-1}(1 - D_{n-1})} = (A - .5A^2 + .5B)\,(\overline{X_n X_{n-1}} + \overline{X_n Y_{n-1}}) + A\,\overline{X_n^2} \quad \text{(III 13)}$$

$$\overline{C_n Y_{n-1}(1 + D_{n-1})} = (A + .5B)\,(\overline{Y_n Y_{n-1}} + \overline{X_n Y_{n-1}}) + A\,\overline{Y_n^2} \quad \text{(III 14)}$$

The above equations are then substituted into Equation (III 8). The result is given in Equations (III 15 - III 20).

$$\overline{C_n^2} = \Big[K_2(\overline{X_n^2} + \overline{Y_n^2}) + K_3\,\overline{Y_n Y_{n-1}} + K_4\,\overline{X_n X_{n-1}} + K_5\,\overline{X_n Y_{n-1}} \Big] / K_1 \quad \text{(III 15)}$$

$$K_1 = -A^2 - 3B^2 - 4AB + .5A^2B - .5B^3 \quad \text{(III 16)}$$

$$K_2 = 2A^2 + 2B^2 + 4AB - .5A^2B + .5B^3 \quad \text{(III 17)}$$

$$K_3 = 2A^2 + 2B^2 + 4AB - .5AB^2 + .5A^3 \quad \text{(III 18)}$$

$$K_4 = 2A^2 + 2B^2 + 4AB - 4A^2B - 2.5AB^2 - 1.5A^3 - .5AB^3 + .5A^3B \quad \text{(III 19)}$$

$$K_5 = 4A^2 + 4B^2 + 8AB - 3AB^2 - 4A^2B - A^3 + .5A^3B - .5AB^3 \quad \text{(III 20)}$$

In order to determine the bit jitter variance, the various cross products on the right side of Equation (III 15) must be evaluated. Once the cross products are evaluated Equation (III 15) provides an expression for tracking performance of the bit synchronization loop.

Figure III-2 will aid in evaluating the cross products.

BIT SYNCHRONIZATION INTEGRALS

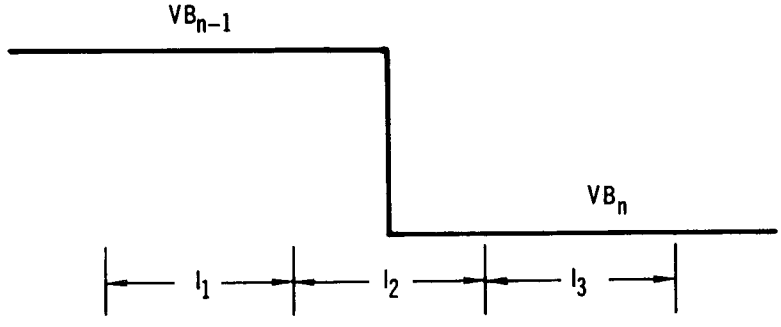

FIGURE III-2

The error signal is determined by integrating over the limits indicated above, and then evaluating Equation (III 21).

$$E = (I_1 + I_2)^2 - (I_2 + I_3)^2 \quad \text{(III 21)}$$

If $B_nB_{n-1} = -1$, the error signal will have the form given in Equation (III 22). The random variables n_1, n_2, and n_3 are uncorrelated, have a mean value of zero, and a variance of $\frac{1}{2}\sigma^2$.

$$X_n = \left[(.5V + n_1 + n_2)^2 - (- .5V + n_2 + n_3)^2 \right] / 4V^2 \qquad \text{(III 22)}$$

If both sides of Equation (III 22) are squared and averaged,

Equations (III 23 - III 24) are obtained.

$$\overline{X_n^2} = (3V^2\sigma^2 + 3\sigma^4) / 16\ V^4 \qquad \text{(III 23)}$$

$$\overline{X_n^2} = (6S + 3) / 64S^2 \qquad \text{(III 24)}$$

$$S = V^2/2\sigma^2$$

If $B_nB_{n-1} = 1$, the value of $\overline{Y_n^2}$ can be derived in a similar manner.

$$\overline{Y_n^2} = (8S + 3) / 64S^2 \qquad \text{(III 25)}$$

The cross product terms can be determined in a similar manner. If $B_n = 1$, $B_{n-1} = -1$, and $B_{n-2} = 1$, the value of X_nX_{n-1} can be determined as shown in Equations (III 26 - III 27).

The random variables n_1, n_2, n_3, n_4 and n_5 are uncorrelated, have a mean value of zero, and a variance of $\frac{1}{2}\sigma^2$.

$$\overline{X_nX_{n-1}} = \left[\overline{(.5V + n_1 + n_2)^2 - (.5V + n_2 + n_3)^2 \quad (-.5V + n_3 + n_4)^2 \quad -(.5V + n_4 + n_5)^2} \right] / 16V^4 \qquad \text{(III 26)}$$

$$\overline{X_nX_{n-1}} = -(2S + 1) / 128S^2 \qquad \text{(III 27)}$$

The other cross product terms can be determined in a similar manner.

$$\overline{Y_nY_{n-1}} = -(8S + 1) / 128S^2 \qquad \text{(III 28)}$$

$$\overline{X_nY_{n-1}} = -(4S + 1) / 128S^2 \qquad \text{(III 29)}$$

A graph of Equation (III 15) as a function of (S) is shown in Figure III-3 where it is compared to equivalent simulation results.

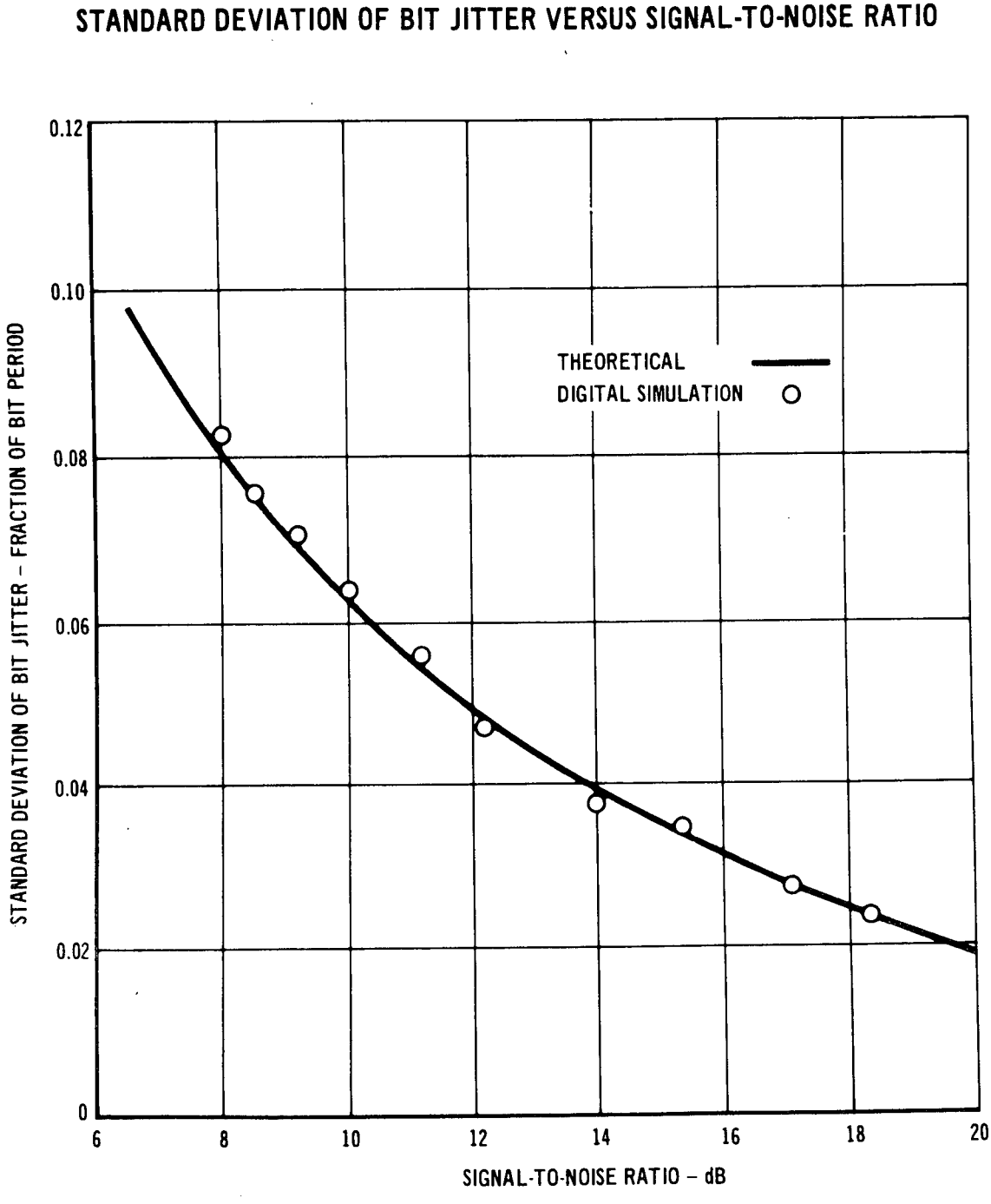

FIGURE III-3

APPENDIX IV

LISTING OF DIGITAL RECEIVER WITHOUT SAMPLE STORAGE BIT SYNCHRONIZATION

```
      PROGRAM BIT
      COMMON ICS
C MCDONNELL DOUGLAS DIGITAL PSK RECEIVER
      DIMENSION ICS(6500)
      DIMENSION INT(100)
      DIMENSION NOUT(2)
      NPTS=4
C SNR IS SIGNAL TO NOISE RATIO IN DB
C NTAU IS NUMBER OF BIT PERIODS IN TIME CONSTANT OF LPF IN DC BIAS REMOVER
      READ (5,119) SNR,NTAU
119   FORMAT (F20.6,I10)
      IF (SNR.LT.-18.00) 120,121
120   IEXP=1
      GO TO 124
121   IF (SNR.LT.5.00) 122,123
122   IEXP=2
      GO TO 124
123   IEXP=3
124   IEXQ=IEXP+2
      IEXR=IEXP+3
      I3=10**IEXP
      I5=10**IEXQ
      I6=10**IEXR
      I33=I3/10
      PI=3.14159
      PI2=2*PI
      IPI=3142
      IPI2=2*IPI
      IPI4=IPI/2
C N IS NUMBER OF BIT PERIODS IN TIME CONSTANT OF BIT SYNC FILTER FOR ACQUISITION
C ISR IS THE NUMBER OF SAMPLES PER BIT
C BR IS THE NUMBER OF BITS PER SECOND
C BWN3DB IS NOISE BANDWIDTH IN HZ FOR COSTAS LOOP FOR ACQUISITION
C SP IS PEAK SIGNAL VOLTAGE
      READ (5,102) N,ISR,BR,BWN3DB,SP
102   FORMAT (2I10,3F20.6)
      ISQ=(10.*I3)/SP
      LSF=100*N**2
      LSF2=LSF/2
      LG=4*N
      KH=ISR/4+1
      KI=ISR/2
      KJ=2*KI
      KK=3*KI
      IS=ISR/2+1
      ITP=4*ISR
      H=1./(ISR*BR)
      AMP=1.0
      ZETA=SQRT(2.)/2.0
      T=1./BR
C BITBW IS THE NOISE BANDWIDTH FOR THE BIT SYNCHRONIZATION LOOP
      BITBW=(2.*ZETA+1./(2.*ZETA))/(4.*ZETA*N*T)
C BW IS OMEGA 0 IN RAD/SEC FOR COSTAS LOOP
      BW=(4*BWN3DB)/(2.*ZETA+1./(2.*ZETA))
C BK AND AK ARE LOOP GAIN CONSTANTS FOR THE COSTAS LOOP
      BK=8.*ZETA*BW/(AMP*AMP)
```

```
      AK=4.*BW*BW/(AMP*AMP)
      DO 771 M=1,IPI2
771   ICS(M)=I3*COS(M*PI2/IPI2)
C ICS(M) IS TABLE OF COSINES
      IX1=IPI2
      IX1=IX1*I3
      IX2=0
      IXA=IPI2
      IXB=IPI4
      I10=IPI2*I3
      I32=I3/2
      ICR=0
      IERR=0
      IOBIT=0
      ITX=0
      NTHAT=0
      NTHAM=0
      ICN=0
      IR=0
      IAZ=0
      ICOUNT=0
      IDUM=0
      IIR=1
      JJ=0
      IIZ=0
      KCOUNT=0
C CONSTANTS FOR IX1
      MP=-I3/2
      D=H*EK
      LD=D*I6
      MHD=ISR*BR
C CONSTANTS FOR IX2
      G=H*AK
      LLG=G*I6
C NB IS NUMBER OF BIT PERIODS IN TIME CONSTANT OF BIT SYNC FILTER
C FOR TRACKING
C BWA IS NOISE BANDWIDTH IN HZ FOR COSTAT LOOP FOR TRACKING
      READ (5,103) NB,BWA
103   FORMAT (I10,F20.6)
      NSF=100*NB**2
      NSF2=NSF/2
      NG=4*NB
      BITBX=(2.*ZETA+1./(2.*ZETA))/(4.*ZETA*NB*T)
      BWN=(4.*BWA)/(2.*ZETA+1./(2.*ZETA))
      BN=8.*ZETA*BWN/(AMP*AMP)
      AN=4.*BWN*BWN/(AMP*AMP)
      DA=H*BN
      ND=DA*I6
      GA=H*AN
      NNG=GA*I6
      WRITE (6,500)
500   FORMAT (41X,38HMCDONNELL DOUGLAS DIGITAL PSK RECEIVER)
      WRITE (6,503) BR
503   FORMAT (/42X,11HBIT RATE IS,F10.5,2X,15HBITS PER SECOND)
      WRITE (6,505) ISR
505   FORMAT (/42X,14HSAMPLE RATE IS,I5,2X,15HSAMPLES PER BIT)
```

```
      WRITE (6,506)
  506 FORMAT (/44X,32HACQUISITION BANDWIDTH PARAMETERS)
      WRITE (6,501) BWN3DB
  501 FORMAT (/39X,30HCOSTAS LOOP NOISE BANDWIDTH IS,F10.5,2X,2HHZ)
      WRITE (6,502) BIT3W
  502 FORMAT (/32X,43HBIT SYNCHRONIZATION LOOP NOISE BANDWIDTH IS,
     $F10.5,2X,2HHZ)
      WRITE (6,507)
  507 FORMAT (/47X,29HTRACKING BANDWIDTH PARAMETERS)
      WRITE (6,501) BWA
      WRITE (6,502) BIT3X
      IAX=0
      IAY=0
      IAA=10000
      IF (IEXP.EQ.1) 410,411
  410 IAA=10*IAA
  411 IALPHA=NTAU*ISR
      IFIV=IAA/ISR
C ENTRY POINT FOR X AND Y IS 101
C X AND Y ARE QUADRATURE COMPONENTS
  101 CALL INDATA(INT,NPTS)
C SSWTCHF(3) ON FOR TRACKING
C SSWTCHF(3) OFF FOR ACQUISITION
      GO TO (789,788) SSWTCHF(3)
  788 ISF=LSF
      ISF2=LSF2
      IG=LG
      MD=LD
      MG=LLG
      GO TO 790
  789 ISF=NSF
      ISF2=NSF2
      IG=NG
      MD=ND
      MG=NNG
  790 CONTINUE
      IX=(ISQ*INT(1))/2048
      IY=(ISQ*INT(2))/2048
C DC BIAS REMOVER
      IAX=IAX-IAX/IALPHA+IFIV*IX/NTAU
      IAY=IAY-IAY/IALPHA+IFIV*IY/NTAU
      IX=IX-IAX/IAA
      IY=IY-IAY/IAA
      ICOUNT=ICOUNT+1
      IDUM=IDUM+1
      IR=0
      IF (IAZ.EQ.1) 8,609
  609 IF (ICN.EQ.1) 78,610
  610 IF (ICOUNT.GE.KH) 7,613
    7 IIR=IIR-1
      I=0
      IA=0
      IB=0
      IC=0
      GO TO 8
   78 ICN=0
```

```
      IA=IC
      IB=0
      IC=0
      I=KI
8     IAZ=0
      I=I+1
      ICOUNT=KH
C COMMON TERMS FOR X1AND X2
C FIRST TERM
613   MA=-(IX**2-IY**2)/4
      MAP=MA/I3
      MB=-ICS(IXA)*ICS(IXB)
      MBP=MB/I3
      MC=MAP*MBP
      MCP=MC/I3
C SECOND TERM
      MM=-(IX*IY)/2
      MMP=MM/I3
      MN=ICS(IXA)**2
      MNP=MN/I3
      MQ=MNP+MP
      MR=MNP*MQ
      MRP=MR/I3
C COMBINE MRP AND MCP TO USE IN BOTH EQUATIONS
      MIRV=MCP+MRP
C BEGIN CALCULATION OF IX1
      ME=MD*MIRV
      MEP=ME/I3
      MF=IX2/MHD
      IX1=IX1+MF+MEP
      L=IX1/I10
      IX1=IX1-L*I10
      IF (IX1.LE.0) 202,203
202   IX1=IX1+I10
203   IF (IX1.LT.I3) 204,205
204   IXA=IPI2
      IXB=IPI4
      GO TO 206
205   IXA=IX1/I3
      IXB=IXA+IPI4
      IF (IXB.EQ.IPI2) 206,207
207   L=IXB/IPI2
      IXB=IXB-L*IPI2
206   NNN=IX1/IPI+ISIGN(I32,IX1)
      NN=NNN/I3
      IXX=IX1-NN*IPI*I3
      IXX=IXX/I3
C BEGIN CALCULATION OF IX2
      MT=MG*MIRV
      MTP=MT/I3
      IX2=IX2+MTP
      IZAZ=(IX*ICS(IXA)+IY*ICS(IXB))/I3
      ITX=ITX+IZAZ
      IF (ICOUNT.GE.KH) 612,100
612   IF (IDUM.LT.ISR) 12,614
614   ICBIT=0
```

```
            IF (ITX.GT.0) 615,616
      615   IOBIT=1
      616   ITX=0
            IDUM=0
      12    IF (IIR.GT.0) 100,625
      625   IF (I.LE.KI) 626,627
      626   IA=IA+IZAZ
      627   IF (I.GT.KI.AND.I.LE.KJ) 628,629
      628   IB=IB+IZAZ
      629   IF (I.GT.KJ.AND.I.LE.KK) 630,631
      630   IC=IC+IZAZ
      631   IF (I.LT.KK) 632,633
      632   IAZ=1
      633   IF (IAZ.EQ.1) 100,634
      634   L1=IA+IB
            L1=L1/I33
            L2=IB+IC
            L2=L2/I33
            IEI=(L1*L1-L2*L2)/ITP
            IE=IERR+2*IEI
            IERR=IE
            IERRR=IE+IG*IEI
            NTHAT=NTHAT+IERRR
            JTHAT=NTHAT+ISIGN(ISF2,NTHAT)
            L=JTHAT/ISF
            JTHAT=L*ISF
            ICR=JTHAT-NTHAM
            NTHAM=JTHAT
            IF (IABS(NTHAT).GE.7000000) 700,701
      700   NTHAT=NTHAT-ISIGN(7000000,NTHAT)
            NTHAM=NTHAM-ISIGN(7000000,NTHAM)
      701   IF (IABS(ICR).LT.ISF) 635,637
      635   ICN=1
            GO TO 100
      637   IR=ICR/ISF
            IDUM=IDUM-IR
            IIR=IS+IR
      100   CONTINUE
      C SSWTCHF(1) OFF FOR DEMODULATED BITS AND INPUT SIGNAL
      C SSWTCHF(1) ON AND SSWTCHF(2) OFF FOR DEMODULATED BITS AND COSTAS LOOP PHASE
      C SSWTCHF(1) ON AND SSWTCHF(2) ON FOR CORRELATOR INTEGRAL AND BIT SYNC
      C ERROR SIGNAL
            GO TO (300,301) SSWTCHF(1)
      300   GO TO (303,304) SSWTCHF(2)
      303   NOUT(1)=((ITX+I3*ISR)/I3)*15
            NOUT(2)=40*IR+600
            GO TO 302
      304   NOUT(1)=IOBIT*1000
            NOUT(2)=(IXX+IPI4)/4
            GO TO 302
      301   NOUT(1)=IOBIT*1000
            NOUT(2)=INT(1)+512
      302   CONTINUE
            CALL DISTWO(NOUT)
            GO TO 101
            END
```

APPENDIX V

LISTING OF DIGITAL RECEIVER WITH SAMPLE STORAGE BIT SYNCHRONIZATION

```
      PROGRAM BIT
      COMMON ICS
C MCDONNELL DOUGLAS DIGITAL PSK RECEIVER
C RECEIVER HAS DC BIAS REMOVER, AGC, SAMPLE STORAGE BIT SYNC
      DIMENSION ICS(6285),LS( 50),NOUT(2),INT( 22)
      NPTS=4
      DO 9 INDX=1, 50
    9 LS(INDX)=0
C SNR IS SIGNAL TO NOISE RATIO IN DB
C NTAU IS NUMBER OF BIT PERIODS IN TIME CONSTANT OF LPF IN DC BIAS REMOVER
      READ (5,119) SNR,NTAU
  119 FORMAT (F20.6,I10)
  121 IF (SNR.LT.5.00) 122,123
  122 IEXP=2
      GO TO 124
  123 IEXP=3
  124 IEXQ=IEXP+2
      IEXR=IEXP+3
      I3=10**IEXP
      I5=10**IEXQ
      I6=10**IEXR
      I33=I3/10
      I38=I33
      I39=I3
      I36=I33
      I37=I3
      PI=3.14159
      PI2=2*PI
      IPI=3142
      IPI2=2*IPI
      IPI4=IPI/2
C N IS NUMBER OF BIT PERIODS IN TIME CONSTANT OF BIT SYNC FILTER FOR ACQUISITION
C ISR IS THE NUMBER OF SAMPLES PER BIT
C BR IS THE NUMBER OF BITS PER SECOND
C BWN3DB IS NOISE BANDWIDTH IN HZ FOR COSTAS LOOP FOR ACQUISITION
C SP IS PEAK SIGNAL VOLTAGE
      READ (5,102) N,ISR,BR,BWN3DB,SP
  102 FORMAT (2I10,3F20.6)
      ISQ=(10.*I3)/SP
      ISF=100*N**2
      ISF2=ISF/2
      IG=4*N
      KH=ISR/4+1
      KI=ISR/2
      KJ=2*KI
      KK=3*KI
      KHI=KI+1
      KII=KI-1
      KJ1=KJ+1
      KK1=KK+1
      I=0
      ITP=4*ISR
      H=1./(ISR*BR)
      AMP=1.0
      ZETA=SQRT(2.)/2.0
      T=1./BR
```

```
      IAX=0
      IAY=0
      IAA=10000
411   IALPHA=NTAU*ISR
      IFIV=IAA/ISR
C BITBW IS THE NOISE BANDWIDTH FOR THE BIT SYNCHRONIZATION LOOP
      BITBW=(2.*ZETA+1./(2.*ZETA))/(4.*ZETA*N*T)
C BW IS OMEGA 0 IN RAD/SEC FOR COSTAS LOOP
      BW=(4*BWN3DB)/(2.*ZETA+1./(2.*ZETA))
C BK AND AK ARE LOOP GAIN CONSTANTS FOR THE COSTAS LOOP
      BK=8.*ZETA*BW/(AMP*AMP)
      AK=4.*BW*BW/(AMP*AMP)
      DO 771 M=1,IPI2
771   ICS(M)=I3*COS(M*PI2/IPI2)
C ICS(M) IS TABLE OF COSINES
      IX2=0
      IXA=IPI2
      IXB=IPI4
      I10=IPI2*I3
      I32=I3/2
      ICR=0
      IE=0
      IOBIT=0
      ITX=0
      NTHAT=0
      NTHAM=0
      ICN=0
      IR=0
      IAZ=0
      ICOUNT=0
      IDUM=0
C CONSTANTS FOR IX1
      MP=-I3/2
      D=H*BK
      MHD=H*I5
C CONSTANTS FOR IX2
      G=H*AK
      JFL=I10
      JFM=I3
      JFN=I32
C NB IS NUMBER OF BIT PERIODS IN TIME CONSTANT OF BIT SYNC FILTER
C FOR TRACKING
C BWA IS NOISE BANDWIDTH IN HZ FOR COSTAT LOOP FOR TRACKING
      READ (5,103) NB,BWA
103   FORMAT (I10,F20.6)
      NSF=100*NB**2
      NSF2=NSF/2
      NG=4*NB
      BITBX=(2.*ZETA+1./(2.*ZETA))/(4.*ZETA*NB*T)
      BWN=(4.*BWA)/(2.*ZETA+1./(2.*ZETA))
      BN=8.*ZETA*BWN/(AMP*AMP)
      AN=4.*BWN*BWN/(AMP*AMP)
      DA=H*BN
      GA=H*AN
      IF (.0118.LE.BWA.AND.0.0187.GT.BWA) 740,741
740   ND=DA*I6
```

```
      NNG=GA*I6*10
      NIX=10*I3
      NIXX=10*I3
      NLSCAL=I3/10
      NNSCA=1
      IF (SNR.LT.5.00) 742,741
  742 I38=100
  741 IF (.0187.LE.BWA.AND..0375.GT.BWA) 743,744
  743 ND=DA*I5
      NNG=GA*I6*10
      NIX=I3
      NIXX=10*I3
      NLSCAL=I3
      NNSCA=10
      IF (SNR.LT.5.00) 745,744
  745 I38=100
  744 IF (.0375.LE.BWA.AND..118.GT.BWA) 746,747
  746 ND=DA*I5
      NNG=GA*I6
      NIX=I3
      NIXX=I3
      NLSCAL=I3
      NNSCA=10
      IF (SNR.LT.5.00) 748,747
  748 I38=100
  747 IF (.118.LE.BWA.AND..187.GT.BWA) 749,750
  749 ND=DA*I5
      NNG=GA*I5
      NIX=I3
      NIXX=I3/10
      NLSCAL=I3
      NNSCA=10
      IF (SNR.LT.5.00) 751,750
  751 I38=100
  750 IF (.187.LE.BWA.AND..375.GT.BWA) 752,753
  752 ND=DA*(I5/10)
      NNG=GA*I5
      NIX=I3/10
      NIXX=I3/10
      NLSCAL=I3*10
      NNSCA=100
      IF (SNR.LT.5.00) 754,753
  754 I38=100
  753 IF (.375.LE.BWA.AND.1.18.GT.BWA) 755,756
  755 ND=DA*(I5/10)
      NNG=GA*(I5/10)
      NIX=I3/10
      NIXX=I3/100
      NLSCAL=I3*10
      NNSCA=100
      IF (SNR.LT.5.0) 757,756
  757 I38=100
  756 IF (1.18.LE.BWA.AND.1.87.GT.BWA) 758,759
  758 ND=DA*(I5/10)
      NNG=GA*I3
      NIX=100
```

```
      NIXX=1
      NLSCAL=I3*I3/100
      NNSCA=I3/10
      IF (SNR.LT.5.00) 760,759
760   I38=100
      I39=10
759   IF (1.87.LE.BWA.AND.3.75.GT.BWA) 761,762
761   ND=DA*I3
      NNG=GA*I3
      NIX=10
      NIXX=1
      NLSCAL=I3*I3/10
      NNSCA=I3
      IF (SNR.LT.5.00) 763,762
763   I38=100
      I39=10
762   IF (3.75.LE.BWA.AND.11.8.GT.BWA) 764,765
764   ND=DA*I3
      NNG=GA*100
      NIX=I3/10
      NIXX=1
      NLSCAL=I3*10
      NNSCA=100
      I39=100
      IF (SNR.LT.5.00) 766,765
766   I38=100
      I39=10
765   CONTINUE
      WRITE (6,500)
500   FORMAT (41X,38HMCDONNELL DOUGLAS DIGITAL PSK RECEIVER)
      WRITE (6,503) BR
503   FORMAT (/42X,11HBIT RATE IS,F10.5,2X,15HBITS PER SECOND)
      WRITE (6,505) ISR
505   FORMAT (/42X,14HSAMPLE RATE IS,I5,2X,15HSAMPLES PER BIT)
      WRITE (6,506)
506   FORMAT (/44X,32HACQUISITION BANDWIDTH PARAMETERS)
      WRITE (6,501) BWN3DB
501   FORMAT (/39X,30HCOSTAS LOOP NOISE BANDWIDTH IS,F10.5,2X,2HHZ)
      WRITE (6,502) BIT3W
502   FORMAT (/32X,43HBIT SYNCHRONIZATION LOOP NOISE BANDWIDTH IS,
     $F10.5,2X,2HHZ)
      WRITE (6,507)
507   FORMAT (/47X,29HTRACKING BANDWIDTH PARAMETERS)
      WRITE (6,501) BWA
      WRITE (6,502) BIT3X
      IZZZ=0                                                    BPL
      IF (.0118.LE.BWN3DB.AND..0187.GT.BWN3DB) 710,711
710   MD=D*I6
      MG=G*I6*10
      KIX=10*I3
      KIXX=10*I3
      LSCAL=I3/10
      NSCA=1
      IF (SNR.LT.5.00) 82,711
82    I36=100
711   IF (.0187.LE.BWN3DB.AND..0375.GT.BWN3DB)  712,713
```

```
      712   MD=D*I5
            MG=G*I6*10
            KIX=I3
            KIXX=10*I3
            LSCAL=I3
            NSCA=10
            IF (SNR.LT.5.00) 83,713
       83   I36=100
      713   IF (.0375.LE.BWN3DB.AND..118.GT.BWN3DB) 714,715
      714   MD=D*I5
            MG=G*I6
            KIX=I3
            KIXX=I3
            LSCAL=I3
            NSCA=10
            IF (SNR.LT.5.00) 84,715
       84   I36=100
      715   IF (.118.LE.BWN3DB.AND..187.GT.BWN3DB) 716,717
      716   MD=D*I5
            MG=G*I5
            KIX=I3
            KIXX=I3/10
            LSCAL=I3
            NSCA=10
            IF (SNR.LT.5.00) 85,717
       85   I36=100
      717   IF (.187.LE.BWN3DB.AND..375.GT.BWN3DB) 718,719
      718   MD=D*(I5/10)
            MG=G*I5
            KIX=I3/10
            KIXX=I3/10
            LSCAL=I3*10
            NSCA=100
            IF (SNR.LT.5.00) 86,719
       86   I36=100
      719   IF (.375.LE.BWN3DB.AND.1.18.GT.BWN3DB) 720,721
      720   MD=D*(I5/10)
            MG=G*(I5/10)
            KIX=I3/10
            KIXX=I3/100
            LSCAL=I3*10
            NSCA=100
            IF (SNR.LT.5.00) 87,721
       87   I36=100
      721   IF (1.18.LE.BWN3DB.AND.1.87.GT.BWN3DB) 722,723
      722   MD=D*(I5/10)
            MG=G*I3
            KIX=100
            KIXX=1
            LSCAL=I3*I3/100
            NSCA=I3/10
            IF (SNR.LT.5.00) 730,723
      730   JFL=JFL/10
            JFM=JFM/10
            JFN=JFN/10
            I36=100
```

```
                I37=10
          723   IF (1.87.LE.BWN3DB.AND.3.75.GT.BWN3DB) 724,725
          724   MD=D*I3
                MG=G*I3
                KIX=10
                KIXX=1
                LSCAL=I3*I3/10
                NSCA=I3
                IF (SNR.LT.5.00) 731,725
          731   JFL=JFL/10
                JFM=JFM/10
                JFN=JFN/10
                I36=100
                I37=10
          725   IF (3.75.LE.BWN3DB.AND.11.8.GT.BWN3DB) 726,727
          726   MD=D*I3
                MG=G*100
                KIX=I3/10
                KIXX=1
                LSCAL=I3*10
                NSCA=100
                JFL=JFL/10
                JFM=JFM/10
                JFN=JFN/10
                I37=100
                IF (SNR.LT.5.00) 180,727
          180   I36=100
                I37=10
          727   IX1=JFL
                IFLG=0
                LIX=1
                IF (SNR.LT.5.00) 796,797
          797   IF (BWN3DB.GE.3.75.AND.BWA.LT.3.75) 794,795
          794   LIX=10
                GO TO 795
          796   IF (BWN3DB.GE.1.18.AND.BWA.LT.1.18) 798,795
          798   LIX=10
          795   CONTINUE
                KCK=2
                KOM=2
                MTAU=30
                KZAZ=0
          C ENTRY POINT FOR X AND Y IS 101
          C x AND Y ARE QUADRATURE COMPONENTS
          C SSWTCHF(3) ON FOR TRACKING
          C SSWTCHF(3) OFF FOR ACQUISITION
          101   CALL INDATA(INT,NPTS)
                GO TO (789,788) SSWTCHF(3)
          788   MT=MD
                MR=MG
                KCK=2
                KIA=KIX
                KIAA=KIXX
                LSCAN=LSCAL
                NSCB=NSCA
                IBF=ISF
```

```
      IBF2=ISF2
      IO=IG
      I34=I36
      I35=I37
      IF (KWK.EQ.KQM) 790,792
  792 IX1=IX1/LIX
      IX2=IX2/LIX
      JFL=JFL/LIX
      JFM=JFM/LIX
      JFN=JFN/LIX
      GO TO 790
  789 MT=ND
      MR=NNG
      KWK=1
      KIA=NIX
      KIAA=NIXX
      LSCAN=NLSCAL
      NSCB=NN.CA
      IBF=NSF
      IEF2=NSF2
      IO=NG
      I34=I38
      I35=I39
      IF (KQK.EQ.KQM) 790,793
  793 IX1=IX1*LIX
      IX2=IX2*LIX
      JFL=JFL*LIX
      JFM=JFM*LIX
      JFN=JFN*LIX
  790 KWM=KWK
      IX=(ISQ*INT(1))/2048
      IY=(ISQ*INT(2))/2048
C UC BIAS REMOVER
      IAX=IAX-IAX/IALPHA+IFIV*IX/NTAU
      IAY=IAY-IAY/IALPHA+IFIV*IY/NTAU
      IX=IX-IAX/IAA
      IY=IY-IAY/IAA
      ICOUNT=ICOUNT+1
      IOUM=IOUM+1
      IF (IAZ.EQ.1) 8,609
  609 IF (ICN.EQ.1) 78,610
  610 IF (ICOUNT.GE.KH) 7,613
    7 IA=0
      IB=0
      IC=0
      IF (IR.EQ.0) 8,305
  305 IF (IR.LT.0) 303,304
  303 KHJ=KJ1+IR
      KHJ=KHJ+KII
      DO 300 IJK=KHJ,KHJJ
      IA=IA+LS(IJK)
  300 KK2=KK1+IR
      LSS=KHI
      DO 301 IJK=KK2,KK
      IB=IB+LS(IJK)
      LS(LSS)=LS(IJK)
```

```
  301   LSS=LSS+1
        I=KI-IR
        GO TO 8
  304   IF (IR.EQ.KI) 306,307
  307   KA=KJ1+IR
        DO 302 IKJ=KA,KK
  302   IA=IA+LS(IKJ)
  306   I=K1-IR
        GO TO 8
   78   ICN=0
        IA=IC
        IB=0
        IC=0
        I=KI
  8     IAZ=0
        I=I+1
        ICOUNT=KH
C COMMON TERMS FOR X1AND X2
C FIRST TERM
  613   MAP=(IX**2-IY**2)/4/I3
        MBP=ICS(IXA)*ICS(IXB)/I3
        MCP=MAP*MBP/I33
C SECOND TERM
        MMP=(IX*IY)/2/I3
        MNP=ICS(IXA)*ICS(IXA)/I3
        MQ=MNP+MP
        MRP=MMP*MQ/I33
C COMBINE MRP AND MCP TO USE IN BOTH EQUA
        MIRV=MCP+MRP
        MF=IX2*MHD/I34
C AGC FOR COSTAS LOOP
        MAA=(IX**2+IY**2)/LSCAN
        IF (MAA.EQ.0) 166,167
  166   MAA=1
  167   MEP=MT*MIRV/MAA
        IX1=IX1+MF+MEP
        L=IX1/JFL
        IX1=IX1-L*JFL
        IF (IX1.LE.0) 202,203
  202   IX1=IX1+JFL
  203   IF (IX1.LT.JFM) 204,205
  204   IXA=IPI2
        IXB=IPI4
        GO TO 206
  205   IXA=IX1/I35
        IXB=IXA+IPI4
        IF (IXB.EQ.IPI2) 206,207
  207   L=IXB/IPI2
        IXB=IXB-L*IPI2
  206   NNN=IX1/IPI+ISIGN(JFN,IX1)
        NN=NNN/JFM
        IXX=IX1-NN*IPI*JFM
        IXX=IXX/I35
        MTP=MR*MIRV/KIAA
        MTP=MTP/MAA/NSCB
        IX2=IX2+MTP
```

```
      IZZZ=(IX*ICS(IXA)-IY*ICS(IXB))/I3
C AGC FOR BIT SYNC LOOP
      IZAZ=-I3
      IF (IZZZ.GE.0) 563,564
563   IZAZ=I3
564   IF (I.GE.KHI.AND.I.LE.KK) 412,413
412   LS(I)=IZAZ
413   ITX=ITX+IZZZ
      IF (ICOUNT.GE.KH) 612,100
612   IF (IDUM.LT.ISR) 625,614
614   IOBIT=0
      IF (ITX.GT.0) 615,616
615   IOBIT=1
616   ITX=0
      IDUM=0
625   IF (I.LE.KI) 626,627
626   IA=IA+IZAZ
627   IF (I.GT.KI.AND.I.LE.KJ) 628,629
628   IB=IB+IZAZ
629   IF (I.GT.KJ.AND.I.LE.KK) 630,631
630   IC=IC+IZAZ
631   IF (I.LT.KK) 632,633
632   IAZ=1
633   IF (IAZ.EQ.1) 100,634
634   L1=(IA+IB)/I33
      L2=(IB+IC)/I33
      IEI=(L1*L1-L2*L2)/ITP
      IE=IE+2*IEI
      IERRR=IE+IO*IEI
      NTHAT=NTHAT+IERRR
      JTHAT=NTHAT+ISIGN(IBF2,NTHAT)
      L=JTHAT/IBF
      JTHAT=L*IBF
      ICR=JTHAT-NTHAM
      NTHAM=JTHAT
      IF (IABS(NTHAT).GE.7000000) 700,701
700   NTHAT=NTHAT-ISIGN(7000000,NTHAT)
      NTHAM=NTHAM-ISIGN(7000000,NTHAM)
701   IF (IABS(ICR).LT.IBF) 635,637
635   ICN=1
      GO TO 100
637   IR=ICR/IBF
      IF (IABS(IR).GT.KI) 14,15
14    IR=ISIGN(KI,IR)
15    IDUM=IDUM-IR
      IF (IDUM.GE.ISR) 1,100
1     IDUM=IDUM-ISR
      IOBIT=0
      IF (ITX.GT.0) 2,3
2     IOBIT=1
3     ITX=0
100   CONTINUE
C SSWTCHF(1) OFF FOR DEMODULATED BITS AND INPUT SIGNAL
C SSWTCHF(1) ON AND SSWTCHF(2) OFF FOR DEMODULATED BITS AND COSTAS LOOP PHASE
C SSWTCHF(1) ON AND SSWTCHF(2) ON FOR CORRELATOR INTEGRAL AND BIT SYNC
C ERROR SIGNAL
```

```
      GO TO (400,401) SSWTCHF(1)
  400 GO TO (403,404) SSWTCHF(2)
  403 NOUT(1)=((IIX+I3*ISR)/I3)*15
      NOUT(2)=40*IR+600
      GO TO 402
  404 NOUT(1)=IOBIT*1000
      NOUT(2)=(IXX+IFI4)/4
      GO TO 402
  401 NOUT(1)=IOBIT*1000
      NOUT(2)=INT(1)+512
  402 CONTINUE
      CALL DISTWO(NOUT)
      GO TO 101
      END
```

APPENDIX VI

LISTING OF DIGITAL RECEIVER WITH SAMPLE STORAGE BIT SYNCHRONIZATION (SPLIT-PHASE DATA)

```
      PROGRAM BIT
      COMMON ICS
C MCDONNELL DOUGLAS DIGITAL PSK RECEIVER FOR SPLIT-PHASE DATA
C RECEIVER HAS DC BIAS REMOVER, AGC, SAMPLE STORAGE BIT SYNC
      DIMENSION ICS(6288),LS( 50),NOUT(2),INT( 22)
C MV AND IV ARE PARAMETERS FOR M-OUT-OF-N DETECTOR
      IV=90
      MV=66
      NPTS=4
      DO 9 INDX=1, 50
9     LS(INDX)=0
C SNR IS SIGNAL-TO-NOISE RATIO IN DB
C NTAU IS NUMBER OF BIT PERIODS IN TIME CONSTANT OF LPF IN DC BIAS REMOVER
      READ (5,119) SNR,NTAU
119   FORMAT (F20.6,I10)
121   IF (SNR.LT.5.00) 122,123
122   IEXP=2
      GO TO 124
123   IEXP=3
124   IEXQ=IEXP+2
      IEXR=IEXP+3
      I3=10**IEXP
      I5=10**IEXQ
      I6=10**IEXR
      I33=I3/10
      I38=I33
      I39=I3
      I36=I33
      I37=I3
      PI=3.14159
      PI2=2*PI
      IPI=3142
      IPI2=2*IPI
      IPI4=IPI/2
C N IS NUMBER OF BIT PERIODS IN TIME CONSTANT OF BIT SYNC FILTER FOR ACQUISITION
C ISR IS THE NUMBER OF SAMPLES PER BIT
C BR IS THE NUMBER OF BITS PER SECOND
C BWN3DB IS NOISE BANDWIDTH IN HZ FOR COSTAS LOOP FOR ACQUISITION
C SP IS PEAK SIGNAL VOLTAGE
      READ (5,102) N,ISR,BR,BWN3DB,SP
102   FORMAT (2I10,3F20.6)
      ISQ=(10.*I3)/SP
      LSF=100*N**2
      LSF2=LSF/2
      LG=4*N
      KZ2=2*ISR
      KH=ISR/4+1
      KI=ISR/2
      KJ=2*KI
      KK=3*KI
      KHI=KI+1
      KII=KI-1
      KJ1=KJ+1
      KK1=KK+1
      I=0
      ITP=4*ISR
```

```
      H=1./(ISR*BR)
      AMP=1.0
      ZETA=SQRT(2.)/2.0
      T=1./BR
      IAX=0
      IAY=0
      IAA=10000
411   IALPHA=NTAU*ISR
      IFIV=IAA/ISR
C BITBW IS THE NOISE BANDWIDTH FOR THE BIT SYNCHRONIZATION LOOP
      BITBW=(2.*ZETA+1./(2.*ZETA))/(4.*ZETA*N*T)
C BW IS OMEGA 0 IN RAD/SEC FOR COSTAS LOOP
      BW=(4*BWN3DB)/(2.*ZETA+1./(2.*ZETA))
C BK AND AK ARE LOOP GAIN CONSTANTS FOR THE COSTAS LOOP
      BK=8.*ZETA*BW/(AMP*AMP)
      AK=4.*BW*BW/(AMP*AMP)
      DO 771 M=1,IPI2
771   ICS(M)=I3*COS(M*PI2/IPI2)
C ICS(M) IS TABLE OF COSINES
      IX1=IPI2
      IX1=IX1*I3
      IX2=0
      IXA=IPI2
      IXB=IPI4
      I10=IPI2*I3
      I32=I3/2
      ICR=0
      IZZZ=0
      IE=0
      IOBIT=1
      ITX=0
      NTHAT=0
      NTHAM=0
      ICN=0
      IR=0
      IAZ=0
      ICOUNT=0
      IOUM=0
      MP=-I3/2
      D=H*BK
      MHD=H*I5
      G=H*AK
      JFL=I10
      JFM=I3
      JFN=I32
C NB IS NUMBER OF BIT PERIODS IN TIME CONSTANT OF BIT SYNC FILTER
C FOR TRACKING
C BWA IS NOISE BANDWIDTH IN HZ FOR COSTAT LOOP FOR TRACKING
      READ (5,103) NB,BWA
103   FORMAT (I10,F20.6)
      NSF=100*NB**2
      NSF2=NSF/2
      NG=4*NB
      BITBX=(2.*ZETA+1./(2.*ZETA))/(4.*ZETA*NB*T)
      BWN=(4.*BWA)/(2.*ZETA+1./(2.*ZETA))
      BN=8.*ZETA*BWN/(AMP*AMP)
```

```
      AN=4.*BWN*BWN/(AMP*AMP)
      DA=H*BN
      GA=H*AN
      IF (.0118.LE.BWA.AND.0.0187.GT.BWA) 740,741
  740 ND=DA*I6
      NNG=GA*I6*10
      NIX=10*I3
      NIXX=10*I3
      NLSCAL=I3/10
      NNSCA=1
      IF (SNR.LT.5.00) 742,741
  742 I38=100
  741 IF (.0187.LE.BWA.AND..0375.GT.BWA) 743,744
  743 ND=DA*I5
      NNG=GA*I6*10
      NIX=I3
      NIXX=10*I3
      NLSCAL=I3
      NNSCA=10
      IF (SNR.LT.5.00) 745,744
  745 I38=100
  744 IF (.0375.LE.BWA.AND..118.GT.BWA) 746,747
  746 ND=DA*I5
      NNG=GA*I6
      NIX=I3
      NIXX=I3
      NLSCAL=I3
      NNSCA=10
      IF (SNR.LT.5.00) 748,747
  748 I38=100
  747 IF (.118.LE.BWA.AND..187.GT.BWA) 749,750
  749 ND=DA*I5
      NNG=GA*I5
      NIX=I3
      NIXX=I3/10
      NLSCAL=I3
      NNSCA=10
      IF (SNR.LT.5.00) 751,750
  751 I38=100
  750 IF (.187.LE.BWA.AND..375.GT.BWA) 752,753
  752 ND=DA*(I5/10)
      NNG=GA*I5
      NIX=I3/10
      NIXX=I3/10
      NLSCAL=I3*10
      NNSCA=100
      IF (SNR.LT.5.00) 754,753
  754 I38=100
  753 IF (.375.LE.BWA.AND.1.18.GT.BWA) 755,756
  755 ND=DA*(I5/10)
      NNG=GA*(I5/10)
      NIX=I3/10
      NIXX=I3/100
      NLSCAL=I3*10
      NNSCA=100
      IF (SNR.LT.5.0) 757,756
```

```
      757   I38=100
      756   IF (1.13.LE.BWA.AND.1.87.GT.BWA) 758,759
      758   ND=DA*(I5/10)
            NNG=GA*I3
            NIX=100
            NIXX=1
            NLSCAL=I3*I3/100
            NSCA=I3/10
            IF (SNR.LT.5.00) 760,759
      760   I38=100
            I39=10
      759   IF (1.87.LE.BWA.AND.3.75.GT.BWA) 761,762
      761   ND=DA*I3
            NNG=GA*I3
            NIX=10
            NIXX=1
            NLSCAL=I3*I3/10
            NSCA=I3
            IF (SNR.LT.5.00) 763,762
      763   I38=100
            I39=10
      762   IF (3.75.LE.BWA.AND.11.8.GT.BWA) 764,765
      764   ND=DA*I3
            NNG=GA*100
            NIX=I3/10
            NIXX=1
            NLSCAL=I3*10
            NNSCA=100
            I39=100
            IF (SNR.LT.5.00) 766,765
      766   I38=100
            I39=10
      765   CONTINUE
            WRITE (6,500)
      500   FORMAT (41X,38HMCDONNELL DOUGLAS DIGITAL PSK RECEIVER)
            WRITE (6,503) BR
      503   FORMAT (/42X,11HBIT RATE IS,F10.5,2X,15HBITS PER SECOND)
            WRITE (6,505) ISR
      505   FORMAT (/42X,14HSAMPLE RATE IS,I5,2X,15HSAMPLES PER BIT)
            WRITE (6,506)
      506   FORMAT (/44X,32HACQUISITION BANDWIDTH PARAMETERS)
            WRITE (6,501) BWN3DB
      501   FORMAT (/39X,30HCOSTAS LOOP NOISE BANDWIDTH IS,F10.5,2X,2HHZ)
            WRITE (6,502) BITBW
      502   FORMAT (/32X,43HBIT SYNCHRONIZATION LOOP NOISE BANDWIDTH IS,
     $F10.5,2X,2HHZ)
            WRITE (6,507)
      507   FORMAT (/47X,29HTRACKING BANDWIDTH PARAMETERS)
            WRITE (6,501) BWA
            WRITE (6,502) BITBX
            MCT=0                                                    21
            IDUN=0                                                   21
            MAS=0
            MAR=0
            MFLAG=0
            IF (.0118.LE.BWN3DB.AND..0187.GT.BWN3DB) 710,711
```

```
710   MD=D*I6
      MG=G*I6*10
      KIX=10*I3
      KIXX=10*I3
      LSCAL=I3/10
      NSCA=1
      IF (SNR.LT.5.00) 82,711
82    I36=100
711   IF (.01o7.LE.BWN3DB.AND..0375.GT.BWN3DB) 712,713
712   MD=D*I5
      MG=G*I6*10
      KIX=I3
      KIXX=10*I3
      LSCAL=I3
      NSCA=10
      IF (SNR.LT.5.00) 83,713
83    I36=100
713   IF (.0375.LE.BWN3DB.AND..118.GT.BWN3DB) 714,715
714   MD=D*I5
      MG=G*I6
      KIX=I3
      KIXX=I3
      LSCAL=I3
      NSCA=10
      IF (SNR.LT.5.00) 84,715
84    I36=100
715   IF (.118.LE.BWN3DB.AND..187.GT.BWN3DB) 716,717
716   MD=D*I5
      MG=G*I5
      KIX=I3
      KIXX=I3/10
      LSCAL=I3
      NSCA=10
      IF (SNR.LT.5.00) 85,717
85    I36=100
717   IF (.187.LE.BWN3DB.AND..375.GT.BWN3DB) 718,719
718   MD=D*(I5/10)
      MG=G*I5
      KIX=I3/10
      KIXX=I3/10
      LSCAL=I3*10
      NSCA=100
      IF (SNR.LT.5.00) 86,719
86    I36=100
719   IF (.375.LE.BWN3DB.AND.1.18.GT.BWN3DB) 720,721
720   MD=D*(I5/10)
      MG=G*(I5/10)
      KIX=I3/10
      KIXX=I3/100
      LSCAL=I3*10
      NSCA=100
      IF (SNR.LT.5.00) 87,721
87    I36=100
721   IF (1.18.LE.BWN3DB.AND.1.87.GT.BWN3DB) 722,723
722   MD=D*(I5/10)
      MG=G*I3
```

```
      KIX=100
      KIXX=1
      LSCAL=I3*I3/100
      NSCA=I3/10
      IF (SNR.LT.5.00) 730,723
730   JFL=JFL/10
      JFM=JFM/10
      JFN=JFN/10
      I36=100
      I37=10
723   IF (1.87.LE.BWN3DB.AND.3.75.GT.BWN3DB) 724,725
724   MD=D*I3
      MG=G*I3
      KIX=10
      KIXX=1
      LSCAL=I3*I3/10
      NSCA=I3
      IF (SNR.LT.5.00) 731,725
731   JFL=JFL/10
      JFM=JFM/10
      JFN=JFN/10
      I36=100
      I37=10
725   IF (3.75.LE.BWN3DB.AND.11.8.GT.BWN3DB) 726,727
726   MD=D*I3
      MG=G*100
      KIX=I3/10
      KIXX=1
      LSCAL=I3*10
      NSCA=100
      JFL=JFL/10
      JFM=JFM/10
      JFN=JFN/10
      I37=100
      IF (SNR.LT.5.00) 180,727
180   I36=100
      I37=10
727   CONTINUE
      IX1=JFL
      IFLG=0
      LIX=1
      IF (SNR.LT.5.00) 796,797
797   IF (BWN3DB.GE.3.75.AND.BWA.LT.3.75) 794,795
794   LIX=10
      GO TO 795
796   IF (BWN3DB.GE.1.13.AND.BWA.LT.1.18) 798,795
798   LIX=10
795   CONTINUE
      KuK=2
101   CALL INDATA(INT,NPTS)
C SSWTCHF(3) ON FOR TRACKING
C SSWTCHF(3) OFF FOR ACQUISITION
      GO TO (789,788) SSWTCHF(3)
788   MT=MD
      MR=MG
      KIA=KIX
```

```
      KIAA=KIXX
      LSCAN=LSCAL
      NSCB=NSCA
      IBF=LSF
      IBF2=LSF2
      IC=LG
      I34=I36
      I35=I37
      IF (KQK.EQ.SSWTCHF(3)) 790,792
  792 IX1=IX1/LIX
      IX2=IX2/LIX
      JFL=JFL/LIX
      JFM=JFM/LIX
      JFN=JFN/LIX
      GO TO 790
  789 MT=ND
      MR=NNG
      KIA=NIX
      KIAA=NIXX
      LSCAN=NLSCAL
      NSCB=NNSCA
      IBF=NSF
      IBF2=NSF2
      IC=NG
      I34=I38
      I35=I39
      IF (KQK.EQ.SSWTCHF(3)) 790,793
  793 IX1=IX1*LIX
      IX2=IX2*LIX
      JFL=JFL*LIX
      JFM=JFM*LIX
      JFN=JFN*LIX
  790 KQK=SSWTCHF(3)
      IX=(ISQ*INT(1))/2048
      IY=(ISQ*INT(2))/2048
C DC BIAS REMOVER
      IAX=IAX-IAX/IALPHA+IFIV*IX/NTAU
      IAY=IAY-IAY/IALPHA+IFIV*IY/NTAU
      IX=IX-IAX/IAA
      IY=IY-IAY/IAA
      IDUN=IDUN+1
      ICOUNT=ICOUNT+1
      IDUM=IDUM+1
      IF (IAZ.EQ.1) 8,609
  609 IF (ICN.EQ.1) 78,610
  610 IF (ICOUNT.GE.KH) 7,613
    7 IA=0
      IB=0
      IC=0
      IF (IR.EQ.0) 8,305
  305 IF (IR.LT.0) 303,304
  303 KHJ=KJ1+IR
      KHJJ=KHJ+KII
      DO 300 IJK=KHJ,KHJJ
  300 IA=IA+LS(IJK)
      KK2=KK1+IR
```

```
      LSS=KHI
      DO 301 IJK=KK2,KK
      IB=IB+LS(IJK)
      LS(LSS)=LS(IJK)
  301 LSS=LSS+1
      I=K1-IR
      GO TO 8
  304 IF (IR.EQ.KI) 306,307
  307 KA=KJ1+IR
      DO 302 IKJ=KA,KK
  302 IA=IA+LS(IKJ)
  306 I=KI-IR
      GO TO 8
   78 ICN=0
      IA=IC
      IB=0
      IC=0
      I=KI
    8 IAZ=0
      I=I+1
      ICOUNT=KH
C COMMON TERMS FOR X1AND X2
C FIRST TERM
  613 MAP=(IX**2-IY**2)/4/I3
      MBP=ICS(IXA)*ICS(IXB)/I3
      MCP=MAP*MBP/I33
      MMP=(IX*IY)/2/I3
      MNP=ICS(IXA)*ICS(IXA)/I3
      MQ=MNP+MP
      MRP=MMP*MQ/I33
C COMBINE MRP AND MCP TO USE IN BOTH EQUATIONS
      MIRV=MCP+MRP
      MF=IX2*MHD/I34
C AGC FOR COSTAS LOOP
      MAA=(IX**2+IY**2)/LSCAN
      IF (MAA.EQ.0) 166,167
  166 MAA=1
  167 MEP=MI*MIRV/MAA
      IX1=IX1+MF+MEP
      L=IX1/JFL
      IX1=IX1-L*JFL
      IF (IX1.LE.0) 202,203
  202 IX1=IX1+JFL
  203 IF (IX1.LT.JFM) 204,205
  204 IXA=IPI2
      IXB=IPI4
      GO TO 206
  205 IXA=IX1/I35
      IXB=IXA+IPI4
      IF (IXB.EQ.IPI2) 206,207
  207 L=IXB/IPI2
      IXB=IXB-L*IPI2
  206 NNN=IX1/IPI+ISIGN(JFN,IX1)
      NN=NNN/JFM
      IXX=IX1-NN*IPI*JFM
      IXX=IXX/I35
```

```
      MTP=MR*MIRV/KIAA
      MTP=MTP/MAA/NSCB
      IX2=IX2+MTP
C AGC FOR BIT SYNC LOOP
      IZZZ=(IX*ICS(IXA)-IY*ICS(IXB))/I3
      IZAZ=-I3
      IF (IZZZ.GE.0) 317,318
  317 IZAZ=I3
  318 CONTINUE
      IF (I.GE.KHI.AND.I.LE.KK) 412,413
  412 LS(I)=IZAZ
  413 ITX=ITX+IZZZ
      IF (ICOUNT.GE.KH) 612,100
  612 IF (IDUN.LT.ISR) 625,614
  614 IOU=IOBIT
      IOBIT=0
      IF (ITX.GT.0) 615,616
  615 IOBIT=1
  616 IF (IDUN.LE.ISR) 617,618
  617 NUM=ITX
  618 IDUM=0
  625 IF (IDUN.LT. KZ2   ) 25,26
   26 IOUTT=1                                                    12
      IF ((NUM-ITX).LE.0) 400,401
  400 IOUTT=0
  401 IDUN=0
      ITX=0
      MAS=MAS+1
      IF (IOU.NE.IOBIT) 402,403
  402 MAR=MAR+1
  403 IF (MAS.GE.IV) 28,25
   28 MAS=0
      IF (MAR.GE.MV) 80,30
   80 MAR=0
      GO TO 25
   30 IDUN=ISR
      MAR=0
   25 IF (IDUN.NE.ISR) 27,29
   29 ITX=0
   27 IF (I.LE.KI) 626,627
  626 IA=IA+IZAZ
  627 IF (I.GT.KI.AND.I.LE.KJ) 628,629
  628 IB=IB+IZAZ
  629 IF (I.GT.KJ.AND.I.LE.KK) 630,631
  630 IC=IC+IZAZ
  631 IF (I.LT.KK) 632,633
  632 IAZ=1
  633 IF (IAZ.EQ.1) 100,634
  634 L1=(IA+IB)/I33
      L2=(IB+IC)/I33
      IEI=(L1*L1-L2*L2)/ITP
      IE=IE+2*IEI
      IERRR=IE+IO*IEI
      NTHAT=NTHAT+IERRR
      JTHAT=NTHAT+ISIGN(IBF2,NTHAT)
      L=JTHAT/IBF
```

```
      JTHAT=L*IBF
      ICR=JTHAT-NTHAM
      NTHAM=JTHAT
      IF (IABS(NTHAT).GE.7000000) 700,701
  700 NTHAT=NTHAT-ISIGN(7000000,NTHAT)
      NTHAM=NTHAM-ISIGN(7000000,NTHAM)
  701 IF (IABS(ICR).LT.IBF) 635,637
  635 ICN=1
      GO TO 100
  637 IR=ICR/IBF
      IF (IABS(IR).GT.KI) 14,15
   14 IR=ISIGN(KI,IR)
   15 IDUM=IDUM-IR
      IDUN=IDUN-IR
      IF (IDUM.GE.ISR) 1,100
    1 IDUM=IDUM-ISR
      IOU=IOBIT
      IOBIT=0
      IF (ITX.GT.0) 2,3
    2 IOBIT=1
    3 IF (IDUN.GE.KZ2) 35,100
   35 IDUN=IDUN-KZ2
      IOUTT=1
      IF ((NUM-ITX).LE.J) 845,846
  845 IOUTT=0
  846 MAS=MAS+1
      IF (IOU.NE.IOBIT) 840,841
  840 MAR=MAR+1
  841 IF (MAS.GE.IV) 828,843
  828 MAS=0
      IF (MAR.GE.MV) 800,830
  800 MAR=0
      GO TO 843
  830 IDUN=IDUN+ISR
      MAR=0
  843 ITX=0
  100 CONTINUE
C SSWTCHF(1) OFF FOR DEMODULATED BITS AND COSTAS LOOP PHASE
C SSWTCHF(1) ON AND SSWTCHF(2) OFF FOR CODED SPLIT-PHASE AND INPUT SIGNAL
C SSWTCHF(1) ON AND SSWTCHF(2) ON FOR DEMODULATED BITS AND BIT SYNC ERROR SIGNAL
      GO TO (404,405) SSWTCHF(1)
  404 GO TO (406,407) SSWTCHF(2)
  406 NOUT(1)=IOUTT*1000
      NOUT(2)=40*IR+600
      GO TO 408
  407 NOUT(1)=IOBIT*1000
      NOUT(2)=INT(2)+512
      GO TO 408
  405 NOUT(1)=IOUTT*1000
      NOUT(2)=(IXX+IPI4)/4
  408 CONTINUE
      CALL DISTWO(NOUT)
      GO TO 101
      END
         FINIS
```

APPENDIX VII

LISTING OF BASEBAND DIGITAL RECEIVER

```
C MCDONNELL DOUGLAS BASEBAND DIGITAL PSK RECEIVER
      DIMENSION LS(50),NOUT(2),INT(22)
      NPTS=4
      DO 9 INDX=1, 50
9     LS(INDX)=0
C SNR IS SIGNAL-TO-NOISE RATIO
C NTAU IS NUMBER OF BIT PERIODS IN LPF TIME CONSTANT IN DC BIAS REMOVER
      READ (5,119) SNR,NTAU
119   FORMAT (F20.6,I10)
121   IF (SNR-LT.5.00) 122,123
122   IEXP=2
      GO TO 124
123   IEXP=3
124   IEXQ=IEXP+2
      IEXR=IEXP+3
      I3=10**IEXP
      I5=10**IEXQ
      I6=10**IEXR
      I33=I3/10
      PI=3.14159
      PI2=2*PI
      IPI=3142
      IPI2=2*IPI
      IPI4=IPI/2
C N IS THE NUMBER OF BIT PERIODS IN TIME CONSTANT OF THE BIT SYNC FILTER
C FOR ACQUISITION
C ISR IS THE NUMBER OF SAMPLES PER BIT
C BR IS THE NUMBER OF BITS PER SECOND
C SP IS PEAK SIGNAL VOLTAGE
      READ (5,102) N,ISR,BR,SP
102   FORMAT (2I10,3F20.6)
      ISQ=(10.*I3)/SP
      LSF=100*N**2
      LSF2=LSF/2
      LG=4*N
      KH=ISR/4+1
      KI=ISR/2
      KJ=2*KI
      KK=3*KI
      KHI=KI+1
      KII=KI-1
      KJ1=KJ+1
      KK1=KK+1
      I=0
      ITP=4*ISR
      H=1./(ISR*BR)
      AMP=1.0
      ZETA=SQRT(2.)/2.0
      T=1./BR
      IAX=0
      IAY=0
      IAA=10000
411   IALPHA=NTAU*ISR
      IFIV=IAA/ISR
C BITBW IS THE NOISE BANDWIDTH FOR THE BIT SYNCHRONIZATION LOOP
      BITBW=(2.*ZETA+1./(2.*ZETA))/(4.*ZETA*N*T)
```

```
      ICR=0
      IZZZ=0
      IE=0
      IOBIT=1
      ITX=0
      NTHAT=0
      NTHAM=0
      ICN=0
      IR=0
      IAZ=0
      ICOUNT=0
      IDUM=0
C NB IS NUMBER OF BIT PERIODS IN TIME CONSTANT OF BIT SYNC FILTER
C FOR TRACKING
      READ (5,103) NB
103   FORMAT (I10,F20.6)
      NSF=100*NB**2
      NSF2=NSF/2
      NG=4*NB
      BITBX=(2.*ZETA+1./(2.*ZETA))/(4.*ZETA*NB*T)
      BWN=(4.*BWA)/(2.*ZETA+1./(2.*ZETA))
      WRITE (6,500)
500   FORMAT (41X,38HMCDONNELL DOUGLAS DIGITAL PSK RECEIVER)
      WRITE (6,503) BR
503   FORMAT (/42X,11HBIT RATE IS,F10.5,2X,15HBITS PER SECOND)
      WRITE (6,505) ISR
505   FORMAT (/42X,14HSAMPLE RATE IS,I5,2X,15HSAMPLES PER BIT)
      WRITE (6,506)
506   FORMAT (/44X,32HACQUISITION BANDWIDTH PARAMETERS)
      WRITE (6,502) BITBW
502   FORMAT (/32X,43HBIT SYNCHRONIZATION LOOP NOISE BANDWIDTH IS,
     $F10.5,2X,2HHZ)
      WRITE (6,507)
507   FORMAT (/47X,29HTRACKING BANDWIDTH PARAMETERS)
      WRITE (6,502) BITBX
      MCT=0
      IDUN=0
101   CALL INDATA(INT,NPTS)
C SSWTCHF(3) ON FOR TRACKING
C SSWTCHF(3) OFF FOR ACQUISITION
      GO TO (789,788) SSWTCHF(3)
788   ISF=LSF
      ISF2=LSF2
      IG=LG
      GO TO 790
789   ISF=NSF
      ISF2=NSF2
      IG=NG
790   CONTINUE
      IX=(ISQ*INT(1))/2048
      IY=(ISQ*INT(2))/2048
C DC BIAS REMOVER
      IAX=IAX-IAX/IALPHA+IFIV*IX/NTAU
      IAY=IAY-IAY/IALPHA+IFIV*IY/NTAU
      IX=IX-IAX/IAA
      IY=IY-IAY/IAA
```

```
            ICOUNT=ICOUNT+1
            IDUM=IDUM+1
            IF (IAZ.EQ.1) 8,609
      609   IF (ICN.EQ.1) 78,610
      610   IF (ICOUNT.GE.KH) 7,613
          7 IA=0
            IB=0
            IC=0
            IF (IR.EQ.0) 8,305
      305   IF (IR.LT.0) 303,304
      303   KHJ=KJ1+IR
            KHJJ=KHJ+KII
            DO 300 IJK=KHJ,KHJJ
      300   IA=IA+LS(IJK)
            KK2=KK1+IR
            LSS=KHI
            DO 301 IJK=KK2,KK
            IB=IB+LS(IJK)
            LS(LSS)=LS(IJK)
      301   LSS=LSS+1
            I=KI-IR
            GO TO 8
      304   IF (IR.EQ.KI) 306,307
      307   KA=KJ1+IR
            DO 302 IKJ=KA,KK
      302   IA=IA+LS(IKJ)
      306   I=KI-IR
            GO TO 8
         78 ICN=0
            IA=IC
            IB=0
            IC=0
            I=KI
      8     IAZ=0
            I=I+1
      613   CONTINUE
            ICOUNT=KH
            IY=0
      C AGC FOR BIT SYNC
            IZAZ=-I3
            IF (IX.GE.0) 150,151
      150   IZAZ=I3
      151   IZZZ=IX
            IF (I.GT.KHI.AND.I.LE.KK) 412,413
      412   LS(I)=IZAZ
      413   ITX=ITX+IZZZ
            IF (ICOUNT.GE.KH) 612,100
      612   IF (IDUM.LT.ISR) 625,614
      614   IOBIT=0
            IF (ITX.GT.0) 615,616
      615   IOBIT=1
      616   ITX=0
            IDUM=0
      625   IF (I.LE.KI) 626,627
      626   IA=IA+IZAZ
      627   IF (I.GT.KI.AND.I.LE.KJ) 628,629
```

```
      628   IB=IB+IZAZ
      629   IF (I.GT.KJ.AND.I.LE.KK) 630,631
      630   IC=IC+IZAZ
      631   IF (I.LT.KK) 632,633
      632   IAZ=1
      633   IF (IAZ.EQ.1) 100,634
      634   L1=(IA+IB)/I33
            L2=(IB+IC)/I33
            IEI=(L1*L1-L2*L2)/ITP
            IE=IE+2*IEI
            IERRR=IE+IG*IEI
            NTHAT=NTHAT+IERRR
            JTHAT=NTHAT+ISIGN(ISF2,NTHAT)
            L=JTHAT/ISF
            JTHAT=L*ISF
            ICR=JTHAT-NTHAM
            NTHAM=JTHAT
            IF (IABS(NTHAT).GE.7000000) 700,701
      700   NTHAT=NTHAT-ISIGN(7000000,NTHAT)
            NTHAM=NTHAM-ISIGN(7000000,NTHAM)
      701   IF (IABS(ICR).LT.ISF) 635,637
      635   ICN=I
            GO TO 100
      637   IR=ICR/ISF
            IF (IABS(IR).GT.KI) 14,15
      14    IR=ISIGN(KI,IR)
      15    IDUM=IDUM-IR
            IF (IDUM.GE.ISR) 1,100
      1     IDUM=IDUM-ISR
            IOBIT=0
            IF (ITX.GT.0) 2,3
      2     IOBIT=1
      3     ITX=0
      100   CONTINUE
      C SSWTCHF(1) OFF FOR DEMODULATED BITS AND INPUT SIGNAL
      C SSWTCHF(1) ON AND SSWTCHF(2) OFF FOR DEMODULATED BITS AND BIT SYNC
      C ERROR SIGNAL
      C SSWTCHF(1) ON AND SSWTCHF(2) ON FOR DEMODULATED BITS AND CORRELATOR INTEGRAL
            GO TO (404,405) SSWTCHF(1)
      404   GO TO (406,407) SSWTCHF(2)
      406   NOUT(1)=IOBIT*1000
            NOUT(2)=((ITX+I3*ISR)/I3)*15
            GO TO 408
      407   NOUT(1)=IOBIT*1000
            NOUT(2)=40*IR+600
            GO TO 408
      405   NOUT(1)=IOBIT*1000
            NOUT(2)=INT(2)+512
      408   CONTINUE
            CALL DISTWO(NOUT)
            GO TO 101
            END
               FINIS
```

APPENDIX VIII

LISTING OF DIGITAL RECEIVER WITH SWEPT FREQUENCY ACQUISITION

```
      PROGRAM BIT
      COMMON ICS
C MCDONNELL DOUGLAS DIGITAL PSK RECEIVER
C RECEIVER HAS DC BIAS REMOVER,AGC,SAMPLE STORAGE BIT SYNC,AND SWEPT
C FREQUENCY ACQUISITION
      DIMENSION ICS(6285),LS( 50),NOUT(2),INT( 22)
      NPTS=4
      DO 9 INDX=1, 50
9     LS(INDX)=0
C SNR IS SIGNAL TO NOISE RATIO IN DB
C NTAU IS TIME CONSTANT OF LPF IN DC BIAS REMOVER IN BIT PERIODS
      READ (5,119) SNR,NTAU
119   FORMAT (F20.6,I10)
121   IF (SNR.LT 5.00) 122,123
122   IEXP=2
      GO TO 124
123   IEXP=3
124   IEXQ=IEXP+2
      IEXR=IEXP+3
      I3=10**IEXP
      I5=10**IEXQ
      I6=10**IEXR
      I33=I3/10
      I38=I33
      I39=I3
      I36=I33
      I37=I3
      PI=3.14159
      PI2=2*PI
      IPI=3142
      IPI2=2*IPI
      IPI4=IPI/2
C N IS TIME CONSTANT OF BIT SYNC FILTER IN BIT PERIODS
C ISR IS THE NUMBER OF SAMPLES PER BIT
C BR IS THE NUMBER OF BITS PER SECOND
C BWN3DB IS NOISE BANDWIDTH IN HZ FOR COSTAS LOOP
C SP IS PEAK SIGNAL VOLTAGE
      READ (5,102) N,ISR,BR,BWN3DB,SP
102   FORMAT (2I10,3F20.6)
      ISQ=(10.*I3)/SP
      LSF=100*N**2
      LSF2=LSF/2
      LG=4*N
      KH=ISR/4+1
      KI=ISR/2
      KJ=2*KI
      KK=3*KI
      KHI=KI+1
      KII=KI-1
      KJ1=KJ+1
      KK1=KK+1
      I=0
      ITP=4*ISR
      H=1./(ISR*BR)
      AMP=1.0
      ZETA=SQRT(2.)/2.0
```

```
      T=1./BR
      IAX=0
      IAY=0
      IAA=10000
  411 IALPHA=NTAU*ISR
      IFIV=IAA/ISR
C BITBW IS THE NOISE BANDWIDTH FOR THE BIT SYNCHRONIZATION LOOP
      BITBW=(2.*ZETA+1./(2.*ZETA))/(4.*ZETA*N*T)
C BW IS OMEGA 0 IN RAD/SEC FOR COSTAS LOOP
      BW=(4*BWN3DB)/(2.*ZETA+1./(2.*ZETA))
C BK AND AK ARE LOOP GAIN CONSTANTS FOR THE COSTAS LOOP
      BK=8.*ZETA*BW/(AMP*AMP)
      AK=4.*BW*BW/(AMP*AMP)
      DO 771 M=1,IPI2
  771 ICS(M)=I3*COS(M*PI2/IPI2)
C ICS(M) IS TABLE OF COSINES
      IX2=0
      IXA=IPI2
      IXB=IPI4
      I10=IPI2*I3
      I32=I3/2
      ICR=0
      IE=0
      IOBIT=0
      ITX=0
      NTHAT=0
      NTHAM=0
      ICN=0
      IR=0
      IAZ=0
      ICOUNT=0
      IDUM=0
C CONSTANTS FOR IX1
      MP=-I3/2
      D=H*BK
      MHD=H*I5
C CONSTANTS FOR IX2
      G=H*AK
      JFL=I10
      JFM=I3
      JFN=I32
      WRITE (6,500)
  500 FORMAT (41X,38HMCDONNELL DOUGLAS DIGITAL PSK RECEIVER)
      WRITE (6,503) BR
  503 FORMAT (/42X,11HBIT RATE IS,F10.5,2X,15HBITS PER SECOND)
      WRITE (6,505) ISR
  505 FORMAT (/42X,14HSAMPLE RATE IS,I5,2X,15HSAMPLES PER BIT)
      WRITE (6,501) BWN3DB
  501 FORMAT (/39X,30HCOSTAS LOOP NOISE BANDWIDTH IS,F10.5,2X,2HHZ)
      WRITE (6,502) BITBW
  502 FORMAT (/32X,43HBIT SYNCHRONIZATION LOOP NOISE BANDWIDTH IS,
     $F10.5,2X,2HHZ)
      IZZZ=0                                                    BPL
      IF (.0118.LE.BWN3DB.AND..0187.GT.BWN3DB) 710,711
  710 MD=D*I6
      MG=G*I6*10
```

```
            KIX=10*I3
            KIXX=10*I3
            LSCAL=I3/10
            NSCA=1
            IF (SNR.LT.5.00) 82,711
      82    I36=100
      711   IF (.0187.LE.BWN3DB.AND..0375.GT.BWN3DB ) 712,713
      712   MD=D*I5
            MG=G*I6*10
            KIX=I3
            KIXX=10*I3
            LSCAL=I3
            NSCA=10
            IF (SNR.LT.5.00) 83,713
      83    I36=100
      713   IF (.0375.LE.BWN3DB.AND..118.GT.BWN3DB) 714,715
      714   MD=D*I5
            MG=G*I6
            KIX=I3
            KIXX=I3
            LSCAL=I3
            NSCA=10
            IF (SNR.LT.5.00) 84,715
      84    I36=100
      715   IF (.118.LE.BWN3DB.AND..187.GT.BWN3DB) 716,717
      716   MD=D*I5
            MG=G*I5
            KIX=I3
            KIXX=I3/10
            LSCAL=I3
            NSCA=10
            IF (SNR.LT.5.00) 85,717
      85    I36=100
      717   IF (.187.LE.BWN3DB.AND..375.GT.BWN3DB) 718,719
      718   MD=D*(I5/10)
            MG=G*I5
            KIX=I3/10
            KIXX=I3/10
            LSCAL=I3*10
            NSCA=100
            IF (SNR.LT 5.00) 86,719
      86    I36=100
      719   IF (.375 LE BWN3DB.AND.1.18.GT.BWN3DB) 720,721
      720   MD=D*(I5/10)
            MG=G*(I5/10)
            KIX=I3/10
            KIXX=I3/100
            LSCAL=I3*10
            NSCA=100
            IF (SNR.LT.5.00) 87,721
      87    I36=100
      721   IF (1.18.LE.BWN3DB.AND.1.87.GT.BWN3DB) 722,723
      722   MD=D*(I5/10)
            MG=G*I3
            KIX=100
            KIXX=1
```

```
      LSCAL=I3*I3/100
      NSCA=I3/10
      IF (SNR.LT.5.00) 730,723
730   JFL=JFL/10
      JFM=JFM/10
      JFN=JFN/10
      I36=100
      I37=10
723   IF (1.87.LE.BWN3DB.AND.3.75.GT.BWN3DB) 724,725
724   MD=D*I3
      MG=G*I3
      KIX=10
      KIXX=1
      LSCAL=I3*I3/10
      NSCA=I3
      IF (SNR.LT.5.00) 731,725
731   JFL=JFL/10
      JFM=JFM/10
      JFN=JFN/10
      I36=100
      I37=10
725   IF (3.75.LE.BWN3DB.AND.11.8.GT.BWN3DB) 726,727
726   MD=D*I3
      MG=G*100
      KIX=I3/10
      KIXX=1
      LSCAL=I3*10
      NSCA=100
      JFL=JFL/10
      JFM=JFM/10
      JFN=JFN/10
      I37=100
      IF (SNR.LT.5.00) 180,727
180   I36=100
      I37=10
727   IX1=JFL
      LIX=1
      KQK=2
      MTAU=800
      KZAZ=0
      KFLAG=0
      MENT=10
      IF (SNR.LE.5.00  .AND.BWN3DB.GE.1.18) 3000,3001
3000  MENT=1
3001  CONTINUE
      IF (SNR.GT.5.00  .AND.BWN3DB.LT.3.75) 3002,3003
3002  MENT=100
3003  CONTINUE
      ICAN=0
      ITY=0
      IDELT=(-PI*H)*10000
      LANG=0
C SWEEP START IS -PI RAD/SEC
C DW IS ONE HALF THE SWEEP RATE IN RAD/SEC/SEC
C DW IS NOMINALLY SET AT 0.025 RAD/SEC/SEC
      READ (5,119) DW
```

```
      IPRA=2.*DW*H*1000000
      PROD=DW*H**2
      IPROD=PROD*10000*10000
      MANG=0
      NANG=0
      JPHAS=0
      KZAX=0
C PERC SETS THRESHOLD ON ACQUISITION INDICATOR
C PERC HAS MAXIMUM VALUE OF 1.0 AND IS NOMINALLY SET AT .98
      PERC=.98
      ITH1=(ISR*I3)*PERC
C ENTRY POINT FOR X AND Y IS 101
C X AND Y ARE QUADRATURE COMPONENTS
101   CALL INDATA(INT,NPTS)
C TURN SSWTCHF(3) ON AND THEN OFF TO MANUALLY RESET SWEEP
      GO TO (398,399) SSWTCHF(3)
398   KFLAG=0
      IX1=JFL
      IXA=IPI2
      IXB=IPI4
      IX2=0
      IX3=0
      ICAN=0
      KZAZ=0
399   CONTINUE
788   MT=MD
      MR=MG
      KIA=KIX
      KIAA=KIXX
      LSCAN=LSCAL
      NSCB=NSCA
      IBF=LSF
      IBF2=LSF2
      IO=LG
      I34=I36
      I35=I37
      IX=(ISQ*INT(1))/2048
      IY=(ISQ*INT(2))/2048
C DC BIAS REMOVER
      IAX=IAX-IAX/IALPHA+IFIV*IX/NTAU
      IAY=IAY-IAY/IALPHA+IFIV*IY/NTAU
      IX=IX-IAX/IAA
      IY=IY-IAY/IAA
      ICOUNT=ICOUNT+1
      IDUM=IDUM+1
      IF (IAZ.EQ.1) 8,609
609   IF (ICN.EQ.1) 78,610
610   IF (ICOUNT.GE.KH) 7,613
    7 IA=0
      IB=0
      IC=0
      IF (IR.EQ.0) 8,305
305   IF (IR.LT.0) 303,304
303   KHJ=KJ1+IR
      KHJJ=KHJ+KII
      DO 300 IJK=KHJ,KHJJ
```

```
      300   IA=IA+LS(IJK)
            KK2=KK1+IR
            LSS=KHI
            DO 301 IJK=KK2,KK
            IB=IB+LS(IJK)
            LS(LSS)=LS(IJK)
      301   LSS=LSS+1
            I=KI-IR
            GO TO 8
      304   IF (IR.EQ.KI) 306,307
      307   KA=KJ1+IR
            DO 302 IKJ=KA,KK
      302   IA=IA+LS(IKJ)
      306   I=KI-IR
            GO TO 8
       78   ICN=0
            IA=IC
            IB=0
            IC=0
            I=KI
        8   IAZ=0
            I=I+1
            ICOUNT=KH
      613   MAP=(IX**2-IY**2)/4/I3
            MBP=ICS(IXA)*ICS(IXB)/I3
            MCP=MAP*MBP/I33
            MMP=(IX*IY)/2/I3
            MNP=ICS(IXA)*ICS(IXA)/I3
            MQ=MNP+MP
            MRP=MMP*MQ/I33
            MIRV=MCP+MRP
            MF=IX2*MHD/I34
      C AGC FOR COSTAS LOOP
            MAA=(IX**2+IY**2)/LSCAN
            IF (MAA.EQ 0) 166,167                                    BPL
      166   MAA=1                                                    BPL
      167   MEP=MT*MIRV/MAA
            IX1=IX1+MF+MEP
            L=IX1/JFL
            IX1=IX1-L*JFL
            IF (IX1.LE.0) 202,203
      202   IX1=IX1+JFL
      C FREQUENCY SWEEP LOGIC
      C SWEEP WILL AUTOMATICALLY RESET IF RECEIVER DOES NOT ACQUIRE
      C SWEEP WILL AUTOMATICALLY START IF ACQUISITION INDICATOR FALLS BELOW
      C THRESHOLD AFTER ACQUISITION
      203   IF (KFLAG.EQ.0) 215,214
      215   CONTINUE
            ICAN=ICAN+1
            IF (ICAN GT 100000) 1114,1115
     1114   ICAN=0
            MANG=0
            NANG=0
            JPHAS=0
            LANG=0
     1115   CONTINUE
```

```
      MANG=MANG+IDELT
      L=MANG/62832
      MANG=MANG-L*62832
      IF (MANG.LE.0) 2000,2001
 2000 MANG=MANG+62832
 2001 CONTINUE
      NDEL=IPROD+2*IPROD*ICAN
      L=LANG/6283185
      LANG=LANG-L*6283185
      IF (LANG.LE.0) 2022,2023
 2022 LANG=LANG+6283185
 2023 CONTINUE
      LANG=LANG+NDEL/100
      NANG=LANG/100
      L=NANG/62832
      NANG=NANG-L*62832
      IF (NANG.LE.0) 2010,2011
 2010 NANG=NANG+62832
 2011 CONTINUE
      JPHAS=MANG+NANG
      JPHAS=JPHAS*MENT
 1199 CONTINUE
      L=JPHAS/JFL
      JPHAS=JPHAS-L*JFL
      IF (JPHAS.LE.0) 220,221
  220 JPHAS=JPHAS+JFL
  221 CONTINUE
      IF (KZAX.GE.ITH1) 212,214
  212 IX2=-IPI+(IPRA*ICAN)/1000
      KFLAG=1
      JPHAS=0
      LANG=0
      MANG=0
      NANG=0
  214 CONTINUE
C END FREQUENCY SWEEP LOGIC
      IX3=IX1+JPHAS
      L=IX3/JFL
      IX3=IX3-L*JFL
      IF (IX3.LE.0) 230,231
  230 IX3=IX3+JFL
  231 IF (IX3.LT.JFM) 204,205
  204 IXA=IPI2
      IXB=IPI4
      GO TO 206
  205 IXA=IX3/I35
      IXB=IXA+IPI4
      IF (IXB.EQ.IPI2) 206,207
  207 L=IXB/IPI2
      IXB=IXB-L*IPI2
  206 NNN=IX3/IPI+ISIGN(JFN,IX3)
      NN=NNN/JFM
      IXX=IX3-NN*IPI*JFM
      IXX=IXX/I35
      NNN=JPHAS/IPI+ISIGN(JFN,JPHAS)
      NN=NNN/JFM
```

```
                IXY=JPHAS-NN*IPI*JFM
                IXY=IXY/I35
                MTP=MR*MIRV/KIAA
                MTP=MTP/MAA/NSCB
                IX2=IX2+MTP
          C AGC FOR BIT SYNC LOOP
                IZZZ=(IX*ICS(IXA)-IY*ICS(IXB))/I3                    BPL
                IZAZ=-I3                                             BPL
                IF (IZZZ.GE.0) 563,564
          563   IZAZ=I3
          564   IF (I.GE.KHI.AND.I.LE.KK) 412,413
          412   LS(I)=IZAZ
          413   ITX=ITX+IZZZ
                ITY=ITY+IZAZ
                IF (ICOUNT.GE.KH) 612,100
          612   IF (IDUM.LT.ISR) 625,614
          614   IOBIT=0
                IVARB=IABS(ITY)
                IVARB=IVARB*1000
                KZAZ=KZAZ-KZAZ/MTAU+IVARB/MTAU
                KZAX=KZAZ/1000
                IF (ITX.GT.0) 615,616
          615   IOBIT=1
          616   ITX=0
                ITY=0
                IDUM=0
          625   IF (I.LE.KI) 626,627
          626   IA=IA+IZAZ
          627   IF (I.GT.KI.AND.I.LE.KJ) 628,629
          628   IB=IB+IZAZ
          629   IF (I.GT.KJ.AND.I.LE.KK) 630,631
          630   IC=IC+IZAZ
          631   IF (I.LT.KK) 632,633
          632   IAZ=1
          633   IF (IAZ.EQ.1) 100,634
          634   L1=(IA+IB)/I33
                L2=(IB+IC)/I33
                IEI=(L1*L1-L2*L2)/ITP
                IE=IE+2*IEI
                IERRR=IE+IO*IEI
                NTHAT=NTHAT+IERRR
                JTHAT=NTHAT+ISIGN(IBF2,NTHAT)
                L=JTHAT/IBF
                JTHAT=L*IBF
                ICR=JTHAT-NTHAM
                NTHAM=JTHAT
                IF (IABS(NTHAT).GE.7000000) 700,701
          700   NTHAT=NTHAT-ISIGN(7000000,NTHAT)
                NTHAM=NTHAM-ISIGN(7000000,NTHAM)
          701   IF (IABS(ICR).LT.IBF) 635,637
          635   ICN=1
                GO TO 100
          637   IR=ICR/IBF
                IF (IABS(IR).GT.KI) 14,15
          14    IR=ISIGN(KI,IR)
          15    IDUM=IDUM-IR
```

```
      IF (IDUM GE.ISR) 1,100
    1 IDUM=IDUM-ISR
      IOBIT=0
      IVARB=IABS(ITY)
      IVARB=IVARB*1000
      KZAZ=KZAZ-KZAZ/MTAU+IVARB/MTAU
      KZAX=KZAZ/1000
      IF (ITX.GT.0) 2,3
    2 IOBIT=1
    3 ITX=0
      ITY=0
  100 CONTINUE
C SSWTCHF(1) OFF FOR ACQUISITION INDICATOR AND PHASE OF FREQUENCY SWEEP
C SSWTCHF(1) ON AND SSWTCHF(2) OFF FOR DEMODULATED BITS AND COSTAS LOOP PHASE
C SSWTCHF(1) ON AND SSWTCHF(2) ON FOR DEMODULATED BITS AND INPUT SIGNAL
      GO TO (400,401) SSWTCHF(1)
  400 GO TO (403,404) SSWTCHF(2)
  403 NOUT(1)=IOBIT*1000
      NOUT(2)=INT(1)+512
      GO TO 402
  404 NOUT(1)=IOBIT*1000
      NOUT(2)=(IXX+IPI4)/4
      GO TO 402
  401 NOUT(1)=(KZAX/I3)*40
      NOUT(2)=(IXY+IPI4)/4
  402 CONTINUE
      CALL DISTWO(NOUT)
      GO TO 101
      END
          FINIS
```